MOLECULAR REGULATION OF NUTRIENT SENSING AND IMMUNOMETABOLISM BY CALORIE RESTRICTION

BY

DIEGO HERNÁNDEZ-SAAVEDRA

DISSERTATION

Submitted in partial fulfillment of the requirements
for the degree of Doctor of Philosophy in Nutritional Sciences
in the Graduate College of the
University of Illinois at Urbana-Champaign, 2018

Urbana, Illinois

Doctoral Committee:

Associate Professor Juan J. Loor, Chair
Associate Professor Yuan-Xiang Pan, Director of Research
Professor Jongsook Kim Kemper
Assistant Professor Nu-Chu Liang

ABSTRACT

"*'You'll live longer and you'll be healthier too,' he answered. 'Because as we were saying today, there's nothing in the world like eating moderately to live a long life.' 'If that's the way things are,' I thought to myself, 'I never will die.' Because I've always been forced to keep that rule, and with my luck I'll probably keep it all my life.*"—Anonymous, The Life of Lazarillo de Tormes and of His Fortunes and Adversities 1554.

Adaptive mechanisms in response to calorie restriction are evolutionarily conserved and necessary to promote longevity and increase health span. Caloric restriction (CR) without malnutrition, constitutes an effective strategy for weight reduction and ameliorates the chronic inflammatory burden of many chronic metabolic diseases. CR is known to impact nutrient sensing and immuno-metabolic processes in immune cells, but not much is known about skeletal muscle, the largest tissue in the body. We first delve into the literature that describes the interaction of CR and epigenetic mechanisms: DNA methylation, histone modifications, and microRNAs. We explore the impact of CR on nutrient sensing and immuno-metabolic processes and provide a comprehensive view of the adaptive and epigenetic machinery coordinated by CR. In our first study, we aimed to uncover the long-term effect of CR following early-life high fat-diet exposure. We analyzed physiological, biochemical, and transcriptional changes in muscle following chronic CR. Our results indicate that CR activates nutrient sensing pathways, promotes protein recycling, and stimulates myogenesis, possibly due to inhibition of cachexia-inducing inflammatory pathways. Then, our second experiment was designed to titrate the effects of CR by using a novel approach with clinical translatability. We used alternate-day CR (ADCR) in 1-3 days a week and 25-75 % energy restriction to delineate the physiological, biochemical, and transcriptional changes in muscle following chronic ADCR. Effective strategies with high translatable potential, such as 50% CR more than 2 days a week or 75% CR more than 1 day a week, produced similar effects to

the gold standard of 25% chronic CR. Finally, on our third experiment we dissected the series of adaptive, epigenetic mechanisms employed by CR to decrease muscle inflammation. Chronic CR activates a series of inhibitors of inflammatory factor NF-kB, while increasing promoter DNA methylation and decreasing transcription factor binding of cytokine *Tnf*, as well as fine-tuning miRNA expression to prevent inflammation. Here we describe that CR orchestrates a series of adaptive nutrient sensing and anti-inflammatory checkpoints to inhibit inflammation and promote skeletal muscle maintenance.

ACKNOWLEDGEMENTS

To the members of my doctoral committee, Dr. Juan J. Loor, Dr. Jongsook Kim Kemper, and Dr. Nu-Chu Liang, thank you for providing extensive constructive criticism and helping my scientific development. To Dr. Gustavo Caetano-Anollés, a previous committee member, for helping me with the development of my project.

Special thanks to Dr. Yuan-Xiang Pan, my thesis director, for providing support throughout my Ph.D., as well as helping me become a productive and competitive scientist. Additionally, I want to thank Dr. Hong Chen for being more than a mentor to me, and making sure that I was eating, learning, and writing!

To unofficial mentors, Dr. Michael de Lisio, Dr. Janice Juraska, and Dr. R. Scott Rector, for believing in my abilities and helping me expand my knowledge.

To previous and current members of the Pan-Chen Lab, Laura Moody, Dr. Huan Wang, Dr. Dan Zhou, Bianca Xu, and Adam Kriska, for always supporting me and being there for me at all times. You were all good friends and teachers to me.

Special thanks to Dr. Rita S. Strakovsky, for taking me under her wing and making sure I got the best preparation. Also, for showing me what a true friendship looks like; being there in the good, the sad, and the happiest moments.

To my army of undergrads over my 5 years at UIUC, thank you all for putting up with my crazy requirements, and extreme schedules, and for keeping me company during the long incubation times.

To the Division of Nutritional Sciences staff, Dr. Jessica Hartke, Ashley Browning, and Sarah Wells, for keeping me on track and making sure that I was always smiling.

To Toni M. Burkhalter, for believing in my teaching skills and for trusting me to improve FSHN 120. Without you I wouldn't be as confident in front of a large crowd, nor will I be able to have self-confidence to apply for different positions.

Special thanks to my family, my Mom (Lulú), my Dad (Don Gus), my siblings (Clau and Gus), and their partners (Diego and Michelle), as well as my nieces (Sofia, Victoria, Valentina, and the new addition), for being my compass and a shining beacon of hope for this foolish dreamer. Your company and your laughs guided me through the roughest times.

To my family in Leon and Queretaro and family friends, for being my most avid supporters throughout my college and Ph.D. years.

Special thanks to Dr. Brett Loman, for showing me a life outside the lab. For being a partner in crime in multiple adventures, and continuing to be by my side to me in the next chapter of my life.

To my DNS friends, Patricia Wolf, Dr. Tzu-wen Liu Cross, Dr. Annabel Biruete, Dr. Adrienne Antonson, thank you for the unconditional love and support. You are truly the best friends for life I could've asked for.

To my friends from Champaign, Queretaro, and Leon, for always be willing to listen to me rambling for hours and hours and hugging me every time I came home.

Finally, to my host families, the Graebe and Mitchell families for being my family away from home, and making me feel welcome even after 12 years.

TABLE OF CONTENTS

CHAPTER 1: INTRODUCTION

1.1. MUSCLE PHYSIOLOGY, METABOLISM AND INFLAMMATION

Skeletal muscle is one of the largest and most metabolically relevant tissues in the body, and its correct function and balance is required for maintenance of health. Skeletal muscle can respond to insulin, as it accounts for 85% of the insulin-mediated glucose uptake and lipid metabolism (F. Li et al., 2016; Peppa, Koliaki, Nikolopoulos, & Raptis, 2010). Remarkably, this tissue can respond to different environmental conditions, such as pollutants, and lifestyle factors (i.e. nutrition and exercise), mounting a specific adaptation mechanism that responds to the metabolic needs of the body. Thus, the importance of skeletal muscle as an endocrine organ has gained notoriety in the past decade (F. Li et al., 2016).

Obesity can regulate the metabolic function of skeletal muscle and thus impair its ability to respond to the metabolic needs of the body. Insulin resistance, a pathology commonly observed in obese patients, is mainly driven by skeletal muscle's inability to respond, possibly through lower IRS-1 content and phosphorylation, or failure to activate PI3K (Peppa et al., 2010; Saltiel & Kahn, 2001). Therefore, metabolic stress and over nutrition impact the ability of muscle to uptake nutrients, which in turn stimulates a sustained stress response that worsens the obese state.

Muscle mass is dynamically regulated by two opposite actors: on one side protein synthesis in an anabolic state allows for nutrient and energy conversion into structural proteins through the Insulin/IGF-1 pathway and mTOR (Mercken, Crosby, et al., 2013), on the other proteolysis through the Ubiquitin proteasome, autophagy (Bowen, Schuler, & Adams, 2015) and activation of cysteine proteases (Teixeira Vde, Filippin, & Xavier, 2012) dictate the amount and specific degradation protein targets that will supply an amino acid pool during catabolic conditions. Recently it has been suggested that even during hypertrophy, a certain degree of degradation of

cytosolic proteins occurs through the ubiquitin proteasomal proteins Atrogin1 and MuRF1(Baehr, Tunzi, & Bodine, 2014). Muscle fibers can increase in size and number through the activation of the adjacent stem cell niche, which contains not only stem cells, but also fibroblasts and immune cells. Satellite cell functions include but are not restricted to maintenance of preexistent muscle fibers, which in response to stress or mechanical strain, form myoblasts that can regenerate lost tissue or stimulate myofiber repair (Garg & Boppart, 2016). Muscle stem cells are able to regulate fiber regeneration and repair through the active expression of myogenic regulatory factors *Myf5* (Myogenic Factor 5) and *MyoD1* (Myogenic Differentiation 1) (Garg & Boppart, 2016), *Mrf4* (Muscle-Specific Regulatory Factor 4), MyoG (Myogenin), *Pax3* and *Pax7* (Paired Box 3 and 7) (Bentzinger, Wang, & Rudnicki, 2012).

The impact of obesity on skeletal muscle is known as sarcopenic obesity, and it entails the impairment of not only metabolic functions, but also the ability of skeletal muscle to regenerate and repair (Bowen et al., 2015). Therefore, it is important to develop strategies that prevent sarcopenia in obese patients.

1.2. HIGH FAT DIET EFFECT ON SKELETAL MUSCLE

Skeletal muscle can adapt to different nutritional and environmental queues. In an obese state, those queues prompt muscle to induce changes in energy expenditure and fat accumulation, leading to the development of insulin resistance. Insulin resistance in skeletal muscle has often been observed with increased circulating fatty acids and triglycerides, as well as the intra- and intercellular deposition of fat intermediates, together with the marked reduction in fatty acid oxidation (Latouche et al., 2014; Turcotte & Fisher, 2008). Moreover, maternal high fat diet has been shown to prime muscle mitochondrial catalytic activity in the offspring (S. M. Kwon, Park, Jun, & Lee, 2014; Pileggi, Hedges, et al., 2016), resulting in atrophy and inflammation, resulting

in fetal wasting (Pileggi, Segovia, et al., 2016). Acute exposure to a high-fat and high-sucrose diet alters muscle integrity and promotes inflammation (Collins et al., 2016), and high fat diet alone induces muscle inflammation and endoplasmic reticulum stress (Dai et al., 2016)

Myokines, or muscle-specific cytokines, are inflammatory mediators capable of regulating both muscle hypertrophy and wasting. Recently the role of proinflammatory cytokines TNFα and the novel TNF superfamily member, TNF-Related Weak Inducer of Apoptosis (TWEAK), have been implicated in muscle wasting and cachexia, given their strong contribution to degradation and myogenesis (Yadava et al., 2015). TNF or cachexin is known to induce muscle breakdown (Bach et al., 2013), and its inhibition is known to increase muscle strength (Subramaniam et al., 2015). Downstream targets of TNF include apoptosis mediator Caspase-8 and the transcription factor NF-κB, which activates proteasomal degradation (MuRF-1), while inhibiting proliferation of muscle fibers (MYOD1) (J. Zhou, Liu, Liang, Li, & Song, 2016). In turn, the role of TWEAK on muscle degradation/regeneration is less clear; Low intracellular concentration can inhibit myogenesis through the activation of NIK/IKKα, whereas high concentrations of TWEAK activate the canonical IKKβ that inhibits differentiation (Enwere et al., 2012). Therefore, the regulation of both TNF and TWEAK is vital for the regulation of muscle mass accretion and metabolism.

1.3. CALORIC RESTRICTION AND MUSCLE NUTRIENT SENSING AND INFLAMMATION

Caloric restriction (CR), without malnutrition, is considered an effective dietary intervention to extend lifespan and quality of life in different organisms (Fontana & Partridge, 2015). The reduction of calories by 25% (Weindruch, Walford, Fligiel, & Guthrie, 1986) is thought to act through energy sensing mechanisms which allow the cell to adapt to the energy restricted state without causing significant strain. Caloric restriction is known to impact the growth and

development of tissues. Studies on old human skeletal muscle have demonstrated the effects CR, restoring the phenotype similarly to that of a young muscle (Mercken, Crosby, et al., 2013). Thus, during prolonged caloric restriction, muscle hypertrophy is spared and in turn the low synthetic rate is efficiently used to perform basic processes. As a dietary intervention to prevent aging, CR is able to stimulate hematopoietic stem cells (Ertl, Chen, Astle, Duffy, & Harrison, 2008) and satellite cells (Cerletti, Jang, Finley, Haigis, & Wagers, 2012). Stimulation of satellite cells by CR appears to be sufficient to initiate new fiber formation and muscle repair in a stem cell transplantation mouse model (Cerletti et al., 2012). The activation of satellite cells from their quiescent state will ultimately lead to proliferation and differentiation into mature myocytes (Buckingham & Rigby, 2014). Chronic caloric restriction (CR) is known to impact the dynamic balance of protein recycling. CR can induce systems that sense amino acid input as well as the ones implicated in the replenishment of the amino acid pool, thus improving muscle health of aged muscles (Mercken, Crosby, et al., 2013). In muscle, chronic CR induces a differential expression of heat shock proteins and associated transcription factors, as well as autophagic mediators that indicate enhanced protein quality assessment (L. Yang et al., 2016a). Under normal conditions, protein anabolism and catabolism can be regulated by different hormonal or inflammatory pathways, with inflammation being the major contributor in metabolic diseases (Hotamisligil, 2006; Hotamisligil & Davis, 2016). Therefore, the reduction of inflammation could prevent skeletal muscle wasting and improve metabolic function.

Aside from weight loss, physiological effects of chronic CR include the reduction of systemic inflammation, as observed in different animal models (Mercken, Crosby, et al., 2013; Robertson & Mitchell, 2013; L. Yang et al., 2016a) and human subjects (Mercken, Crosby, et al., 2013; H. Wang & Ye, 2015; L. Yang et al., 2016a), thus conferring beneficial effects to muscle

metabolism. While CR is a potent inhibitor of inflammation (Fontana, 2009; Holloszy & Fontana, 2007), no information is available regarding the effect of chronic CR on muscle TNFα and TWEAK signaling. The TNF superfamily are a canonical type of inflammatory cytokines that are able to regulate intracellular signaling in different tissues, and whose function is related to insulin resistance (Hotamisligil, 2006), tissue inflammation and cell death (Ting & Bertrand, 2016). The canonical inflammatory marker TNF is able to down-regulate muscle hypertrophy and induce wasting (J. Zhou et al., 2016), however the epigenetic mechanisms elicited by CR that act on *Tnf* gene regulation remain largely unknown.

Caloric restriction and other weight loss protocols have proven to be effective at altering the methylation pattern of several inflammatory cytokines, especially TNF (Phillips & Leeuwenburgh, 2005). Studies assessing weight loss through a low calorie diet or Roux-en Y gastric bypass in overweight and obese patients, have found an altered promoter methylation pattern of the TNF gene in whole blood (Campion, Milagro, Goyenechea, & Martinez, 2009; Kirchner et al., 2014), subcutaneous adipose tissue (Cordero et al., 2011).

1.4. EPIGENETIC REGULATION OF INFLAMMATION

Tnf gene transcription is known to be regulated by epigenetic mechanisms such as DNA methylation and histone modifications. Studies using immune cells constitute the larger body of evidence that demonstrate the regulation of the TNF gene (Falvo, Jasenosky, Kruidenier, & Goldfeld, 2013). Regarding histone modifications (Fig. 1.1.), TNF regulation by LPS is thought to act downstream of the promoter by increasing H3S10 phosphorylation independent of NF-κB (Thorne, Ouboussad, & Lefevre, 2012). Moreover, H3S10p displaces HP1 from the chromatin (Fischle et al., 2005), thus creating a conformational change towards a euchromatic landscape. Activating histone modifications include those mediated by histone deacetylase CBP/p300

(Barthel & Goldfeld, 2003; Falvo et al., 2013), ATF2 (Kawasaki et al., 2000), CRE, PCAF and GCN5 (Ranjbar, Rajsbaum, & Goldfeld, 2006), as well as histone deacetylases HDAC1 and HDAC3 (Falvo et al., 2013) within the proximal promoter of TNF. This new landscape could facilitate the binding of transcription factors or insulators such as CCCTC-binding factor (CTCF) and others that can stabilize long-range interactions, as seen in the TNF/LT locus for the mRNA transcription (Tsytsykova et al., 2007). Likewise, other histone marks that are able to activate TNF are H3K4me1, H3K4me2, and H3K4me3 in stimulated cells (Sullivan et al., 2007), as well as H3K4me3 an H3Ac in unstimulated cells (Hargreaves, Horng, & Medzhitov, 2009) within the promoter. Following histone changes, the binding of the transcription machinery is observed in unstimulated cells (RNA Pol II, TBP, and CBP/p300) (Hargreaves et al., 2009), as well as poised state chromatin changes such as H3Ac and H4Ac (Garrett, Dietzmann-Maurer, Song, & Sullivan, 2008). Interestingly, most regulatory epigenetic mechanisms known for TNF are known to be tissue and stimulus specific (Fig. 1.1.). Although the TNF locus has been extensively characterized in immune cells, little is known about it regulation in skeletal muscle.

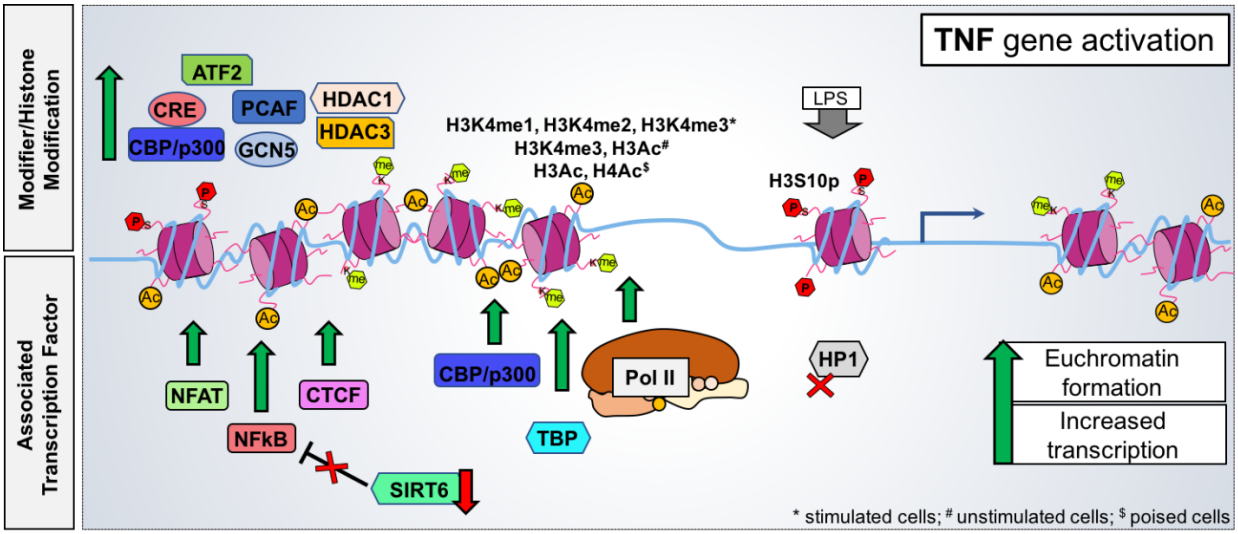

Figure 1.1. Summary of Histone modifications and Transcription factors that regulate TNF gene expression in immune cells. Top half of the diagram depicts modifiers (colored boxes) and corresponding modifications (letters without outline) onto the histones, as well as the relative location within the TNF

Figure 1.1. (cont.) promoter. Bottom half of the diagram shows the transcription factors involved in the regulation of gene transcription.

Epigenetic regulation occurs through covalent modifications exerted by a myriad of chromatin and DNA modifiers. As previously discussed, epigenetic modifiers such as HDAC3 are known to regulate the expression of the TNF gene; however, other modifiers are known to act within proximal or distal regions to modulate its expression. A novel NAD+-dependent deacetylase, SIRT6, has emerged as a possible candidate that extends lifespan (Kanfi et al., 2012; Michishita et al., 2008) and inhibits the activity of NF-kB in different cellular models (N. Zhang et al., 2016). Interestingly, no information is available regarding the modulation of cytokine signaling in muscle during CR, less so on the regulation of TNF by the epigenetic modifiers *SIRT6*. The Histone-Lysine N-Methyltransferase, suppression of variegation 3-9 homolog 1 (SUV39H1), has been regarded as an important regulator of inflammation, where silencing of SUV39H1 in vascular smooth muscle cells produces the upregulation of inflammatory genes (T. T. Chen et al., 2017; Villeneuve et al., 2008). Similarly, the Polycomb group protein Enhancer of Zeste Homolog 2 (EZH2), is silenced in hepatocytes from animals with NAFLD and causes the upregulation of inflammatory genes (*Tnf* and *Tgf-β*), and pharmacological silencing of *Ezh2* generates enhanced fat accumulation and inflammation (Vella et al., 2013). Interestingly, TNF itself can interact with Ezh2 (within the PRC2), to produce the silencing of the myogenic transcription factor Pax7 that stimulates satellite cell differentiation (Palacios et al., 2010). Moreover, aside from its important role in cell development and differentiation (J. E. Lee et al., 2013), Lysine N-methyltransferase 2b (Kmt2b) is able to methylate H3K4 at the promoter of inflammatory marker IL-20 (Su, Lin, Tzeng, Hsieh, & Hsu, 2016), and when interacting with the lysine demethylase KDM6A (KDM6A-KMT2B complex) induces the full action of the enhancer of IFN-β, an acute response inflammatory cytokine (X. Li et al., 2017). Finally, both DNA methyltransferases, Dnmt1 and

Dnmt3a, are known to impact inflammation and specifically TNF production upon stimulation with different stimuli (Cheng et al., 2014; Falvo, Tsytsykova, & Goldfeld, 2010; J. Yu et al., 2016).

CHAPTER 2: SIGNIFICANCE

The dissection of nutrient-sensing epigenetic mechanisms that respond to caloric restriction and prevent inflammation in peripheral tissues remain poorly understood. Therefore, the study of conserved epigenetic mechanisms will help us understand the signals that participate in cytokine repression. In particular, *Tnf* as a major myokine, regulates myogenesis and metabolic processes, but the epigenetic silencing that occurs during calorie limitation remains unknown (Fig. 2.1.).

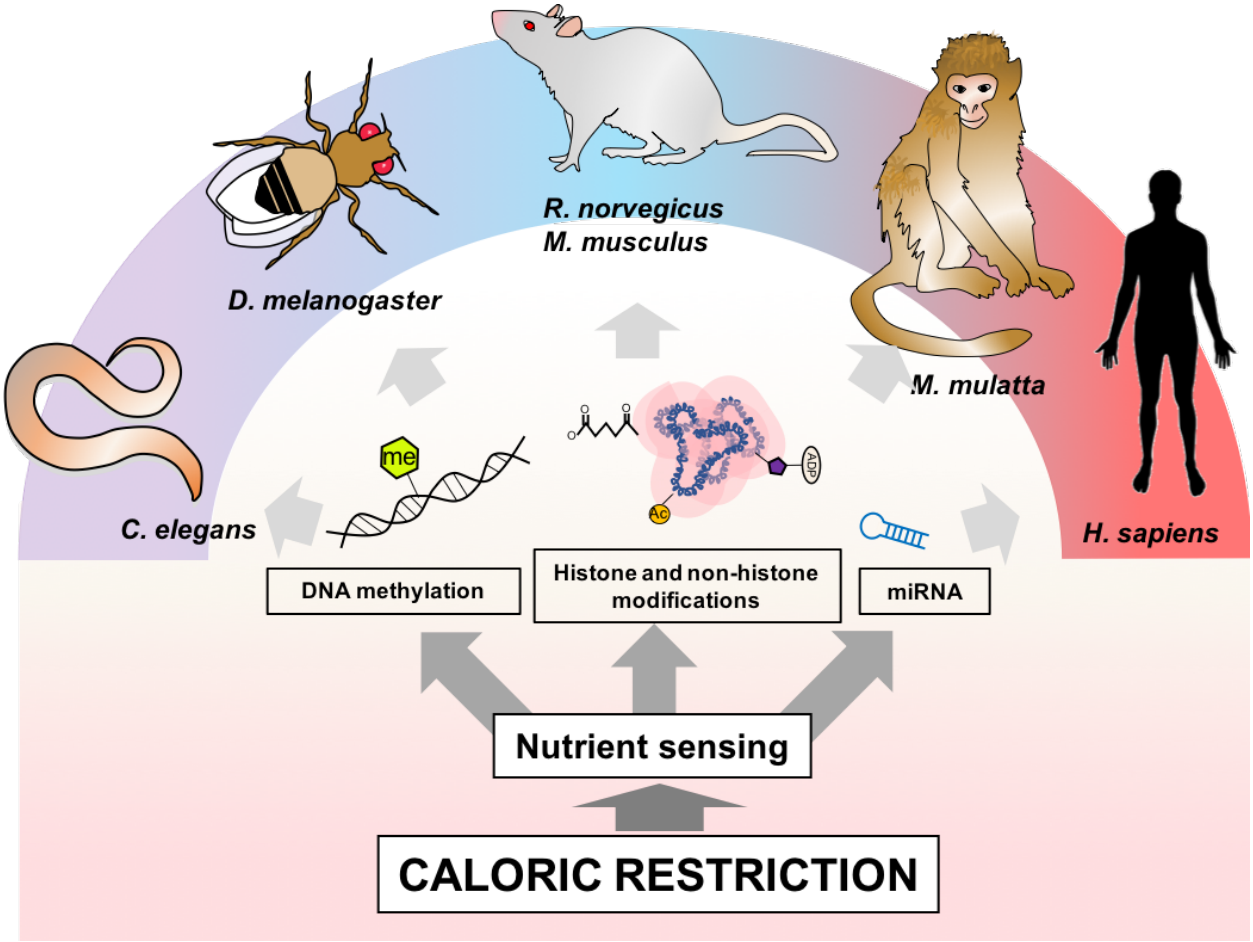

Figure 2.1. Summary of the effects of chronic caloric restriction on nutrient sensing and long-lasting epigenetic effects across different species.

CHAPTER 3: EPIGENETIC REGULATION OF NUTRIENT SENSING AND IMMUNE-METABOLISM BY CALORIE RESTRICTION

3.1. ABSTRACT

Chronic caloric restriction (CR) without malnutrition is known to impact different cellular processes such as stem cell function, nutrient sensing, cell senescence, inflammation and metabolism. In spite of the differences in CR implementation, the reduction of calories produces a widespread beneficial effect in non-communicable chronic diseases, which can be explained by improvements in immuno-metabolic adaptation. Cellular adaptation that occur in response to dietary patterns can be explained by alterations in epigenetic mechanisms such as DNA methylation, histone modifications, and microRNA (miRNA). In this review, we define these modifications and systematically summarized the current evidence related to CR and the epigenome. We then explain the significance of genome-wide epigenetic modifications in the context of disease development. Although substantial evidence exists for the widespread effect of CR on longevity, no consensus exists epigenetic regulation of the underlying cellular mechanisms that lead to improved health. We provide compelling evidence of the long-lasting epigenetic effect of CR on genes related to immuno-metabolic processes. Epigenetic reprogramming of nutrient-sensing pathways by CR can lead to immuno-metabolic adaptations that will enhance quality of life, extend life and delay chronic disease onset.

3.2. INTRODUCTION

Caloric restriction (CR) without malnutrition is constitutes a safe and effective way to promote weight loss, decrease metabolic complications, increase lifespan, and improve quality of life. Caloric restriction refers to a reduction in the intake of net calories, with no limitation in specific macronutrients, while meeting the necessary micronutrient requirements. Caloric intake can be restricted to an individual through a variety of ways: percent CR, macronutrient limitation, or exercise-induced restriction. Restriction percentage of total calories span from mild (15% energy restriction) to a severe restriction of calories (60% restriction), and can be achieved in a variety of way, either with calorie or amount of food provided (Anton et al., 2009; Civitarese et al., 2007; Heilbronn & Ravussin, 2003; Parra, Gonzalez, Martinez, Labayen, & Diez, 2003), or with supplementation of physical activity (Anton et al., 2009; Civitarese et al., 2007; Lefevre et al., 2009). Other alternatives for calorie restriction have proposed changes in the proportion of macronutrients, such as hyperproteic vs. hypoproteic diets (Larsen et al., 2010), or ketogenic diets with a high lipid, low carbohydrate content (Goday et al., 2016; Lv, Zhu, Wang, Wang, & Guan, 2014; Rogovik & Goldman, 2010). In animal studies, CR can also be achieved by increasing the litter size or access to food, and while this approach provides a natural method of energy limitation, often the amount of food cannot be measured (Branquinho et al., 2017; N. Li et al., 2016).

Different dietary approaches have been used to treat and prevent chronic disease development, among which chronic CR has provided widespread beneficial effects. In obese patients, CR is able to provide additional health benefits to weight loss, such as decreasing visceral adipose tissue(Verheggen et al., 2016) and inflammation (Meydani et al., 2016) while improving kidney function (Giordani et al., 2014; Ruggenenti et al., 2017), and cellular quality control (L. Yang et al., 2016a). Moreover, such effects have also been documented for type 2 diabetic animals

(Kanda et al., 2015) and patients (Bhatt et al., 2017; Ghalandari, Kamalpour, Alimadadi, & Nasrollahzadeh, 2018; C. Li et al., 2017; Oshakbayev et al., 2017; Urbanova et al., 2017), where insulin sensitivity is improved. Additionally, 12-week CR treatment (30% restriction) reduced the circulating levels of the risk marker fetuin-A, improved blood pressure in patients and hepatic steatosis in rats (K. M. Choi et al., 2013). Lastly in cancer patients, CR or fasting can effectively prevent malignancies through a variety of cellular responses and can improve the efficacy of therapeutic agents (Brandhorst & Longo, 2016). Different forms of CR are able to reduce progression of cancer types with the highest morbidity rates, including colorectal, pancreas, breast, liver, prostate, esophagus, and kidney malignancies. In monkeys from the Wisconsin National Primate Research Center (WNPRC), 30% lifelong restriction was sufficient to cause a 50% decrease in neoplasic events, gastrointestinal adenocarcinoma being the most common (Simpson, Le Couteur, Raubenheimer, et al., 2017). Similarly, young-onset CR (30% restriction) improved the incidence of cancer in monkeys from the National Institute on Aging (NIA), despite the great genetic differences with the WNPRC monkeys.

3.2.1. Nutrient Sensing and Protein Quality Control

The way cellular energetics are partitioned in the cell is the result of active and passive mechanisms that respond to the needs of the cell and the tissue it resides in. Depending on the energy availability and requirements, the cell must decide whether to expend or to save energy, this in turn will guarantee its long-term survival. During the feeding period, the cell is exposed to a rapid surge of nutrients that must be utilized or stored for times for times of scarcity; however, during the fasting period, it must be resourceful and effectively communicate its needs to produce adequate amounts of nutrients and energy. In this section, we will try to define what is known about the nutrient

sensing mechanisms during fasting periods, as they closely mimic the conditions during times of starvation and chronic CR.

Macronutrient sensing and energy sensing pathways are highly conserved among different species and are used to adapt to limited nutrient availability. Lipid sensing pathways encompass fatty acid and cholesterol/sterol recognition, which are released from energy stores during starvation and CR. Fatty acid sensing is enabled by membrane-bound and intracellular receptors that are able to bind fatty acids within their ligand binding domains, thus activating signal transduction or activate transcription of target genes. Among the fatty acid sensors, there are membrane bound receptors such as Fatty acid transporter proteins (FATPs, SLC27A1-6)(Kazantzis & Stahl, 2012; Luiken, Miskovic, Arumugam, Glatz, & Bonen, 2001) (Gimeno, 2007), G-protein coupled receptors (FFARs) (Nakamura, Yudell, & Loor, 2014), and co-receptors (CD36)(Hotamisligil & Bernlohr, 2015; Nakamura et al., 2014), as well as intracellular binding proteins (FABPs)(Hotamisligil & Bernlohr, 2015; Syamsunarno et al., 2013), and intracellular receptors with transcriptional activity (PPARs, HNF4, RXR/LXP, etc.) (Nakamura et al., 2014), altogether will sense the extra- and intracellular compartments and activate fasting-specific signaling pathways. During CR, adipose tissue synthesizes a greater amount of fatty acids (Bruss, Khambatta, Ruby, Aggarwal, & Hellerstein, 2010) and decreases serum long-chain saturated fatty acids (Hardy, Meckling-Gill, Williford, Desmond, & Wei, 2002), the former will be in turn oxidized to meet the energy requirements (Bruss et al., 2010). Fatty acid uptake appears to be decreased in myocardiac tissue following CR, with the concomitant reduction of myocardial mass and cardiac work (Viljanen et al., 2009). Regarding lipid trafficking, FABP4 and 5 share immunometabolic functions, and whole-body depletion protects against high-fat diet consumption, steatosis, and improves insulin sensitivity (Hotamisligil & Bernlohr, 2015; Maeda et al., 2005).

Short term CR (40% restriction) decreases circulating FABP4, possibly originated from non-adipose tissues, as CR does not affect subcutaneous adipose expression, but increased adipose FABP5 expression (Charles et al., 2017). Additionally, deletion of FABP4/5 recapitulates the lipidomic changes seen in CR, but without lifespan extension, which suggests that CR improves metabolic health by fine tuning lipid trafficking proteins. Although evidence exists for the effect of short term fasting on fatty acid receptors, limited data is available on the long-term adaptation of FATPs, FFARs, and FABPs during chronic CR.

PPARs appear to be vital for metabolic adaptation to short- and long-term fasting, this is evidenced by knockout experiments with PPARα mice, which display hypoglycemia, impaired ketosis, increased steatosis, impaired lipolysis, hypothermic, leading to death within 24hrs (Hashimoto et al., 2000; Kersten et al., 1999; Le May et al., 2000; G. Y. Lee, Kim, Zhao, Cha, & Kim, 2004; S. S. Lee et al., 2004; Leone, Weinheimer, & Kelly, 1999; Nakamura et al., 2014). Moreover, the effects of CR in the liver appear to be solely dependent on PPARα, given that 30% CR activates its transcription and translation, while PPARγ remains unchanged and PPARβ/δ decreases (Masternak et al., 2004; Masternak et al., 2005), which is responsible for the adaptive response to prolonged food restriction while preventing hypoglycemia (Kersten et al., 1999; Leone et al., 1999). In skeletal muscle, the expression of PPARs appears to be reduced (Masternak et al., 2005), perhaps to allow for protein recycling and fiber maintenance, whereas in cardiac muscle and adipose tissue the expression of PPARs remains unchanged by CR (Jones et al., 2005; Masternak & Bartke, 2007; Y. X. Wang et al., 2003; Z. Wang, Al-Regaiey, Masternak, & Bartke, 2006). Lastly, Peroxisome proliferator-activated receptor gamma coactivator 1α (PGC-1α), a well-known and extensively studied coactivator is responsible for the short- and long-term adaptations to fasting and CR in some metabolic tissues (R. Anderson & Prolla, 2009). As

discussed later, CR is able to stimulate SIRT1 activation in different tissues, thus stimulating the deacetylation of PGC-1α and in turn contributes to mitochondrial biogenesis and function (Fernandez-Marcos & Auwerx, 2011; Guarente, 2006). Nevertheless, skeletal muscle PGC-1α activation is dispensable for the CR-induced whole-body adaptations (Finley et al., 2012), hence highlighting the redundant and robust response following CR.

Regarding amino acid sensing, the mechanistic Target of rapamycin complex 1 (mTORC1) pathway is the master regulator of cell growth and is known to be modulated in response to growth factors, cell stress, energy and amino acids supply. mTORC1 is at the crossroad of catabolism and anabolism, as it modulates both mRNA translation into proteins and protein recycling through autophagy. Both the vacuolar H^+-Adenosine triphosphatase ATPase (V-ATPase) that interacts with the Ragulator and the Sodium-coupled neutral amino acid transporter 9 (SLC38A9) sense lysosomal amino acid signals and stimulate in turn the lysosome-residing complexes Rheb and Rag GTPases, leading to their interaction and activation of mTORC1 complex (Wolfson & Sabatini, 2017). In the cytosol, the presence of amino acids such as leucine and arginine can prevent the inhibitory actions of Sestrin2, CASTOR1, and GATOR1, thus promoting enhancement of the mTORC1 complex, leading to mRNA translation activation (Wolfson & Sabatini, 2017). These amino acid sensing mechanisms appear to be conserved in nematodes (*C. elegans*), flies (*D. melanogaster*), mice (*M. musculus*), and humans (*H. sapiens*) (Chantranupong, Wolfson, & Sabatini, 2015; Wolfson & Sabatini, 2017), which highlights the great degree of specialization of amino acid sensing through evolution. Theories surrounding the aging process have pointed out that activation of nutrient-sensing mTORC1 leads to cell senescence and age-related disease development, and that CR is capable of preventing age-related decline, at least in part, by slowing down the activity of the mTORC1 pathway (Blagosklonny, 2010). During CR, energy and nutrient

availability are scarce and the mTORC1 complex is inhibited, giving rise to the activation of other nutrient sensors such as SIRT1; both processes cannot occur in the same cell as they are activated by opposing signals. Interestingly, in the intestine of CR mice, both SIRT1 and mTORC1 appear to cooperate to promote the self-renewal of the adult stem cell pool (Igarashi & Guarente, 2016). Briefly, anti-microbial peptide secreting Paneth cells produce cyclic ADP-ribose promotes SIRT1-mediated deacetylation of S6K1 in neighboring intestinal stem cells (ISCs), this in turn facilitates its phosphorylation by the mTORC1 complex within ISCs, leading to mTORC1-directed cell division and SIRT1-mediated self-renewal (Igarashi & Guarente, 2016). Extension of lifespan and health span by CR appear to be intricately related to mTORC1 inhibition, as low protein diets seem to have more robust effects (Cummings & Lamming, 2017; Lamming et al., 2015; Solon-Biet et al., 2014). Whether directly mediated though mTORC1 inactivation or downstream effector molecules, CR nutrient-sensing adaptations are vital for the survival and function of the cell.

Protein quality assessment must be conducted within the cell in order to guarantee the safeguarding of the cell's functions. During times of starvation or energy deprivation (CR), the cell initiates a recycling process in an effort to ensure that the nutrient pool is used effectively, such recycling processes include cysteine proteases, autophagy, and proteasomal degradation. While autophagy is regarded as a non-specific, widespread protein turnover event, degradation through the ubiquitin-proteasome pathway utilizes E3-ligase enzymes to tag specific protein targets, thus ensuing protein turnover (Bento et al., 2016). Consumption of high-fat, calorically dense diets decreases autophagy (van Niekerk, du Toit, Loos, & Engelbrecht, 2018) as well as degradation of ubiquitinated proteins (Otoda et al., 2013), leading to the cellular stress and insulin resistance. Remarkably, CR is able to significantly activate protein turnover by increasing autophagy to promote muscle quality control in humans (L. Yang et al., 2016a) and prevent

sarcopenia (Fan et al., 2016). Likewise, CR with resveratrol supplementation has been found to be protective against oxidative stressor doxorubicin, which promotes cardioprotection by inducing autophagy in aged rats (Dutta, Xu, Dirain, & Leeuwenburgh, 2014). Moreover, similar strategies to CR such as intermittent fasting or alternate-day CR (ADCR) are able to elicit protein quality control (autophagy and proteasome) in the context of peripheral nerve damage (S. Lee & Notterpek, 2013). Therefore, CR-based strategies should be able to stimulate protein quality control and cell renewal, both hallmarks of CR-mediated lifespan and health span extension.

CR-based strategies that are able to increase patient compliance, while conferring all the benefits associated with CR remain a poorly studied area of CR research. Alternate-day or intermittent CR (ADCR) has demonstrated, despite the limited literature, to be as effective as chronic CR protocols and maximizes the amenability of the restriction protocols in a clinical setting. ADCR has a potent and robust effects on a variety of animal and human experiments: it's capable of ameliorating inflammation due to sepsis (Hasegawa et al., 2012), decrease hepatic inflammation in obese mice (W. Yang, M. Cao, et al., 2016), decrease oxidative stress and inflammation in obese, asthmatic subjects (Johnson et al., 2007), increase fat-free mass and decrease leptin secretion in overweight and obese individuals (Trepanowski et al., 2017), etc. Furthermore, a meta-analysis identified this form of restriction to be effective and possibly superior to CR given the improvement of patient compliance, while increasing the lean-to-fat mass ratio (Alhamdan et al., 2016). In the coming years, research that focuses on the comparison of CR vs. ADCR will determine the great benefit of such modified strategies on health- and lifespan extension.

Overall, chronic CR has been demonstrated to be an effective dietary intervention for the treatment of many non-communicable chronic diseases. Given the impact that CR has on the

prevention, development, and treatment of chronic diseases, we sought to review three epigenetic mechanisms that might be related to the long-term programming of cellular functions. Epigenetic mechanisms are at the forefront of cellular changes that can be modulated by CR, which can lead to long-lasting cellular adaptations and improved health outcomes. In our review, we will provide an overview of different epigenetic mechanism that can be targeted (DNA methylation, histone modifications, and miRNAs). We will then explore the effect of CR and fasting patterns on such mechanisms. Lastly, we will delineate the epigenetic regulation of immunometabolic processes that leads to improvements for many non-communicable chronic diseases.

3.3. CALORIC RESTRICTION AND DNA METHYLATION

3.3.1. Dynamic regulation of DNA Methylation

DNA methylation or the modification of a cytosine nucleotide to 5-methyl cytosine (5mC) is an epigenetic process intricately associated with the regulation of gene expression. DNA methylation has been associated with the control of gene expression at all stages of development, genomic imprinting and X-chromosome inactivation (Jurkowska, Jurkowski, & Jeltsch, 2011; Klose & Bird, 2006). DNA methyltransferases (DNMTs) are the proteins involved in de novo and maintenance methylation state of cytosine residues. This protein family has been studied extensively, from its physiology and biochemistry, to its evolution and pervasiveness across species (Jurkowska et al., 2011; Zemach, McDaniel, Silva, & Zilberman, 2010). Broadly, DNMT1, DNMT3A and 3B, are the enzymes in charge of regulating the addition of a methyl group to the cytosines, yet they carry out specific functions during development and adaptation to the environment. For instance, DNMT1 is responsible for the establishment of methylation patterns that define different tissues, whereas DNMT3A and 3B oversee the dynamic turnover of novel methylation marks, or *de novo* methylation. Other DNMTs include DNMT2, which is involved in

the methylation of tRNA (methylation of aspartic acid transfer RNA onto the cytosine-38 residue in the anticodon loop), and DNMT3L, which activates DNMT3A and 3B. Transcriptionally related DNMTs are required for the silencing and transcription of target genes.

The mechanisms and enzymes involved in the process of DNA demethylation are poorly understood. In eukaryotes, the recently described Ten Eleven Translocation (TET) family of proteins has been found to play an important role on DNA demethylation (Kinney et al., 2011). The TET family of proteins consists of TET1, TET2 and TET3; and genomic analysis across species has found them to be conserved across vertebrates. Structural analysis of TETs reveals a catalytic domain similar to an 2-oxoglutarate oxygenase (Loenarz & Schofield, 2009). TET1 has a Zn-chelating domain, CXXC region and a nuclear localization signal that is missing from both TET2 and TET3 (Kinney et al., 2011). Nevertheless, the whole protein family shares a DNA sequence homology of 70% and a double-stranded B-helix (DSBH), which has been proposed as being sufficient and necessary for the catalytic activity. Various isoforms have been described, but many of them appear to be missing the DBSH and iron binding sites. The proposed mechanism for DNA demethylation involves TET-mediated oxidation, starting with the conversion of 5mC to 5-hydroxymethyl cytosine (5hmC), followed by oxidation to 5-formyl cytosine (5fC), and finally to 5-carboxyl cytosine (5caC) (Wu & Zhang, 2011). Both 5caC and/or 5fC DNA residues can be recognized by other proteins that will restore the nucleotide to the demethylated cytosine (R. M. Kohli & Zhang, 2013).

Zemach et al. (Zemach et al., 2010) proposed that the process of gene methylation originated before the divergence of plants and animals and that both groups use DNA methylation to repress transposable elements. Additionally, the phylogenetic analysis of DNMTs found that eukaryotic DNMTs are most likely to descend from prokaryotic DNMTs, and not from RNA

methyltransferases as it was previously thought (Jurkowska et al., 2011). This indicates a conserved, yet divergent mechanism for DNA methylation across domains of life. On the other hand, TET proteins in fungi have been evolutionarily associated with transposons, which could explain the lineage specific expansion or loss in various eukaryotes (Iyer et al., 2014).

3.3.2. Early-Onset Caloric restriction and DNA Methylation

CR has been found to impact the methylation pattern of certain genes, and thus alter biological processes such as metabolism, oxidative stress, senescence, and aging (Maegawa et al., 2017; Mendelsohn & Larrick, 2017; Unnikrishnan et al., 2017) (Fig. 3.1). Specific macronutrient limitation, or CR without accounting for malnutrition, can have deleterious effects. A form of dietary restriction by limiting protein (not CR) to pregnant rat dams was found to induce transcriptional changes across 3 subsequent generations (F1 through F3), and the changes observed in fasting glucose could be explained by alterations in the methylation pattern of gluconeogenic enzyme phosphoenol pyruvate carboxykinase (PEPCK) (Hoile, Lillycrop, Thomas, Hanson, & Burdge, 2011). Transgenerational changes induced by protein restriction alone do not seem consistent between generations, but accumulation of genetic alterations might be conducive to a hyperglycemic state. Low birth weight (LBW) is a predictor of suboptimal outcomes in humans and non-human primates, having altered expression and methylation of the inflammatory marker CXCL14 in cord blood, which is thought to be responsible for the metabolic abnormalities (Cheong et al., 2014). Late-gestation CR has been observed to alter global placental DNA methylation (P. Y. Chen et al., 2013), specifically of the glucose transporter GLUT-3 and decrease its expression through a mechanism involving the binding of Methyl-CpG Binding Protein 2 (MeCP2) in mice (Ganguly, Chen, Shin, & Devaskar, 2014). This in turn limits the supply of nutrients and specifically glucose to the fetus. In utero undernutrition (50% calories) produced

significant changes in the methylation pattern of adult sperm, having that lower methylation (hypomethylation) in differentially methylated regions (DMR, compared to control) are low in coding and repetitive regions and hypomethylation was found in intergenic regions and CpG islands in mice(Radford et al., 2014). Although methylation patterns were not consistent between generations, accumulation of the effects related to differential epigenome alterations at early developmental stages could lead to long-lasting alterations in chromatin, transcriptional changes, and ultimately affect their differentiation potential or the supramolecular tissue organization (Radford et al., 2014). However, despite the detrimental effects observed in IUGR, LBW populations and CR animals with malnutrition, CR protocols that compensate for malnutrition can combat chronic disease development by shaping the epigenome during early developmental stages. Most importantly, the timing of the restriction onset as well as the diet formulation (Mattison et al., 2017) are the most important factor that can predict the positive outcomes related to CR (Fig. 3.1A).

3.3.3. Late-Onset Caloric Restriction and DNA Methylation

CR without malnutrition in adults appears to provide protection against chronic illness, produces weight loss, and helps prevent the development of metabolic abnormalities (Fig. 3.1B). Comparison of two non-human primate longitudinal CR studies from the National Institute of Aging (NIA) and the Wisconsin National Primate Research Center (WNPRC), revealed differences in CR onset and diet formulation (Mattison et al., 2017). Early CR onset appears to be linked to lower life-expectancy and reduced quality of life, whereas mid- to late-CR onset produced significant health benefits (Mattison et al., 2017) (Fig. 3.1B). Hence, we sought to review the effects of mid- and late-onset CR and diet specifications associated with longevity and better quality of life, with an epigenetic focus. In a clinical population, 8 weeks of CR-induced weight

loss significantly reduced DNA methylation of inflammatory cytokine Tumor Necrosis Factor (*TNF*), and provided a striking biomarker differences for prediction of the degree of weight reduction (Campion et al., 2009). Moreover, similar methylation patterns for TNF and Leptin were observed for obese women who were prescribed an 8-week long low-calorie diet protocol (Cordero et al., 2011), thus lessening the inflammatory burden of obese patients. Other genes that are known to be modified by CR-induced weight loss are ATPase phospholipid transporting 10A (*ATP10A*) and CD 44 molecule (*CD44*) in overweight and obese men (Milagro et al., 2011). Similarly, in overweight and obese postmenopausal women, CR differentially affected the methylation pattern of genomic loci involved in weight control and insulin secretion analyzed in adipose tissue biopsies (Bouchard et al., 2010). Maintenance of weight following weight loss, can alter the methylation pattern similar to that of normal weight individuals, rather than the obese counterparts who did not lose weight (Y. T. Huang et al., 2015).

Interestingly, the weight loss method, CR or bariatric surgery, impact the methylation status in different directions (Nicoletti et al., 2016).

3.3.4. CR-Induced DNA Methylation Changes and Nutrient Sensing

Cellular nutrient sensors represent the first line of detection of a cell and its environment. Nutrient intake is "sensed" by numerous different receptor proteins or "sensors" that are capable of relaying the message to downstream pathways, and it turn, these downstream actors compose a specific adaptive response in accordance to the sensed metabolite. Nutrients, primarily macronutrients are sensed in two different ways, either through the direct binding to the macronutrient (fatty acid, amino acid, carbohydrate), or by indirect detection of the energy levels following anabolism. Nutrient-sensing actors are thus referred to hereafter as nutrient sensors and not energy sensors. Among the nutrient sensors, fatty acids are one of the best characterized molecules that can be

sensed; from membrane receptors such as Free fatty acid receptor 1 (FFAR1), FFAR4, CD36 (Efeyan, Comb, & Sabatini, 2015), and the well-known Peroxisome proliferator activated receptors (PPAR-α,δ,γ) (Contreras, Torres, & Tovar, 2013; Poulsen, Siersbaek, & Mandrup, 2012). In overweight women, energy restriction resulted in reduced coding region methylation (CpG +477) within CD36 (do Amaral, Milagro, Curi, & Martinez, 2014), and a promoter polymorphism of CD36 is associated with differential effect on LDL-c (Goyenechea et al., 2008). Moreover, CR is known to activate FOXO-1 and in turn, FOXO-1 can modulate prime C2C12 muscle cells to rely on fatty acid metabolism by inducing CD36 membrane enrichment (Bastie et al., 2005). However, no information is available regarding the effect of CR on DNA methylation other fatty acid membrane-sensors in animals or humans (FFARs). As for PPARs, limited information exists regarding their direct modulation by CR. As discussed later, activation of SIRT1 by CR leads PGC-1α-mediated enhanced activity of PPARα, but no direct changes in DNA methylation of PPARα have been documented in postnatal- and adult-onset CR. Prenatal protein restriction are able to alter promoter DNA methylation of PPARα in the liver of offspring (Lillycrop et al., 2008), and the methylation status of PPARα appears to be related to NAFLD pathogenesis, which can be ameliorated by DNA methylation inhibitors (5-Aza-2'-deoxycytidine or curcumin) (Ju et al., 2018; Y. Y. Li et al., 2018). Moreover, very long chain fatty acids are positively associated with maternal methylation level of PPARα during pregnancy in serum of 40 mother-infant dyads (Marchlewicz et al., 2016). Similarly, the adipogenic function of pre-adipocytes from obese subjects appears to be epigenetically reprogrammed at PPAR-related pathways (Andersen et al., 2018), which highlights the possible use of CR to prevent lipid and adipogenic reprogramming. PPARγ is regarded as the master regulator of adipogenesis. Effective weight loss strategies such as CR and intermittent fasting (IF) are able to decrease PPARγ

expression in visceral adipose (Yang et al., 2017) and liver (Mulligan, Stewart, & Saupe, 2008). Weight loss induced through roux-en-y gastric bypass (RYGB) decreases the ability of subcutaneous adipose tissue to store lipids, while increasing lipolysis, this by directly targeting the activities of PPARγ/δ (Jahansouz et al., 2018). Both RYGB and CR are able to reduce the adipogenic potential of adipose stromal progenitor cells, but protect these cells from DNA damage and extends their lifespan (Mitterberger, Mattesich, & Zwerschke, 2014), possibly due to the hallmark activation of SIRT1 by CR (Picard et al., 2004). Although promoter hypermethylation of PPARγ is associated with hepatic inflammation and fibrosis in chronic hepatitis B (Zhao et al., 2013), the effect of CR on PPARγ methylation status has not been defined. Altogether, CR appears to affect PPAR activity by directing SIRT1 and PGC-1α, but future research should focus on the DNA demethylation potential of CR on adipogenesis and lipid metabolism.

Other factors that are known to be involved in disease development, particularly non-alcoholic fatty liver disease (NAFLD), are susceptible to DNA methylation changes following bariatric surgery-induced weight loss. NAFLD-specific expression and DNA methylation were partially reversed by bariatric surgery, and it produced a differential methylation pattern within transcription factor binding sites of ZNF274 (zinc finger protein 274), PGC1A (Peroxisome proliferator-activated receptor γ coactivator 1 alpha), SREBF2 (Sterol regulatory element binding factor 2), GRP20 (Glycine-rich protein 20), ZEB1 (Zinc finger E-box binding homeobox 1), and FOXA1 (Forkhead box A1), FOXA2 (Forkhead box A1). Moreover, the epigenetic remodeling effect in liver following bariatric surgery was possibly due to the changes observed in transcription factors NRF1 (nuclear respiratory factor 1), HSF1 (heat shock factor 1), ESRRA (estrogen-related receptor alpha), SRF (serum response factor), TR4 (testicular receptor 4), CEBPZ

(CCAAT/enhancer binding protein zeta), and SREBP1(sterol regulatory element binding protein 1) (Ahrens et al., 2013).

The intricate regulation of energy-sensing sirtuins (SIRTs) will be discussed later; however, their DNA methylation patterns can be modulated by CR. In adipose tissue of obese individuals (BMI>40 kg/m^2), DNA methylation status to the promoter of SIRT1 or 7 was not correlated with the expression, but rather to the miRNAs targeting their degradation (miR-22-3p, miR-34a-5p, miR-181a-3p for SIRT1 and miR-125a-5p, miR-125b-5p with SIRT7), compared to normal-weight individuals (BMI 20-24.9 kg/m^2) (Kurylowicz et al., 2016). SIRT6 promoter DNA methylation can be modified by age in humans. Aging is known to increase SIRT6 promoter DNA methylation from 43.21% at a young age (9-19 years old), to an average methylation of 65.63% in the after 19-years-of-age (20-79 years old) in whole blood (Sahin, Yilmaz, & Gozukirmizi, 2014). Therefore, whether it is through direct activation of gene transcription or indirect enhancement with NAD^+ production, CR facilitates the robust activation of SIRTs.

3.3.5. CR-Induced DNA Methylation Changes and Immunometabolism

In human studies, weight loss via CR has been shown to alter DNA methylation in blood, adipose tissue, and skeletal muscle (Fig. 3.1C). In one study, obese and overweight men were subjected to 30% energy restriction for 8 weeks (Milagro et al., 2011). Greater weight loss was associated with hypermethylation of Wilms tumor 1 (*WT1*) and *ATP10A* in peripheral blood mononuclear cells (PBMCs). In a similar study involving overweight women, an 8-week intervention involving 30% CR resulted in decreased methylation of CD 36 molecule (*CD36*), CD 14 molecule (*CD14*), pyruvate dehydrogenase kinase 4 (*PDK4*) and fatty acid desaturase 1 (*FADS1*) in PBMCs (do Amaral et al., 2014). Examination of subcutaneous adipose tissue from these women revealed no change in DNA methylation within the leptin (*LEP*) promoter (Cordero et al., 2011). Another study

focused on overweight and obese postmenopausal women who underwent a 6-month calorie restriction weight loss program. Subcutaneous adipose tissue was biopsied after an additional 4-week weight stability period. Those participants that had a greater than 3%

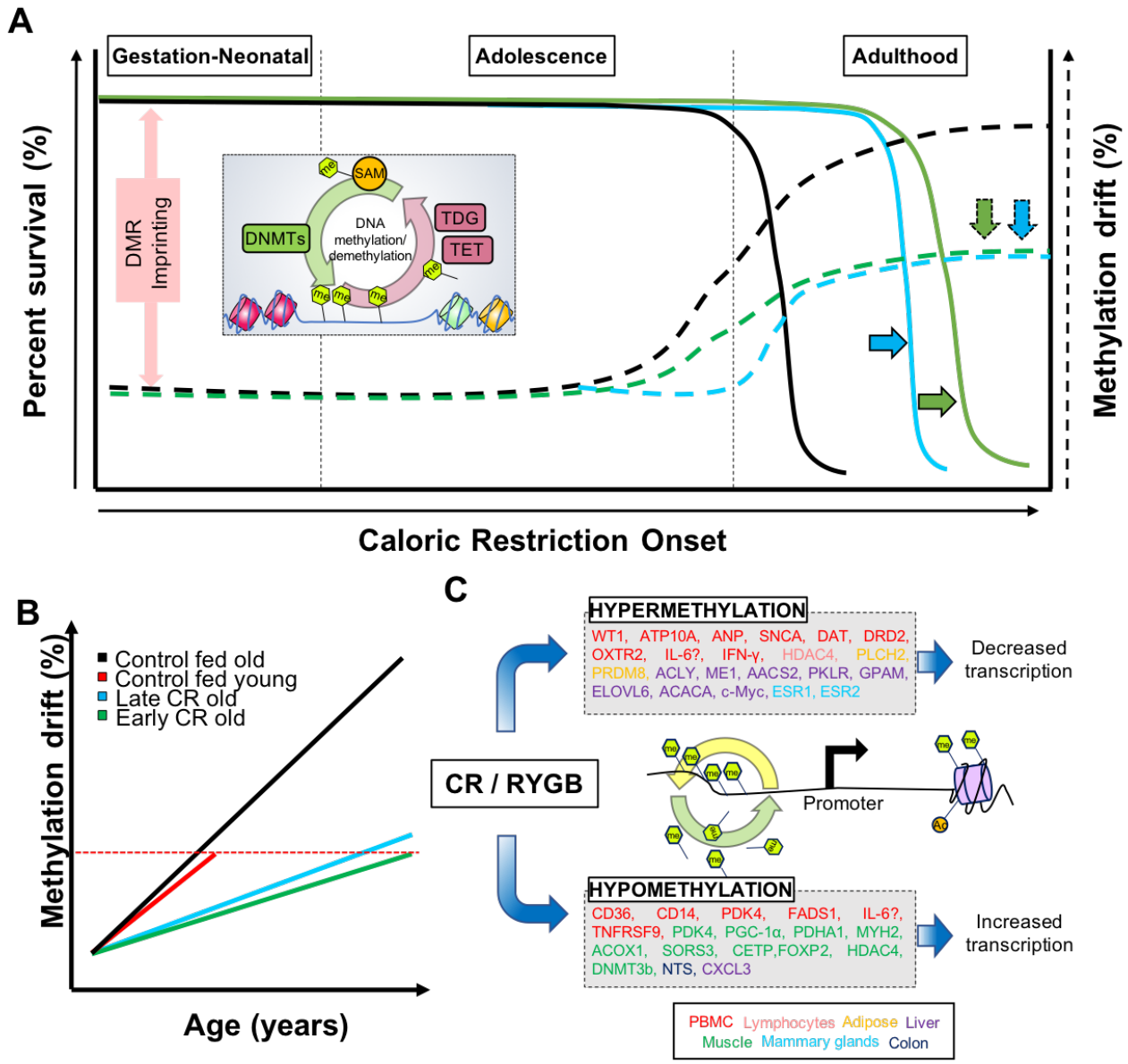

Figure 3.1. Age-related changes in DNA methylation drift and the effect of caloric restriction. A) DNA methylation is a dynamic process that is regulated during development and throughout life. Early life DNA methylation patterns are established through genetic and epigenetic imprinting of differentially methylated regions (DMR). Early- (green solid line) vs. late-onset of CR (blue solid line) are able to extend lifespan with differences in health span. Both early (green dotted line) and late onsets (green dotted line) are able to ameliorate age-related methylation drifts, thus producing significant changes in the B) DNA methylation dysregulation with age. C) Weight loss strategies such as CR and roux en y gastric bypass (RYGB) are able to produce distinct patterns of either hyper- or hypomethylation in many metabolic tissues, compared to their obese counterparts.

reduction in body fat percentage were found to have hypermethylated loci associated with phospholipase C eta 2 (*PLCH2*) and PR/SET domain 8 (*PRDM8*) (Bouchard et al., 2010). Thus, it appears that weight loss strategies, regardless of the form or severity, are able, to some extent, to alter DNA methylation patterns of metabolism- or immune-related genes but a significant variability in the response is expected.

In extreme cases of obesity, bariatric surgery may be used as a weight loss strategy to reduce the capacity of the stomach and reduce food intake, thus providing some form of artificial calorie restriction. One study found that gastric bypass patients had higher methylation of *PDK4* in whole blood at 12 months post-surgery (Kirchner et al., 2014). In skeletal muscle biopsies 6 months after surgery, gastric bypass patients had normalized DNA methylation in 11 metabolic gene promoters, including *PDK4*, PPARG coactivator 1 alpha (*PPARGC1A*), pyruvate dehydrogenase E1 alpha 1 subunit (*PDHA1*), myosin heavy chain 2 (*MYH2*), acyl-CoA oxidase 1 (*ACOX1*), and others (Barres et al., 2013). Another study found reduced methylation in skeletal muscle at 30 CpGs associated with sorbin and SH3 domain containing 3 (*SORBS3*) following Roux-en-Y gastric bypass surgery (Day et al., 2017). In addition to muscle, DNA methylation profiles of omentum and subcutaneous adipose tissue were altered by gastric bypass surgery (Benton et al., 2015). Results found 3,601 differentially methylation CpGs in subcutaneous and 15 in omentum. CpGs were associated with genes involved in obesity and epigenetic regulation, such as cholesteryl ester transfer protein (*CETP)*, forkhead box P2 (*FOXP2)*, histone deacetylase 4 (*HDAC4)*, and DNA methyltrasferase 3B (*DNMT3B)*. Overall, CR resulting from bariatric surgery

is able to mediate DNA methylation of metabolic genes from metabolic tissues such as muscle and adipose tissue in humans.

In addition to weight loss intervention for overweight and obesity, CR is also observed in normal and underweight patients with eating disorders (Fig. 3.1C). Previous literature highlights the role of DNA methylation in endocrine and psychiatric pathways. One study found increased global methylation in lymphocytes of anorexia patients (Booij et al., 2015; Kesselmeier et al., 2018). In particular, 14 hypermethylated probes were associated with genes involved in histone acetylation (*HDAC4*), RNA modification, cholesterol storage and lipid transport, and dopamine and glutamate signaling. In other studies, these findings were not reproduced in whole blood samples, as a global hypomethylation was observed in anorexic patients (Frieling et al., 2007; Tremolizzo et al., 2014); nor were the findings reproduced in saliva samples, as *HDAC4* was hypomethylated in anorexic and bulimic patients (Subramanian, Braun, Han, & Potash, 2018). Other studies have suggested that CR impacts fluid regulation and neuronal function, as hypermethylation of atrial natriuretic peptide (*ANP*) promoter was observed in bulimic patients, while hypermethylation of alpha synuclein (*SNCA*), dopamine transporter (*DAT*), dopamine receptor D2 (*DRD2*), and oxytocin receptor (*OXTR*) was seen in anorexics (Frieling et al., 2008; Frieling et al., 2007; Frieling et al., 2010; Y. R. Kim, Kim, Kim, & Treasure, 2014). Thus, voluntary CR is able to directly modulate DNA methylation to perpetuate the long-term cellular program.

While human studies have primarily focused on CR as a means of weight loss, animal models have examined CR in the context of longevity and cancer. Studies in *Drosophila* found dietary restriction to extend the lifespan without changing methylation patterns (Lian, Gaur 2018), while several others have shown that CR mitigates age-associated DNA methylation in a range of

tissues (Cole et al., 2017; C. H. Kim et al., 2016; Maegawa et al., 2017; T. Wang et al., 2017). In WI-38 lung fibroblasts, glucose restriction extended the lifespan and downregulated p16 gene expression (Y. Y. Li, Liu, & Tollefsbol, 2010). Such effect might be due to elevated DNMT activity and hypermethylation of the promoter of p16 in the restricted cells. A study in mice used 60% energy restriction starting at 12 weeks of age and examined genome-wide methylation in the liver (Hahn et al., 2017). Not only did restricted animals have longer lifespans, but dietary restriction was also shown to ameliorate age-related hepatic DNA methylation changes. Additional analysis revealed hypermethylation of gene bodies. CR-induced methylation was enriched for fatty acid, triglyceride, and ketone body metabolism related genes, including ATP-citrate lyase (*Acly*), Malic enzyme 1 (*Me1*), acetoacetyl-CoA synthetase (*Aacs2*), pyruvate kinase (*Pklr*), glycerol-3-phosphate acyltransferase (*Gpam*), fatty acid elongase 6 (*Elovl6*), and acetyl-CoA carboxylase 1 (*Acaca*). In addition to metabolic pathways, CR also impacts hepatic methylation of proto-oncogene, *Myc*. One study showed that aging mice steadily decreased methylation in the promoter and increased methylation in the gene body of *Myc* (Miyamura et al., 1993). After both 11 months and 21 months of 42% CR, age-related methylation changes surrounding *Myc* were significantly diminished. In hippocampal tissue of mice exposed to 40% CR, over 30% of age-related differentially methylated CpGs were prevented by CR (Hadad et al., 2018). Furthermore, CR produced changes in DNA methylation that were independent of aging. Genes affected by CR were enriched for pathways related to energy regulation, inflammation, and phagocytosis. DNA methylation in other brain regions also depends on age and diet. In mouse cerebellum, aging induced a significant increase in 5-mC immunoreactivity (Lardenoije et al., 2015). A 15% calorie reduction had no effect on Purkinje cell methylation in 12-month old mice. However, the same CR regimen decreased global DNA methylation in Purkinje cells of 24-month old mice. Thus, the

importance of CR in a variety of tissues is not only able to improve lifespan-associated mechanisms, but also improve health span.

The duration of CR appears to be critical in producing methylation changes. Female mice were 30% calorie restricted starting at 6-8 weeks of age, and genome-wide DNA methylation in mammary tissue was measured at 5 months and 22 months (Rossi et al., 2017). After 5 months of dietary treatment, there were 759 differentially methylated CpGs between CR and control mice. After prolonged treatment, the number of differentially methylated loci substantially increased to 7,552 with the majority (6,901) being hypermethylated in the CR group. Closer investigation of Estrogen receptor 1 and 2 (*Esr1* and *Esr2*) uncovered minimal methylation differences at 5 months. However, in aged animals, CR resulted in greater methylation at three loci within the first intron. Aged CR mice also showed hypermethylation upstream and downstream of the *Esr2* gene body. Another study in mice found that 40% restriction for 4 months was sufficient to observe an increase in neurotensin (*Nts*) expression in the colon as well as lower promoter DNA methylation in restricted mice. Interestingly, this DNA methylation change persisted even when mice were switched back to an *ad libitum* diet for 5 months (Unnikrishnan et al., 2017).

While CR is known to regulate systemic inflammation, it remains unclear how DNA methylation contributes to altered cytokine levels. In humans, weight loss studies have revealed various changes across adipose tissue and blood. One report found that after an 8-week 30% energy restricted intervention there was no change in promoter DNA methylation of *TNF* subcutaneous adipose tissue of obese women (Cordero et al., 2011). However, results in whole blood were contradictory, as gastric bypass patients had elevated methylation of interleukin 1B (*IL1B*), interleukin 6 (*IL6*), and *TNF* 12 months after surgery (Kirchner et al., 2014). Findings regarding *IL6* were reproduced in white blood cells, as *women subjected to 6 months of 30% energy*

restriction had increased IL6 methylation (Nicoletti et al., 2016). However, *IL6* methylation in bariatric surgery patients decreased. Interestingly, these changes were not correlated with circulating levels of the cytokines. In another study, obese and overweight men were subjected to 30% energy restriction for 8 weeks. Analysis revealed hypomethylation of TNF receptor superfamily member 9 (*TNFRSF9*) and hypermethylation of interferon gamma (*IFNG*) in PBMCs (Milagro et al., 2011). Overall, investigation of CR-mediated DNA methylation of inflammatory genes has yielded inconsistent results in humans.

In animal models, CR and DNA methylation in inflammatory pathways has only been examined in a limited number of studies. One study showed that age-related DNA methylation drift is accelerated under conditions of chronic inflammation (Issa, Ahuja, Toyota, Bronner, & Brentnall, 2001). In ulcerative colitis patients, there was hypermethylation in age-related CpG islands in colon epithelial cells. Because CR also impacts DNA methylation in aging, it is reasonable to hypothesize that CR could be affecting systemic inflammation via DNA methylation. Indeed, in mouse hippocampus, CR resulted in hypermethylation of CpGs that fell within genes that were enriched for inflammatory pathways, including FC epsilon receptor signaling, signaling by the B cell receptor (BCR), antigen activation of BCR leading to generation of second messengers, FC gamma receptor dependent phagocytosis, and interleukin-2 signaling (Hadad et al., 2018). Similarly, in monkey liver, CR reduced age-related DNA methylation drift associated with several genes including the neutrophil chemoattractant C-X-C motif chemokine ligand 3 (*CXCL3*) (Maegawa et al., 2017). Collectively, evidence suggests an association between CR and inflammation as well as CR and DNA methylation; however more work is necessary to uncover the role of DNA methylation in mediating inflammatory outcomes in CR.

3.4. HISTONE MODIFICATIONS AND CALORIC RESTRICTION

3.4.1. The Basis of Histone Remodeling

The chromatin landscape determines the availability of the genome, whether it is found in an open and accessible conformation (euchromatin), or a tightly packed in a closed arrangement (heterochromatin). Chromatin changes are mainly driven by covalent modifications to the nucleosomal histones, hence producing a change in the availability of genes; specific amino acid residues (lysine, serine, arginine, glutamine, etc.) within the histone globular core and tails can be modified covalently, thus altering the interaction with the DNA that is wound around the histone octamer (Lawrence, Daujat, & Schneider, 2016). Modifications to the histones, such as acetylation, methylation, phosphorylation, SUMOylation, among others, can interact with each other and other factors (Lawrence et al., 2016) to control the rate of transcription in of several genes in a variety of tissues, which in turn dictates tissue-specific gene expression. One such modification, histone acetylation is a post-transcriptional addition of and acetyl group facilitated by the enzymes histone acetyltransferases (HATs), and removed by histone deacetylases (HDACs). HATs act by transferring acetyl groups from acetyl CoA (Coenzyme A) onto the histone tails (lysine residues), neutralizing their positive charge and causing the DNA to decondense to allow transcription, mainly driven by an increased frequency of transcription factor binding within the target genes. For instance, the addition of acetyl groups to Histone 4 (H4K16ac) increases transcription in vivo and in vitro (Akhtar & Becker, 2000; Shogren-Knaak et al., 2006). Conversely, HDACs remove acetyl groups from the histones and restore the positive charge on the histone, restoring the heterochromatic state (Ng & Bird, 2000; Taunton, Hassig, & Schreiber, 1996). Both HAT and HDAC appear to be evolutionarily conserved across species (Smith, 2003; Akhtar, 2000). Other histone modifications have been described and their activating/repressive mechanisms have been reviewed previously (Lawrence et al., 2016; Y. Zhang & Reinberg, 2001).

Given the potent effect of CR on health and lifespan, several authors have described the relationship between nutrient sensing and chromatin modifications and the modifiers (H. C. Chang & Guarente, 2014).

3.4.2. Caloric Restriction as Regulator of Protein Modifications

During CR, energy depletion in the cell is evidenced by the increased catabolic state, alteration of nutrient sensing pathways (Fontana & Partridge, 2015), and increased NAD+ production (Mouchiroud, Houtkooper, & Auwerx, 2013), but the production of the latter seems to only improve health span, but not lifespan in mice (S. J. Mitchell et al., 2018). Alteration of the nutrient pool and its sensors, will in turn be able to influence nuclear gene transcription, which can be mediated by protein, and specifically histone modifiers susceptible to CR (Vaquero & Reinberg, 2009; Wood et al., 2015). CR is known to impact Sirtuins, a family of nutrient sensing HDACs (Guarente, 2000) (Fig. 3.2). Sirtuins are NAD^+-dependent protein deacetylases and HDACs (F. Wang, Nguyen, Qin, & Tong, 2007) and exert their function on lysine residues, some of them found in the nucleosomal histone tails. The first identified Sirtuin in *Saccharomyces* cerevisiae, Sir2, has been well studied in the context of lifespan extension that is thought to occur by silencing ribosomal DNA, thus decreasing the frequency of ribosomal DNA circles that cause aging in yeast (Sinclair & Guarente, 1997). Furthermore, deletion of Sir2 results in a shorter lifespan (Kennedy, Austriaco, & Guarente, 1994), whereas deletion of DNA replication fork-blocking protein 1 (FOB1) (required for generation of rDNA circles) (Defossez et al., 1999) or overexpression of Sir2 increases lifespan (Kaeberlein, 2004), providing evidence that a decrease in cellular stress could impact longevity. In addition, telomeres, the genomic regions that protect the ends of each chromosome from deterioration, are shortened when Sir2 expression is low (Dang et al., 2009). Conversely, when Sir2 is overexpressed, the longevity phenotype is restored. Increased cellular

stress coming from increased ribosomal circles, shorter telomeres, or epigenomic insults could lead to cell senescence and long-term exposure could impact aging, and Sir2 appears to be a strong regulator of this process.

Sirtuins are at the crossroads of metabolism and the epigenome. The SIRT family is comprised of 7 mammalian isoforms (SIRT1-7), that localize either in the nucleus (SIRT1, SIRT2, SIRT6) where they influence histones and other trans-activating factors, in the mitochondria (SIRT3-5) where they can participate in metabolic-related processes and modulate oxidative stress (H. C. Chang & Guarente, 2014), or in the nucleolus (SIRT7) where they aid in cell division. Their role as nutrient sensors allows them to identify the cell's energy status, as it is the case in CR where the energy status is lower. Then, they couple the signal with both deacetylation (DAC) of target proteins (such as histones within target genes), as well as mono [ADP-ribosyl] transferase (mADPRT) in the cytosol (Tanny, Dowd, Huang, Hilz, & Moazed, 1999) or deacylation (malonylation, succinylation, glutarylation, etc.) of mitochondrial matrix proteins (Carrico, Meyer, He, Gibson, & Verdin, 2018). Mono ADP-ribosylation (MARylation) was first observed in yeast Sir2 (Frye, 1999; Tanny et al., 1999) and later confirmed (Haigis et al., 2006; Liszt, Ford, Kurtev, & Guarente, 2005) with the transfer of ADP-ribose from NAD^+ to diverse substrates by SIRT4 and 6. Although the function of SIRTs as MARylation mediators has been established, the identification of sensitive and reliable detection methods as well as the lack of a consensus sequence for MARylation complicate the study of such function of SIRTs (Butepage, Eckei, Verheugd, & Luscher, 2015). Future experiments that are able to identify MARylation targets of SIRTs will shed light of the implications of CR on the MAR code. Moreover, the functions of SIRTs beyond DAC, i.e. demyristoylation, desuccinylation, demalonylation, deglutarylation,

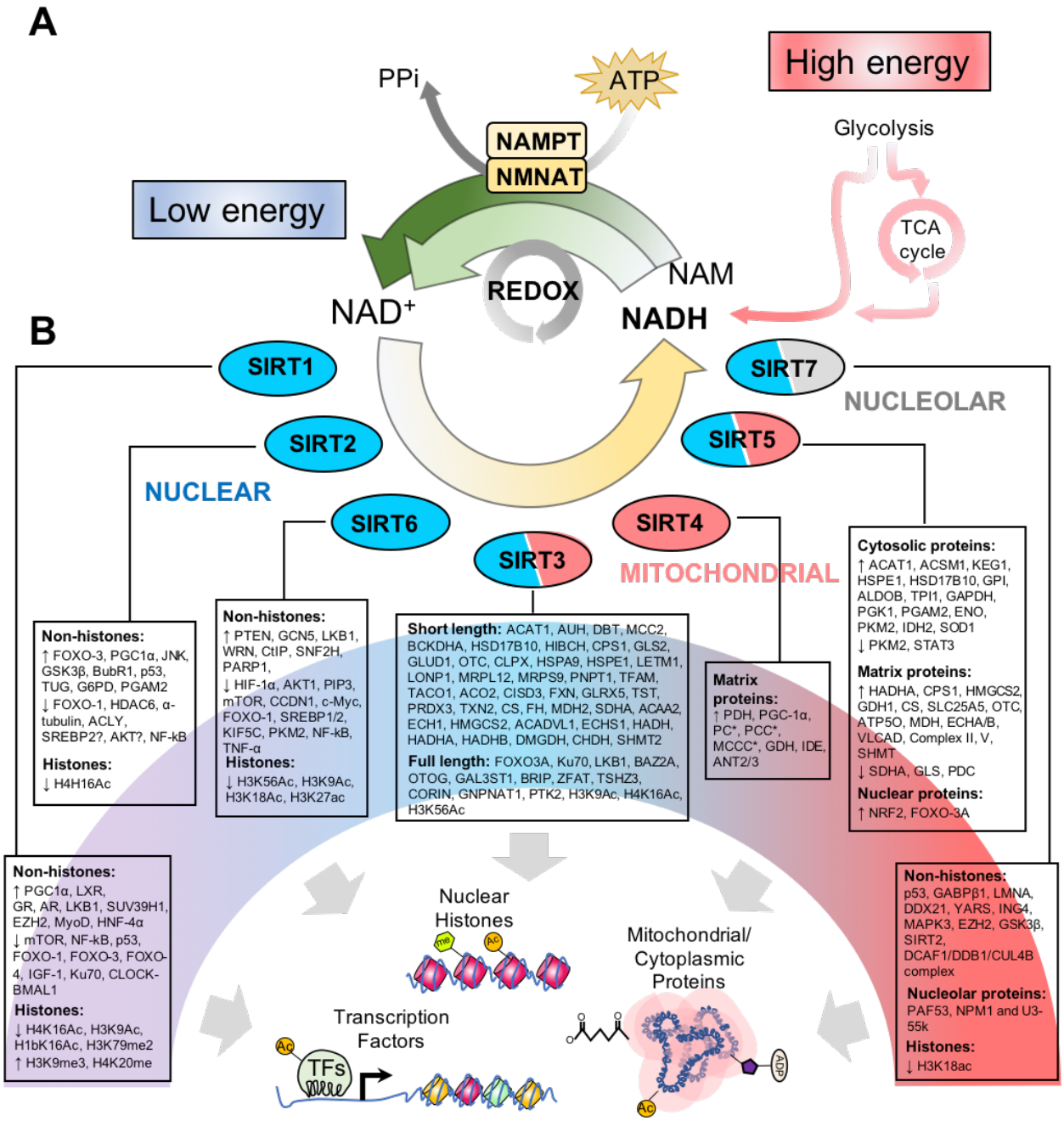

Figure 3.2. Epigenetic and genetic regulation of sirtuins by caloric restriction. A) High energy levels following a feeding period contribute directly to the elevated levels of NAM and NADH originated from catabolic pathways. Diverse cells and cellular processes deplete the concentration of NADH, and together with the biosynthetic transformation by NAMPT and NMNAT, high intracellular levels of NAD^+ are produced. B) Intracellular NAD^+ is sensed by NAD^+-dependent enzymes, such as sirtuins that add or remove posttranslational protein modifications from nuclear (blue), cytosolic, nucleolar (grey), and mitochondrial (red) proteins. Seven sirtuins, or SIRTs, have been defined in mammals, and participate in deacetylation, mono ADP-ribosylation, and defattyacylation (demyristoylation, desuccinylation, demalonylation, deglutarylation, demethyglutarylation, and de-3-hydroxy-3-methylglutaryl(HMG)-ation) of nuclear transcription factors, nucleosomal histones and various nuclear, nucleolar, and mitochondrial proteins.

demethyglutarylation, and de-3-hydroxy-3-methylglutaryl(HMG)-ation (HMGylation), provide a broader perspective of the role of SIRTs in fine-tuning metabolism according to cellular energetics.

Nutrient and energy sensing within the cells can be achieved through the monitoring of cellular energetics during feeding and fasting periods. Among the determinants of cellular energetics, the ratio of NAD^+:NADH is an adequate indicator of the energy status, in that the NAD^+:NADH ratio is high when energy levels are low, while the NAD^+:NADH decreases when nutrient and energy availability is high. Large concentrations of NADH can be utilized as reducing agents for oxidized substrates (Redox reactions), and together with biosynthetic pathways that use a Nicotinamide phosphoribosyl transferase and Nicotinamide nucleotide adenylyl transferase (NAMPT and NMNAT, respectively) to convert nicotinamide (NAM), both can yield high levels of oxidized NAD+ (Fig. 3.2A), and these reactions are catalyzed by. During fasting or CR, the levels of NAD+ increase and catalyze reactions mediated by all SIRTs (Fig. 3.2B), given that during each round of DAC SIRTs consume one NAD^+ molecule (Imai, Armstrong, Kaeberlein, & Guarente, 2000). Following activation of the SIRTs, a variety of posttranslational modifications are removed (acetyl, acyl, myristoyl, succinyl, etc.) or added (ADP-ribosylation) to proteins and histones within the nucleus, mitochondria, and nucleolus. We have subdivided the functions of SIRTs according to their subcellular localization (Fig. 3.2B), and we will give a brief overview of their role on metabolism and immunity.

3.4.3. Sirtuin 1

Sirtuin 1 (SIRT1) is the mammalian homologue of yeast Sir2 (F. Wang et al., 2007), and it is thought to have a major role at extending lifespan with CR in mammals. It localizes within the nucleus and cytosol and is involved in DAC reactions of different substrates such as cytosolic proteins, and nuclear histones and transcription factors (Fig. 3.2B). In the cytosol, SIRT1

deacetylates and activates transcription factors such as nuclear receptor liver X receptor (LXR), glucocorticoid receptor (GR), and androgen receptor (AR), which then translocate to the nucleus and bind to target genes to promote transcription. Likewise, SIRT1 activates peroxisome proliferator-activated receptor gamma coactivator 1-alpha (PGC-1α), the master regulator of mitochondrial biogenesis and muscle fiber type determination. Additionally, it is able to activate serine/threonine kinase 11 (or liver kinase B1, LKB1), which in turn activates AMP-activated protein kinase (AMPK) to mediate metabolism, apoptosis, and DNA damage responses. Similar to other sirtuins, SIRT1 requires NAD+ to perform a round of DAC. In pathological conditions such as obesity, a miRNA (miR-34a) inhibits the rate limiting step of NAD+ formation (NAMPT)(Fig. 3.2B) and contributes to the downregulation of SIRT1 activity (S. E. Choi et al., 2013). Thus, both energy availability and disease state have a great impact on SIRT expression and function.

On the other hand, SIRT1 deacetylates and inactivates multiple factors associated with anabolic processes including mammalian target of rapamycin (mTOR), a master regulator of protein synthesis, and insulin-like growth factor-1 (IGF-1). SIRT1 has a role in stress resilience where it binds stress-dependent factors forkhead box O1 (FOXO-1), FOXO-3, and FOXO-4, p53, and Nuclear factor kappa B(NF-kB), and promotes transcription of stress protection genes while inhibiting those that increase cell cycle arrest, senescence, or apoptosis(Vaquero & Reinberg, 2009). Moreover, SIRT1 deacetylates Ku70 (X-ray repair cross complementing 6) (Ku70-dependent apoptosis and DNA repair), indicating that it plays a role in non-homologous end joining (NHEJ) and double strand break (DSB) repair pathways (Vaquero & Reinberg, 2009). Finally, SIRT1 counteracts the effect of circadian machinery protein Clock by deacetylating its

target histones and BMAL1, the other major component of the machinery. This function is tightly related to the circadian fluctuations of NAD+.

Although SIRT1 has many targets within the cytosol, long-lasting effects of CR that are known to be mediated by SIRT1 are thought to be linked to its HDAC role in the nucleus (Fig. 3.2B). SIRT1 maintains a heterochromatic environment by removing the active transcription mark H3K79me2 (Vaquero et al., 2004). Additionally, SIRT1 interacts with histone methyltransferase (HMT) SUV39H1 (Suppressor of Variegation 3-9 Homolog 1) to allow the methylation of H3K9 (H3K9me3) and H4K20 (H4K20me), both hallmark histone modifications of heterochromatin (Peters et al., 2001; Trojer & Reinberg, 2007). Although heterochromatin is known to be located within virtually inactive regions of the genome such as centromeres, telomeres, and retrotransposons (LINEs and SINEs), transcription from certain heterochromatic regions called facultative heterochromatin is known to occur. Interestingly, the state of constitutive and facultative chromatin is responsive to both micronutrient and macronutrient availability, as we have previously reviewed (Hernandez-Saavedra, Strakovsky, Ostrosky-Wegman, & Pan, 2017). SIRT1 provides stability to facultative heterochromatin, as it deacetylates H3K9Ac and H4K16Ac marks, and is able to interact with linker histone modification H1bK26Ac and recruit it to promote higher order organization (Vaquero et al., 2004), which in turn is modified by EZH2 to generate H1bK26me (Vaquero & Reinberg, 2009). Thus, it seems that SIRT1 can respond to nutrient availability in CR and induce several changes within the acetylation landscape of cytosolic and nuclear proteins and histones to mount an adaptive response to the low energy status.

3.4.4. Sirtuin 2

SIRT2 is regarded as the most conserved SIRT across species, and due to this feature, it is thought to regulate important cellular processed that are shared by multiple organisms. SIRT2 localizes

within the nucleus and cytosol where it can act on cell cycle control and cell division as well as metabolism of fatty acids, which is thought to be mediated through its control on acetylation and myristoylation. This sirtuin deacetylates and activates transcription factors FOXO-3, PGC-1α, p53, and NF-kB, key regulatory kinases JNK and GSK3β, and histone deacetylase HDAC6. The main function of SIRT2 is to localize to microtubules where it deacetylates the stable acetylated α-tubulin, thus promoting their polymerization/depolymerization cycle. This process is sensitive to the levels of NAD^+ (Skoge, Dolle, & Ziegler, 2014),which is of particular importance given that during CR the levels of NAD+ rise and can directly regulate the SIRT2-mediated DAC of α-tubulin. Moreover, the deletion of SIRT2 in mouse oocytes results in higher rates of spindle defects, chromosome disorganization, and impaired kinetochore interaction with the centromere (L. Zhang et al., 2014). This function appears to be intricately related to the direct acetylation of a component of the spindle assembly checkpoint complex BubR1 (BubR1-K243) (D. Qiu et al., 2018) and DAC of nucleosomal H4K16Ac (L. Zhang et al., 2014). CR may prevent genomic instability by regulating mitotic and spindle control, inspecting cell division checkpoints (i.e. spindle assembly checkpoint), and promoting the fidelity of the chromosomal distribution (Fig. 3.2B).

Additionally, recent reports have highlighted the effect of SIRT2 on fatty acid metabolism and adipocyte differentiation. In rapidly growing cells, the need for lipid synthesis increases and in a condition of nutrient excess, ATP-citrate lyase is acetylated on three different sites by p300/PCAF (K540, K546, K554), which results in its stabilization followed by rapid lipid synthesis, proliferation, and tumor growth. On the other hand, SIRT2 acts on these lysine residues to promote the ubiquitination and degradation of ACLY (R. Lin et al., 2013). Lastly, in adipocytes, SIRT2 is capable of inhibiting adipogenesis by deacetylating FOXO-1 and thus strengthening its inhibitory

action on adipogenic transcription factor PPARγ (Jing, Gesta, & Kahn, 2007; F. Wang & Tong, 2009). On the other hand, SIRT2 is known to alter glucose metabolism by deacetylating PEPCK1 and increase gluconeogenesis (Q. Wang et al., 2010; M. Zhang et al., 2017), or by activating the pentose phosphate pathway (PPP) and glycolysis by deacetylating Glucose-6-Phosphate Dehydrogenase (G6PD) and Phosphoglycerate Mutase 2 (PGAM2), respectively, under oxidative stress conditions (Y. P. Wang et al., 2014). Lastly, SIRT2 can also have insulin sensitizing effects, which occurs through the direct DAC of TUG (Tethering protein containing a UBX domain for GLUT4), thus establishing a stable link for the uptake of glucose (Belman et al., 2015; Bogan, Hendon, McKee, Tsao, & Lodish, 2003; Xu et al., 2011). Altogether, activation of SIRT2 due to increased NAD+ availability directs the cell cycle checkpoints and inhibits the rapid growth of tumor cells, thus rendering SIRT2 as an important anti-cancer agent.

3.4.5. Sirtuin 6

Similar to other nuclear sirtuins, SIRT6 is known to localize to the cytosol but primarily remains in the nuclear compartment where it is involved in DAC, ADP-ribosylation, and defatty-acylation (myristoyl residues) of numerous proteins related to cell cycle and metabolism. Interestingly, unlike other sirtuins, SIRT6 appears to add O-acetyl-ADP-ribose residues ~1,000X slower and is capable of binding NAD^+ in the absence of acetylated substrate, implying that this sirtuin might act as an NAD^+ metabolite sensor (Pan et al., 2011). NAD^+ sensing constitutes a key function of SIRT6 in health and disease (Fig. 3.2B). Conflicting evidence exists on the role of SIRT6 in cancer progression. Evidence suggests that SIRT6 is sufficient to upregulate the expression of the tumor suppressor PTEN and prevent its ubiquitination and subsequent degradation, whilst reducing the levels of AKT1, PIP3, mTOR, c-Myc, and CCND1, and decreasing colon cancer progression (Tian & Yuan, 2018). This deacetylase is also known to inhibit Hypoxia inducible factor 1 α (HIF-1α)

binding to its target genes (Kuang et al., 2018; Zhong et al., 2010). This downregulates glycolysis and accelerates metastasis, angiogenesis, and resistance to therapy (Masoud & Li, 2015). In addition, this sirtuin binds to and deacetylates nuclear pyruvate kinase M2 (PKM2), which directs its expulsion from the nucleus by exportin 4 and contributes to decreased cell proliferation, migration, and invasiveness (Bhardwaj & Das, 2016). In addition, SIRT6 is known to regulate pluripotency of stem cells and their differentiation through Tet-mediated production of 5hmC (Etchegaray et al., 2015). SIRT6 has also been shown to inhibit glioma cell growth (X. Chen, Li, Gao, Cao, & Hao, 2018), growth of colorectal cancer stem cells (W. Liu et al., 2018), hepatocellular carcinoma aided by FOXA-2 (J. Liu et al., 2018), gastric cancer (J. Zhou, Wu, Yu, Zhu, & Dai, 2017), non-small cell lung cancer (Zhu, Yan, Shao, Tian, & Zhou, 2018), breast carcinoma (Bae et al., 2016), and its downregulation by miR-34c-5p is associated with promotion of colon cancer and poor prognosis (N. Li et al., 2018). Conversely, evidence exists to demonstrate the oncogenic role of SIRT6 in esophageal cancer (N. Huang et al., 2017), hepatocellular carcinoma (S. Kohli, Bhardwaj, Kumari, & Das, 2018; N. Lee et al., 2016), neuroblastoma (Song et al., 2018), melanoma (Garcia-Peterson et al., 2017; L. Wang et al., 2018), malignant colon cancer (Geng et al., 2018), osteosarcoma (H. Lin, Hao, Zhao, & Tong, 2017). Therefore, it appears that the role of SIRT6 as a tumor suppressor or oncogene is dependent on the tissue type and severity of the disease, pointing to the possible epigenetic regulation of SIRT6 in cancer progression.

Cancer and other normal cellular functions are both dependent on the correct division of chromosomes and preservation of the genetic information following each cell division step. To that end, SIRT6 is known to interact with the DNA damage machinery both at breakage sites and highly susceptible telomeric regions. SIRT6 deacetylates and activates the C-terminal-binding

protein interacting protein (CtIP) and recruits Sucrose non-fermenting protein 2 homolog (SNF2H) to promote double strand break and resection, which in turn facilitates homologous recombination of chromosomes in collaboration with BRCA1 (Kugel & Mostoslavsky, 2014; Toiber et al., 2013). In addition to chromosomal stability, SIRT6 also cooperates with different telomeric maintenance systems to protect these important regions. In the nucleus, SIRT6 is able to deacetylate H3K9Ac and H3K56Ac within telomeric regions, and facilitates the recruitment of Werner syndrome recQ like helicase (WRN) to aid in telomere capping during cell division (Michishita et al., 2008; Vaquero & Reinberg, 2009). Moreover, upon oxidative damage, SIRT6 promotes directional telomeric movement, which grants protection and is related to telomeric length conservation (Y. Gao et al., 2018). In a similar way, SIRT6 can act on equally important genomic regions such as enhancers; SIRT6 deacetylates H3K27ac and thus activates cis-regulatory loci (Tasselli, Zheng, & Chua, 2017; W. W. Wang, Zeng, Wu, Deiters, & Liu, 2016). Altogether, SIRT6 and other members (SIRT1) can prevent genomic instability by ensuring proper cell division and protecting or activating important genomic loci.

Another function that has been described for SIRT6 is related to energy and nutrient metabolism in liver, muscle, and brain (Cui et al., 2017). As an NAD^+-dependent deacetylase, SIRT6 can activate the Liver Kinase B1 or LKB1 (also called STK11), which can in turn activate AMPK and improve insulin sensitivity (Cui et al., 2017; Kuang et al., 2018). Moreover, SIRT6 is known to impact insulin secretion in response to glucose by deacetylating H3K56Ac within the Thioredoxin interacting protein (Txnip) promoter in pancreatic β-cells to enhance insulin secretion (Qin et al., 2018). SIRT6 can also participate in lipid metabolism regulation, from adipogenesis and lipid synthesis to fatty acid oxidation. SIRT6 inhibits SREBP1/2, master lipogenic transcription factors. Conversely, miRNA contained in intronic regions of SREBP1 and 2 (miR-

33a and miR-33b) are known to downregulate SIRT6 expression (Elhanati et al., 2013). Similarly, SIRT6 downregulates miR-122 in the liver by deacetylating H3K56Ac within the promoter and thus increase fatty acid β-oxidation (Elhanati et al., 2016). Lastly, SIRT6 inhibits adipogenesis by blocking mitotic clonal expansion through the inactivation of kinesin KIF5C, thus preventing hyperplasia in adipose tissue (Q. Chen et al., 2017) (Fig. 3.2B).

Other functions of this sirtuin include the removal of fatty acids from diverse proteins, in particular the removal of myristoyl residues from lysine residues. This process appears to be dependent on $NAD^{+.}$ If NAD^{+} is present, SIRT6 deacetylates rather than removes myristoyl residues, and this process mediates the secretion of various proteins (X. Zhang et al., 2016). Interestingly, SIRT6 is known to regulate TNF-α secretion, a potent inflammatory and signaling cytokine, through removal of fattyacyl modifications on K19 and K20, thus stimulating its cellular export in macrophages (Jiang et al., 2013), other immune cells (Van Gool et al., 2009), and pancreatic cancer cells (Bauer et al., 2012). Nevertheless, in pathological conditions SIRT6 is sufficient to inhibit inflammation (Y. He et al., 2017) by decreasing NF-kB binding to its target genes (Kawahara et al., 2009; N. Zhang et al., 2016). SIRT6 deacetylates H3K9Ac tails within p65 (NF-kB)-responsive regions thus impeding binding of this transcription factor and inhibiting aging-associated inflammation (Kawahara et al., 2009). Finally, given the potent inhibition of inflammation by CR in aged animals (Phillips & Leeuwenburgh, 2005) and humans (L. Yang et al., 2016a), SIRT6-mediated inactivation of cytokines might be related to the dual action of the enzyme (deacetylase vs. defattyacylase) (Fig. 3.2B), which is sensitive to cellular NAD+ levels..

3.4.6. Sirtuin 3

Of all the members of the sirtuin family, SIRT3 is one of the most studied proteins in relation to stress and longevity due to its subcellular localization within the mitochondria (Albani et al., 2014;

Dhillon & Denu, 2017). Mitochondria are the powerhouse of the cell and are intimately related to nutrient and energy metabolism. As such, mitochondrial protein decetylases that respond to the cell's energy status are primordial for the coupling of metabolic reactions and preservation of the mitochondrial integrity. SIRT3 exists in two forms, the full-length form (40kD) and the mitochondrial-exclusive short length form (28kD). The full-length form of SIRT3 is cleaved by a Matrix processing peptidase (MPP) upon entering the mitochondrial matrix, yielding a short form SIRT3 with deacetylase activity (Schwer, North, Frye, Ott, & Verdin, 2002). The full-length (FL) SIRT3 is known to act as a histone deacetylase given that it localizes within the nucleus and cytosol. Nuclear FL SIRT3 is able to regulate transcription of PGC-1α, SOD2, and stress related genes (BAZ2A, OTOG, GAL3ST1, and BRIP), and deacetylate FOXO3A and Ku70 (Iwahara, Bonasio, Narendra, & Reinberg, 2012; Sundaresan, Samant, Pillai, Rajamohan, & Gupta, 2008). Under conditions of cellular stress FL SIRT3 is targeted for ubiquitin-proteasome degradation by E3-ligase SKP2, and this process is thought to initiate its translocation to the mitochondria and processing to the short-length form (Iwahara et al., 2012). Lastly, FL SIRT3 might be responsible for the changes to chromatin observed in stress-induced DNA damage. For instance, SIRT3 is capable of deacetylating H4K16Ac and H3K56Ac upon DNA damage induction (Scher, Vaquero, & Reinberg, 2007; Vempati et al., 2010), but translocates to the mitochondria following a rapid remodeling of the nuclear chromatin. While the regulation of stress-response genes is important in the context of disease, limited information is available on the genome-wide binding targets of the FL SIRT3 form and its regulation during CR.

On the other hand, the short-length, mitochondrial form of SIRT3 has been well-characterized in relation to the mitochondrial acetylome (mitochondria-wide acetylation/DAC) and its regulation. From here on, we will refer to the short-length, mitochondrial form of SIRT3 as plainly

"SIRT3". In the mitochondrial matrix, SIRT3 is able to interact with a myriad of factors that are involved in energy metabolism, such as the electron transport chain, tricarboxylic acid cycle, β-oxidation and ketogenesis, as well as stress resilience and reactive oxygen species quenching (Giralt & Villarroya, 2012; Hallows et al., 2011; Hirschey et al., 2010; Jing et al., 2011; X. Qiu, Brown, Hirschey, Verdin, & Chen, 2010; Shimazu et al., 2010). Altogether, it appears that the effect of SIRT3 revolve around mitochondrial-performance enhancement and increasing resistance to stress. Interestingly, higher NAD^+ availability as in the case of CR, is able to activate SIRT3 that in turn directs the DAC of two lysine residues within SOD2 (K53 and K89), thus improving the response to oxidative stress (X. Qiu et al., 2010). Similarly, fasting or CR could increase fatty acid β-oxidation by reversibly deacetylating long-chain acyl co-enzyme A dehydrogenase (LCAD) at lysine 42 (K42) (Hirschey et al., 2010). Moreover, in addition to LCAD, SIRT3 is known to directly deacetylate Acetyl-CoA synthetase 2 (ACSS2), Ornithine carbamoyltransferase (OTC), and Isocitrate dehydrogenase 2 (IDH2) (Hallows et al., 2011; W. Yu, Dittenhafer-Reed, & Denu, 2012), to promote acetate and urea metabolism, and antioxidant defenses, respectively. Finally, SIRT3 is able to direct the DAC of 3-Hydroxy-3-methylglutaryl CoA synthase 2 (HMGCS2) within lysine residues 310, 447, and 473, thus increasing its activity and enabling the generation of ketone bodies during fasting and CR (Shimazu et al., 2010). As it is readily apparent, SIRT3 modifies mitochondrial enzymes that participate in the hallmark processes of CR (Hirschey, Shimazu, Huang, Schwer, & Verdin, 2011), thus making SIRT3 an attractive target for therapeutic strategies.

SIRT3, like SIRT1, is highly responsive to CR and is involved in the age-related benefits of this dietary therapeutic strategy. SIRT3, is able to reshape the entire acetylome of the liver in response to CR, and experiments that have defined the acetyl-proteome have identified three

different types of acetyl residues: those that are responsive to CR and are acted on by SIRT3 (class I), those that are responsive to CR and are unresponsive to SIRT3 (class II), and those that are unresponsive to CR or SIRT3 (class III)(Hebert et al., 2013). Class I acetylated proteins are involved in amino acid and branched chain amino acid catabolism, transamination and ammonia detoxification, mitochondrial integrity, mitochondrial DNA (mtDNA) transcription and translation, iron homeostasis, antioxidant response, TCA cycle, acetyl CoA metabolism, fatty acid oxidation and one-carbon metabolism (Hebert et al., 2013) (Fig. 3.2B). Thus, other mitochondrial sirtuins like SIRT4 or other deacetylases can be responsible for those acetyl marks that are not removed by SIRT3, and might be related to the aging-dependent mitochondrial decline. Evidence points to the inactivation of SIRT3 activity by other SIRTs. In obese and aged mice, SIRT1 levels are reduced and SIRT3 becomes hyperacetylated due to the inability of SIRT1 to remove SIRT3-K57Ac (S. Kwon et al., 2017). Consequently, SIRT3 deacetylase activity is by nature, highly dynamic and can be modulated by other deacetylases and disease conditions.

This close relationship between SIRT3 and other acetylated proteins and deacetylases (SIRT4 and 5) becomes obvious in light of the efforts to map the mitochondrial sirtuin network (W. Yang, K. Nagasawa, et al., 2016) (Fig. 3.2B). Yang et al. (W. Yang, K. Nagasawa, et al., 2016) performed a systematic interaction proteomic analysis to identify specific SIRT3-5-interacting proteins, as well as define SIRT3-5-associated subnetworks, to provide a complete map of the SIRT3-5 interactome. They found that upon loss mitochondrial membrane potential, SIRT3 dissociates from the ATP5O subunit of the Complex V embedded within the inner mitochondrial membrane and initiates the rapid remodeling of the matrix acetylome. Conversely, during the extraction of energy from nutrients (high membrane potential) SIRT3 is anchored to ATP5O through a histidine residue (H135), where it remains inert. Just like ATP5O, SIRT3 might interact with other proteins to

modulate its action. Exploration of the partners and regulators of SIRT3 might provide a complete view of the dynamic remodeling of the mitochondrial acetylome and acylome (Carrico et al., 2018).

3.4.7. Sirtuin 4

Among the other mitochondrial sirtuins, SIRT4 is strictly localized within the matrix and its primary function does not involve the DAC of target proteins, but rather entails ADP-ribosylation and deacylation, mainly removing glutaryl, methylglutaryl and HMGyl residues from mitochondrial proteins. Unlike other sirtuins, SIRT4 is negatively regulated by CR and its crystal structure hints at a higher inhibitory potential of NADH due to its higher preference over NAD^+ (Pannek et al., 2017). The role of SIRT4 in energy metabolism is not as well studied as other mitochondrial sirtuins(Chalkiadaki & Guarente, 2012), but studies indicate that it participates in crucial steps of glycolysis by controlling the pyruvate dehydrogenase (PDH) complex by removing lipoyl and biotinyl residues from the complex(Mathias et al., 2014) (Fig. 3.2B). Moreover, SIRT4 is known to regulate fatty acid β-oxidation in the liver by controlling PPARα, the master regulator of fatty acid oxidation, which controls CPT1a, PDK4, and ACOX1(Laurent et al., 2013), as well as AMPK (Nasrin et al., 2010). During fasting conditions or prolonged nutrient limitation, SIRT4 is suppressed and SIRT1 is upregulated to initiate the oxidative program of the mitochondria. The effects of SIRT4 oppose that of CR. In pancreatic β-cells, SIRT4 ADP-ribosylates Glutamate dehydrogenase (GDH) to inhibit glutamate and glutamine usage and a subunit of the ATP/ADP translocase. This decreases ATP production and interacts with insulin degrading enzyme (IDE2) that in turn prevents insulin secretion. Such effects can be reversed by CR (Ahuja et al., 2007; Haigis et al., 2006). Additionally, SIRT4 knockout mice (SIRT4KO) have dysregulated leucine metabolism (Methylcrotonoyl-CoA Carboxylase [MCCC]) and increased insulin secretion, which

progressively leads to insulin resistance (K. A. Anderson et al., 2017). Such interaction with biotin-dependent carboxylases (PC, PCC, and MCCC) has also been observed in yeast (Wirth et al., 2013).

3.4.8. Sirtuin 5

The final "mitochondrial" sirtuin actor is SIRT5, a particularly interesting sirtuin whose function spans not mitochondrial protein modifications, but nuclear and cytosolic as well (Fig. 3.2B). SIRT5 does not possess deacetylase activity, which set it apart from other SIRTs, but it removes glutaryl, malonyl and succinyl residues from its target proteins (Carrico et al., 2018). SIRT5 (and SIRT4) is involved in deglutarylation of proteins belonging to oxidation/reduction, generation of precursor metabolites and energy, fatty acids and coenzyme metabolism, as well as aerobic respiration (Tan et al., 2014). From all these cellular processes, Tan *et al.* (Tan et al., 2014) were able to identify that SIRT5 targets Carbamoyl phosphate synthase 1 (CPS1), and possibly other glutarylation targets such as HADHA (Hydroxyacyl-CoA dehydrogenase trifunctional multienzyme complex subunit alpha), GOT2 (Glutamic-oxaloacetic transaminase 2), MDH2 (Malate Dehydrogenase 2), SDHA (Succinate dehydrogenase complex flavoprotein subunit A), ACAA2 (Acetyl-CoA acyltransferase 2), ACAT1 (Acetyl-CoA acetyltransferase 1), HADH (Hydroxyacyl-CoA dehydrogenase), SCP2 (Sterol carrier protein 2), and OTC. Regarding energy metabolism, SIRT5 is known to impact the lysine (K) malonylation of several glycolytic enzymes such as Phosphoglucose isomerase (GPI), Triosephosphate isomerase (TPI1), Glyceraldehyde 3-phosphate dehydrogenase (GAPDH), Phosphoglycerate kinase (PGK1), Phosphoglycerate Mutase 2 (PGAM2), Enolase (ENO), and Pyruvate kinase (PK), thus activating glycolytic flux, as well as urea cycle and other mitochondrial enzymes (Nishida et al., 2015). Likewise, SIRT5 is also able to regulate several mitochondrial proteins related to β-oxidation and ketogenesis; for instance,

SIRT5 removes succinyl residues (K83 and K310) from on HMGCS2, thus regulating the critical step in ketogenesis (Rardin et al., 2013). Also, protein succinylation networks have revealed that several proteins can be acted on by SIRT5, like the PDH complex, Succinate dehydrogenase complex (SDH, Complex II), Glutathione S transferases, ribosomes, and the chaperonin-containing TCP1 complex (Park et al., 2013). SIRT5 not only regulates the mitochondrial acylome, but also protects against mitochondrial fragmentation and mitophagy (mitochondrial degradation). Thus, it is vital for starvation-induced (or CR) mitochondrial elongation (Guedouari, Daigle, Scorrano, & Hebert-Chatelain, 2017). Interestingly, two well-known CR actors have opposing regulatory effects on SIRT5 expression: while PGC-1α promotes the transcription of SIRT5, AMPK inhibits its expression in the liver, while increasing the other sirtuins (Buler, Aatsinki, Izzi, Uusimaa, & Hakkola, 2014). Finally, although the role of SIRT5 in metabolism has been defined, several avenues of research indicate the great potential of this sirtuin in health and age-related diseases (Bringman-Rodenbarger, Guo, Lyssiotis, & Lombard, 2018; Kumar & Lombard, 2018; van de Ven, Santos, & Haigis, 2017; Zou et al., 2018), highlighting the potential benefits of CR and SIRT5 activation.

3.4.9. Sirtuin 7

The last member of the sirtuin family is one of the least understood and understudied NAD^+-dependent deacetylases. SIRT7 localizes within cytosol and nucleus in its high-molecular weight form (47.5 kDa), but unlike other sirtuins, SIRT7 is processed to a lower-molecular weight form (45 kDa) that allows for its import into the nucleolus (Kiran et al., 2013)(Fig. 3.2B). This subcellular nucleolar SIRT7 is depleted in senescent cells, which indicates that SIRT7 is related to replicative senescence (Kiran et al., 2013). Disorganized spindles and disruption of chromosomal syzygy is observed in SIRT7 depleted cells and obese mice (M. Gao et al., 2018), but

overexpression of SIRT7 is associated with cancer growth (Barber et al., 2012; W. Li et al., 2018). The latter, is thought to be regulated through miR-125b-5p and miR-340 (W. Li et al., 2018; X. Wang & Song, 2018), or C/EBPα-mediated HDAC3 recruitment (Liu et al., 2016), which negatively regulates SIRT7 expression. Moreover, among the proteins known to interact with SIRT7 are histone H3K18Ac, p53, GABPβ1 (GA Binding Protein Transcription Factor Beta Subunit 1), and nucleolar proteins PAF53 (Polymerase associated factor 53), NPM1 (Nucleophosmin 1), and U3-55k (U3 Small nucleolar ribonucleoprotein-associated 55 KDa protein) (Simonet & Vaquero, 2017), but recently the protein interaction network has been expanded to ~176 proteins involved in metabolic processes (C. Zhang et al., 2017). DAC of H3K18Ac by SIRT7 decreases mRNA transcription mediated by the Pol II machinery, which demonstrates its effect on chromatin and ability to promote cell transformation and tumorigenesis (Barber et al., 2012). Further, SIRT7 interacts with and represses the RNA pol I and other nucleolar chromatin remodeling complexes (MYBBP1a, WSTF, and SNF2H), which emphasizes the role of SIRT7 in transcription (Tsai, Greco, Boonmee, Miteva, & Cristea, 2012). Moreover, SIRT7 increases transcription of rRNA genes and then binds to rRNAto catalyze SIRT7's deacetylase and defattyacylase (myristoyl) activities (Tong et al., 2017).

Further important functions related to SIRT7 include mitochondrial gene expression and hepatic lipid metabolism (Wronska, Lawniczak, Wierzbicki, & Kmiec, 2016). SIRT7 is known to be affected differently by aging and CR, in a tissue-specific manner (Wronska et al., 2016). SIRT7 and SIRT6 appear to have a shared proportion of protein targets that are related to DNA repair, chromatin assembly, and aging (N. Lee et al., 2014). Furthermore, aging-dependent Nucleophosmin (NPM1) acetylation is dependent on SIRT6-SIRT7, thus shedding light on the anti-aging effects of SIRT7. Finally, SIRT7 is known to play a role in fat uptake, opposing the

effects of SIRT1, SIRT3, and SIRT6 in fat utilization (Houtkooper, Pirinen, & Auwerx, 2012). SIRT7 enhances fat uptake by upregulating hepatic *Cd36* and promotes triglyceride synthesis and storage through the elevation of *Mogat* and *Cidea*/*Cidec* (Yoshizawa et al., 2014). Moreover, SIRT7 was identified as a direct inhibitor of the E3-Ubiquitin complex CAF1/DDB1/CUL4B, which is known to target the nuclear receptor Testicular receptor 4 (TR4 or NR2C2) (J. Lee & Zhou, 2007). In turn TR4 activates genes involved in fat uptake and lipid storage in the liver (Yoshizawa et al., 2014). SIRT7 regulation therefore, might constitute an attractive target to counteract the effects of a high-fat diet to prevent fatty liver disease.

3.5. SMALL NON-CODING RNA AND CALORIC RESTRICTION

3.5.1. Epigenetic basis of small ncRNA

When discussing the epigenetic regulation of genes, one must take into account the ubiquitous and silencing/activating nature of the epigenetic small non-coding RNAs. MicroRNAs (miRs) are small, non-coding RNA molecules that regulate post-transcriptional stability of genes through base pair recognition within the 3'-UTR in the target gene. Technologies such as microarray, q-PCR-based or sequencing approaches, have allowed for the stabilization and identification of numerous miRNA present *in vivo* (Vasudevan, Tong, & Steitz, 2007). The binding of miRs to the target gene recruits the multiprotein complex RNA-induced silencing complex (RISC) which cleaves the target gene through one of its components, Argounaute (Carthew & Sontheimer, 2009; Orom et al., 2012; Orom, Nielsen, & Lund, 2008). This highly orchestrated process is responsible for the post-transcriptional stability of mRNAs in the cytosol. Therefore, environmental stimuli that affect the presence of a particular set of miRs will determine the gene expression pattern. During early eukaryotic mRNA translation, cytoplasmic poly(A)-binding protein (PABPC) and the poly(A) tail of the mature mRNA interact to form a complex that can then associate with the eukaryotic

translation-initiation factor 4G (eIF4G) by recognizing the 5'-cap. Formation of the mRNA/PABPC/eIF4G complex is necessary to protect the circular mRNA, but miRs hinder the interaction of PABPC and eIF4G at the early stages of translation. Binding of miRs to 3'-UTR recruits the RISC complex, which activates one of its components, GW182 (Trinucleotide Repeat Containing 6A) (Braun, Huntzinger, & Izaurralde, 2013). Following GW182 activation, deadenylation of the mRNA occurs by recruiting the CAF1-CCR4-NOT deadenylase complex, leading to mRNA degradation together with the decapping enzyme DCP2 and cytoplasmic 5'-3' exonuclease XRN1 (Calvopina, Coleman, Lewindon, & Ramm, 2016). RISC-mediated degradation is a fine-tuned degradation machinery, but its specificity is ultimately dependent on the presence of the miRs.

Due to the ubiquitous nature of miRs (Calvopina et al., 2016), research in this area can provide valuable knowledge in the exploration of the etiology of human diseases (Nezami et al., 2014). In time, miRs could be used as a predictive biomarker for different tissues given their adaptability to different environmental stimuli (Calin et al., 2004; Negrini, Nicoloso, & Calin, 2009; Simone et al., 2009). To harness the power of miRs in disease prevention, environmental stimuli must be strong enough to alter the expression pattern of these small nucleotide modulators. The mechanisms by which CR is able to promote health benefits is thought to be mediated through alteration of miR patterns in different tissues. In the following section, we will explore the powerful effect of CR on miR regulation in different tissues.

3.5.2. Caloric Restriction and microRNAs

CR onset is important when considering the possible short- and long-term effects on health and disease. For instance, CR during pregnancy leads to glucose intolerance, fat mass accretion, and

hypercholesterolemia in adult offspring (Bhasin et al., 2009; Burton, Jauniaux, & Charnock-Jones, 2010), and 50% CR at gestational day 10 induces differential expression in the placenta similar to

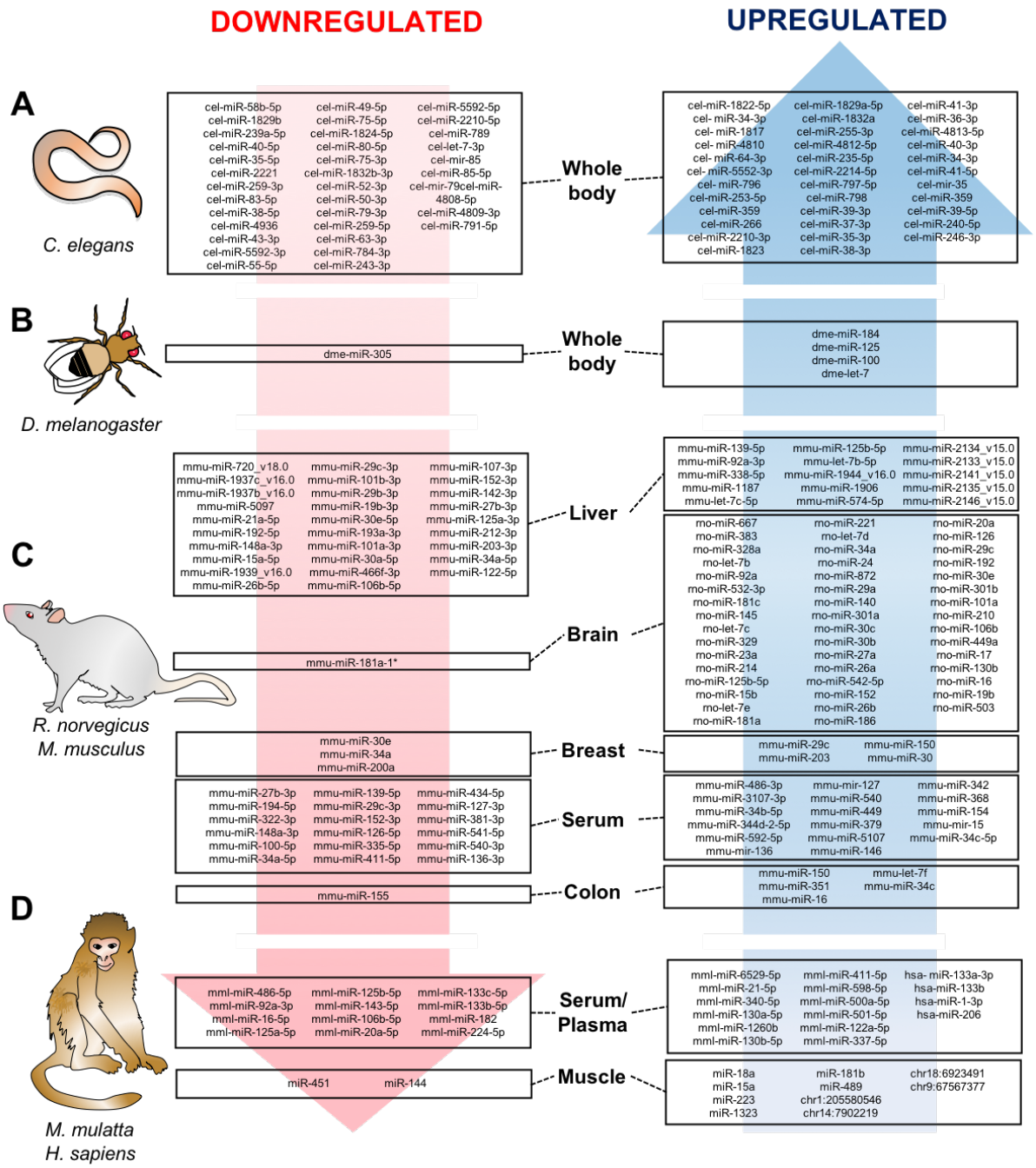

Figure 3.3. Caloric restriction (CR) conservation of miRNA changes across species and tissues. Caloric restriction and starvation are able to upregulate or downregulate miR signatures in A) *C. elegans*, B) *D. melanogaster*, C) rodents (*R. norvegicus* and *M. musculus*), and D) Rhesus macaques (*M. mulatta*) and humans (*H. sapiens*). miR signatures associated with CR are involved in anti-aging pathways such as immunometabolic regulation in different peripheral and central tissues.

Intrauterine growth restriction (IUGR), all the while decreasing global methylation level, and specific altered methylation pattern of miRs associated with vital homeostatic processes (P. Y. Chen et al., 2013). On the other hand, late-onset CR has been associated with beneficial miR patterns that are able to prevent or treat chronic diseases (Mico, Berninches, Tapia, & Daimiel, 2017). Nevertheless, the effects of early- vs. late-onset CR should be studied in the context of miRNAs.

The effects of CR on miR expression patterns appear to be conserved in different species, from *Caenorhabditis elegans* and *Drosophila*, to rodents (*R. norvegicus* and *M. musculus*), Rhesus macaques (*Macaca mulatta*) and humans (*Homo sapiens*). Different CR levels and protocols have been investigated for their miR-modulating effect in many tissue types (Fig. 3.3). In the following section, we will revisit all the evidence surrounding CR using a systematic review algorithm in PubMed (Appendix A Suppl. Table 3.1). In *C. elegans*, 12-hr or 2-day starvation is sufficient to produce significant changes in miR whose target genes are related to metabolism, development, and oogenesis processes (Garcia-Segura et al., 2015) (Fig. 3.3A; Appendix A Suppl. Table 3.1). Further, 2-day fasting produced whole body miR changes that were related to longevity, and such changes were dependent on DRSH-1 (*Drosha* ortholog) (Kogure, Uno, Ikeda, & Nishida, 2017). Additionally, 12-hr fasting induced physiological changes seen in higher organisms such as decreased lipid accumulation, reduced reproductive function, and increased lifespan (Garcia-Segura et al., 2015)(Fig. 3.3A; Appendix A Suppl. Table 3.1). Limited evidence exists for miR regulation by CR in fruit flies (*D. melanogaster*), but studies point to metabolic improvements and an increased lifespan. Comparing high- versus low-nutrient diets (CR mimic), CR flies had altered expression of miR-184, let-7, miR-125, and miR-100, but it was let-7 overexpression in female nervous tissue the one responsible for ~22% increase in lifespan (Gendron & Pletcher, 2017). In a

model of muscular dystrophy in flies, Marrone et al. (Marrone, Edeleva, Kucherenko, Hsiao, & Shcherbata, 2012) elucidated a circuit that involves miR in the Dystrophin glycoprotein complex and is responsible for cellular adaptations during stress. Finally, starvation-induced miR-305 downregulation was capable of activating Dp53 (p53) in the fat body and thus produce metabolic adaptations through nutrient sensing pathways (Barrio, Dekanty, & Milan, 2014). Altogether, the use of CR in lower organisms highlights the great contribution of nutrient sensing pathways to lifespan and healthspan.

In rodents, different tissue types with varied restriction protocols have demonstrated the effectiveness of CR at controlling miR production and exocytosis (Fig. 3.3C; Appendix A Suppl. Table 3.1). In long-lived B6C3F1 mice, ~40% CR for 27 months was able to produce a miR pattern in serum that is related to longevity (Dhahbi et al., 2013). Certain miR appear to be genotype-specific and age-specific in long-lived Ames dwarf mice. Additionally, the pathways these miR impact are related to tumor suppression, inflammation, WNT-, insulin-, mTOR-, and MAPK-signaling pathways (Victoria et al., 2015). Similarly, miR that are commonly observed in serum (Dhahbi et al., 2013) were upregulated in liver in C57B6J mice following increasing CR from 10-30% for two years, and miR-125a-5p was identified as a direct contributor to age-related CR effects (Makwana et al., 2017). When compared to metformin, another life-extending intervention, CR was able to produce a distinguishable signature in liver of mice leading to the alteration of miR-20a, miR-34a, miR-130a, miR-106b, miR-125, and let-7 expression (Noren Hooten et al., 2016) (Fig. 3.3C; Appendix A Suppl. Table 3.1).

In colon and colon mucosa CR seems to be related to anti-inflammatory and anti-carcinogenic effects. In a murine colon cancer model, ten miRs were found to be significantly differentially expressed between three treatment groups (CR, diet-induced obese, and control):

miR-425, miR-196a, miR-155, miR-150, miR-351, miR-16, let-7f, miR-34c, miR-138a and miR-21 (Olivo-Marston et al., 2014). Interestingly, another study showed that one of the functions of miR-150 is increasing cell susceptibility to apoptosis and reducing cell proliferation through decreasing cell cycle progression via initiator of eukaryotic translation protein, eIF5A (Watanabe et al., 2011). A previous study indicated a potential mechanism by which eIF5a used to regulate apoptosis by upregulating p53 protein expression, which in turn increases *Bax* expression (pre-apoptotic member from Bcl-2 family) while decreasing expression of *Blc2* (A. L. Li et al., 2004). Consequently, p53-dependent apoptosis is promoted by the activation of *Bax*, while cell survival signals are repressed (Basu & Haldar, 1998). A balance between these BCL2/BAX and BAX/BAX homodimer formation in mammalian cells is necessary to regulate survival and death signals (Mo, Yu, Theodosiou, Ee, & Beck, 2005). Thus, the upregulation of miR-150 by CR might be linked to the modulation of apoptosis and alteration of cell proliferation. CR is able to significantly downregulate the expression of miR-155 in colon, which is linked to cell apoptosis (Shibuya, Iinuma, Shimada, Horiuchi, & Watanabe, 2010) and proliferation (B. He et al., 2015). Interestingly, miR-155 targets TP53INP1, which is a pro-apoptotic stress-induced gene that activates p53 (Fig. 3.3C; Appendix A Suppl. Table 3.1).

In breast tissue, CR is sufficient to produce miR patterns associated to longevity and aging (Orom et al., 2012). This study demonstrated several miR that were altered after CR treatment, among which the most significantly increased were miR-29c, miR-203, miR-150 and miR-30. Co-transfection assays suggested that miR-203 can downregulate the translation of Caveolin-1 (*Cav-1*). Cav-1 is a scaffolding protein that functionally interacts and regulates signaling molecules such as Protein Kinase A (PKA), Protein Kinase C (PKC), H-Ras, Epidermal Growth Factor Receptor (EGFR), and G-protein α subunit, and its interaction with such proteins is related to Ku70-

mediated apoptosis regulation (Martinez-Outschoorn, Sotgia, & Lisanti, 2015). In a similar way, other miR such as miR-10a, miR-10b, miR-21, miR-124, miR-125b, miR-126, miR-145 and miR-200a (Devlin et al., 2016). In particular, miR-100a has been useful for the detection of stage-specific breast cancer, and might constitute a beneficial CR target for breast cancer patients.

Besides the beneficial effects of CR in peripheral tissues, it also has shown a neuroprotective role by inducing the loss of age-dependent miRs, thus establishing a balance between pro-apoptotic and survival signals in the brain. Data has shown age-dependent miRs, miR-181a-1, miR-30e and miR-34a, to be downregulated by CR in brain tissue, which correspond with the upregulation of *Bcl-2* and downregulation of *Bax*, leading to apoptosome inhibition (Khanna, Muthusamy, Liang, Sarojini, & Wang, 2011) (Fig. 3.3C; Appendix A Suppl. Table 3.1). In primary cerebromicrovascular endothelial cells (CMVECs), CR also reduced oxidative stress, enhanced of *Nrf2* function, and increased miRs related to angiogenic, proliferative, adhesive, anti-apoptotic and anti-inflammatory processes (Csiszar et al., 2014). Collectively, evidence from rodent models shows that CR modulates the expression of several immunometablic and oncogenic miR across tissue types.

Although the evidence in distinct animal models is strong, clinical trials that aim to identify markers relevant to human populations are needed to provide efficacious and sensitive miR biomarkers (Fig. 3.3D; Appendix A Suppl. Table 3.1). Relevant studies have been conducted in Rhesus monkeys to assess the CR miR signature, showing a conserved miR pattern related to growth and insulin signaling as well as regulation of ribosomal, mitochondrial, and spliceosomal pathways (Schneider et al., 2017). Similarly, a study analyzing old monkeys revealed an age-dependent decline in muscle-specific miRs, but CR improved health span and rescued the expression of miR-181b and chr1:205580546, while decreasing miR-451 and miR-144 levels

(Mercken, Majounie, et al., 2013). Finally, one of the only interventions in humans revealed that whole body protein synthesis was inversely related with circulating levels of muscle-specific miRs (myomiRs) (miR-1-3p, miR-133a-3p, miR-133b, and miR-206) in energy restricted (35 days) overweight men (Margolis et al., 2017). Altogether, the evidence suggests that CR-based therapies could target muscle miR and muscle immunometabolism to prevent age-related comorbidities.

3.6. CONCLUSION

Modulation of age-related decline by CR is robust and is related to genetic and epigenetic adaptations to nutrient availability. Short- and long-term CR are able to produce significant changes in different tissues and across species, thus indicating that CR acts through conserved mechanisms, such as immunometabolic pathways. Lastly, CR directly modifies the dynamic DNA methylation/demethylation cycle, as well as histone and protein modifiers like sirtuins, and miRNA to orchestrate the adaptive and long-lasting response, leading to increased lifespan and health span.

CHAPTER 4: CHRONIC CALORIC RESTRICTION FOLLOWING A HIGH FAT-DIET ACTIVATES SKELETAL MUSCLE NUTRIENT SENSING AND PROTEIN RECYCLING IN RATS

4.1. ABSTRACT

Background: Caloric restriction (CR) is an effective strategy for weight loss and risk reduction of chronic diseases. However, the reduction on body weight induces both lean and fat mass loss, and the cellular implications of the loss of muscle mass remains largely unknown. **Objective:** To explore the CR-induced effect on skeletal muscle homeostasis following early life high-fat feeding. **Method:** 5-week old male Sprague-Dawley rats were fed a high-fat diet (45% Kcal fat) ad libitum for 3 months, thereafter maintenance energy required was calculated and were randomized into: HF group ad libitum (HFD), maintenance group fed a control diet (MTN, 100% energy requirement), or the CR group (25% energy restriction) for 6 months. Food intake, body weight (BW), and body composition were regularly monitored and recorded. Six months after the dietary intervention, rats were sacrificed, serum metabolic profile was measured (IGF-1, Insulin, lipid profile), and gene expression analysis was performed in muscle. **Results:** The HFD group showed a 30.5% increase of BW (83.0% of which was from fat), whereas MTN showed a steady weight gain (8.4%). The CR group showed a marked decrease in BW (16.9%), and a significant lean mass reduction of 12.4%. Serum IGF-1 together with peripheral gene expression of Igf1 and Igf1r, and fasting TAG were decreased by CR. Muscle gene expression analysis showed differences in nutrient sensing (Cpt1a, Pgc1a, Pon1, Pon2, mTor), autophagy markers (Atf4, Atg2a, Chop, Gcn2, Lc3a), protein degradation (Atrogin1, Capn1, Capn2, Fst, Inha, Murf1), myogenic markers (Mapk14, Myod1, Pax3, Pax7), and Inflammatory markers (Ifng, Il-1b, Il-6, Nfatc4, Nfkb, Tnf) in CR compared to HFD, and such changes might be related to DNA and histone modifiers (Dnmt1, Sirt1, Sirt6, Suv39h1). **Conclusion:** chronic CR in rats resulted in the activation of nutrient sensing

and protein degradation pathways, which explain the lean mass loss in response to the reduced energy, while preserving the myogenic signals.

4.2. INTRODUCTION

Caloric restriction (CR), without malnutrition, is considered an effective dietary intervention to extend lifespan and quality of life in different organisms (Fontana & Partridge, 2015; Mercken, Crosby, et al., 2013; L. Yang et al., 2016b). The reduction of calories by 25% in CR is thought to act through energy sensing mechanisms that allow the cell to adapt to energy restriction without causing significant stress (Weindruch et al., 1986). However, several studies suggest that the relative ratio of macronutrients, rather than the total energy intake is what drives the increase in lifespan, improvements in metabolic health, and ultimately healthy aging (Solon-Biet, Walters, et al., 2015) (Solon-Biet et al., 2014).

Skeletal muscle is the largest and most metabolically active tissue in the body. It accounts for 85% of the insulin-mediated glucose uptake and lipid metabolism (Esposito, Petrizzo, Maiorino, Bellastella, & Giugliano, 2016; Peppa et al., 2010), and can adaptively respond to a variety of different environmental conditions, nutrition and exercise (Bohnert, McMillan, & Kumar, 2018; Kitessa & Abeywardena, 2016; Meng et al., 2017; Mercken et al., 2017; Sharples, Stewart, & Seaborne, 2016). For example, skeletal muscle function is impaired in obese patients, decreasing its capacity to respond to the metabolic needs of the body. Insulin resistance, a pathology commonly observed in obese patients, is mainly driven by skeletal muscle's inability to respond to insulin-mediated glucose uptake, possibly through lower IRS-1 content and phosphorylation, or failure to activate PI3K (Peppa et al., 2010; Saltiel & Kahn, 2001). Therefore, metabolic stress and over nutrition ultimately impact the ability of muscle to uptake glucose, which in turn activates a sustained stress response that exacerbates the obese state (Meng et al., 2017).

Muscle mass is dynamically regulated by two opposing metabolic pathways; the first is protein synthesis occurring in the anabolic state (Insulin/IGF-1/mTOR pathway), while the second is proteolysis which dictates the amount and specific degradation of protein targets (Ubiquitin proteasome, autophagy and cysteine proteases), which contributes to the amino acid pool during the catabolic condition (Bowen et al., 2015; Mercken, Crosby, et al., 2013; Teixeira Vde et al., 2012). Caloric restriction is a potent stimulator of metabolic homeostasis and maintenance of myofibers. A study in older individuals showed that CR can induce a transcriptional profile in skeletal muscle similar to that of younger individuals (Mercken, Crosby, et al., 2013), and is able to maintain myofiber number and decrease inflammation (Phillips & Leeuwenburgh, 2005). During prolonged caloric restriction, muscle hypertrophy is spared while the low rate of protein synthesis is efficiently used to contribute to basal cellular needs (R. M. Anderson, Shanmuganayagam, & Weindruch, 2009). In humans, chronic CR (15 years) was shown to induce autophagy, oxidative stress and DNA repair systems, mainly mediated through heat shock proteins leading to higher protein-quality control, compared to a population consuming a Western diet (L. Yang et al., 2016b). Therefore, while CR has been shown to induce beneficial cellular adaptation, it is unclear whether the degradation pathways can lead to positive effects in skeletal muscle.

As a dietary mean to prevent aging, CR is shown to stimulate hematopoietic stem cells (Ertl et al., 2008) and satellite cells (Cerletti et al., 2012). Stimulation of satellite cells by CR appears to initiate new fiber formation and muscle repair in a stem cell transplantation mice model (Cerletti et al., 2012). The activation of adjacent stem cells increases the size and number of muscle fibers, which fuse to preexisting muscle fibers in response to stress. The activation of satellite cells from their quiescent state will ultimately lead to proliferation and differentiation into mature myocytes (Buckingham & Rigby, 2014).

Although advances have been made to understand the cellular mechanisms that are at play during CR, most studies compare only the effects of a diseased state such as obesity and then the changes that occur after the dietary intervention. In this study, we sought to investigate the physiological effect of chronic CR following early-life high-fat diet consumption. Additionally, we explored the CR-induced transcriptional signature on skeletal muscle markers of homeostasis (nutrient sensing, protein recycling, myogenesis, inflammation, epigenetic modifiers).

4.3. METHODS

4.3.1. Experimental Design

In the present study, 5-wk-old male Sprague–Dawley rats (N=33) were fed a high fat diet *ad libitum* (HF, 45% calories from fat) (Table 4.1) for 3 months (Fig. 4.1). Thereafter, animals showed a 15% increase in fat mass and were randomized into 3 groups High fat- diet *ad libitum* (HFD), weight maintenance (MTN), and chronic caloric restriction (CR).

Total average daily energy consumption or maintenance energy requirement (MER) was calculated (average Kcal/day) for each individual animal in the MTN and CR groups by feeding AIN-93M (CON, 16% calories from fat) (Table 4.1) diet for 3 weeks *ad libitum* prior to the start of the treatment. During this period, the HFD group continued on the same HF diet. For this period, food intake was recorded daily and the body weight weekly. Following the MER calculation period, animals started their respective 6-month treatment where the HFD group continued on HF diet (n=9), whereas the Maintenance group (MTN) was fed 100% of their MER (100% MER) with AIN-93M diet to maintain body weight without weight gain (n=12), and the Caloric Restriction (CR) group was fed daily 75% of calories (25% MER restriction) with AIN-93M supplemented with micronutrients to reach the vitamin and mineral levels consumed by MTN animals (n=12).

Table 4.1. Diet composition.

	CON	*HF*
Casein‡	14.5	19.7
L-Cystine‡	0.2	0.3
Corn Starch‡	51.5	7.2
Maltodextrin‡	13.0	9.9
Sucrose‡	10.4	17.0
*Cellulose**	50	50
Soybean oil‡	9.4	5.5
Lard‡	-	39.4
*t-Butylhydroquinone**	0.008	-
*Mineral mix**	35	10
*DiCalcium Phosphate**	-	13
*Calcium Carbonate**	-	5.5
*Potassium Citrate**	-	16.5
*Vitamin mix**	10	10
*Choline Bitartrate**	2.5	2

Protein‡	14.7	20
Carbs‡	75.9	35
Fat‡	9.4	45

‡ Kcal percentage. *Grams per 1000g of food.

Animals were individually housed with 12-h light/dark cycles, and given free access to water throughout the study. Food intake and body weight were measured and recorded weekly during the treatment period. After 6 months of treatment, rats were euthanized with CO_2 after an overnight fast (12 hours) to collect blood and tissues for subsequent analysis. To ensure that all rats were presented with comparable metabolic and feeding statuses, food was provided starting at 6:00 PM for all groups. Food was removed starting at 8:00 PM, and the animals were sacrificed starting at 8:00 AM the following day. All applicable institutional and governmental regulations regarding the ethical use of animals were followed during this research (University of Illinois Institutional Animal Care and Use Committee protocol no. 09112).

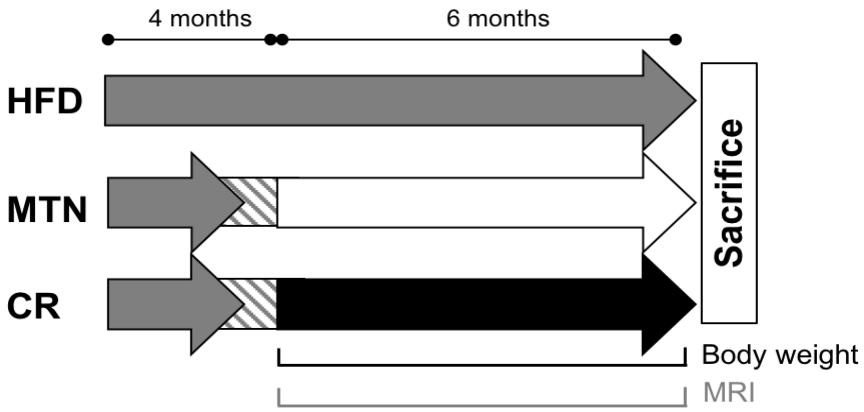

Figure 4.1. Experimental Design. Animals were fed a high fat diet (HFD) for 3 months (45% Kcal from fat), at which point they were randomized into each of the experimental treatments. Following high fat-feeding, the animals were switched to a control diet to calculate the maintenance energy requirements (MER) for each animal. MTN group received 100% of their MER, whereas the CR group received 75% of their MER. HFD group continued on a HFD ad libitum until the end of the study. Body weight was measured weekly, and body composition was performed on a monthly basis. The total duration of the study was 10 months.

4.3.2. Body Composition Measurement

Body composition was measured on Day 1 (initial) and every 30 days after until the end of the study (final), using the EchoMRI-700 Body Composition Analyzer (Echo Medical Systems, Houston, Texas). This approach allows the analysis of fat and lean mass simultaneously in conscious animals using magnetic resonance imaging (MRI) (Strakovsky et al., 2014). Total fat mass was measured using a pure oil standard prior to each measurement, whereas lean mass was calculated as non-water free lean mass.

4.3.3. Biochemical measurements

Trunk blood was collected at necropsy by decapitation, and the subsequent serum samples were prepared and stored at -70°C until future use. Serum lipids were analyzed using the Abaxis Piccolo Xpress^{TM} Lipid Panel Disc, which allows for the simultaneous measurement of total cholesterol (Chol), high-density lipoprotein cholesterol (HDL), low-density lipoprotein cholesterol (LDL), very low-density lipoprotein cholesterol (VLDL), non-high-density lipoprotein cholesterol

(nHDL), and triglycerides (TAG). Serum glucose was determined using TRUE result™ glucose meter (Florida, USA) blood glucose meter. Serum Insulin (Mercodia, Uppsala, Sweden) and IGF-1 (R&D systems, Minneapolis, USA) levels were quantified using rat ELISA kits per manufacturer's instructions. HOMA-IR was calculated using fasting serum glucose and insulin values: $HOMA - IR = \frac{Glucose\left(\frac{mmol}{L}\right) x\ Insulin\left(\frac{mU}{L}\right)}{22.5}$.

4.3.4. RNA Isolation and Two-Step Real Time qPCR

For tissue preparation, 50 mg of liver, 100 mg of muscle and visceral adipose tissue (VAT) were homogenized in liquid nitrogen prior to RNA isolation. Total RNA was isolated and DNAse I treated using the Direct-zol™ RNA MiniPrep (Zymo Research, Irvine, CA, USA) according to manufacturer's instructions. RNA quality was assessed with a Nanodrop (Thermo Fisher Scientific) with a ratio of absorbance at 260/230 and 260/280 both at >1.8. Reverse transcription was performed on 2 µg of RNA using the High Capacity cDNA Reverse Transcription Kit (Applied Biosystems). Quantitative Real time PCR was using the StepOnePlus™ Real-Time PCR System with Power SYBR® Green PCR Master Mix. Quantification was performed using a standard curve with serial dilutions and the dissociation curve was analyzed in each experiment. Real-time PCR primers were designed using the VectorNTI software (Life Technologies, Grand Island, New York), analyzed using BLAST, and synthesized by IDT (Coralville, IA; Appendix B Supplemental Table 4.1). Genes included in our experiment have been previously reported as known markers for each pathway analyzed. mRNA data were normalized to the reference gene encoding ribosomal protein L7a (L7a) as previously reported (Strakovsky et al., 2014).

4.3.5. Statistical Analysis

Average caloric intake, body weight, body composition, and serum biochemical parameters were analyzed one-way ANOVA with a Tukey post hoc comparison in R 3.3.2. All data assumptions

(normality, homogeneity of variances, linearity) were met. Differences were considered significant at $p<0.05$.

4.4. RESULTS

4.4.1. Body Weight and Body Composition

Body weight (BW) and body composition reported here show only the treatment period (6 months), but the 3-month HF feeding nor the 1-month MER assessment periods are not shown as they were not statistically different and no weight loss was observed (Fig. 4.1). Hereafter, initial BW is prior to the start of the treatment and the final BW corresponds to the end of the experiment (6 months of dietary intervention) (Fig. 4.2A). Initial BW was significantly higher in the HFD group, compared to the other two groups. After the dietary intervention, the animals in the HFD and MTN groups showed an increase in BW. BW was the lowest for CR (387.26 ± 15.05, $p<0.05$), followed by MTN (496.50 ± 10.28, $p<0.05$), and the highest in HFD group (635.40 ± 13.33, $p<0.05$). There are significant net increases in BW in HFD and MTN groups, and a decrease in CR group (Δweight final-initial: increase by 129.53 g, 24.47 g and a decrease of 86.09 g for HFD, MTN, and CR respectively) ($p<0.05$). Average daily calorie consumption was different between treatments (Fig. 4.2B), where the lowest energy intake was 44. 70 ± 0.45 Kcal ($p<0.05$) for CR that accounts for ~75% of MER in the MTN group, followed by MTN consuming 100% MER of 60.18 ± 0.64 Kcal ($p<0.05$), and the highest for the HFD group which consumed the average of 76.58 ± 0.57 Kcal ($p<0.05$).

Body composition is presented for fat and lean mass as the initial measurement (after MER establishment) and as the final measurement at the last day of the dietary intervention (Fig. 4.2C

and D). There was a slight difference in total fat mass at the beginning of the intervention (HFD: 74.37 ± 4.93 g; CR: 62.04 ± 5.99 g, MTN: 51.67 ± 3.70 g, $p<0.05$) (Fig. 4.2D), but no differences

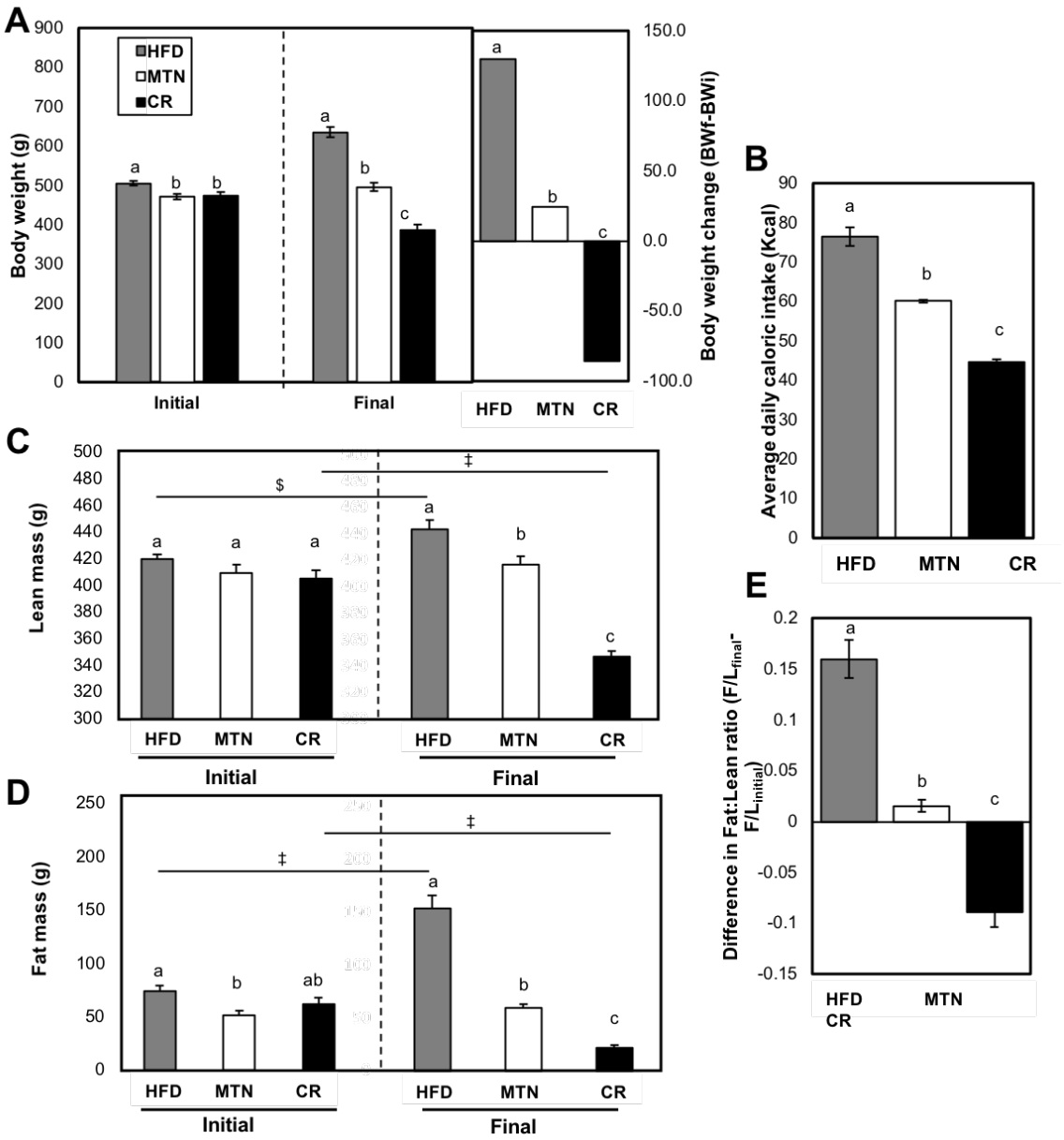

Figure 4.2. Body weight and composition of animals following 6 months of CR. A) Initial (4 months), final (10 months) body weight, and weight change of rats, showed significant differences between all treatments. B) Average caloric intake from the beginning of the dietary intervention (4 months) until the end of the experiment (10 months) highlights the energy consumed based on the energy requirements for each experimental group. Body composition measurement with EchoMRI-700 Body Composition Analyzer showing C) total lean, and D) total fat mass before and after dietary intervention, as well as lean and E) the difference in fat-to-lean ratio. Values are expressed as means ± SEM. ^{abc} Different letters between treatments indicate significant statistical difference with Tukey post hoc test $^{\$}p<0.05$ and $^{\ddagger}p<0.001$.

in total muscle mass were observed (Fig. 4.2C). Fat mass percentage (relative to body weight) was not different between treatment groups at the beginning of the study (data not shown). Significant statistical differences were observed in the CR group for lean (p<0.0001) (Fig. 4.2C) and fat (p<0.0001) (Fig. 4.2D) mass from initial to final assessment (after 6 months of dietary intervention). No differences were observed in lean mass (p=0.42) or fat mass (p=0.22) from the beginning to the end of the study for the MTN group (after 6 months of dietary intervention). At the end of the study (after 6 months of dietary intervention), rats in the HFD group showed a significant increase in lean (p<0.05) (Fig. 4.2C) and fat mass (p<0.001) (Fig. 4.2D), with the highest values among all groups. Differences in fat-to-lean ratio (final-initial) were the lowest for CR (decreased 0.08 units; lean mass 346.96 ± 4.66 g and fat mass 21.95 ± 2.41 g) then MTN (increased by 0.01 units; lean mass 416.91 ± 6.58 g and fat mass 59.35 ± 4.17 g), and highest in HFD (increased by 0.16 units; lean mass 443.55 ± 6.84 g and fat mass 153.79 ± 11.66 g) (Fig. 4.2E).

4.4.2. Growth Signal Assessment

Changes in growth responses were estimated through the analyses of serum hormones insulin and IGF1, as well as gene expression of *Igf1* and its receptor *Igf1r* in different metabolic tissues. Serum insulin levels were not significantly different between groups (Fig. 4.3A). A marginal decrease in insulin was observed in the CR group, but it was not statistically different (CR: 0.65 ± 0.12 ng/mL vs. MTN: 0.95 ± 0.10 ng/mL, HFD: 0.74 ± 0.18 ng/mL). Moreover, serum IGF-1 levels were significantly lower in CR (0.75 ± 0.04 ng/mL, p<0.05), compared to both MTN and HFD (1.01 ± 0.02 and 1.02 ± 0.04 ng/mL, respectively, Fig. 4.3A). Given that growth signals known to originate from different metabolic tissues (H. R. Chang, Kim, Xu, & Ferrante, 2016), we characterized the gene expression of *Igf-1* in different metabolic tissues (liver, muscle, and visceral adipose tissue

[VAT]). In liver, gene expression of both *Igf-1* and its receptor *Igf1r* were decreased by CR (Fig. 4.3B, $p<0.05$), and only *Igf1r* for MTN, compared to HFD. This corresponded to a significant

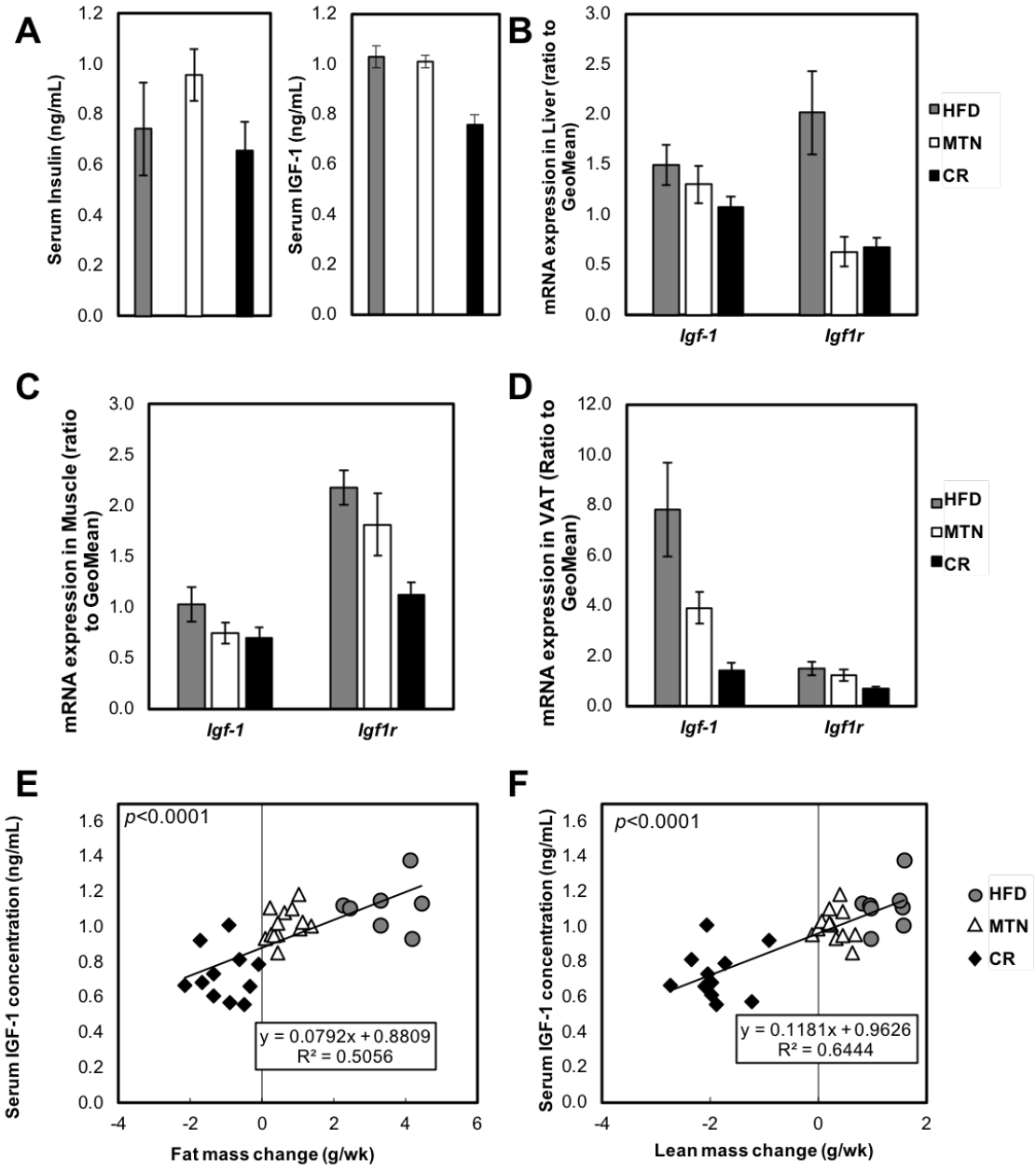

Figure 4.3. Growth signal and receptor expression are altered with chronic CR. A) Serum IGF-1 and Insulin levels are expressed in ng/mL. Gene expression of Igf-1 and Igf-1r from B) liver, C) Muscle, and D) Visceral Adipose Tissue (VAT) shows alterations in the expression of both hormone and receptor gene expression. Linear regression of IGF-1 to E) Fat and F) Lean mass slope. Fat and lean mass changes are represented as the slope of the regression vs. time of treatment.

reduction in liver weight by CR ($p<0.05$), compared to MTN and HFD (Data not shown). Additionally, VAT expression of *Igf1* was decreased CR ($p<0.05$), compared to HFD (2-fold) and MTN (1.8-fold); no changes were observed for *Igf1r* in VAT (Fig. 4.3D). Skeletal muscle *Igf1r* mRNA expression was decreased in CR compared to both MTN and HFD, whilst no differences were observed for *Igf1* mRNA expression in muscle (Fig. 4.3C). Finally, a regression analysis of body composition and serum IGF1 revealed a significant predictive Pearson correlation of fat (R^2= 0.505) (Fig. 4.3E), and lean mass (R^2= 0.644) (Fig. 4.4F) with the serum IGF1 levels. Additionally, a high Pearson correlation coefficient was found between the average caloric intake and IGF1 (R^2= 0.639), but not for insulin (R^2=0.04) (Data not shown).

4.4.3. Biochemical measurements

Table 4.2. Serum Biochemical Analysis of CR Animals Following Early Life HF-Feeding.

	HFD		MTN		CR	
Chol[1]	103.80	± 14.3	100.17	± 9.6	98.71	± 12.9
HDL-c[1]	59.00	± 9.7	50.67	± 6.8	45.83	± 2.5
TAG[1]	160.80	± 19.8 [ab]	186.83	± 27.4 [a]	109.43	± 10.9 [b]
Glu[1]	156.40	± 21.4	126.67	± 11.8	173.29	± 18.9
HOMA-IR[2]	5.95	± 1.4	5.39	± 0.4	3.85	± 0.6
nHDL[1]	44.40	± 6.9	49.83	± 3.2	41.00	± 2.6
TC/H[2]	1.82	± 0.1	2.03	± 0.1	1.92	± 0.1
LDL-c[1]	13.60	± 6.2	14.83	± 4.3	19.00	± 3.1
VLDL-c[1]	32.20	± 4.0 [ab]	37.33	± 5.6 [a]	21.86	± 2.2 [b]
ALT[3]	47.80	± 1.4	59.57	± 8.7	54.71	± 3.7
AST[3]	170.40	± 8.7	180.43	± 24.7	168.43	± 18.7

Values are presented as means ± SEM. [1]Data are expressed as mg/dL; [2]Data are expressed as arbitrary units; [3]Data are expressed as U/L. [ab] Different letters between treatments indicate significant statistical difference at $p<0.05$ with Tukey's post hoc test. Chol: Total cholesterol; HDL-c: high-density lipoprotein cholesterol; TAG: triglycerides; Gluc: Fasting Glucose; LDL-c: low-density lipoprotein cholesterol; VLDL-c: very low-density lipoprotein cholesterol; nHDL: non-high-density lipoprotein cholesterol; HOMA-IR: Homeostatic Model Assessment-Insulin Resistance; AST: aspartate aminotransferase; ALT: alanine aminotransferase.

To assess the metabolic status of the animals, lipid profile and hepatic function enzymes were assessed in serum samples at the end of the experiment (6 months after dietary intervention) (Table 4.2). Circulating levels of TAG were lowest for CR (109.43 ± 10.94 mg/dL, 41% decrease) ($p<0.05$), compared to MTN group (186.83 ± 27.38 mg/dL) ($p<0.05$) and HFD (160.80 ± 19.77 mg/dL). Similar results were observed for fasting VLDL (CR: 21.86 ± 2.21 mg/dL vs. MTN: 37.33 ± 5.52 mg/dL and HFD: 32.20 ± 3.99 and). A numerical decrease was observed for HOMA-IR index for CR compared to HFD but no statistical difference was observed. No other changes in lipid profile or liver enzymes were observed between groups (Table 4.2).

4.4.4. Skeletal muscle gene expression analysis

To elucidate the metabolic and immunologic mechanisms that mediate the changes observed for muscle mass, we assessed the effect of the dietary intervention in gene expression pattern of nutrient sensing, autophagy-related, myogenic-related, inflammatory genes and chromatin modifier markers. Statistical differences are reported using the HFD group consuming high fat-diet throughout the study as a control (Fig. 4.4). Nutrient sensing systems are vital for appropriate nutrient uptake and usage in skeletal muscle. Therefore, nutrient sensing genes were analyzed in skeletal muscle of rats. Mamalian target of Rapamicyn (*mTor*) was significantly different in CR compared to HFD (1.1-fold), but not MTN (Fig. 4.4A). Beta-oxidation markers *Cpt1a* (Carnitine Palmitoyltransferase 1A) and *Mlycd* (Malonyl-CoA Decarboxylase) were both increased in the HFD group compared to CR and MTN. Antioxidant enzymes Paraoxonase 1 and 2 (*Pon1* and *Pon2*) differed significantly in the CR compared to both MTN and HFD (-1.8 and -1.5-fold for *Pon1*; -1.2-fold for *Pon2*) (Fig. 4.4A).

Protein turnover genes related to autophagy were not different between CR and MTN. Significant differences were observed for *Atf4*, between CR and HFD (Fig. 4.4B).

Autophagosome-formation proteins *Atg2a* and *Lc3a* (microtubule associated protein light chain α) were increased in CR and MTN, compared to HFD (-1.2- and -1.4-fold). Cysteine proteases *Capn1* and Capn2 and proteasomal E3 ligase *Murf1* were significantly increased by CR, whereas E3 ligase *Atrogin1* was significantly upregulated by HFD group (1.3-fold) (Fig. 4.4B).

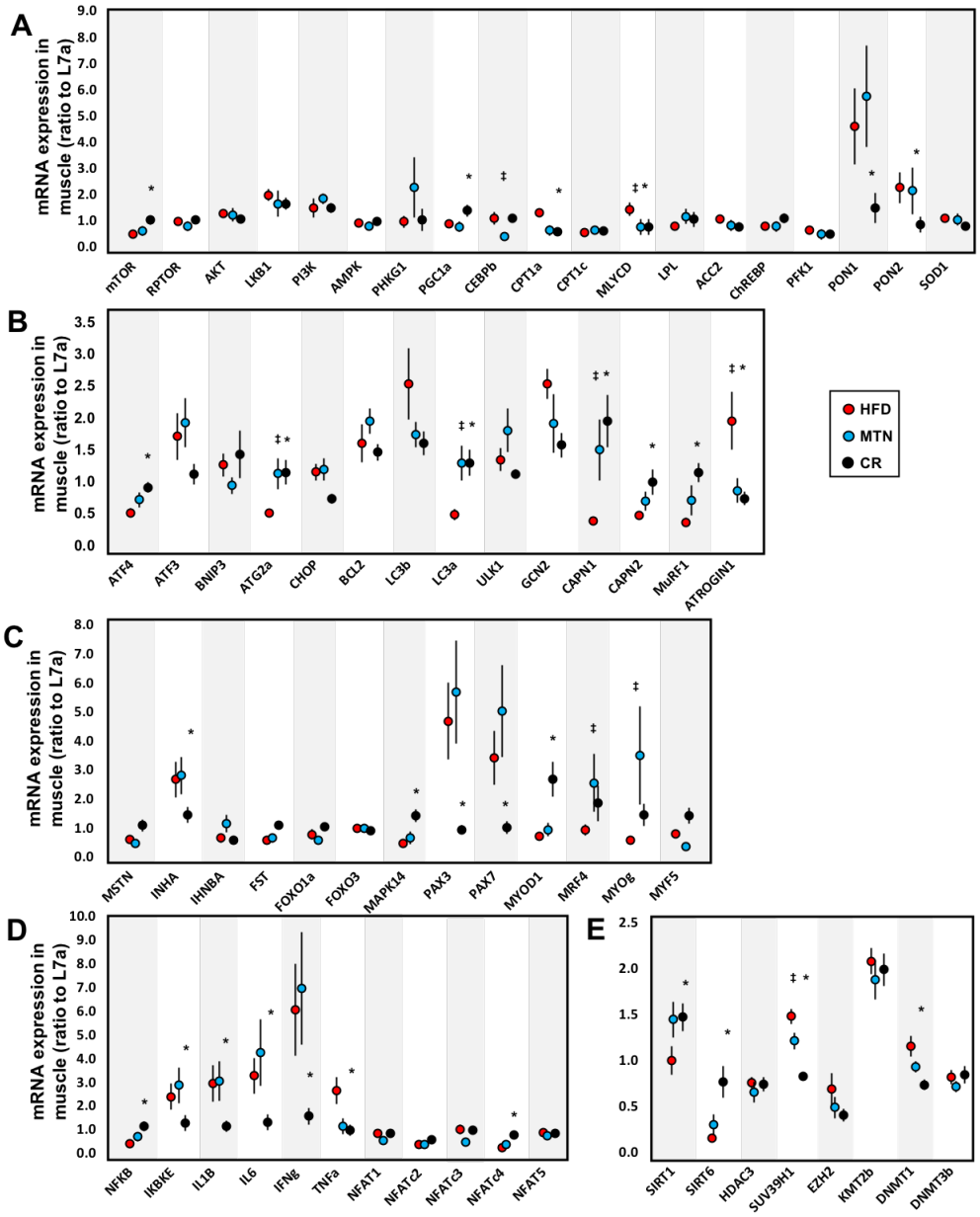

Figure 4.4. Gene expression of nutrient sensing, proteostasis-, and inflammatory- related pathways and epigenetic modifiers from skeletal muscle using qPCR. Values are means of the ratio to L7a ± SEM; HFD (n=9), MTN (n=12), CR (n=12). *$p \leq 0.05$ for CR vs. HFD and ‡for MTN vs. HFD.

The pathways that lead to atrophy were analyzed, mainly the Activin-Myostatin-Follistatin system (Fig. 4.4C). No significant changes were observed for myogenic activator *Fst*; however, the myogenic inhibitor Myostatin (*Mstn*) was significantly upregulated in the CR group compared to MTN (1.2-fold), but was not different from HFD. No changes were observed for Activin A (*Inhba*) and inhibin (*Inha*). Myogenic transcription factor *Mapk14* was upregulated by CR, compared to both MTN and HFD (1.2- and 1.5-fold, respectively) (Fig. 4.4C). Early myoblast differentiation factors *Pax3* and *Pax7* showed an inverse pattern (-2.0-fold), with CR having the lowest values. Concurrent pathways that are known to impact atrophy such as inflammation were explored. Markers of skeletal muscle precursor proliferation, differentiation, and fiber homeostasis were measured. CR showed higher expression values for *MyoD* compared to HFD (1.8-fold). The main differences between HFD and MTN were for the expression of *MyoG* and *Mrf4*, where the first two had significantly higher values in MTN (-2.5- and -1.4-fold, respectively) (Fig. 4.4C). Inflammatory markers that are known to regulate myogenesis and muscle wasting were assessed (Fig. 4.4D). Inflammatory cytokine expression of *Tnf-α*, *Ifn-γ, Il-1β, and Il-6* was significantly reduced in CR, despite the increased expression of *Nfkb* (p50 subunit), and possibly due to the reduced *Ikbke* expression in the CR group, compared to HFD

Finally, chromatin modifiers were measured in skeletal muscle to assess possible epigenetic regulation by CR. Maintenance DNA methyltransferase *Dnmt1* was reduced by CR (Fig. 4.4E). Significant increases in mRNA expression were observed for NAD-dependent protein deacetylases *Sirt1* and *Sirt6* in CR animals, compared to HFD (Fig. 4.4E). Both CR and MTN were able to reduce the expression of histone-lysine methyltransferase *Suv39h1*. An integrative view of the epigenetic regulation of gene expression in muscle is summarized in Fig. 4.5.

4.5. DISCUSSION

In this paper, we assessed the effectiveness or a chronic caloric restriction (CR) protocol in high fat-fed animals. We observed that when animals are subjected to a 25% restriction of calories, striking changes in body weight and composition are observed, which are not observed with a maintenance diet. Furthermore, synthesis of growth hormone IGF-1 appears to be modulated by CR in liver and visceral adipose, and it impacts the circulating levels of this hormone, which are

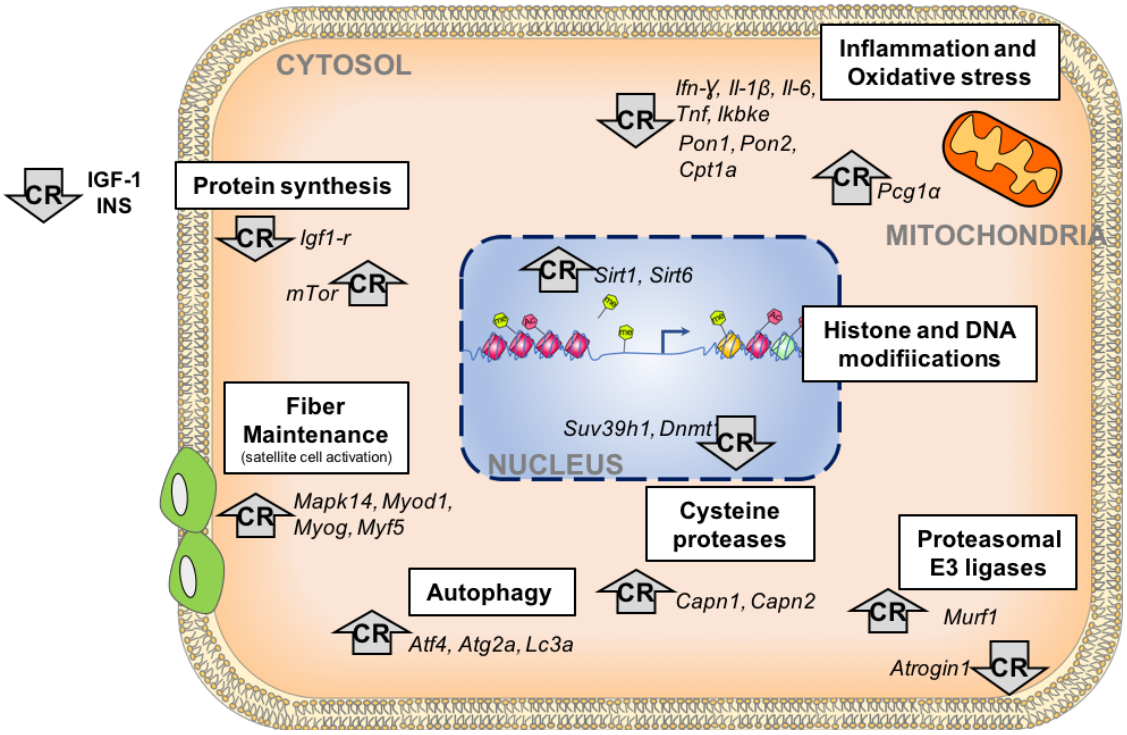

Figure 4.5. Transcriptional Regulation of Skeletal Muscle by CR compared to High Fat Diet. Genes where a significant effect was found are highlighted in yellow. Arrows for CR group indicate the direction of the effect compared to the HFD control. IGF-1, Insulin-like Growth Factor -1; *Igf1r*, Insulin-like Growth Factor -1 Receptor; INS: Insulin; *mTor*, mammalian Target of Rapamycin; *Ifn-ɣ*, Interferon-ɣ*, IL-6, Interleukin-6; IL-1β,* Interleukin-1β; *Tnf,* Tumor necrosis factor-α; *Ikbke*, Inhibitor of nuclear factor kappa-B kinase subunit epsilon; *Pgc-1α*, Peroxisome proliferator-activated receptor gamma coactivator 1-alpha; *Pon1*, Paraoxonase 1; *Pon2*, Paraoxonase 2; *Cpt-1α*, Carnitine palmitoyl transferase-1α; *Suv39h1*, Histone-Lysine methyltransferases Suppressor of variegation 39 homolog 1; *Dnmt1*, DNA methyltransferase 1; *Sirt1*, Sirtuin 1; *Sirt6*, Sirtuin 6; *Mapk14*, Mitogen Activated Protein Kinase 14; *Myod1*: Myogenic Differentiation 1; *Atf4*, Activating Transcription Factor 4; *Lc3a*, Microtubule-Associated Protein 1 Light Chain 3 Alpha; *Atg2a*, Autophagy Related 2A; *Capn1*, Calpain 1; *Capn2*, Calpain 2; *MuRF-1*, Muscle-Specific RING Finger Protein 1; *Atrogin 1*: Muscle Atrophy F-Box Protein.

predicted by the changes in fat and lean mass. Finally, for the first time we report and integrative view of the cellular transcriptional adaptation to CR in skeletal muscle, where nutrient sensors and protein degradation pathways are impacted, whereas myogenic signals are increased to compensate the nutrient restriction. Additionally, pathways that inhibit myogenenesis, such as inflammation and oxidative stress are silenced by CR. We propose a direct effect of CR on epigenetic modulators that can in turn revert the programming of high fat diet.

Caloric restriction (CR) is regarded as an effective tool for weight management control, as well as the long-term effects on lifespan. Previous studies have highlighted the potential effects of chronic CR on quality of life, but recognizing the importance of skeletal muscle as one of the major contributors to metabolic homeostasis. In our study, we aimed to define the molecular mechanisms that are at play in skeletal muscle of high fat-fed rats after a period of chronic caloric restriction. Following the high fat-diet (HFD) feeding period, the animals underwent a CR regiment for six months. For the first time, we used a maintenance control (MTN) to account for normal growth and weight changes, and to to assess the differential response attributed exclusively to CR. Compared to traditional CR studies, the addition of a control group that is neither obese nor restricted (MTN) eliminates the growth bias while highlighting the effects of chronic restriction, compared to a HFD overconsumption animal model (HFD). Compared to HFD, the CR group presented a preferential decrease of fat and lean mass, as observed for calorie restriction protocols without exercise (S. E. Mitchell, Delville, et al., 2015). Weight maintenance (MTN) does not produce the same effect on weight and composition as the 25% restriction (CR), nor the HFD overconsumption (HFD). Meanwhile a positive energy balance in the HFD group, not only in fat but also lean mass, delineate the phenotypical differences with the CR group that might be able to explain the molecular discrepancies observed in both fat and muscle mass.

The effects on body composition are regulated, at least in part, by hormonal adaptations to the energy intake. Hormones such as Insulin and Insulin-like Growth Factor-1 (IGF-1) can elicit an anabolic response in a variety of tissues, stimulating the uptake of glucose from the blood, synthesis of proteins and fatty acids, thus contributing to the overall positive contribution of overfeeding to body mass. We observed a reduction on circulating levels of IGF-1, which is consistent with previous studies (S. E. Mitchell, Delville, et al., 2015). Increased synthesis of IGF-1 at the primary site of production and stimulation ability through the binding to IGF1R in the liver, are hallmarks of obese individuals (Sharples et al., 2016), which lead to the development of metabolic abnormalities. Liver size, and hepatic levels of *Igf-1* and *Igf1r* transcripts appear to be responsive to the consumption of HFD or 25% caloric reduction. Likewise, peripheral metabolic tissues such as skeletal muscle and adipose tissue showed significant differences in the expression of *Igf-1* and *Igf1r*, indicating an adaptation mechanism to the energy intake that can be reverted by chronic CR. Recently, the secretion of IGF-1 by the adipose tissue has been explored as a major site of synthesis (H. R. Chang et al., 2016), thus the greater ability of fat depots to secrete IGF-1 provides an insight into the elevation of circulating hormone, without changes in the ability of the liver. Lastly, the levels of circulating IGF-1, but not insulin, appear to be responsive to the restriction of calories and could help to explain the adaptive mechanism of liver, skeletal muscle, and adipose tissue that reduce the stimulation by anabolic hormones. Peripheral adaptations to the reduced anabolic stimulation in the CR group, lead to the progressive reduction in fat and lean mass that are correlated with the circulating hormone levels. Consequently, given the reduction in the stimulatory capacity of IGF-1 by CR, the liver and adipose reduce their synthetic capabilities as well as the possible stimulation through IGF1R, therefore contributing to the concomitant reduction in both fat a lean mass.

Given the changes in body composition observed in CR, we sought to explore the changes at the transcriptional level that are mediated by the caloric input in muscle. Aside from being the largest tissue in the body, skeletal muscle plays a key role in metabolic and hormonal regulation. In this study, three major pathways that are known to contribute to muscle mass accretion or loss were explored: Nutrient sensing, autophagy, and myogenesis and atrophy. Regarding skeletal muscle nutrient sensing systems, *mTor* and *Pgc1-α* appeared to be significantly increased by CR, and it's in agreement with positive changes in nutrient sensing epigenetic regulators *Sirt1* and *Sirt6*. Consistent with the insulin resistant phenotype, the HFD group displayed a switch towards a fatty acid oxidation-dependent metabolism given the high expression of both *Cpt1a*. This indicates that the adaptation of skeletal muscle to HFD is to obtain energy mainly from fatty acids, compared to MTN and CR. Both 25% restriction (CR) and no restriction (MTN), seem to be efficient at utilizing nutrients, and are not entirely dependent on fat, whilst reducing the expression of inflammatory markers *Tnf-α*, *Ifn-γ, Il-1β,* and *Il-6, and* increased antioxidant enzymes *Pon1* and *Pon2*, indicating a reduction of stress burden in skeletal muscle by CR.

Protein turnover in skeletal muscle is vital for growth, adaptation and maintenance of skeletal muscle fibers. The major pathways that lead to protein recycling are the autophagosome, Ubiquitin-proteasome, and cysteine proteases (Bowen et al., 2015). This allows the cell to target the degradation of proteins that are not necessary, this to obtain resources needed for "dynamic proteostasis" or proper adaptation to the lack of nutrient availability. Autophagic responses are vital for the proper recycling of cellular components during prolonged starvation (L. Yang et al., 2016b). Marked differences in autophagic markers (*Atf4, Atg2a*, and *Map1Lc3a*) were observed between MTN and CR vs. HFD. Moreover, E3 Ligases were differentially expressed in skeletal muscle in response to CR, where *Murf1* was significantly increased compared to both MTN and

HFD groups, indicating that a higher degradation of potential targets such as enzymes able to generate ATP indirectly, as well as directly such as ATP synthase and creatine kinase, and also those proteins related to myofibrils like Titin, TnI, TnT, Myotilin among others (Witt, Granzier, Witt, & Labeit, 2005). On the other hand, E3 Ubiquitin ligase *Atrogin-1* was highly expressed in skeletal muscle from HFD rats, compared to both MTN and CR. Unlike MuRF1, proteasomal protein Atrogin1 can target eIF3-f (Lagirand-Cantaloube et al., 2008) and MyoD1, a potent transcription factor that induces cell cycle exit and activation of differentiation, for proteasomal degradation (Lagirand-Cantaloube et al., 2009). Both IFNγ and TNFα are known activators of *Atrogin 1* (Y. P. Li et al., 2005), which is consistent with our findings of increased inflammation in HFD that leads to targeted MyoD-degradation through Atrogin1. Activation of proteosomal ligases seems to be indicative of atrophy, despite the increase in muscle mass for the HFD group. Finally, calcium-dependent cysteine proteases *Capn1* and *Capn2* expression was increased by CR and MTN. The Calpain family of proteins are thought to act upstream of the Ubiquitin proteasome by initiating the cleavage of nebulin an titin (J. Huang & Forsberg, 1998), proteins related to sarcomere integrity. Interestingly, during CR the levels of *Capn 1* and *2* were increased as well as proteasomal activation (*Murf1*), both of which are thought to be required for differentiation to myocytes to occur (Ueda et al., 1998). Moreover, the transcript level of *MyoD1* in CR animals was significantly higher compared to both MTN and HFD, indicating a possible link between the recycling of proteins (autophagy, proteasome, calpains) and funneling of substrate towards differentiation. No indication of myogenesis (*Mrf4*, *MyoG*, *MyoD*) was found for the HFD group, suggesting that the *Atrogin 1* levels might be more related with atrophy rather than with differentiation and proliferation. In the context of energy restriction, myogenic factors (*MyoD, Mrf4, MyoG*, and *Myf5*) can couple the response to lower nutrient influx with the greater

availability of substrate from proteolysis, and in turn they might activate resident stem cells to proliferate and differentiate, as seem with short term caloric restriction (Cerletti et al., 2012). The flux through the autophagosome and ubiquitin-proteasome systems in lean versus obese individuals might differ; In an obese condition the upregulation of the proteasome is the preferred mechanism whereby proteins are recycled and this is an adaptive mechanism to the nutrient influx in HFD (Bollinger, Powell, Houmard, Witczak, & Brault, 2015). On the other hand, the flux through the autophagy/lysosome pathway might be stimulated in CR and the activation of both systems might help to regenerate muscle mass in response to prolonged CR. This explains the preferred activation during caloric overload and deprivation, as well as the downstream effects of the activation of different pathways that perpetuates the phenotype observed in skeletal muscle.

Epigenetic regulation occurs through covalent modifications exerted by a myriad of chromatin and DNA modifiers. As previously discussed, epigenetic modifiers such as HDAC3 are known to regulate the expression of the TNF gene; however, other modifiers are known to act within proximal or distal regions to modulate its expression. A novel NAD^+-dependent deacetylase, SIRT6, has emerged as a possible candidate that extends lifespan (Kanfi et al., 2012; Michishita et al., 2008) and inhibits the activity of NFkB in different cellular models (N. Zhang et al., 2016). Therefore, despite the increased *Nfkb* expression by CR, Sirt6 might act as a repressor of the inflammatory signal. Interestingly, no information is available regarding the epigenetic modulation of cytokine signaling in muscle during CR. The Histone-Lysine N-Methyltransferase, suppression of variegation 3-9 homolog 1 (SUV39H1), has been regarded as an important regulator of inflammation (T. T. Chen et al., 2017; Villeneuve et al., 2008). In our study, we observed a repression of *Suv39h1* by the maintenance group (MTN) or CR. Interestingly, inflammatory cytokine TNF itself can interact with Ezh2 (within the transcriptional inhibitor

complex PRC2), to produce the silencing of the myogenic transcription factor Pax7 that stimulates satellite cell differentiation (Palacios et al., 2010). Finally, both DNA methyltransferases, DNMT1 and DNMT3A, are known to impact inflammation upon stimulation with different stimuli (Cheng et al., 2014; Falvo et al., 2010; J. Yu et al., 2016). In our study, we observed a reduction of Dnmt1 which agrees with the decrease in inflammatory markers in skeletal muscle of CR animals.

In conclusion, the beneficial effects that can be attributed to CR following a HFD consumption are related to weight loss, and the repression of inflammation and oxidative stress, together with the activation of protein turnover pathways can in turn promote myogenesis to maintain a critical muscle mass. Future studies regarding the coupling of caloric restriction signals and epigenetic regulation of metabolic pathways are needed, this to fully understand the programming of adaptive mechanisms by chronic CR.

CHAPTER 5: TITRATION OF ALTERNATE DAY CALORIC RESTRICTION (ADCR) MINIMIZES MUSCLE WASTING AND DECREASES INFLAMMATION IN MALE RATS

5.1. ABSTRACT

Background: Caloric restriction (CR), without malnutrition, is considered an effective dietary intervention to extend lifespan and quality of life, and such effects include those related to musculoskeletal health; however, patient adherence to the CR protocol remains a challenge. Alternate Day Caloric Restriction (ADCR) consists of controlled feeding alternated with CR, and has proven to be overcome adherence limitations as well as to cause weight loss. **Objective:** Using a 3X3 factorial restriction protocol (three degrees of restriction, and 3 restriction schedules) we aim to explore body composition and muscle transcriptomic changes in high fat diet (HFD) model. **Methods:** 4-week old Male rats consumed a HFD (45% calories from fat) for 3 months, maintenance energy requirement (MER) was calculated for 3 weeks, and from then on, ADCR began by consuming a normal chow diet on the feeding days (100% of MER), followed by alternated consumption of 75% (IF1-3), 50% (IF4-6) or 25% (IF7-9) of ER during one, two or three days per week. A chronic CR (25% ER) groups was used as control. Food intake, body weight (BW), and body composition were regularly monitored and following six months of ADCR, animals were sacrificed. **Results:** No significant BW differences were observed for the 25% restriction groups (IF1-3). Of the 50% ER groups, only the 3-day restriction (IF6) produced similar effects to CR. Both 2- and 3-day 75% ER groups (IF8 and 9) produced similar effects to CR. Serum nutrient-sensing intermediates IGF-1 positively correlated with final fat and lean mass (p<0.0001), whereas insulin and HOMA-IR were only correlated to final fat mass (p<0.0001). Skeletal muscle gene expression of nutrient sensing and protein recycling markers showed that CR and 3-day 75% restriction (IF9) produced similar effects, whereas IF5-8 produced a discriminant

transcriptional pattern. Finally, skeletal muscle *Tnf* showed a marked decrease for all 50% and 75% restriction groups similar to CR. **Conclusion:** Energy reduction by 50% 3 days per week, or 75% restriction more than two days per week is an effective weight loss strategy to reduce muscle inflammation.

5.2. INTRODUCTION

Caloric restriction (CR) has been regarded as one of the most effective strategies for weight reduction, with the addition of the long-term benefits such as delayed aging and improved quality of life (Cava & Fontana, 2013; Fontana & Partridge, 2015). Nevertheless, the feasibility of voluntary, chronic CR in humans still remains the greatest challenge in the clinical practice. Novel strategies for weight control have emerged and provide a safer yet effective alternative to reduce or maintain body weight. Such strategies derive from the original ~25% energy restriction that the usual CR protocol describes, and substitute the daily restriction for alternating fasting and feast days. Given the limitations of the current CR protocols, novel strategies are required that can confer the benefits related to CR while providing higher translatability to a clinical setting.

CR is able to act on diverse pathways that permit the extension of lifespan and health span; the benefits associated to caloric restriction and other forms of restriction include but are not limited to improvement of stem cell function, decrease in oxidative stress, improvement of nutrient sensing pathways, protein recycling enhancement, reduction of insulin resistance, prevention of genomic instability, and modulation of inflammation and immune function (Fontana & Partridge, 2015). Dietary or calorie restriction protocol that provide the same energy by implementing modified protocols have found similar if not better health outcomes. Protocols that implement “fasting” and “feasting” days alternated are termed Alternate Day Fasting or Alternate day CR (ADCR) (Varady & Hellerstein, 2007), and can modulate risk factors that lead

to the development of chronic diseases in animal models. However, despite the great potential ADCR on chronic disease risk reduction, the feasibility of such restrictive protocols for long periods of time has been questioned given that the hunger sensation during fasting days does not seem to decrease, and the addition of small meal during those days was not able to increase the fullness sensation (Johnstone, 2015). Nevertheless, such modification to the widely used CR method has been used in many human studies (Johnson et al., 2007; Varady, Tussing, Bhutani, & Braunschweig, 2009) (Stockman, Thomas, Burke, & Apovian, 2018), proving the effectiveness of ADCR to both improve patient compliance and improve risk markers.

Weight loss studies in human populations have found that the partial restriction of calories during the "fasting" day to only 20% of the calories, which resulted in a marked 8% body weight reduction after 8 weeks of ADMF (Johnson et al., 2007). Collectively these studies highlight potential of dietary caloric restriction, in particular ADCR, as a positive strategy for weight loss with the great translational competence. Therefore, the purpose of this study was to assess whether the implementation of different restriction levels (25%, 50% and 75% restriction) during alternated fasting periods (one-, two-, or three- days a week) interspersed with feasting days could elicit comparable effects to chronic CR. To analyze the complexity of the responses we took advantage of the newly developed Geometric Framework for Nutrition (GFN) (Simpson, Le Couteur, James, et al., 2017; Simpson, Le Couteur, Raubenheimer, et al., 2017; Solon-Biet, Mitchell, et al., 2015), which offers a platform for tackling this complexity in terms of macronutrient limitation. Finally, we assessed the transcriptional signature of skeletal muscle, a tissue of great importance for the young and elderly populations undergoing CR, and compared the effects to the gold standard, chronic 25% CR.

5.3. METHODS

5.3.1. Experimental Design

In the present study, post-weaning, 4-5-wk-old male Sprague–Dawley rats (N=144) were fed a high fat diet (HFD, 45% calorie from fat) for 3 months (Fig. 5.1). Food intake and body weight were measured and recorded weekly. Hereafter, the animals were randomized into 12 groups, and one of those groups (OL) was fed with HFD for the entirety of the study, whereas for the remaining 11 groups the Maintenance Energy Requirement (MER) or the basal energy requirement was estimated. To establish MER, the remaining animals in the 11 groups (not OL) were fed AIN-93M diet for 3 weeks *Ad libitum* prior to the start of the treatment diets for the adjustment and establishment of the MER, calculated as the average daily individual caloric intake within 3 weeks (Fig. 5.1). After this feeding period, animals were randomized into 11 groups: Maintenance group (ML) that was provided with 100% MER, to avoid overfeeding (n=12). Caloric Restriction (CR) group, which was fed daily with a diet to meet 75% of MER supplemented with micronutrients to reach optimal vitamin and mineral levels similar to ML group (n=12); lower alternate-day caloric restriction (low ADCR) with 75% MER restriction for 1 (IF1), 2 (IF2), or 3 days (IF3), alternated with days where they received 100% of MER; intermediate alternate-day caloric restriction (mid ADCR) with 50% MER restriction for 1 (IF4), 2 (IF5), or 3 days (IF6), alternated with days where they received 100% of MER; and high alternate-day caloric restriction (high ADCR) with 25% MER restriction for 1 (IF7), 2 (IF8), or 3 days (IF9), alternated with days where they received 100% of MER. Animals continued on their respective maintenance, CR, or ADCR protocols for 6 months, and after this period all rats were euthanized with CO_2 after 12 h of overnight fasting. Body composition was evaluated by scanning fat and lean mass in a Body Composition Analyzer (Echo Medical Systems, Houston, TX, USA). Blood collection, tissue dissection and weighing

were performed at necropsy. To ensure that all rats were presented with comparable feeding statuses, food was placed starting at 6:00 PM for all groups. Food was removed starting at 8:00 PM, and the animals were sacrificed starting at 8:00 AM the following day. The animals were individually housed with 12-h light/dark cycles, and given free access to water throughout the study. All applicable institutional and governmental regulations regarding the ethical use of animals were followed during this research (University of Illinois Institutional Animal Care and Use Committee protocol no. 09112).

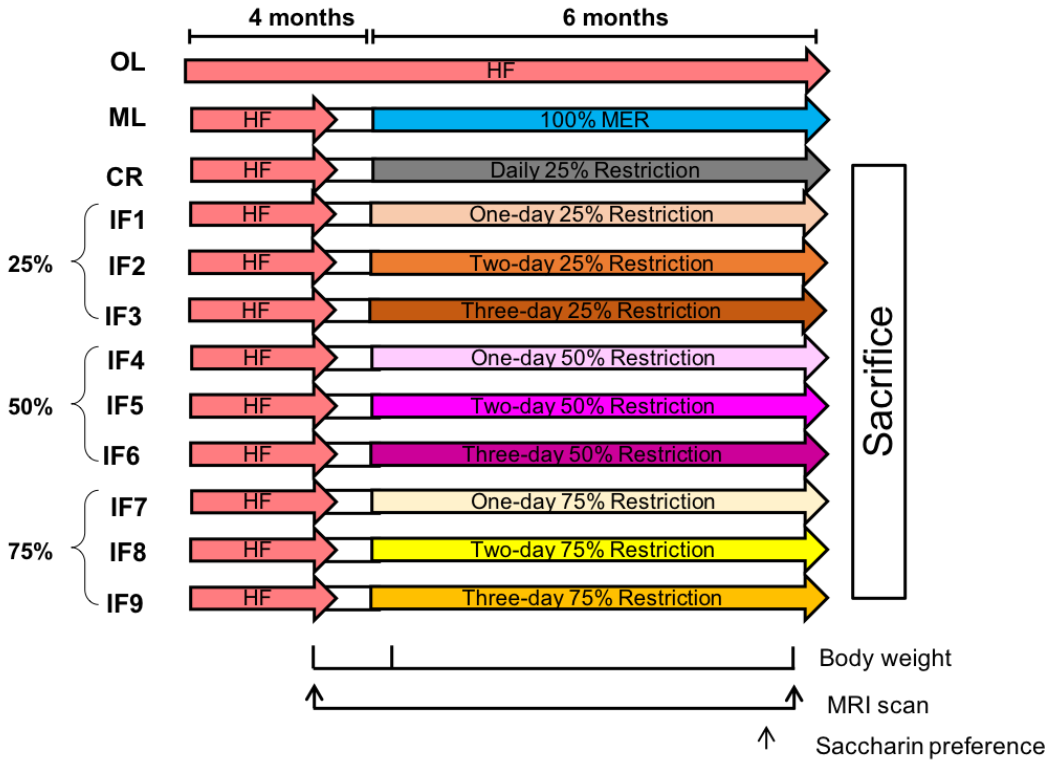

Figure 5.1. Experimental Design. Animals were fed a high fat diet (HFD) for 3 months (45% Kcal from fat), at which point they were randomized into each of the experimental treatments. Following high fat-feeding, the animals were switched to a control diet to calculate the maintenance energy requirements (MER) for each animal. ML group received 100% of their MER, whereas the CR group received 75% of their MER. OL group continued on a HFD ad libitum until the end of the study. Low alternate-day caloric restriction (low ADCR) with 75% MER restriction for 1 (IF1), 2 (IF2), or 3 days (IF3), intermediate alternate-day caloric restriction (mid ADCR) with 50% MER restriction for 1 (IF4), 2 (IF5), or 3 days (IF6), and high alternate-day caloric restriction (high ADCR) with 25% MER restriction for 1 (IF7), 2 (IF8), or 3 days (IF9), alternated with days where they received 100% of MER. Body weight was measured weekly, and body composition was performed on a monthly basis. The total duration of the study was 10 months.

5.3.2. RNA Isolation and Two-Step Real Time qPCR

Total RNA from Skeletal muscle (Gastrocnemius/ Soleus complex) was isolated using TRI reagent (Sigma, St. Louis, MO, USA), followed by Direct-zol™ RNA MiniPrep according to manufacturer's instructions. Reverse transcription was performed using the High Capacity cDNA Reverse Transcription Kit (Applied Biosystems). Quantitative Real time PCR was using the StepOnePlus™ Real-Time PCR System with Power SYBR® Green PCR Master Mix using the respective forward and reverse primer for each gene (Appendix C Supplemental Table 5.1), and were designed by Vector NTI software (Invitrogen Corporation) and synthesized by Integrated DNA Technologies (www.idtdna.com). Standard curves with a slope of -3.30 (SEM 0.30) and $R^2 \geq 0.99$ were accepted. A 60S ribosomal protein (RpL7a) housekeeping gene whose expression was not affected by treatment were used to normalize the gene expression data.

5.3.3. Biochemical measurements

Trunk blood was collected at necropsy by decapitation, and the subsequent serum samples were prepared and stored at -70°C until future use. Serum lipids were analyzed using the Abaxis Piccolo XpressTM Lipid Panel Disc, which allows for the simultaneous measurement of total cholesterol (Chol), high-density lipoprotein cholesterol (HDL), low-density lipoprotein cholesterol (LDL), very low-density lipoprotein cholesterol (VLDL), non-high-density lipoprotein cholesterol (nHDL), and triglycerides (TAG). Serum glucose was determined using TRUE resultTM glucose meter (Florida, USA) blood glucose meter. Serum Insulin (Mercodia, Uppsala, Sweden) and IGF-1 (R&D systems, Minneapolis, USA) levels were quantified using rat ELISA kits per manufacturer's instructions. HOMA-IR was calculated using fasting serum glucose and insulin values: HOMA-IR= (Glucose (mmol/L) x Insulin (mU/L))/22.5.

5.3.4. Saccharin Preference

Saccharin preference test was assessed one week prior to the end of the experiment. Prior to the paradigm test, male rats were habituated to the two-bottle paradigm by allowing them to explore and drink water from two bottles positioned on opposite sides of the cage. On the testing day, results were collected from individual in cages (n=12) for 24 h where they had access to two 250 ml drinking bottles. One tube was filled with water and the other with 0.3% saccharin solution. Food was provided ad libitum. Saccharin preference was calculated as follows: Saccharin preference (AU)= Saccharin volume consumed (ml)/ [saccharin volume consumed (ml) + water volume consumed (ml)].

5.3.5. Statistical Analysis

A one-way ANOVA was used for cumulative caloric intake, body weight and body composition, biochemical measurements, saccharin preference, and gene expression data. Student's t-test was used for body weight and body composition compared to zero with a p value ≤ 0.05. Tukey's LSD was used for *post hoc* tests with a p value ≤ 0.05. Response landscapes describing each mouse's physiological change with nutritional intake were established by fitting generalized additive models to the data (Thin Plate Spline Regression) as previously described (Solon-Biet et al., 2014). Briefly, general additive models (GAM) with thin-plate splines were used to model the changes with diet macronutrient composition (protein, carbohydrate, and fat) or physiological changes. GAMs were fitted with the help of the akima, scatterplot3d, rgl, rglwidget, and plot3D packages of the R language. All statistical tests were performed in R 3.3.4.

5.4. RESULTS

5.4.1. Body Weight and Body Composition of Animals Following Alternate-Day Caloric Restriction.

To examine the effectiveness of different levels of Alternate-day Caloric Restriction (ADCR) we used a 3-day and 3-restriction level experimental design, having the commonly used restriction protocol of chronic 25% restriction (CR), a maintenance group (ML), and a lifelong HFD group (OL) as controls. CR was used each time as a reference to assess each level of restriction separately. To achieve the different levels of ADCR, animals consumed varying calorie levels each week (Fig. 5.2A), the highest being the OL group (77.65 ± 0.57 Kcal/day), followed by ML (60.18 ± 0.65 Kcal/day), IF1 (58.86 ± 0.58 Kcal/day), IF4 (57.72 ± 0.62 Kcal/day), IF2 (58.69 ± 0.58 Kcal/day), and IF7 (56.42 ± 0.66 Kcal/day), then IF3 (54.82 ± 0.53 Kcal/day) and IF5 (53.31 ± 0.53 Kcal/day), and finally IF8 (47.55 ± 0.47 Kcal/day), IF6 (45.64± 0.48 Kcal/day), CR (44.69 ± 0.45 Kcal/day), and IF9 (41.95 ± 0.58 Kcal/day). ADCR at different levels are used to overcome the feasibility issue of CR in humans (Brandhorst et al., 2015), whilst retaining the beneficial effects observed with CR. The effects of CR can be studied based on the total amount calories that are restricted or by the amount of the restrictive macronutrient provided, in this case protein and no carbohydrates or fat intake. Furthermore, several studies have pointed out that CR and protein restriction (PR) can cause similar effects, and it has been hypothesized in different studies and meta-analysis that the CR acts through different ranges of protein restriction (Simpson, Le Couteur, Raubenheimer, et al., 2017; Speakman, Mitchell, & Mazidi, 2016)), as seen in the studied ADCR patterns. In our experiment, we are able to achieve different levels of protein restriction compared to carbohydrate intake (Fig. 5.2B), where the OL group has a similar ratio of

carbohydrate:protein (C:P) intake similar to diets that maximize reproduction (1:1 carbohydrate-to-protein ratio), whereas the ML group shows a C:P ratio that localizes in between commonly

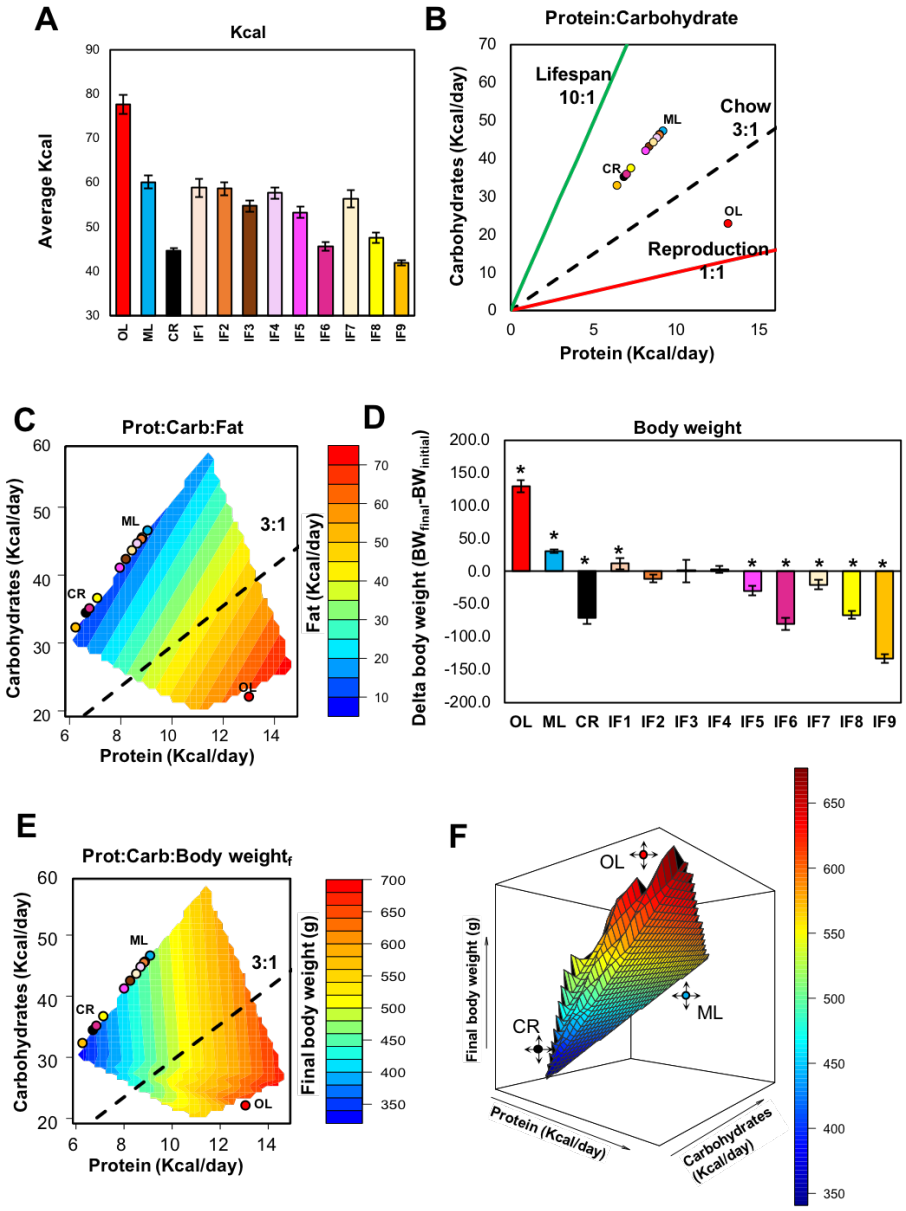

Figure 5.2. Caloric intake and body weight changes following 6-month ADCR. A) Average caloric intake from the beginning of the dietary intervention (4 months) until the end of the experiment (10 months) highlights the energy consumed based on the energy requirements for each experimental group. B) Protein-to-Carbohydrate ratio used in the experimental diets for each ADCR group adapted to Simpson *et al.* 2017 (10.1016/j.arr.2017.03.001). C) Response surfaces showing the relationship between protein intake (Kcal/day) versus carbohydrate and fat content. Response surfaces were fitted with generalized additive models (GAMs) using thin-plate splines. D) Body weight difference from initial (4 months) to final (10 months), showing significant differences between all treatments. Values are expressed as means changes ± SEM. *Indicates significant statistical difference from zero with Student's T test $p<0.05$. Response surfaces

Figure 5.2. (cont.) showing the relationship between protein and carbohydrate intake (Kcal/day) versus final body weight in E) 2 and F) 3 dimensions. Dotted line in all surface plots show the standardized chow diet composition with a carbohydrate-to-protein ratio of 3:1. In all surfaces, red indicates the highest value, while blue indicates the lowest value, with the colors standardized across response surfaces.

used chow diets (3:1 carbohydrate-to-protein ratio) and those that are known to promote longevity (10:1 carbohydrate-to-protein ratio). Finally, the least restrictive ADCR protocols (IF1-3, IF4-5, and IF7) have similar C:P ratios with decreasing rates of protein, whereas the most restrictive ADCR protocols (IF6, IF8-9) and CR group shows the highest C:P ratios (Fig. 5.2B), and localize closely to diets that aim to extend lifespan.

Advances in the field of nutritional geometry have demonstrated the significant effects of macronutrient distribution, mainly protein restriction, by modelling the state-space responses of animals to varying levels of energy or protein, and how they balance the restrictive nutrient intake. In our study, we used this Geometric nutritional framework (GNF) to question whether the restriction of calories and protein was sufficient to erase the effects of early-life HFD consumption. This approach allows for the three-dimension visualization of any given physiological or biochemical parameter; On the x-axis, a limiting macronutrient like protein is loaded, and in the y-axis another macronutrient such as fat or carbohydrates, or a physiological outcome are loaded, and these two define the spatial distribution of the animals. The third component then, is plotted in a heat map with values that range from the minimum (shown in blue) to the maximum (shown in red), and is adjusted according to the state-space of the first two components. In Fig. 5.2C, the relationship of protein:carbohydrate:fat intake can be visualized for each experimental group, with the OL group showing the highest fat consumption (red), and the remaining groups showed a lower consumption of fat (blue).

Given that the animals were provided different levels of calories and P:C, we examined the changes in body weight and body composition. Body weight (BW) is presented as the change from

beginning of the experimental period (following MER, 4 months) to the end of the treatment period (10 months) (Fig. 5.2D). As seen previously, the OL group showed a significant increase in BW

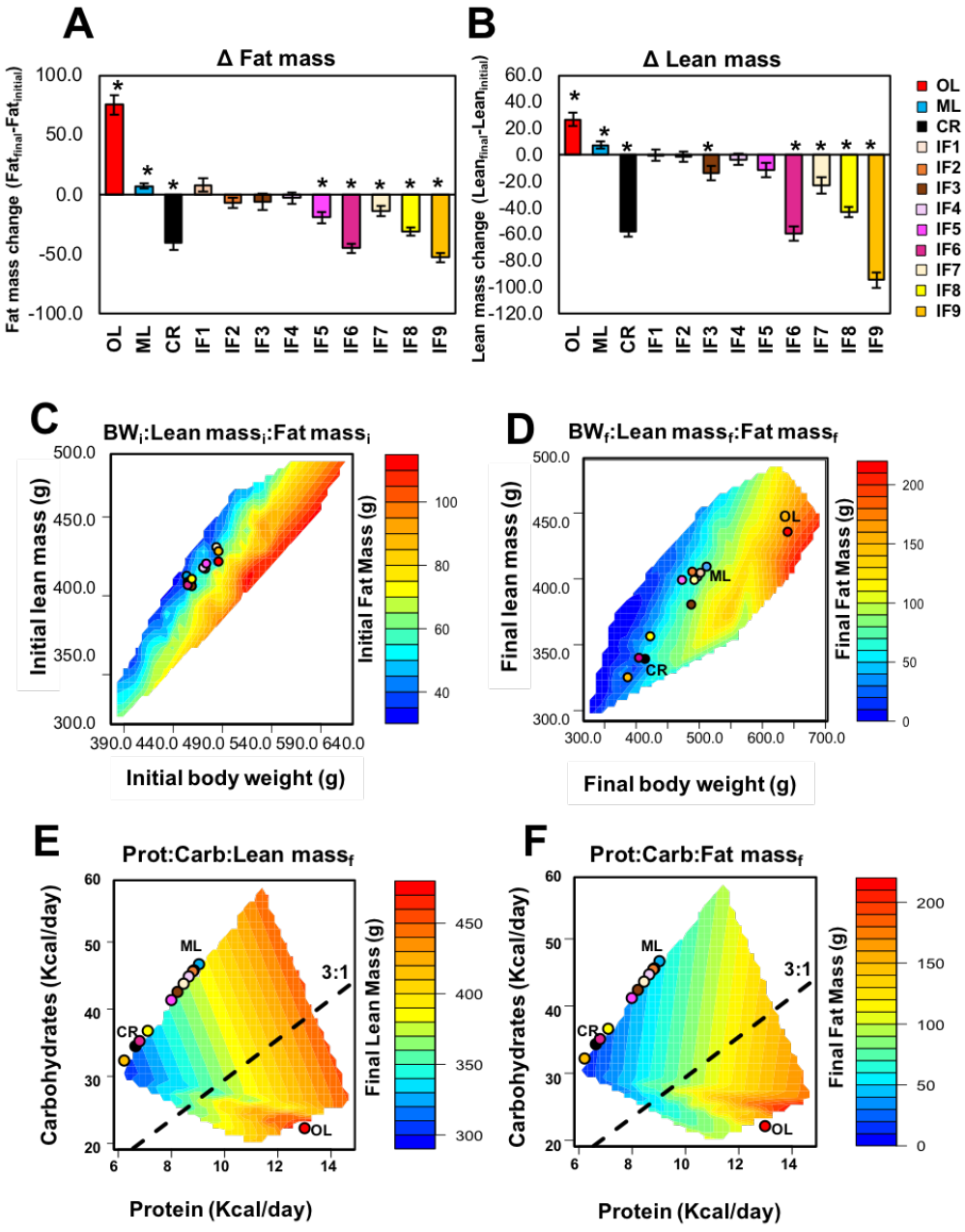

Figure 5.3. Body composition changes following 6-month ADCR. Body composition differences from initial (4 months) to final (10 months), showing significant differences for A) fat and B) lean mass. Values are expressed as means changes ± SEM. *Indicates significant statistical difference from zero with Student's T test $p<0.05$. C) Response surfaces showing the relationship between initial body weight and initial lean and fat mass (4 months). D) Response surfaces showing the relationship between final body weight and final lean and fat mass (10 months). Response surfaces showing the relationship between protein and carbohydrate intake (Kcal/day) versus E) final lean and F) fat mass. Response surfaces were fitted with

Figure 5.3. (cont.) generalized additive models (GAMs) using thin-plate splines. Dotted line in all surface plots show the standardized chow diet composition with a carbohydrate-to-protein ratio of 3:1. In all surfaces, red indicates the highest value, while blue indicates the lowest value, with the colors standardized across response surfaces.

(129.53 ± 8.94) ($p<0.0001$), followed by ML (30.85 ± 2.66) ($p<0.0001$), and CR with a significant decrease in BW (70.60 ± 9.56) ($p<0.0001$). Regarding the ADCR groups, 25% ADCR groups in one (IF1), two (IF2), and three-day (IF3) restriction showed no significant difference between them, and only IF1 increased BW significantly ($p=0.022$) (Fig. 5.2D). Next, 50% one day a week (IF4) produced no significant effect ($p=0.91$) in BW, but both IF5 (two-day 50%) and IF6 (three-day 50%) produced significant reductions in BW ($p<0.0001$). Only 50% restriction three days per week (IF6) produced comparable changes to CR (Fig. 5.2D). Lastly, all 75% restriction ADCR (IF7-9) were sufficient to cause a significant reduction in final BW ($p<0.001$), and only two- and three-day 75% restrictions comparable and superior to CR, respectively (Fig. 5.2D).

Analyzing the macronutrient consumption through nutritional geometry (GNF), we can trace changes in body weight in response to the average consumption of each macronutrients. Final BW is higher for the OL group with the lowest C:P ratio (22.98:13.13, red) (Fig. 5.2E), whereas ML localizes at the at the top of the spatial macronutrient distribution (47.45:9.19, blue) with medium range BW, and the CR group localizes closer to the 10:1 C:P ratio for lifespan extension (35.24:6.82, black) and has the lowest body weight. For the ADCR groups, mid-ADCR show low-to-mild changes in BW, whereas ADCR groups with the highest C:P ratios, show the lowest BW (Fig. 5.2E). This relationship can also be understood in a three-dimensional representation (Fig. 5.2F) with an x-, y-, and z-components.

Body weight changes in response to varying levels of calories indicate adaptive mechanisms and different utilization of nutrients. Body composition was measured before and after MER, showing no changes for all ADCR groups (data not shown). Body composition changes

were assessed comparing the differences at the end of the experiment with the pre-treatment period (following MER estimation), and the results for fat and lean mass are shown on Fig. 5.3A and B, respectively. As reported previously, fat mass changes were significant for all control groups (OL, ML, and CR) (Fig. 5.3A). No significant changes in fat mass were observed with low-ADCR protocols (IF1, IF2, and IF3), or one-day 50% restriction (IF4). Dose response changes were observed for 50% two and three days per week (IF5 and 6, respectively), as well as all high-ADCR protocols (IF7-9) (Fig. 5.3A). On the other hand, lean mass changes were significant for the three control groups, as reported previously (Fig. 5.3B). No changes were observed for one- or two-day 25% ADCR, nor for one- or two-day 50% ADCR. Significant reduction in lean mass was observed for 3-day 25% and 50%, as well as all high-ADCR protocols (IF7-9) (Fig. 5.3B). To understand the changes in body composition that occur in response ADCR, we used a similar approach to GFN using the body weight, lean, and fat mass from the animals before (Fig. 5.3C) and after the ADCR protocol (Fig. 5.3D). Before the ADCR treatment, animals show a similar scattering pattern of the mean values and appear to be normally distributed (Fig. 5.3C). Following ADCR (6-month intervention), animals have adapted and used the excessive or limited amount of nutrients, and show scattering patterns that reflect the level of restriction. The unrestricted OL group consuming HFD shows the highest final BW, lean, and fat mass (Fig. 5.3D, upper right corner), then the ML control shows an intermediate BW, lean and fat mass (Fig. 5.3D, middle), and CR animals localize on the bottom left corner of the plot, indicating a low BW, lean, and fat mass (Fig. 5.3D). Next, we wanted to explore the individual contribution of macronutrients and their impact on both final lean (Fig. 5.3E), and fat mass (Fig. 5.3F).

5.4.2. Serum Anabolic Signals from Animals Following Alternate-Day Caloric Restriction.

Given the changes in body composition in response to long-term ADCR, we sought to explore the systemic biochemical changes that occur and can be used as a biomarker for the degree of caloric limitation. Serum lipid profile, glucose and anabolic hormone signaling can be found on Appendix C Suppl. Table 5.2. No changes were observed in serum cholesterol, HDL-c, nHDL (total cholesterol minus HDL), ratio of TC/HDL, or LDL-c.

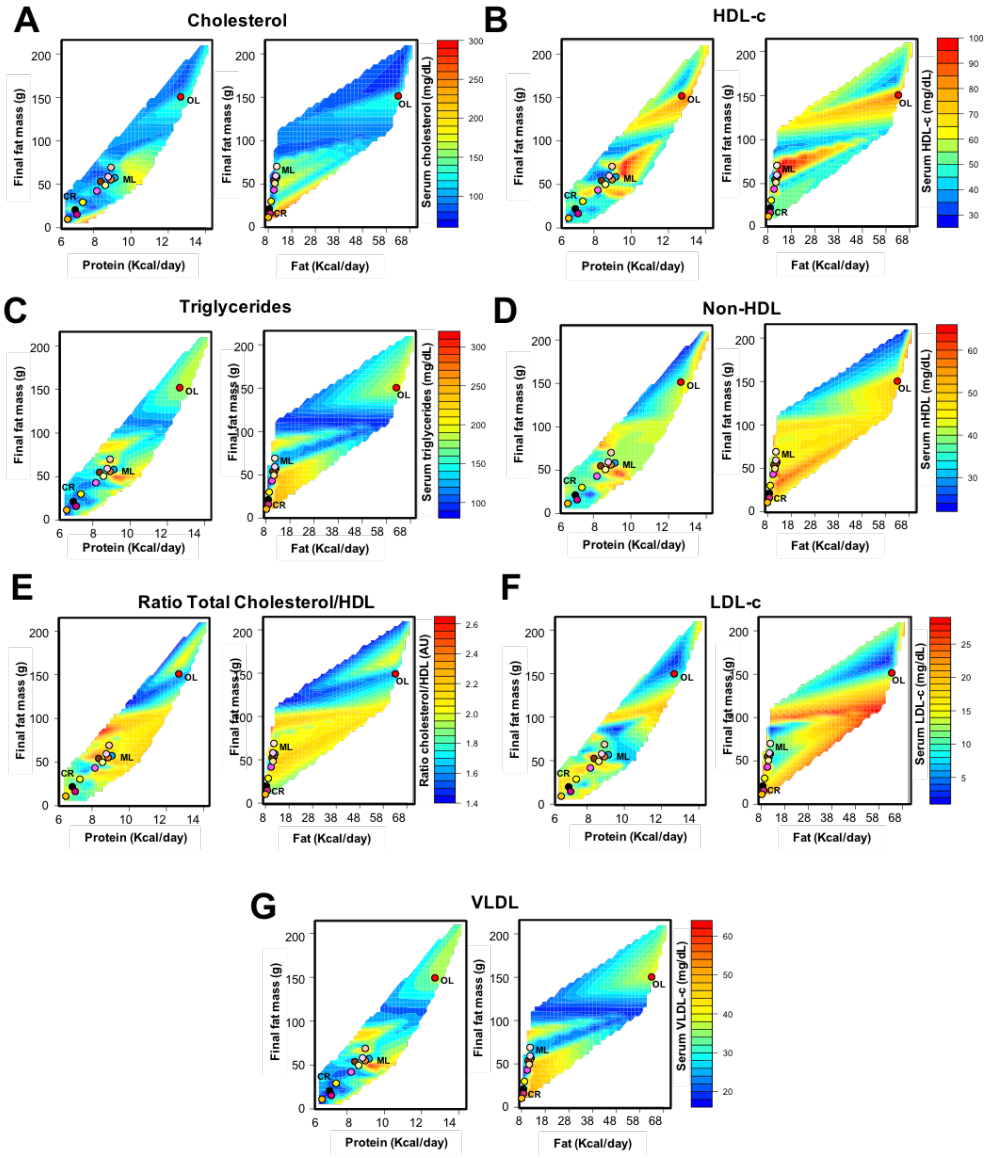

Figure 5.4. Serum lipid profile following 6-month ADCR. Response surfaces showing the relationship between protein or fat consumption (Kcal/day) and final and fat mass (10 months) in relationship with A) serum total cholesterol, B) HDL cholesterol (HDL-c), C) Triglycerides, D) non-HDL particles, E) ratio of

Figure 5.4. (cont.) total cholesterol to HDL, F) LDL cholesterol (LDL-c), and G) VLDL. Individual values are presented on Appendix C Suppl. Table 5.2. Response surfaces were fitted with generalized additive models (GAMs) using thin-plate splines. Dotted line in all surface plots show the standardized chow diet composition with a carbohydrate-to-protein ratio of 3:1. In all surfaces, red indicates the highest value, while blue indicates the lowest value, with the colors standardized across response surfaces.

Significant changes were observed for serum TAG and VLDL, where ML and IF1 (one-day 25%) had the highest values ($p<0.05$), followed by IF2, OL, IF7, IF4, IF3, IF6, IF5, CR, and IF8, and the highest 3-day restriction (IF9) had the lowest value ($p<0.05$) (Appendix C Suppl. Table 5.2). Using GNF, we were able to observe the effect of protein or fat consumption and final fat mass, on the distribution of serum cholesterol (Fig. 5.4A). Similar state-space representations are observed for HDL-c (Fig. 5.4B), nHDL (Fig. 5.4D), ratio of TC/HDL (Fig. 5.4E), and LDL-c (Fig. 5.4F). Interestingly, protein consumption seems to be predictive of TAG and VLDL, when it's graphed against an adiposity measure (final fat mass) (Fig. 5.4C and G, respectively).

We then analyzed changes in serum glucose and anabolic signals Insulin, IGF-1 and the insulin resistant marker HOMA-IR. Results can be found on Appendix C Suppl. Table 5.2. No differences were observed for serum glucose. Serum insulin was higher in animals with the lowest ADCR (IF1), followed by IF7, IF2, ML, IF4, IF3, IF8, IF5, and OL, and the lowest values were found for CR, IF6, and IF9 ($p<0.05$) (Appendix C Suppl. Table 5.2). As expected, HOMA-IR values followed the same trend as serum insulin. Finally, serum IGF-1 proved to be a good predictor of the energy status in ADCR and non-ADCR animals. Animals with lower ADCR at 50% and 75% had similar IGF-1 levels to OL, followed by IF1, ML and IF2 ($p<0.05$), then IF3, IF5, IF8, and lastly the groups with the lowest IGF-1 were IF6, CR and IF9 (Appendix C Suppl. Table 5.2). When plotted against macronutrient distribution (Fig. 5.5A) or final fat mass (Fig. 5.5B), serum glucose shows a uniform pattern across the board. Moreover, HOMA-IR shows that the highest fat accretion is indicative of a higher glucose-to-insulin ratio (Fig. 5.5D), but not macronutrient

distribution (Fig. 5.5C). Finally, as seen on Appendix C Suppl. Table 5.2, serum IGF-1 is able to closely predict the restriction pattern having that the animals with the highest and medium fat mass and protein intake have increased IGF-1, whereas the animals with the lowest protein intake and lowest fat mass have reduced IGF-1 (Fig. 5.5E and F).

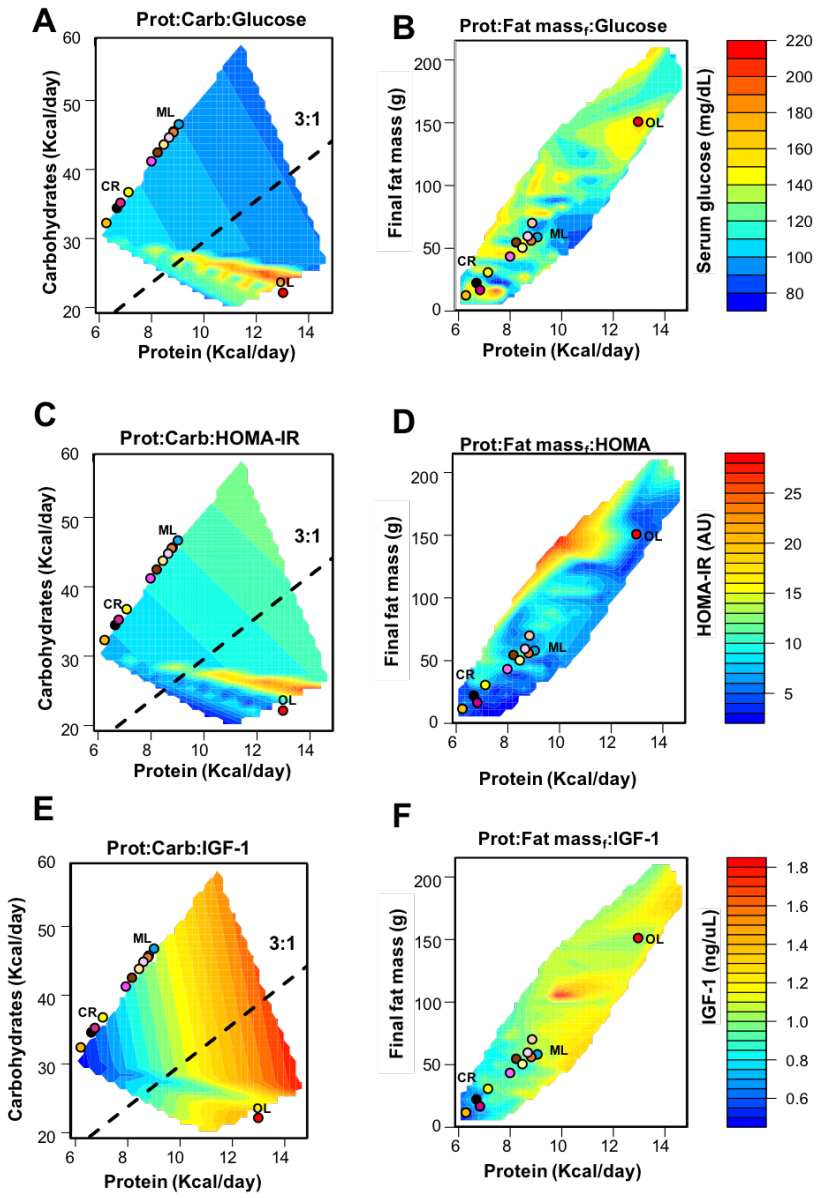

Figure 5.5. Serum IGF-1 and insulin resistant index (HOMA-IR) following 6-month ADCR. A) Response surface showing the relationship between protein and carbohydrate consumption (Kcal/day) and serum glucose. B) Response surface showing the relationship between protein and fat consumption (Kcal/day) and serum glucose. C) Response surface showing the relationship between protein and carbohydrate consumption (Kcal/day) and HOMA-IR. D) Response surface showing the relationship between protein and fat consumption (Kcal/day) and HOMA-IR. E) Response surface showing the

Figure 5.5. (cont.) relationship between protein and carbohydrate consumption (Kcal/day) and serum IGF-1. B) Response surface showing the relationship between protein and fat consumption (Kcal/day) and serum IGF-1. Response surfaces were fitted with generalized additive models (GAMs) using thin-plate splines. Dotted line in all surface plots show the standardized chow diet composition with a carbohydrate-to-protein ratio of 3:1. In all surfaces, red indicates the highest value, while blue indicates the lowest value, with the colors standardized across response surfaces.

Different tissues are known to be impacted by CR; adipose tissue depots are depleted quickly following a short 3-month CR, followed by reproductive organs, kidneys, etc., whereas the liver, brain, heart and pancreas among others, are spared (S. E. Mitchell, Tang, et al., 2015). Here we assessed the effect of long-term ADCR (6 months) on brain and liver weights. Animals with the highest brain weight were OL, ML, IF2, IF4, and IF7 (2.13 ± 0.03, 2.12 ± 0.03, 2.15 ± 0.04, 2.13 ± 0.02, and 2.12 ± 0.02 g, respectively), followed by IF3 and IF5 (2.11 ± 0.02 and 2.11 ± 0.02 g, respectively), and the lowest CR, IF1, IF6, IF8, and IF9 (2.06 ± 0.01, 2.09 ± 0.02, 2.04 ± 0.03, 2.08 ± 0.02, and 2.06 ± 0.03 g, respectively). Using GNF, we can classify each of the groups according to their protein (Fig. 5.6A) or fat consumption (Fig. 5.6B), and observe the spatial distribution of the relative brain weight (ratio to final BW). We can observe that animals consuming the highest protein and fat mass (OL group) do not possess the highest relative brain mass (Fig. 5.6A and B, blue). On the other hand, low to medium ADCR maintain a relative brain weight according to their body weights (ML, IF1, IF2, IF3, IF4, IF5, and IF7, yellow or green), whereas the highest ADCR (IF6, IF8, and IF9) and CR possess the highest relative brain mass (Fig. 5.6A and B, red). Another protected tissue during CR is the liver, and we see that at the end of 6 months of ADCR the highest absolute liver weights belong to OL, ML, low-ADCR (IF1-3), mid-ADCR (IF4,5), and the lowest 75% ADCR (IF7) (16.05 ± 0.89, 15.24 ± 0.56, 15.01 ± 0.93, 15.20 ± 1.26, 13.91 ± 0.60, 14.64 ± 0.67, 14.98 ± 1.25, and 14.79 ± 0.79 g, respectively). The lowest liver weights corresponded to CR, IF6, IF8, and IF9 (11.81 ± 0.45, 10.60 ± 0.59, 12.34 ± 0.92, and 11.26 ± 0.50 g, respectively). Nevertheless, relative liver weight was higher for all CR

and ADCR groups (except IF6), but lower in the HFD consuming animals (OL group). Using GNF, we can observe that relative liver weight remains mostly unchanged by protein (Fig. 5.6C) or fat consumption (Fig. 5.6D).

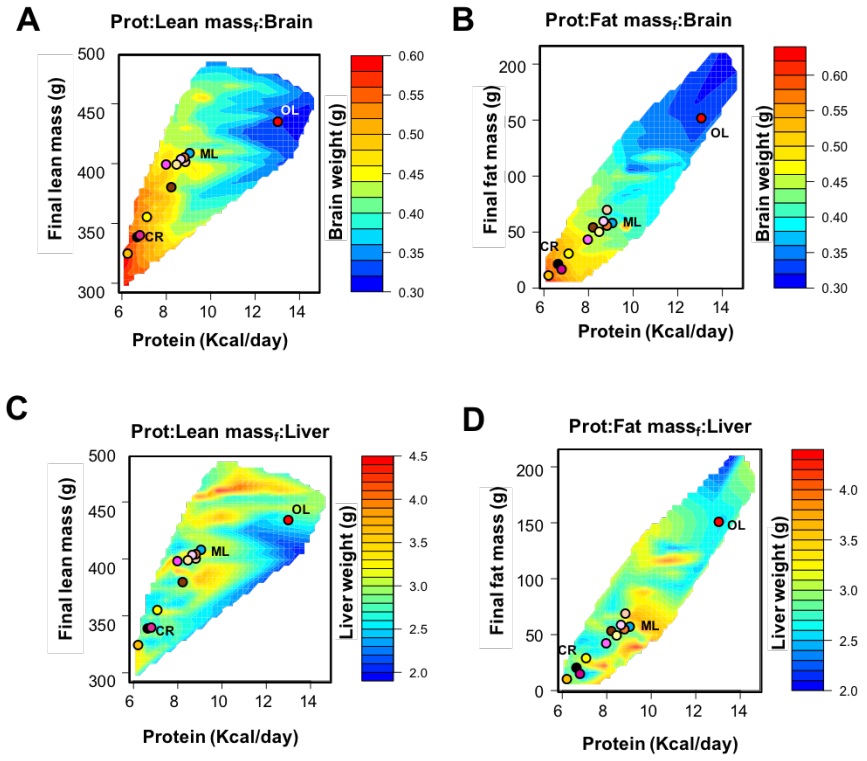

Figure 5.6. Relationship of brain and liver mass to final body weight following 6-month ADCR. Response surfaces showing the relationship between protein intake (Kcal/day) and A) final lean or B) fat mass versus brain mass at the time of collection. Response surfaces showing the relationship between protein intake (Kcal/day) and A) final lean or B) fat mass versus liver mass at the time of collection. Response surfaces were fitted with generalized additive models (GAMs) using thin-plate splines. Dotted line in all surface plots show the standardized chow diet composition with a carbohydrate-to-protein ratio of 3:1. In all surfaces, red indicates the highest value, while blue indicates the lowest value, with the colors standardized across response surfaces.

5.4.3. Saccharin preference test.

One of the limitations of chronic CR is the constant sensation of hunger that patients experiment, but this can be bypassed by using ADCR and allowing the consumption of 100% of the MER on non-restricted days. In our study, we aimed to overcome this limitation and therefore assessed

anhedonic/reward behavior as a direct measure of depressive-like behaviors using a saccharin preference test. In our study, we used a two-bottle testing paradigm with one drinking bottle that contained a solution sweetened with saccharin (0.3% Saccharin in water) and another one with

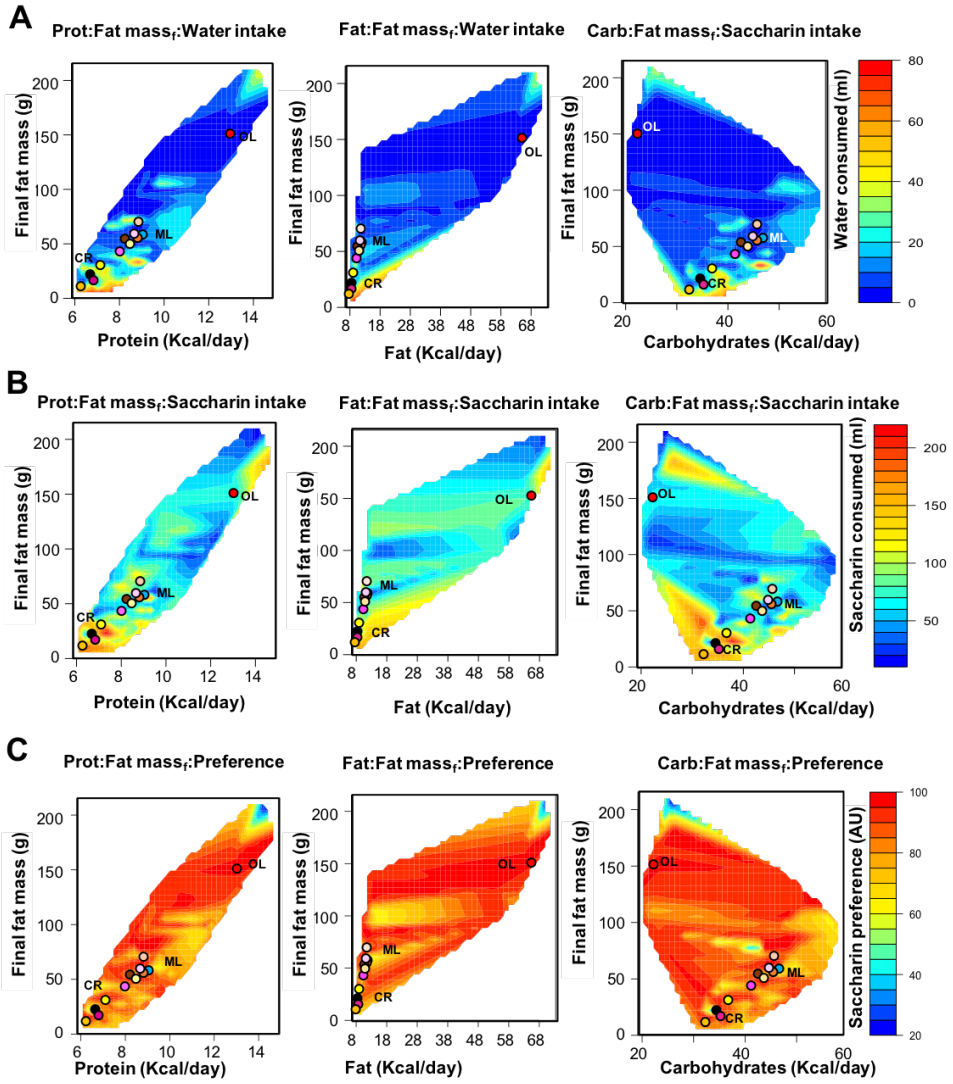

Figure 5.7. Conditioned water, saccharin consumption and saccharin preference following 6-month ADCR. Response surfaces showing the relationship between A) protein, B) carbohydrate, or C) fat intake (Kcal/day) and fat mass versus water consumption (ml). Response surfaces showing the relationship between A) protein, B) carbohydrate, or C) fat intake (Kcal/day) and fat mass versus saccharin (0.3% Saccharin in water) consumption (ml). Response surfaces showing the relationship between A) protein, B) carbohydrate, or C) fat intake (Kcal/day) and fat mass versus saccharin preference (saccharin consumption in ml/total volume consumed in ml). Response surfaces were fitted with generalized additive models (GAMs) using thin-plate splines. Dotted line in all surface plots show the standardized chow diet composition with a carbohydrate-to-protein ratio of 3:1. In all surfaces, red indicates the highest value, while blue indicates the lowest value, with the colors standardized across response surfaces.

plain water. Following habituation to the presence of two bottles, animals were tested overnight and the water/saccharin consumption was assessed for each individual animal. The results indicate that animals with the highest restriction (CR, IF6, IF7, IF8, and IF9) had the greatest consumption of water and saccharin ($p<0.05$), whereas the OL, ML, and the lower ADCR (IF1-3, IF4-5) had the lowest (Appendix C Suppl. Fig. 5.1A and B). However, despite the differences in water and saccharin consumption, only IF6 (3-day 50% ADCR) and IF8 (2-day 75% ADCR) showed significantly lower saccharin preference (p=0.02 and p=0.05, respectively) compared to CR (Suppl. Fig. 5.1C). Using GNF we can observe that lower protein, fat and carbohydrate consumption leads to a higher water and saccharin intake (Fig. 5.7A and B), but no appreciable differences in saccharin preference (Fig. 5.7C).

5.4.4. Skeletal muscle gene expression and Tnf modulation by ADCR.

We previously assessed the effect of skeletal muscle on nutrient sensing genes and inflammatory genes, and our findings indicate that CR is sufficient to erase the early-life HFD feeding, stimulating protein recycling and myogenesis. In order to characterize the response to prolonged ADCR as a suitable alternative strategy to CR, we measured the expression of nutrient sensing genes in skeletal muscle given the observed drastic changes in muscle mass (Fig. 5.8). As previously described, significant differences were observed in nutrient sensing, protein recycling, and myogenesis genes in muscle between OL, ML, and CR, and such differences are apparent in the top three panels of the heatmap (Fig. 5.8A). In regard to low-ADCR groups, 1- and 2-day 25% ADCR (IF1 and 2, respectively) showed similar patterns of expression between them, and were different from 3-day 25% ADCR (IF3). The latter showed a pattern that closely resembled that of the CR group. Mid-ADCR group IF4 (1-day 50% ADCR) showed a pattern of expression similar

to CR, and was different from both IF5 and IF6 (2- and 3-day 50% ADCR, respectively). Finally, high-ADCR groups IF7 and IF8 produced similar effects in the expression of nutrient sensing and protein recycling genes, but were different from CR. The highest restriction, 3-day 75% ADCR (IF9), produced similar effects to CR and had different expression patterns from the other high-ADCR groups (Fig. 5.8A).

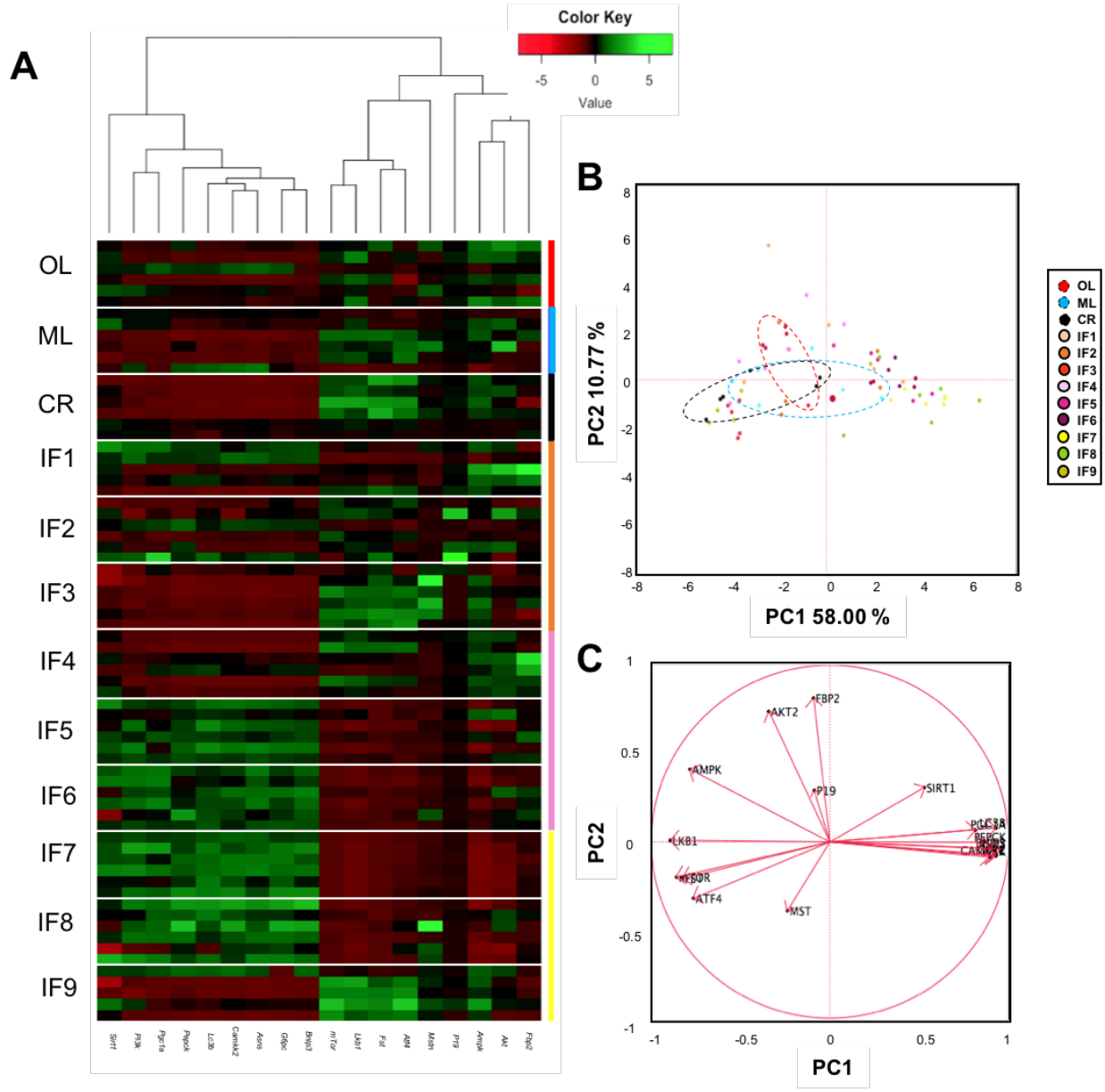

Figure 5.8. Gene expression of nutrient sensing and proteostasis related pathways from skeletal muscle using qPCR following 6-month ADCR. A) Heatmap with one-way hierarchical clustering comparing the overall scaled gene expression pattern of skeletal muscle. B) Principal component analysis of the expression of groups in two components and C) loading plot showing the relationship between the

Figure 5.8. (cont.) genes analyzed in skeletal muscle. Ellipses show 95% confidence interval for each control group. Each dot represents one biological sample.

In order to examine the data as a whole, we performed a principal component analysis (PCA) of the gene expression data from skeletal muscle (Fig. 5.8B). PCA project the data onto the PCs (principal components) in two dimensions, and such PCs provide a new space of uncorrelated variables that best explain the variation in the original data to represent the samples in a succinct way. As seen in Fig. 5.8A and B, a similar pattern of expression was observed for CR, IF3, IF4, and IF9. OL clustered separately, whereas the ML group was dispersed between OL and CR. Lastly, a distinct pattern of expression of nutrient sensing and protein recycling genes was observed for IF5-8 (Fig. 5.8B). Comparison of individual ADCR patterns and CR can be observed in Suppl. Fig. 5.2. Interestingly, the PCA loading plot, which is a representation of the degree of correlation between the tested variables (highly correlated genes appear closer together), shows the commonly CR responsive genes *Sirt1*, *Pgc1a*, and *Lc3b* closer together. Genes such as Lkb1, mTor, Mstn, Atf4, Akt2, and Fbp2 are at 90-degree angle from CR-responsive genes (*Sirt1*, *Pgc1a*, and *Lc3b*), which indicates that there is a degree of negative correlation between them.

Given the significant impact that CR has on inflammation, we sought to examine the effect of long term ADCR on skeletal muscle inflammation, in particular the myokine *Tnf* that is related to muscle cachexia. As seen in Fig. 5.9A, muscle *Tnf* expression is increased by HFD in the OL group, and it's similar to 3-day 25% ADCR (IF3). Intermediate effects were observed for IF2, IF3, IF4, IF5, IF7, and IF9. Finally, the lowest muscle Tnf expression was observed for ML, CR, IF6, and IF8. Interestingly, 50% ADCR was the only strategy that seemed to produce a dose-dependent effect on Tnf expression (IF4>IF5>IF6), whereas 25% (IF1-3) and 75% ADCR (IF7-9) produced a U-shaped effect. Using GNF, we can dissect the effect of protein (Fig. 5.9B) or fat consumption

(Fig. 5.9C) and final fat mass on *Tnf* expression, having that animals that consume the highest protein and fat and accrue the highest fat mass have the greater expression of *Tnf*. On the other

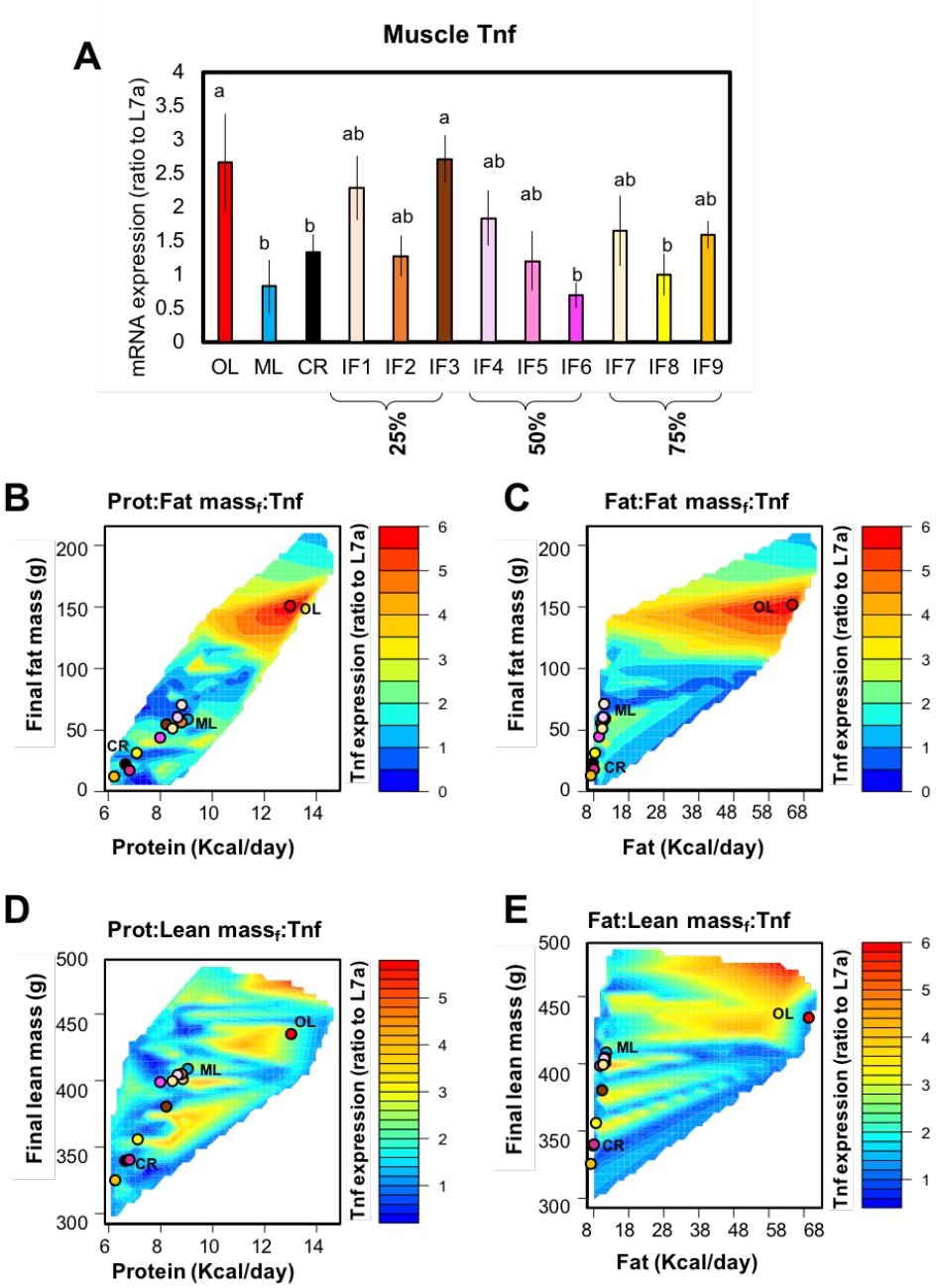

Figure 5.9. *Tnf* gene expression in muscle following 6-month ADCR. A) Gene expression of *Tnf* mRNA in skeletal muscle from animals at the end of the experiment. Values are expressed as means ± SEM. [abc]Different letters between treatments indicate significant statistical difference with Tukey post hoc test at $p<0.05$. Response surfaces showing the relationship between B) protein or C) fat intake (Kcal/day) and fat mass versus *Tnf* mRNA expression in muscle. Response surfaces showing the relationship between D) protein or E) fat intake (Kcal/day) and lean mass versus *Tnf* mRNA expression in muscle. *Tnf* values are normalized to the housekeeping gene *RpL7a*.

hand, medium to high final lean mass accretion is able to predict higher levels of *Tnf* in skeletal muscle, where CR, IF6, and IF8 respond to either low protein (Fig. 5.9D) or low fat (Fig. 5.9E) and mount an adaptive low-grade inflammatory response (Fig. 5.9D and E, bottom left corner).

5.5. DISCUSSION

This study demonstrated the effectiveness of different Alternate Day Caloric Restriction (ADCR) protocols as a measure to overcome the shortcomings of chronic CR. Low-, mid-, and high-ADCR not only impact body weight and body composition, but also induce significant changes in serum biochemical parameters and skeletal muscle transcriptional response. Low-ADCR protocols (IF1-3) showed increases in body weight and body composition, increased cholesterol/HDL ratio, VLDL and TAG, different nutrient sensing, protein recycling, and increased inflammatory signals, compared to chronic CR. Mid-ADCR (50%, IF4-6) on more than two days, and high-ADCR (75%, IF7-9) produced incremental effects on body weight and body composition; the higher restrictions, IF6, IF8, and IF9 produced the biggest decreases in serum biochemical parameters and lipid profile, and produced similar transcriptional signatures in skeletal muscle to that of chronic CR. By using a novel geometric nutrition framework, this study validates ADCR protocols that overcome the limitations of chronic CR and can produce significant changes in body composition and biochemical parameters, while stimulating skeletal muscle adaptation, which can be titrated to find an optimal balance.

Using a novel geometric approach to nutritional interventions, our paper addresses for the first time the long-term effect of ADCR integrating the multidimensionality and dynamic nature of the adaptation to calorie restriction. Previous studies have demonstrated the benefits of using a

Geometric Framework for Nutrition (GFN) on diverse contexts such as the nutritional geometry of liver disease (Simpson et al., 2018), brain and cognition (Wahl et al., 2016), aging and lifespan (Le Couteur et al., 2016; Piper, Partridge, Raubenheimer, & Simpson, 2011), among others, and have concluded that the restriction of calories, rather than being the result of overall energy, results from the restriction of macronutrients. Formulated laboratory diets contain the three macronutrients in different proportions to fulfil a desired function; whether the goal of the study is intended for reproduction (Protein-to-carbohydrate ratio of 1:1), or lifespan (Protein-to-carbohydrate ratio of 1:10), or a chow diet that maximizes both functions simultaneously (Protein-to-carbohydrate ratio of 1:3) (Simpson, Le Couteur, Raubenheimer, et al., 2017). In our study, diets that are used to restrict calories have a ratio that locates between the chow and lifespan compositions, and thus the varying proportions of protein/carbohydrate (P:C) can be used to explain the adaptation to the titration in ADCR animals. The relationship of P:C (or non-protein components) can adequately determine the limiting macronutrient and how that affects metabolic parameters; a conserved mechanisms across species is the prioritization of protein intake rather than calories or carbohydrates or fat requirements (Simpson, Le Couteur, Raubenheimer, et al., 2017), and this phenomenon is called protein leverage (Simpson & Raubenheimer, 2005). Therefore, given the great benefits to assessing nutritional interventions with general additive models (Simpson, Le Couteur, James, et al., 2017), expressing the treatment outcomes in a state-space relative to the macronutrient consumption will improve the translatability of ADCR strategies. To our knowledge, this is the first study that seeks to combine GFN and ADCR to better understand metabolic adaptations to calorie restriction.

A clear consensus exists on the effects of chronic CR; whether the desired effect is lifespan extension, reduced oxidative stress, improved insulin sensitivity, improved proteostasis, or lower

inflammation, chronic CR is known to positively affect diverse cellular mechanisms that improve health span (Fontana & Partridge, 2015). Nevertheless, despite the positive outcomes related to CR in different model organisms and human trials, some limitations of such dietary restrictive protocols include but are not limited to low patient compliance and translatability (Johnstone, 2015; Varady & Hellerstein, 2007). The hypothesis of this study is that titration of CR on different days and at different energy levels can achieve comparable physiological and metabolic benefits to CR. The initial goal was to provide low, medium, and high levels of CR on "fasting" days interspersed with "feeding" days to produce changes in body weight and body composition. By providing varying levels of chronic restriction, ADCR was able to produce significant changes in body weight; lower ADCR was associated with high variability, no changes from baseline, or weight gain, whereas mid-to-high ADCR consistently produced weight loss. The most effective groups that produced similar weight loss to chronic CR were 50% ADCR for 3 days a week and 75% ADCR on 2 or more days a week. The changes in body weight observed for the low-ADCR protocols demonstrate the limitations or "dangers" of fasting trends in which the subject can experience no changes in weight or could induce weight gain and contribute to lower patient compliance. On the other hand, mid- and high-ADCR on more than 2 days a week significantly and consistently produced weight reduction, which provides a solution to improve patient compliance in the clinics. Our surprising findings demonstrate the ability of 50% ADCR for 3 days a week and 75% ADCR on 2 or more days a week to produce similar results to chronic CR in terms of body weight, but without the constant restriction of calories.

Changes in body weight due to ADCR constitute the first indication of the effectiveness of modified restrictions protocols on health span. In addition to body weight, body composition (fat and lean mass) and serum biochemical parameters were also assessed as an outcome of the

restriction. Animals with low-ADCR (IF1-3) and the less frequent mid-ADCR (1-day restriction, IF4) produced none to very little changes in body composition, and small changes in serum lipids and hormones. Restriction of 50% of calories on two or more days and 75% ADCR on 1 or more days produced significant reduction in fat and lean mass. Interestingly, our results indicate that the long term ADCR can be titrated in a 'dose'-dependent manner starting with the medium levels of restriction and optimized for higher levels of energy limitation avoiding chronic CR. Such restrictive patterns could constitute viable alternatives not only for weight loss, but also to improve health and reduce disease states. Moreover, despite the general lack of changes in serum lipids, TAG and VLDL were affected by the mid- and high-ADCR protocols indicating the influence on *de novo* hepatic lipid synthesis. Serum anabolic hormone IGF-1 proved to be an accurate predictor of the restriction level and responded to varying levels of protein intake. Finally, HOMA-IR was improved with the highest levels of restriction, which indicates that the metabolic improvements related to insulin sensitivity might require greater restriction of calories many times per week. Our findings emphasize the versatility of ADCR protocols which can be optimized to accomplish either a reduction in body weight, body fat, improvement of lipid profile, or amelioration of insulin resistance.

Previous studies have assessed the effect if short-term CR on the turnover and utilization of different tissues, and have established that some tissues are preferentially utilized (adipose tissue, spleen, reproductive organs, kidneys and skin), whereas others are protected (liver, pancreas, lungs, heart and brain), or are invested onto (gastrointestinal tract) (S. E. Mitchell, Tang, et al., 2015). In our study, we wanted to focus on the idea of protected tissues such as the brain and the liver, and analyze what are the changes that occur with long-term ADCR. Using GFN, we observed that only the animals with the lowest protein content and lowest final lean or fat mass

tended to preserve brain tissue relative to their body weight, but the liver appeared to be protected by all ADCR groups and ML group. These differential responses could be indicative of the metabolic outcomes to each ADCR protocol and require further exploration. Another feature of chronic CR that needs to be addressed is related to the constant sensation of hunger that these patients experience. For that purpose, we assessed the anhedonic/reward behavior as a direct measure of depressive-like behaviors using two-bottle paradigm for saccharin preference. We saw a consistent elevation of water and saccharin consumption for the groups that had the highest restrictions (CR, IF6, IF8, IF9), but no differences were observed in terms of saccharin preference. The former indicates that the amount of saccharin consumed is related to the increased sensation of hunger or reward that does not dissipate, whereas the latter indicates that the water and the non-nutritive sugar solution are consumed in the same proportion indicating the similar pleasure-seeking behavior for all animals. This study for the first time combined a behavioral test outcome with ADCR titration using GFN, which can be extended in future experiments for the optimization of hunger/satiety tests.

Chronic CR, like protein restriction, is able to activate diverse mechanisms that are related to delayed aging (Mercken et al., 2017; Mercken, Crosby, et al., 2013; Simpson, Le Couteur, Raubenheimer, et al., 2017); Reduces anabolic responses and cell growth (mTOR, IGF-1/Insulin/Growth hormone), while improving protein turnover (autophagy and proteasomal degradation), nutrient sensing (AMPK, SIRT1), and mitochondrial function (PGC1-α). Although such adaptations are beneficial for the overall health of different biological systems and tissues, the negative effects that such CR-specific adaptive mechanisms have on skeletal muscle needs to be addressed (Simpson, Le Couteur, Raubenheimer, et al., 2017). Skeletal muscle, the largest and one of the most metabolically active tissues in the body, is of great concern for young and old

individuals undergoing CR. Therefore, given the significant changes in lean mass following ADCR, we compared the transcriptional signature of skeletal muscle to that of animals with chronic CR. Transcriptional profiles of skeletal muscle indicate that lower restriction levels IF1 and IF2 (1- and 2-day 25% ADCR) are not sufficient to produce significant changes in skeletal muscle gene expression. Interestingly, despite the lack of similarities between IF3 (3-day 25% ADCR) and IF4 (1-day 50% ADCR) with CR, both of these groups together with IF9 (3-day 75% ADCR) produced similar transcriptional responses to CR of protein recycling and nutrient sensing genes. Additionally, low levels of restriction, such as IF3 and IF4 produce genetic patterns that are similar to CR and IF9, but are achieved without the changes in lean or fat mass. This result accentuates the positive effect of lower levels of restriction to modulate the transcriptional response of skeletal muscle, but caution must be exercised when implementing lower ADCR (IF3-4) given the unwanted weight gain, or the highest ADCR (IF9) that has the highest wasting rate. Finally, mid-to-high ADCR, IF5 (2-day 50% ADCR), IF6 (3-day 50% ADCR), IF7 (1-day 75% ADCR), and IF8 (2-day 75% ADCR), generated distinct transcriptional patterns from CR while decreasing lean and fat mass. Importantly, our study is one of the first to define a happy medium restrictive space with either IF5-8 levels of ADCR, where significant changes in body weight, body composition, lipid profile, and insulin sensitivity are achieved, and ultimately result in a consistent improvement of the nutrient sensing and protein recycling pathways in skeletal muscle. Altogether, our results indicate that intermediate levels of restriction are able to produce the desired changes in body composition and establish a new transcriptional signature that can be advantageous to prevent sarcopenia and wasting.

Lastly, along with the features of nutrient sensing and protein turnover, muscle inflammation is of importance given the size and secretory nature of skeletal muscle. The

inflammatory response of muscle was assessed by measuring the expression of the *Tnf* gene or "cachexin", associated with chronic inflammation and muscle wasting. This study demonstrates for the first time, the titration capacity of the inflammatory response in skeletal muscle by using ADCR combined with GFN. Lower restrictions (IF1, IF2, IF3, IF4, IF7) are not sufficient elicit an adaptive response on muscle inflammation. Higher levels of restriction, IF6 and 8 significantly reduced inflammation to the levels of CR, but when the restriction becomes excessive like the case for IF9 (highest restriction level), the level of *Tnf* increases again. The latter highlights the importance of the titration of CR and ADCR to optimize the changes in body composition, while establishing a personalized and beneficial transcriptional profile of skeletal muscle. Strategies such as IF6 and 8 demonstrated great improvement of physiological, biochemical, and metabolic parameters, and could minimize cachexia in multiple clinical populations. Optimization of ADCR in our study using GFN systematically demonstrated that mid-ADCR is most effective at mimicking chronic CR, and that IF6 and 8 represent the superior strategies for the achievement of metabolic adaptation to long-term restriction.

Our study is novel in the context of personalized nutrition because we optimized different levels of restriction with a high translatability potential to achieve body composition, biochemical, and muscle transcriptional changes. We explored the differences between each ADCR level in the context of macronutrient consumption and the observed changes in body mass. This is significant given that it paves the way for personalized ADCR strategies in order to achieve full or partial adjustments. Future studies should address the impact of isocaloric diets that provide varying levels of macronutrients to be able to define the complete state-space following chronic restriction. We found that mid-to-high restriction levels like IF6 and IF8 provide the best results for health span and should be used to replace the widely used chronic CR protocols. In addition, mechanistic

studies are needed to understand the important long-term programming or epigenetic changes that occur in skeletal muscle, and examine if they become permanent and can be transgenerationally inherited.

This study provides validation of modified CR protocols with a high translation potential that overcome the limitations of chronic CR. Such ADCR alternatives produce significant changes in body composition and biochemical parameters, while stimulating skeletal muscle adaptation, and reduced inflammation. Finally, we demonstrate that physiological, biochemical, and transcriptional responses can be titrated to find an optimal balance.

CHAPTER 6: CALORIC RESTRICTION FOLLOWING HIGH FAT-DIET FEEDING EPIGENETICALLY REPRESSES SKELETAL MUSCLE NF- κB SIGNALING AND TNF IN MALE RATS

6.1. ABSTRACT

Caloric restriction (CR), without malnutrition, fosters musculoskeletal health. The canonical inflammatory marker TNF is able to down-regulate muscle hypertrophy and induce wasting, however the epigenetic mechanisms elicited by CR that act on Tnf regulation remains largely unknown. The aim of our study was to evaluate the mechanisms by which muscle Tnf gene is epigenetically modified, as well as the modifiers that are recruited by CR. In our study, 4-week old male Sprague-Dawley rats were fed a high fat diet (HF, 45% Kcal from fat) ad libitum for 4 months. Animals were then divided into HF ad libitum (OL), maintenance group were fed a control diet (ML, 100% energy requirement at baseline adjusted with body weight), and the caloric restriction group (CR, 25% energy reduction). The dietary intervention continued for six months, at this point animals were sacrificed and muscle samples were collected for gene expression and epigenetic analysis. Gene expression in muscle showed a marked decrease in *Ikbkε* and *Tnf* (premRNA, mRNA and protein) in the CR group, accompanied by *Tnf* promoter DNA hypermethylation. Expression of NAD+-dependent histone deacetylase *Sirt6* was increased by CR, whereas methyltransferase of H3K9 *Suv39h1* was downregulated in CR animals. CR decreased promoter and coding region binding of transcription factors (TF) NF-κB (p50) and C/EBP-β within in silico-predicted regions. miRNA data mining retrieved miR-19b and miR-181a, and qPCR analysis in muscle revealed that CR downregulated the pro-inflammatory miR-19b and increased the anti-inflammatory miR-181a and confirmed miR-19b targets (*Kdm2a, Zbtb16, Tnfaip3*). Chronic CR is able to regulate muscle-specific inflammation by targeting the NF-κB pathway as well as transcriptional and post-transcriptional regulation of *Tnf*.

6.2. INTRODUCTION

High fat, calorically dense diet consumption leads to an increased systemic inflammatory state that contributes to the development of several chronic metabolic diseases in humans including Obesity and Cancer. Skeletal muscle is the largest tissue in the body and a major source of inflammatory cytokines and their chronic increase promotes metabolic and immune impairment, which in turn can lead to sarcopenia or wasting (Collins et al., 2016; Dai et al., 2016). The transcriptional and epigenetic regulation of inflammatory cytokines, like Tumor Necrosis Factor (TNF), has been extensively described in immune tissues (T. T. Chen et al., 2017; Cheng et al., 2014; Falvo et al., 2010; J. E. Lee et al., 2013; X. Li et al., 2017; Palacios et al., 2010; Su et al., 2016; Vella et al., 2013; Villeneuve et al., 2008; J. Yu et al., 2016; N. Zhang et al., 2016), but no information is available regarding non-immune tissues like skeletal muscle. TNF and IL-6 are the main myokines (muscle cytokine) that contribute to metabolic regulation, myogenesis and immune function, and if dysregulated they can stimulate tissue wasting.

High-fat (HF) diet induces not only physiological (Helge, 2002; Hotamisligil & Davis, 2016; Kitessa & Abeywardena, 2016; Kraegen, Cooney, Ye, Thompson, & Furler, 2001; Storlien, Pan, Kriketos, & Baur, 1993) but also genome-wide epigenetic changes in various tissues, which are translated into an epigenomic programming of cellular metabolism and inflammation. Both DNA methylation and histone modifications can be altered by HF, and disturbance of gene expression patterns can be transgenerationally inherited. HF diet produces genome-wide epigenetic modifications that impact cellular metabolism and inflammation across many generations (Moody, Chen, & Pan, 2017; Y. Zhang et al., 2015). Given the nature of the widespread and inheritable nature of these epigenetic modifications, strategies that address not

only weight loss, but are able to reprogram the epigenome are needed for the sustained weight loss-effect at the cellular level.

Caloric restriction (CR) without malnutrition has been used as an effective weight management strategy, which can restore metabolic function and decrease inflammation (Cava & Fontana, 2013; Fontana, 2009; Fontana & Partridge, 2015). Studies have demonstrated the beneficial effects of CR on longevity and overall improvements in the quality of life (QOL) (Longo et al., 2015; Weiss & Fontana, 2011). We and others have found that CR is effective at downregulating the *Tnf* gene expression in muscle, leading to a reduction on inflammation-mediated muscle wasting (*Atrogin-1*), increase protein recycling (*Murf1*), whilst increasing myogenic factors (*MyoD1*, *MyoG*, *Myf5*). Interestingly, CR downregulates inflammation independently from weight loss (Mercken, Crosby, et al., 2013; Robertson & Mitchell, 2013; L. Yang et al., 2016b), but the mechanisms that lead to myokine regulation have not been fully described. Moreover, scarce information is available regarding the epigenetic effects of CR on myokines, which can have long-lasting anti-inflammatory effects. A better understanding of the mechanisms that lead to TNF silencing by CR, especially in skeletal muscle is critically needed.

CR is able to modify the epigenome in different tissues, and such actions are thought to be mediated by nutrient-sensing epigenetic modifiers like SIRT1, which can alter the acetylation status of histone H3 (Bordone & Guarente, 2005; Guarente, 2005; Hasty, 2001). Additionally, CR is able to mediate DNA methylation changes that have been associated to the aging and senescence processes (Maegawa et al., 2017; Mendelsohn & Larrick, 2017). Early-life exposure to high-fat diet epigenetically programs inflammation, which could be "erased" and reprogrammed by chronic CR. Therefore, elucidation of the epigenetic mechanism activated by chronic CR can help to determine the basis for the transgenerational and muscle-specific impact on inflammation.

Transgenerational modulation of inflammation by CR could help prevent chronic metabolic diseases, or lessen the impact of poor nutritional choices. Finally, the elucidation of a CR-responsive epigenetic pathway that instructs non-immune tissue to create an anti-inflammatory environment will provide therapeutic alternatives for the treatment of chronic metabolic diseases, such as Obesity.

6.3. METHODS

6.3.1. Experimental Design

In the present study, post-weaning, 4-5-wk-old male Sprague–Dawley rats (N=33) were fed a high fat diet (HF, 45% calorie from fat) (Research Diets, Inc., Cat. No. D12451) for 3 months (Fig. 6.1). Thereafter, from the time the animals showed an increase in fat mass (15% grams of fat) they were randomized into 3 groups: High fat- diet ad libitum (OL), weight maintenance (ML), and chronic caloric restriction (CR). Total average daily energy consumption or maintenance energy requirement (MER) was calculated (average Kcal/day) for each individual animal in the ML and CR groups by feeding AIN-93M (CON, 16% calories from fat) diet for 3 weeks ad libitum prior to the start of their individual dietary treatment. During this time, the OL group continued consuming HF diet. During this period, food intake was recorded daily and the body weight weekly. Following MER estimation, the respective 6-month dietary treatment began where the OL group continued to consume HF diet (n=9), the Maintenance group (ML) was fed 100% of their individual MER (100% MER) with AIN-93M diet to maintain body weight without weight gain (n=12), and finally the Caloric Restriction (CR) group was fed daily 75% of their individual calories (25% MER restriction) with AIN-93M supplemented with micronutrients to reach the vitamin and mineral levels consumed by MTN animals (n=12). Food intake and body weight were measured and recorded weekly during the treatment period. Animals were individually housed

with 12-h light/dark cycles, and given free access to water throughout the study. At the end of the 6-months dietary treatment, animals were euthanized with CO2 after an overnight fast (12 hours) to collect blood and tissues for subsequent analysis. To ensure that all rats were presented with comparable metabolic and feeding statuses, food was provided starting at 6:00 PM for all groups. Food was removed starting at 8:00 PM, and the animals were sacrificed starting at 8:00 AM the following day. All applicable institutional and governmental regulations regarding the ethical use of animals were followed during this research (University of Illinois Institutional Animal Care and Use Committee protocol no. 09112).

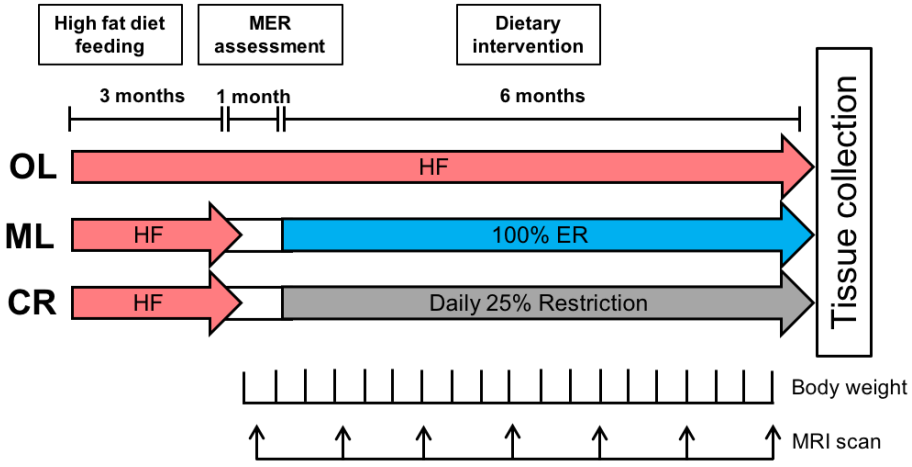

Figure 6.1. Experimental Design. Animals were fed a high fat diet (HFD) for 3 months (45% Kcal from fat), at which point they were randomized into each of the experimental treatments. Following high fat-feeding, the animals were switched to a control diet to calculate the maintenance energy requirements (MER) for each animal. MTN group received 100% of their MER, whereas the CR group received 75% of their MER. HFD group continued on a HFD ad libitum until the end of the study. Body weight was measured weekly, and body composition was performed on a monthly basis. The total duration of the study was 10 months.

6.3.2. RNA Isolation and Two-Step Real Time qPCR

Total RNA from Skeletal muscle (Gastrocnemius/ Soleus complex) was isolated using TRI reagent (Sigma, St. Louis, MO, USA), followed by Direct-zol™ RNA MiniPrep according to manufacturer's instructions (Cat. No. R2072). Reverse transcription was performed using the High

Capacity cDNA Reverse Transcription Kit (Applied Biosystems). Quantitative Real time PCR was using the StepOnePlus™ Real-Time PCR System with Power SYBR® Green PCR Master Mix (Cat. No. 4367659) using the respective forward and reverse primer for each gene (Appendix D Suppl. Table 6.1), and were designed by Vector NTI software (Invitrogen Corporation) and synthesized by Integrated DNA Technologies (www.idtdna.com). Standard curves with a slope of -3.30 (SEM 0.30) and R2 ≥ 0.99 were accepted. A 60S ribosomal protein (RpL7a) housekeeping gene whose expression was not affected by treatment were used to normalize the gene expression data.

6.3.3. Muscle TNF Western Blot

Total protein from skeletal muscle (50 mg) isolated by adding in 500 ul of protein lysis buffer (0·125 MTris–HCl, pH 6·8, 1 % SDS, 0·04 % bromophenol blue and 20 % glycerol, v/v) with 1X proteinase inhibitor (Roche Applied Science) and phosphatase inhibitor cocktail 1 and 2 (Sigma-Aldrich). Then, samples were sonicated with thirty pulses at a power setting of 3 (Fisher Scientific Model 100 Sonic Dismembrator). Diluted protein samples (25 mg) were size-fractionated on a 18 % Tris–HCl polyacrylamide gel and transferred onto a polyvinyl difluoride (PVDF) membrane (Bio-Rad Laboratories, Inc.) with a Trans-Blot® Turbo™ Transfer System (Bio-Rad Laboratories, Inc.) using the Turbo setting. To investigate TNF protein expression, the transferred PVDF membrane was incubated with blocking solution (5% w/v BSA) in TBS/T (20 mmol/L Tris–HCl, pH 7.6, 137 mmol/L NaCl, and 0.1% (v/v) Tween-20) for 1 h at room temperature. A rabbit polyclonal antibody against TNF (Anti-TNF alpha antibody, Abcam Cat. No. ab6671) diluted 1:2,000 in the blocking solution with 5% BSA and incubated with the membrane for overnight at room temperature before washing with 2% BSA in TBS/T 5 times for 5 min. A goat anti-rabbit HRP-conjugated secondary antibody (Kirkegaard & Perry Laboratories, Gaithersburg, MD) was

diluted to 1:10,000 in the blocking solution containing 3% BSA and incubated with the membrane for 1 h at room temperature (Appendix D Suppl. Table 6.2). After washing 5 times for 5 min in the blocking solution containing 1% BSA, the membrane was exposed to the enhanced chemiluminescence reagent ECL signal enhancer for 6 min (Amersham G&E, Cat. No. RPN2232). Signals from the membrane were detected and quantified by the ChemiDoc XRS imaging system (Bio-Rad, Hercules, CA). β-Actin was used as a loading control for the protein expression (Santa Cruz Biotechnology, Cat. No. sc-1616).

6.3.4. Genomic DNA isolation and methylation-sensitive PCR analysis of Tnf

Frozen muscle (50 mg) was ground in liquid nitrogen and genomic DNA (gDNA) was them isolated using ZR Genomic DNA™Tissue MiniPrep (Zymo Research, Irvine, California, Cat. No. D3051) per manufacturer's instruction. gDNA was bisulfite converted using the EZ DNA Methylation-Gold Kit (Zymo Research, Irvine, California, Cat. No. D5005) following the manufacturer's instructions. Quantitative PCR used 20 ng of gDNA as the template using Power SYBR Green PCR Master as the reporter. Primers used for each genomic region were designed using the Primer Express™ Software (Thermo Fisher Scientific) within CpG sites vidualized in the Methprimer website (http://www.urogene.org/methprimer/index.html) (L. C. Li & Dahiya, 2002), to create six primer sets that targeted the promoter (-5000 bp to 0 bp) or coding region (0 bp to 2.61 kb) of rat *Tnf*. Primers were screened in the IDT OligoAnalyzer to minimize dimers and hairpin loops. Primer information can be found in Appendix D Suppl. Table 6.1. Data are presented as fold change calculated with the ΔΔCt method.

6.3.5. Skeletal Muscle Chromatin Immunoprecipitation (ChIP)

To determine specific histone modifications and NF-κB1 and C/EBPb binding on the promoter and coding region of *Tnf*, ChIP analysis was performed according to a modified protocol (D. Zhou,

Wang, Cui, Chen, & Pan, 2015). Briefly, 200 mg frozen liver was ground in liquid nitrogen and suspended in PBS. Protein-DNA cross-linking was performed, and sheered on ice by a Sonic Dismembrator (Fisher Scientific, model F100) for 40 s at power setting 5 with 2 min cooling interval between each burst, four bursts for rat samples. Sheared chromatin incubated with specific antibodies (Appendix D Suppl. Figure 4.2), and precipitated with pre-blocked protein G-agarose beads (Millipore, Cat. 16-266). A normal rabbit IgG was used as a negative control. Supernatant from incubated IgG was saved as the input DNA for each sample. Then protein-DNA complexes were eluted and reverse cross-linked. Chromatin DNA was purified using QiaPrep miniprep kit (Qiagen, Cat. No. 27106) after proteinase K digestion. Immunoprecipitated DNA was then quantified by real-time quantitative PCR using primers specific to the promoter and coding region of gene (Appendix D Suppl. Table 6.1). The results were expressed as percent to input DNA. Antibodies are listed in Appendix D Suppl. Table 6.2.

6.3.6. Transcription Factor Binding In Silico Analysis

Transcription factor binding identification within the promoter and coding region of the rat Tnf gene were analyzed using the PROMO tool version 8.3 of TRANSFAC (Farre et al., 2003; Messeguer et al., 2002). Sequences were retrieved from Ensembl (ENSRNOT00000079677.1) defining the promoter region within 1000 bp upstream of the transcription start site (TSS), and within the coding region only the +600 to +700 containing the highest variation in C/EBPβ and NF-κB1 binding is shown.

6.3.7. Identification of miRNAs targeting Tnf 3'-UTR

To identify rat miRNAs that might target inflammatory pathways or the 3'-UTR of *Tnf* gene, we used a three-pronged analysis. First, we used a bioinformatic approach to map the 3'-UTR of *Rattus norvegicus Tnf* gene in miRDB (http://www.mirdb.org/), Targetscan

(http://www.targetscan.org/), and microRNA.org (http://34.236.212.39/microrna/home.do) to predict miRNAs that interact with *Tnf* or its pathway. Then, we performed a systematic search in PubMed with the keywords "muscle TNF" and "miRNA" for any organism to identify a broadly conserved miRNA family across vertebrates that targeted the gene. Finally, we performed a similar systematic search in PubMed with the keywords "caloric restriction" and "miRNA" for any organism to identify a broadly conserved miRNA family across vertebrates that was targeted by CR. The final miRNA candidates were selected based on broadly conserved families that overlapped in the in the three approaches. The full list of miRNAs for each approach can be found in Appendix D Suppl. Table 6.3. The miRNA that overlapped in the screening process were rno-mir-19b-3p (MIMAT0000788) and rno-mir-181a-1-5p (MIMAT0000858). Quantification of specific miRNA was achieved by performing individual reverse transcription of previously isolated RNA for enrichment, followed by qPCR with the commercially available TaqMan probes for rno-mir-19b-3p (Assay ID: rno478264_mir, Cat. No. A25576), rno-mir-181a-1-5p (Assay ID: rno481485_mir, Cat. No. A25576), following manufacturer's instructions. All miRNA content was normalized to a U6 housekeeping snRNA (NCBI Accession: NR_004394; Assay ID: 001973 [Cat. No. 4440887]).

6.3.8. Statistical Analysis

A repeated measures ANOVA was used for cumulative caloric intake, body weight and body composition changes. A one-way ANOVA was used to analyze the gene expression and protein quantification data. Tukey's LSD was used for post hoc tests with a p value ≤ 0.05. Significant differential expression of miRNA data was defined as a fold change greater than 0.5. Violin plots and statistical tests were performed in in R 3.3.2.

6.4. RESULTS

6.4.1. Caloric intake and Body Composition

Animals were assigned to a high-fat feeding protocol for 3 months until fat mass increased by 10-15% from the initial measurement. Following the high-fat feeding period, the animals were randomly allocated to one of three groups: OL (chronic HF), ML (BW maintenance), and CR (25% restriction). Both ML and CR underwent a 3-week period of maintenance energy requirement (MER) estimation by feeding control AIN-93 diet and measuring the average caloric intake per individual animal. Once the MER was calculated, the ML group was fed 100% of their MER to prevent overfeeding, and the CR group was given 75% of their individual MER. Cumulative caloric intake for each group from the start of the dietary treatment are shown in Fig. 6.2A. Caloric intake was used to define the separation between groups, and so the OL group had a significantly higher intake starting from week 4 of dietary intervention, compared to ML and CR.

Body weight changes were recorded weekly, having that by week 4 of dietary intervention significant differences between all groups were observed (OL: 517.34 ± 5.34 g, ML: 468.58 ± 7.42 g, CR: 440.43 ± 9.85 g), and such differences were maintained throughout the experiment (Fig. 6.2B). Body composition changes for each group can be observed in Fig. 6.2B. Body weight incremented weekly for the OL group, as shown by the final fat mass gain of 75.62 ± 8.24 g and 26.97 ± 4.93 g of lean mass gain, compared to the initial measurement (beginning of dietary intervention). The ML group was used to assess changes following maintenance of body weight, as such, we observed a final fat mass gain 7.36 ± 2.24 g and 7.64 ± 2.76 g of lean mass, and statistically different from OL ($p<0.0001$). The ML group showed a 1:1 ratio of fat-to-lean mass gain, whereas the OL group showed a 3:1 increment ratio. Lastly, the CR group significantly

decreased both final fat (-40.09 ± 5.91 g) and lean mass (-57.89 ± 3.57 g), showing a slight preferential wasting coming from lean mass (1:1.44 fat-to-lean) (Fig. 6.2B).

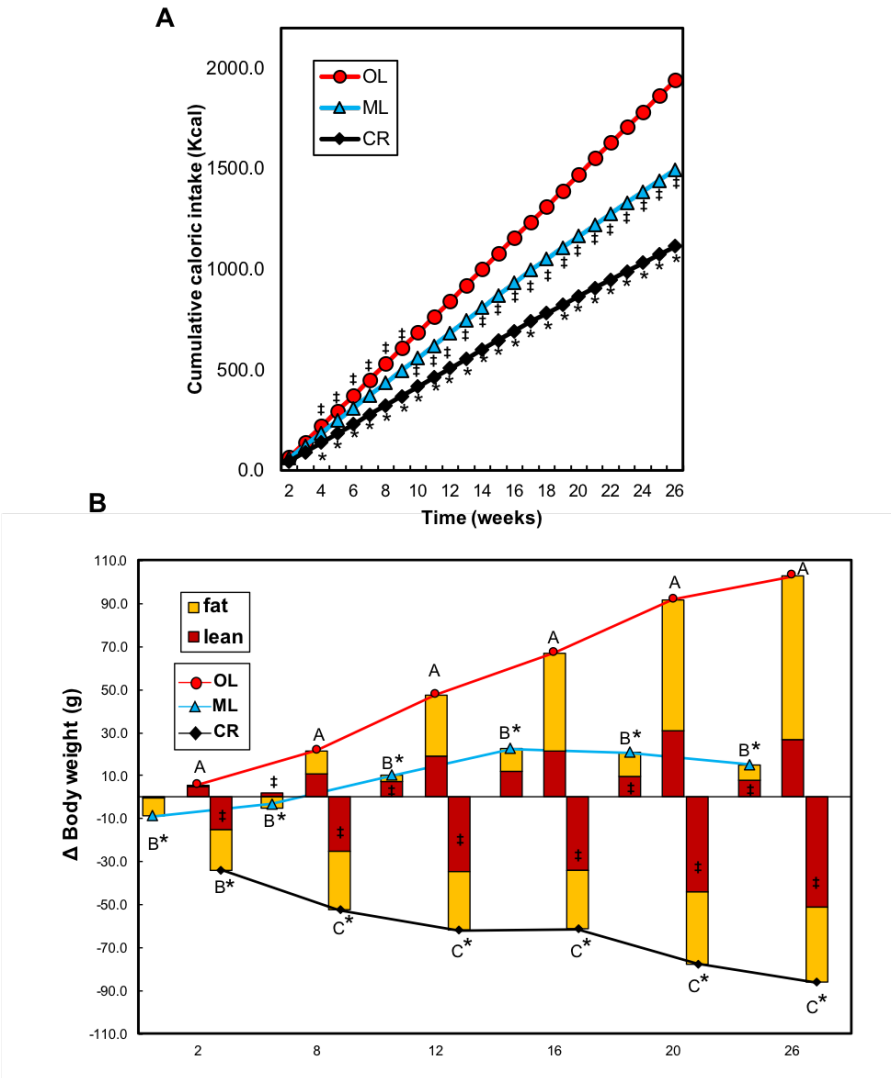

Figure 6.2. Caloric Intake and Body Composition of changes in CR animals following a HF diet. A) Cumulative daily caloric intake highlights the energy consumed based on the energy requirements for each experimental group. Different symbols indicate significant statistical difference with Tukey post hoc test using repeated measures ANOVA at $p<0.05$: ‡ ML vs. OL; * CR vs. OL. B) Body composition changes were analyzed with EchoMRI-700 Body Composition Analyzer showing a sustained change in fat and lean mass for all animals at week 2. Body weight changes can be observed in the lines connecting each time point, whereas fat (yellow bars) and lean (red bars) mass is presented as a proportion to body weight changes. Values are expressed as means ± SEM. Different symbols indicate significant statistical difference in lean mass (‡), fat mass (*), and body weight changes (ABC) with Tukey post hoc test using repeated measures ANOVA at $p<0.05$.

6.4.2. Skeletal Muscle Tnf Expression and Protein Content

Given the preferential loss of lean mass in CR, muscle cachexia was assessed by measuring the gene expression of *Nfκb1* and *Tnf*, both known markers of skeletal muscle wasting. Surprisingly, CR group showed increased expression of *Nfkb1* compared to OL ($p<0.05$), but a significant decrease in its activation kinase Ikbke (Fig. 6.3A), together with a significant upregulation of the Inhibitor of NF-kB (*Nfkbia*) or IKBα. No changes were observed in TNF receptors *Tnfrsf1a* and *Tnfrsf12a*, and upstream kinase *Ripk1*, as well as *Cebpb*, *Rela* (*p65*), or *Ikbkg* between all groups (Fig. 6.3A).

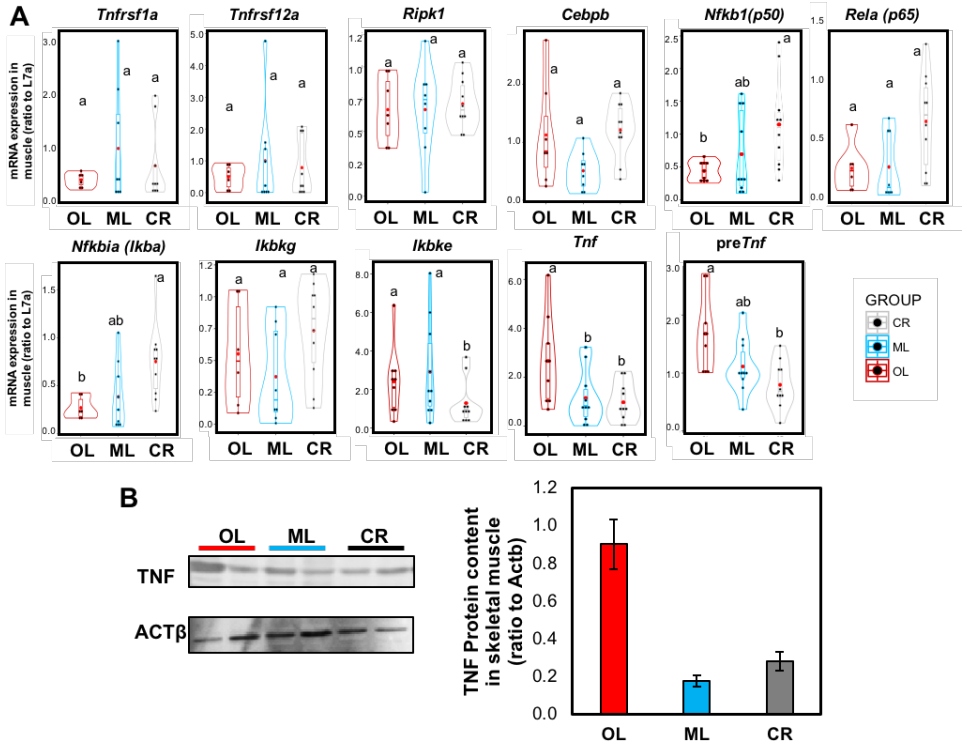

Figure 6.3. Violin Plots of the Distribution of Transcription Rate, Gene and Protein Expression of TNF in Skeletal Muscle of CR Rats Following HF Diet. A) Gene expression distribution of TNF receptors Tnfrsf1a and Tnfrsf12a, Ripk1, Nfkb1 (p50), Rela (p65), Nfkbia (Ikba), Ikbkg, Ikbke, Tnf mRNA and pre-mRNA. abc Different letters indicate significant statistical difference with Tukey post hoc test at $p<0.05$. B) TNF protein content in skeletal muscle shown in representative blots (left) and quantification of the ratio to Actinβ (right). abc Different letters indicate significant statistical difference with Tukey post hoc test at $p<0.05$.

Next, expression of mature *Tnf* RNA was significantly reduced by ML and CR, compared to OL, whereas active translation assessed by measuring immature *Tnf* RNA content was only significantly reduced for CR, compared to OL (Fig. 6.3A). Given the marked reduction in Tnf transcription, we assessed the content of TNF protein in skeletal muscle. Similar to premRNA and mRNA levels, CR was able to significantly reduce TNF protein expression, compared to ML and OL (Fig. 6.3B).

6.4.3. DNA Methylation Analysis of Tnf Promoter

Following assessment of mRNA and protein measurement of TNF in muscle, we aimed to explore the changes in DNA methylation that would lead to an alteration of the transcriptional control of the Tnf gene. DNA methyltransferases are responsible for changes in DNA methylation both maintenance (Dnmt1) and de novo methylation (Dnmt3b).

Gene expression of Dnmt1 was decreased by CR ($p<0.05$), compared to OL indicating alterations in methylation maintenance (Fig. 6.4A). No significant changes were observed for de novo methyltransferase Dnmt3b (Fig. 6.4A). Promoter DNA methylation is known to regulate gene transcription; for that reason, DNA methylation changes were assessed at 5'-upstream sites of the *Tnf* gene (-4850 to -4789 bp, -2922 to -2834 bp, -1902 to -1832 bp, -1018 to -950 bp, and -253 to -155 bp) (Fig. 6.4B). Significant changes in 5'-upstream methylation were observed at -1018 to -950 bp, where the CR group showed the highest methylation at this site ($p<0.05$), followed by and ML and OL groups that showed the lowest levels of methylation (Fig. 6.4C). Other regions within the promoter displayed a trend towards a decrease for CR, but were not statistically significant.

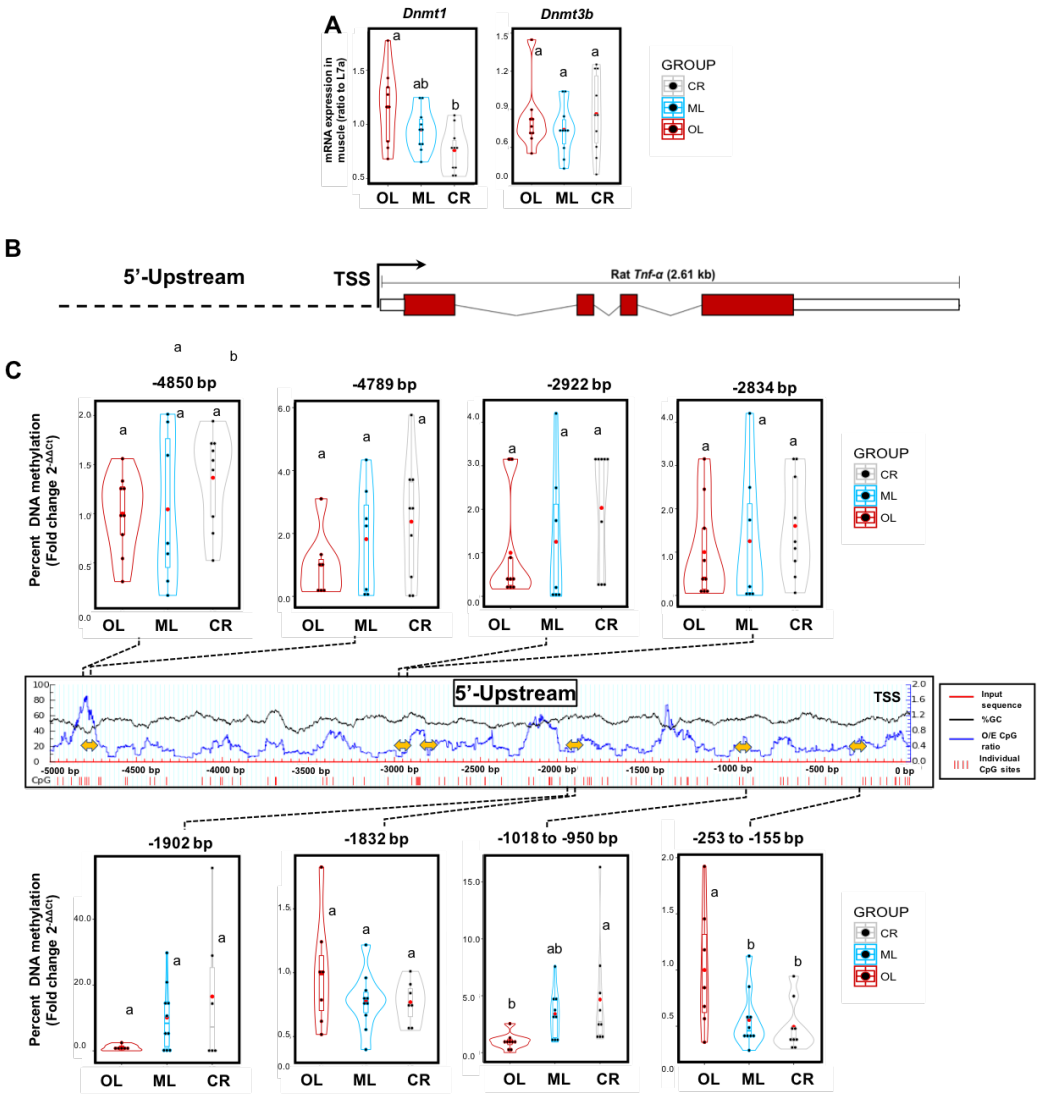

Figure 6.4. Violin Plots of the Distribution of DNA Methyltransferases and DNA Methylation from *Tnf* Promoter in Skeletal Muscle of CR Rats Following HF Diet. A) Gene expression distribution of Dnmt1 and Dnmt3b. [abc] Different letters indicate significant statistical difference with Tukey *post hoc* test at $p<0.05$. **B)** MSP primers for *Tnf* promoter methylation analysis are found within -4850 to -4789bp, -1902 to -1832bp, -1018 to -950 bp, -253 to -155 bp. (—) Red line within the diagram depicts the input sequence of 5000 bp upstream of *Tnf* TSS; (—) Black line within the diagram depicts the intensity of GC percentage (%GC) within 5000 bp upstream of *Tnf* TSS; (—) Blue line within the diagram depicts the ratio of observed vs. expected CpG (O/E CpG) within 5000 bp upstream of *Tnf* TSS; (||||) Vertical red lines within the diagram depict the Individual CpG sites within 5000 bp upstream of *Tnf* TSS; (⇔) Yellow double arrows within the diagram indicate the approximate location of each primer within 5000 bp upstream of *Tnf* TSS. **C)** DNA Methylation percentage (%) within each region analyzed with MSP primers. Data are presented as mean values ± SEM. [abc] Different letters indicate significant statistical difference with Tukey *post hoc* test at $p<0.05$.

6.4.4. Chromatin Immunoprecipitation (ChIP) and In silico Transcription Factor binding

Together with DNA methylation, epigenetic modification such as histone tail modifications have a strong impact on the availability of the underlying DNA sequences to transcription factors and transcriptional machinery. For that reason, we assessed transcription factor binding, namely NF-κB (p50) and C/EBP-β, and histone 3 lysine 4 trimethylation (H3K4me3) and histone 3 acetylation (H3Ac) as marks of a permissive chromatin (Yan & Boyd, 2006). As seen in Fig. 6.5A, *Tnf* from *Rattus norvegicus* has a highly conserved promoter, and coding region mainly spanning exons, and portions of the 3'-UTR. Both NF-κB (p50) and C/EBP-β binding was increased for the OL group within the promoter and along the coding region (Fig. 6.5C & D), compared to the IgG negative control (Fig. 6.5B). OL showed a consistent NF-κB (p50) binding along the *Tnf* gene, whereas C/EBP-β showed a higher peak within Intron 1-2 (+614 to +688 bp) (Fig. 6.5C & D). Both CR and ML displayed a decreased NF-κB (p50) and C/EBP-β binding within the promoter and coding region of *Tnf*. Activating histone marks H3K4me3 and H3Ac were slightly increased within the first exon of *Tnf* (Fig. 6.5E & F), whilst no changes were observed for OL for these two marks.

To characterize the binding sites within the promoter and coding region of *Tnf*, an *in silico* analysis was performed to define the regions of highest NF-**κ**B (p50) and C/EBP-β density. Using a consensus sequence 5'-GGRNNYYCC-3' for NF-**κ**B (p50) and 5'-T[TG]NNGNAA[TG]-3' for and C/EBP-β, we mapped the predicted binding sites. Binding of NF-**κ**B (p50) has numerous cis-elements within the promoter of rat Tnf, and the sequences are can be found in Fig. 6.6A. Given the increased binding of NF-**κ**B (p50) within intron 1-2, we found that 3 different binding sites are

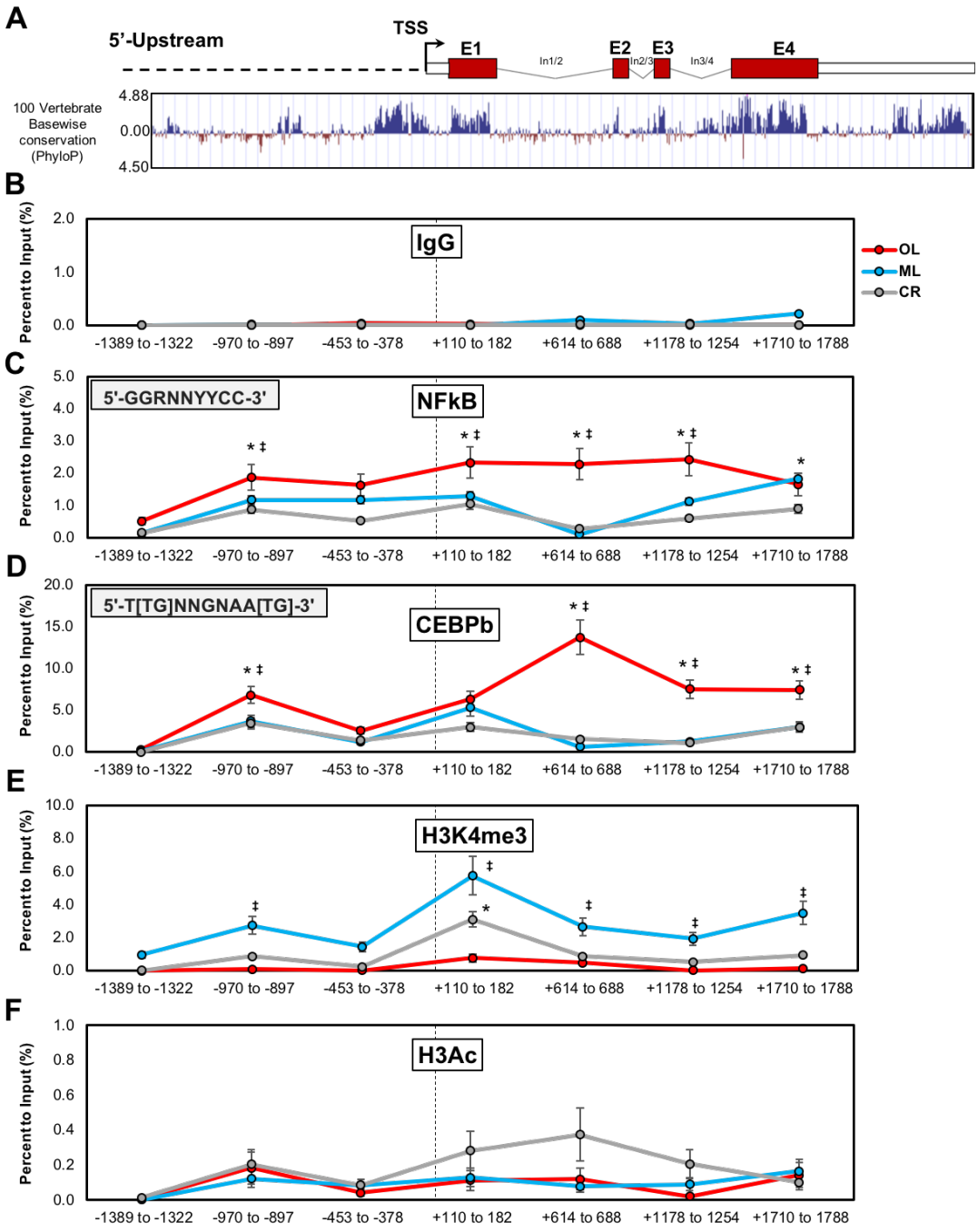

Figure 6.5. NF-κB and CEBP-β Transcription factor binding and Histone modifications within the *Tnf* gene. A) Phylogenetic basewise conservation PhyloP (-Log *p*-value) from 100 vertebrates of the *Tnf* gene. Each site of corresponds to the depicted 5'-upstream region or within the *Tnf* rat gene. **B)** IgG (negative control), **C)** NF-κB (p50 subunit) (inset: consensus sequence), **D)** CEBP-β (inset: consensus sequence), binding within each genomic region depicted in the *Tnf* gene diagram. **E)** Histone 3 Lysine 4 trimethylation (H3K4me3), and **F)** Histone 3 Acetylation (H3Ac) modifications within each genomic region depicted in the *Tnf* gene diagram. Data are presented as mean values ± SEM. ‡, * Different symbols within each site indicate significant statistical difference with Tukey *post hoc* test at $p<0.05$. ‡ ML vs. OL; * CR vs. OL.

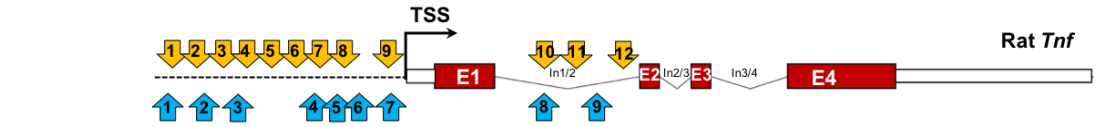

A

NF-kB1 (p50)
Consensus sequence

Binding site	Genomic location	Start	End	Sequence
1	Promoter	-903	-892	AAGTGACTCCCC
2	Promoter	-792	-783	GGGAACCACA
3	Promoter	-655	-646	GTGAATTCCC
4	Promoter	-637	-628	GTTCATTCCC
5	Promoter	-513	-503	GGGGGCTTTCC
5	Promoter	-511	-502	GGGCTTTCCC
6	Promoter	-492	-481	TTGAGTCTCCCC
7	Promoter	-405	-396	GGGAACGGAC
8	Promoter	-210	-199	CTGGGTGTCCCC
9	Promoter	-75	-66	AGCTTTTCCC
10	Intron 1-2	+576	+585	GGGAAGAAGC
11	Intron 1-2	+661	+670	GGGAAACAAC
12	Intron 1-2	+827	+836	AGAAGTTCCC

B

C/EBPb
Consensus sequence

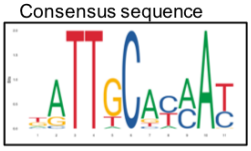

Binding site	Genomic location	Start	End	Sequence
1	Promoter	-939	-932	CAATCCAA
2	Promoter	-842	-835	TTGGAAGA
3	Promoter	-771	-764	TGCTGCAA
3	Promoter	-770	-764	GCTGCAA
3	Promoter	-769	-764	CTGCAA
4	Promoter	-255	-248	TTGCCACA
4	Promoter	-255	-250	TTGCCA
4	Promoter	-255	-249	TTGCCAC
5	Promoter	-196	-189	CTTTCCAA
6	Promoter	-173	-166	TTGGAGAA
7	Promoter	-84	-77	TTGAATGA
8	Intron 1-2	580	587	AGAAGCAA
8	Intron 1-2	581	587	GAAGCAA
8	Intron 1-2	582	587	AAGCAA
9	Intron 1-2	758	765	GCTGGCAA
9	Intron 1-2	759	765	CTGGCAA
9	Intron 1-2	760	765	TGGCAA

C

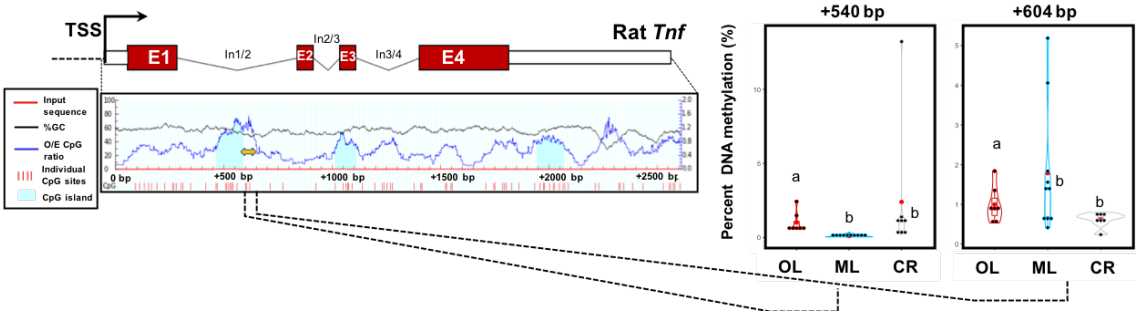

Figure 6.6. ***In silico*** **Prediction of NF-κB and CEBP-β Binding Sites within the** ***Tnf*** **gene.** Consensus sequence and individual predicted binding sites and *cis*-element within the 5'-upstream region or within the *Tnf* rat gene for **A)** NF-κB (p50 subunit) and **B)** CEBP-β. **C)** DNA methylation percentage of *Tnf* coding within +540 to +604bp. (—) Red line within the diagram depicts the input sequence of *Tnf* coding region; (—) Black line within the diagram depicts the intensity of GC percentage (%GC) of *Tnf* coding region; (—) Blue line within the diagram depicts the ratio of observed vs. expected CpG (O/E CpG) of *Tnf* coding region; (||||) Vertical red lines within the diagram depict the Individual CpG sites of *Tnf* coding region; (⇔) Yellow double arrows within the diagram indicate the approximate location of each primer of *Tnf* coding region; ( ) Blue regions within the diagram indicate CpG island prediction of *Tnf* coding region. Data are presented as mean values ± SEM. ^{abc} Different letters indicate significant statistical difference with Tukey *post hoc* test at $p<0.05$.

found within the same region as seen in Fig. 6.5C. On the other hand, C/EBP-β has fewer binding site within the promoter of Tnf (Fig. 6.6B), and can also bind the same genomic location found for C/EBP-β ChIP (Fig. 6.5D). Interestingly, coding region DNA methylation within Intron 1-2 (+540 bp to +604 bp) was significantly increased for the OL group, compared to both the ML and CR groups (Fig. 6.6C). Next, we assessed gene expression of several histone modifiers (histone deacetylases, methyltransferases and demethylases) in skeletal muscle samples from animals. Neither histone deacetylase Hdac3 nor NAD+-dependent deacetylase Sirt1 were affected by CR, although an increasing trend was observed for the latter (Fig. 6.7A).

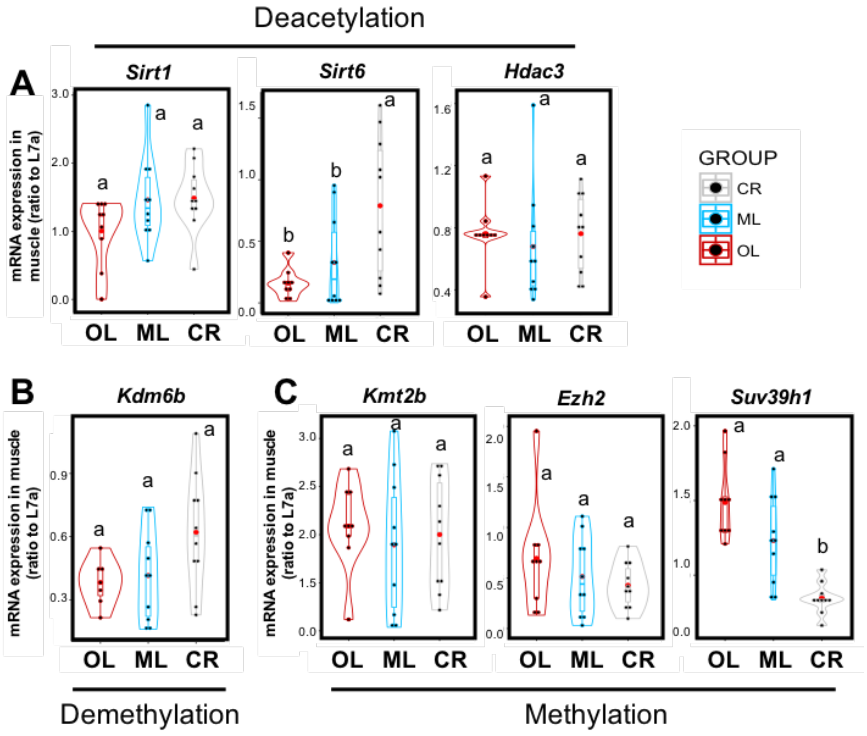

Figure 6.7. Violin Plots of the Distribution Gene Expression of Chromatin Modifiers in Skeletal Muscle of CR Rats Following HF Diet. A) Gene expression distribution of histone deacetylases *Sirt1*, *Sirt6*, and *Hdac3*, **B)** histone demetylase *Kdm6b* and **C)** histone methyltransferases *Kmt2b*, *Ezh2*, and *Suv39h1*. Data are presented as mean values ± SEM. [abc] Different letters indicate significant statistical difference with Tukey *post hoc* test at $p<0.05$.

Gene expression of another NAD+-dependent deacetylase, Sirt6 was highly induced by chronic CR, compared to ML and OL (Fig. 6.7A). Lysine-Specific Demethylase 6b (*Kdm6b*) showed an increasing trend for CR, but was not statistically significant (Fig. 6.7B). Likewise, histone methyltransferases Lysine N-Methyltransferase 2b (Kmt2b) and Enhancer of Zeste 2 (*Ezh2*) were unchanged by treatment, but the Suppressor of Variegation 3-9 Homolog 1 (*Suv39h1*), which targets specifically H3K9 methylation, was suppressed by CR, compared to OL and ML (Fig. 6.7C).

6.4.5. miRNA Analysis

To define the epigenetic mechanisms at play during CR that are able to revert the HF-induced epigenetic program, we sought to explore the involvement of miRNA in skeletal muscle inflammation regulation. Following the bioinformatics analysis using *Tnf* 3'-UTR with online databases, PubMed search with algorithms that target "muscle *Tnf*" AND "miRNA" and "caloric restriction" AND "miRNA", we found a total of 207 miRNA. Of the 207 miRNAs, 37 unique miRNA that are able to target the *Tnf* 3'-UTR region were identified, whereas 83 were found with "muscle *Tnf*" and "miRNA" algorithm, and 155 were observed for "CR and miRNA". A total of 2 miRNA that overlapped for all three strategies were selected, both rno-mir-19b-3p and rno-mir-181a-5p are broadly conserved miRNAs that are related to inflammation or *Tnf* mRNA (Fig. 6.8A). rno-mir-181a targets the 3'-UTR of the *Tnf* gene (Fig. 6.8B), and its expression can be found in Fig. 6.8C.

Anti-inflammatory miR-181a-5p was decreased in OL, and was significantly different from ML and CR ($p<0.05$) (Fig. 6.8C). Moreover, LRR Binding FLII Interacting Protein 1 (*Lrrfip1*) a known repressor of *Tnf*, whose function is complimentary to mir-181a-5p, was reduced

in ML and CR groups, compared to OL (Fig. 6.8D). Moreover, mir-19b-3p is able to target the repressors

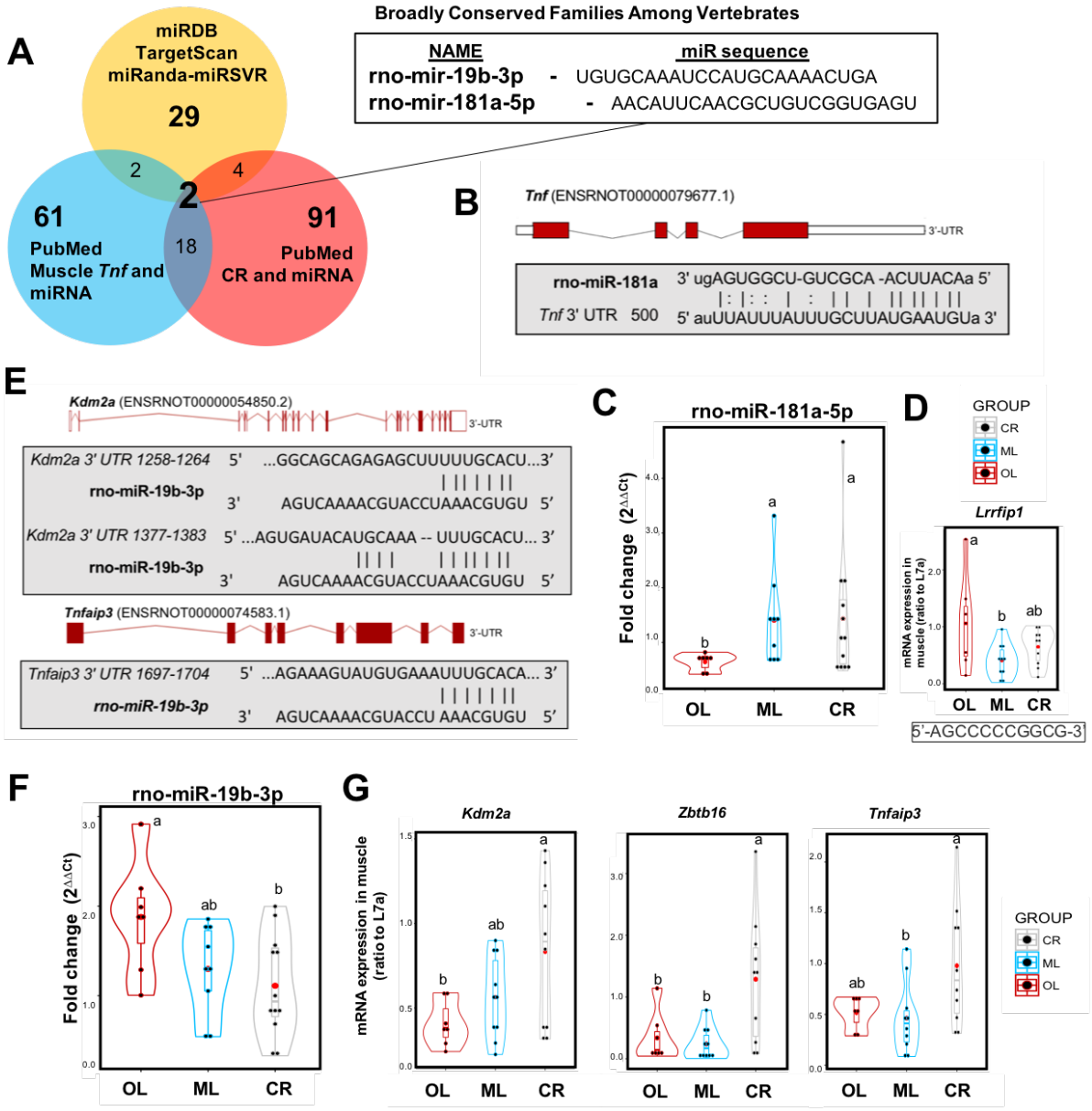

Figure 6.8. Database Mining and Expression of miRNA targeting NF-κB Signaling and *Tnf* Expression in Muscle. **A)** Venn diagram depicting the results from miRNA database and PubMed mining, showing an overlap for rno-mir-181a-5p and rno-mir-19b-3p (Appendix D Suppl. Table 6.3). **B)** rno-mir-181a-5p directly targets the *Tnf* 3'-UTR. **C)** Violin plot of distribution of the fold change in rno-mir-181a-5p in skeletal muscle. **D)** Violin plot of the distribution of TNF inhibitor, Lrrfip1, in skeletal muscle (inset: binding sequence). **E)** rno-mir-19b-3p directly targets the 3'-UTR of *Kdm2a* and *Tnfaip3*. **F)** Violin plot of distribution of the fold change in rno-mir-19b-3p in skeletal muscle. **G)** Violin plot of the distribution of NF-κB inhibitors, *Kdm2a, Zbtb16,* and *Tnfaip3*, in skeletal muscle. Data are presented as mean values ± SEM. [abc] Different letters indicate significant statistical difference with Tukey *post hoc* test at $p<0.05$.

of NF-κB signaling (*Rnf11, Kdm2a, Tnfaip3, Zbtb16*), and thus its increase will lead to an overstimulation of NF-κB and the downstream inflammatory pathway (Gantier et al., 2012). Fig. 6.8D shows a representative binding site of mir-19b-3p to the 3'-UTR of *Kdm2a and Tnfaip3*. In skeletal muscle, OL group showed the highest expression of mir-19b-3p, followed by ML and CR ($p<0.05$) (Fig. 6.8E). Additionally, the inhibitors of NF-κB signaling, *Kdm2a*, *Zbtb16*, and *Tnfaip3* are consistently increased by CR, compared to OL and ML ($p<0.05$) (Fig. 6.8F). *Rnf11* is not adequately annotated in the rat genome, therefore the analysis was not performed.

A summary of the results can be observed in Fig. 6.9, where high-fat diet or its associated chronic inflammatory state are able to stimulate receptors within the muscle cells that lead to the activation of Inhibitor of Nuclear Factor Kappa B Kinase (IKK), which phosphorylates the Inhibitor of Nuclear Factor Kappa B (IkBα) and promote its proteasomal degradation (Fig. 6.9A). Following activation of NF-**κ**B (RelA/p50 complex), NF-**κ**B translocates to the nucleus where it can bind cis-elements within the promoter and coding region of *Tnf* and enhance transcription aided by the decreased promoter DNA methylation in response to high-fat feeding (Fig. 6.9B). Other factors that are mediated by high-fat diet, such as C/EBP-β also bind the promoter and coding region to produce a similar effect. Following transcriptional activation, premRNA from Tnf is exported out of the nucleus where it matures (7-mG cap, poly A tail, and splicing), forming the mature mRNA that can be translated into TNF protein (Fig. 6.9C). CR is able to Inhibit IKK expression (Fig. 6.9A), NF-**κ**B, and C/EBP-β binding (Fig. 6.9B), as well as increase promoter methylation. Chronic CR downregulated the transcriptional activation (premRNA) of Tnf, as well as its mRNA and protein expression (Fig. 6.9C). Furthermore, CR is capable of upregulating miR-181a which depletes *Tnf* mRNA (Fig. 6.9D), and downregulates miR-19b which targets the inhibitors of NF-**κ**B (Fig. 6.9E), leading to the regulation of the inflammatory pathway.

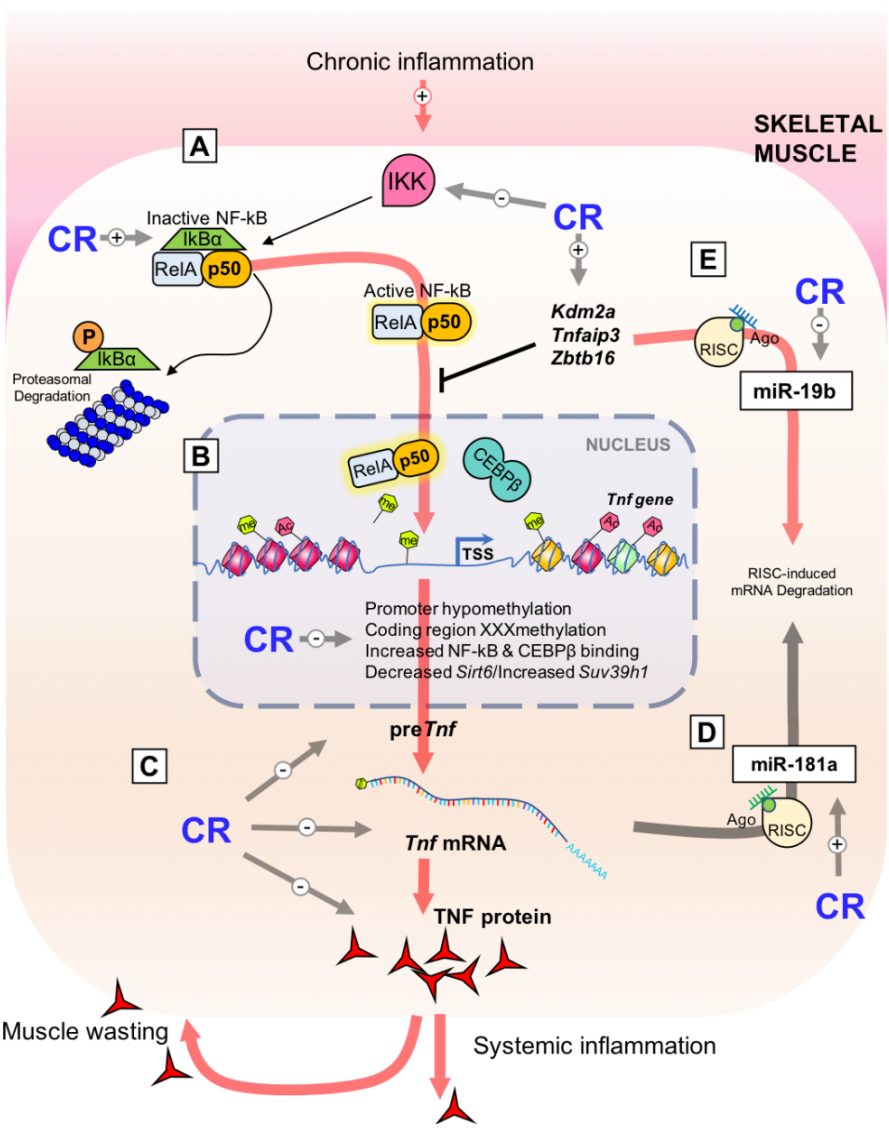

Figure 6.9. Summary of the Effects of Chronic CR on NF-κB Signaling and *Tnf* Expression in Skeletal Muscle. **A)** Chronic high-fat diet or its associated chronic inflammatory state are able to stimulate receptors within the muscle cells, leading to the activation of Inhibitor of Nuclear Factor Kappa B Kinase (IKK), which phosphorylates the Inhibitor of Nuclear Factor Kappa B (IkBα) and promotes its proteasomal degradation. B) Following activation of NF-κB (RelA/p50 complex), NF-κB translocates to the nucleus where it can bind *cis*-elements within the promoter and coding region of *Tnf* and enhance transcription aided by the decreased promoter DNA methylation in response to high-fat feeding. Other factors that are mediated by high-fat diet, such as C/EBP-β also bind the promoter and coding region to produce a similar effect. C) Following transcriptional activation, premRNA from *Tnf* is exported out of the nucleus where it matures and forms mRNA that can be translated into TNF protein by the ribosomal machinery. CR is able to Inhibit IKK expression (Panel A), NF-κB, and C/EBP-β binding, *Suv39h1* expression, and increase *Sirt6* (Panel B), as well as increase promoter methylation that leads to the transcriptional downregulation of *Tnf*, mRNA and protein expression (Panel C). D) Furthermore, CR is capable of upregulating miR-181a that recruits the RNA-induced silencing complex (RISC) to mediate the degradation of *Tnf* mRNA, and **E)** CR also downregulates miR-19b which targets the inhibitors of NF-κB, which fosters the redundant downregulation of the inflammatory pathway.

6.5. DISCUSSION

This study demonstrated for the first time the reprogramming effect of chronic CR on skeletal muscle inflammation, which establishes an adaptive epigenetic response to prevent inflammation and cachexia. Rats were assigned to life-long HF (OL), early-life HF with weight maintenance (ML), or early-life HF with chronic 25% CR (CR). Animals undergoing CR decreased expression of *Ikbkε* and Tnf (premRNA, mRNA and protein), despite the *Nfkb1* increase, compared to OL and ML. *Tnf* promoter DNA methylation was increased by CR, despite *Dnmt1* reduction. Moreover, gene expression of *Sirt6* and *Suv39h1* were altered by CR, although no changes in *Tnf* H3K4me or H3Ac were observed. CR prevented promoter and coding region binding of TFs NF-κB (p50) and C/EBP-β within *in silico*-predicted regions. Finally, miRNA data mining identified miR-19b and miR-181a, and analysis in skeletal muscle revealed that CR downregulated the pro-inflammatory miR-19b and increased the anti-inflammatory miR-181a together with the confirmed miR-19b targets. Chronic CR is able to regulate muscle-specific inflammation by targeting the NF-κB pathway and repressing transcription of *Tnf* through promoter DNA methylation and promoter and coding region TF inhibition, as well as blunting inflammatory miRNA.

Chronic CR is regarded as a safe and effective weight loss strategy, and is associated with increased lifespan and improved metabolic health (Cava & Fontana, 2013; Fontana, 2009; Fontana & Partridge, 2015). To our knowledge, this is the first study that includes a control group (ML) that will facilitate the separation of the CR-specific effects taking into account early life-HF, while maintaining BW and avoiding overfeeding. We observed a marked separation of not only body weight in our experimental groups, but a positive relationship between the caloric intake and the body composition, having that CR preferentially used muscle mass as a dynamic reservoir of energy. Together with this shift in lean mass, CR was able to turn off inflammatory mediators such

as *Ikke* and *Tnf*, compared to its HF-fed counterparts. As reported in previous studies, CR (%) is able to regulate muscle inflammation in aged rats in a muscle-type specific manner similar to younger animals (Phillips & Leeuwenburgh, 2005; L. Yang et al., 2016a). Therefore, CR without malnutrition is effective at decreasing fat and lean mass, as well as inflammation, to overcome the effects of early-life HF feeding.

Epigenetic regulation of inflammatory genes has been extensively described in immune tissues (Falvo et al., 2010), but other metabolically active tissues such as the liver, adipose and more importantly skeletal muscle, are able to transform dietary cues into an immunologic response (Oh et al., 2016; Pedersen & Hojman, 2012). To our knowledge, we are the first to describe a novel mechanism by which CR makes use of the epigenetic machinery to repress NF-κB signaling and specifically TNF expression in skeletal muscle. Despite the decreased *Dnmt1* expression in CR muscle, *Tnf* promoter methylation is in accordance with the transcription rate reduction (*Tnf* premRNA), which in turn limits the amount of mRNA generated and leads to decreased TNF protein content in muscle of CR animals. Intronic DNA methylation is a poorly understood, but warrants exploration given the marked reduction in the CR and ML groups, possibly revealing an unknown regulatory element within the coding region of the gene. In addition, CR is able to block promoter and coding region binding of TFs such as NF-κB and C/EBP-β, which are known modulators of inflammation in response to systemic inflammation or dietary factors (Ertunc & Hotamisligil, 2016; Gregor & Hotamisligil, 2011; Hotamisligil, 2017a, 2017b). Decreased binding of such TFs speaks to the ability of CR to block chromatin accessibility to *in silico* predicted binding sites that are needed for activation of the *Tnf* gene (Falvo et al., 2010). Such blocking might be related to the shifts in expression of chromatin modifiers *Sirt6* and *Suv39h1*, which could directly affect *Tnf* accessibility or indirectly instruct inhibitors of inflammation (IKBα) to regulate

the NF-κB pathway and TNF. Nuclear NAD^+-dependent histone deacetylase, SIRT6, is able to inhibit expression of NF-κB (p65 subunit) and by altering H3K9 acetylation on NF-κB target genes (Kawahara et al., 2009; Lappas, 2012; Mendes, Lelis, & Santos, 2017; Tilstra, Clauson, Niedernhofer, & Robbins, 2011). Additionally, SIRT6 monoubiquitinates cysteine residues within the pre-SET (neighboring SET) domain of SUV39H1, leading to its displacement from the IκBα locus, and in turn IκBα is transcribed to sequester NF-κB within the cytosol (Santos-Barriopedro et al., 2018), which is in accordance with the upregulation of *Nfkbia* (IKBα) in CR muscle. By ensuring the persistent blocking of TFs within cis-regions of the *Tnf* gene and by modulating the expression of modifiers, chronic CR can reprogram skeletal muscle inflammation to prevent wasting and encourage myogenesis (Cerletti et al., 2012).

The mechanism we describe is novel, given that no efforts have been made to understand muscle inflammation and how dietary interventions like CR act to ameliorate the deleterious effects of HF diet. HF consumption is able to produce long-lasting modifications to the epigenome, from genome wide DNA methylation to chromatin accessibility, and miRNA expression. miRNAs are small non-coding nucleotides that direct the multiprotein complex RNA-induced silencing complex (RISC) to degrade target genes, adding another layer of epigenetic regulation. In our study, we used miRNA data mining and current literature to select for miRNAs that can control inflammation and *Tnf* in skeletal muscle. By using this three-pronged approach we found two miRNA that can interfere with NF-κB signaling (miR-19b) and TNF expression (miR-181a). CR not only can prevent the expression of *Tnf* (pre-mRNA, mRNA and protein), but can also increase miR-181a to bind *Tnf* 's 3'-UTR, leading to its RISC-mediated degradation. Similarly, CR selectively inhibits miR-19b, a negative regulator of NF-κB signaling inhibitors (*Kdm2a, Tnfaip3, Zbtb16*), leading to increased NF-κB-inhibitor expression and *Tnf* modulation. Gantier *et al.*

(Gantier et al., 2012) proved that miR-19b directly regulates the expression of *Kdm2a, Tnfaip3,* and *Zbtb16* through direct binding on the 3'-UTR, and ablation of the region prevented miR-19b binding. ZBTB16 (or PLZF) is thought to be a substrate-recognition component of the E3 ubiquitin proteasome and a powerful transcriptional repressor of NF-κB, as seen in HAT1-induced NF-κB signaling inactivation through the formation of a novel repressor complex (ZBTB16/HDAC3/NF-κB) (Sadler et al., 2015). Moreover, TNFAIP3 is induced by TNF and has both ubiquitin-ligase (E3-ligase) and deubiquitinase roles; it deubiquitinates RIPK1 Lysine-63 polyubiquitin chains and catalyzes Lysine-48 polyubiquitination, as well as deubiquitination of NEMO/IKK (upstream of NF-κB) (S. C. Lin et al., 2008), thus promoting proteasomal degradation and termination of NF-κB signaling. Finally, KDM2A (or FBXL11) is known to inhibit NF-kB signaling by demethylating Lysine-218 and -221, and overexpression of KDM2A inhibits NF-κB activity (Lu et al., 2010). Consequently, CR is able to activate anti-inflammatory miR-181a that destabilizes *Tnf* mRNA, and increase selective NF-κB inhibitors through directed silencing of anti-inflammatory miR-19b.

Novel epigenetic mechanisms that respond to chronic CR are vital to understand the immunometabolic regulation that occurs in large, metabolically active non-immune tissues like skeletal muscle. Transcriptional regulation through DNA methylation and TF binding inhibition, as well as miRNA activation are needed to ensure that muscle cells function correctly during calorie restriction. We and others have characterized the transcriptional signature of muscle in response to CR and have defined the beneficial effects, which lead to decreased wasting, senescence, and aging. However, several reports have pointed out the limitations of long-term CR as being a poorly sustainable dietary strategy, and thus not entirely translatable to human subjects. The titration of CR that allows for reprogramming of inflammation (promoter methylation, TF

inhibition, and miRNA), is vital to delineate a viable and highly translatable restriction protocol. Further exploration of the mechanisms that respond to CR entail the generation of a viable animal or cell culture experiment, which is not available to date. Nevertheless, we have uncovered a robust epigenetic silencing mechanism used by CR to block inflammation and prevent muscle wasting. We describe for the first time that CR, in a series of coordinated efforts, redundantly silences inflammation by employing all the epigenetic machinery.

Chronic CR is able to regulate muscle-specific inflammation by targeting the NF-κB pathway and repressing transcription of *Tnf*, which can have significant effects in obese individuals with sarcopenia or those that undergo cachexia. Through a series of redundant epigenetic signaling pathways, chronic CR prevents inflammation in skeletal muscle and leads to a decrease in TNF secretion. Future studies will require the study of the CR-responsive histone modifications that can modulate inflammatory genes and promote protein recycling and myogenesis. The activation of the epigenetic machinery evidenced by increased promoter DNA methylation and TF inhibition, together with anti-inflammatory miRNA are examples of the powerful and long-lasting effect of CR.

CHAPTER 7: FUTURE DIRECTIONS

Given the critical role that skeletal muscle has in homeostatic regulation, in addition to the intricate relationship between inflammation and metabolism, the exploration of mechanisms that modulate skeletal muscle inflammation and specifically TNF signaling requires attention. Animal models provide a good study subject for the exploration of dietary interventions and whole-body homeostasis and inflammation; however, *in situ* manipulation of signaling pathways becomes challenging. Cell culture models provide an excellent tool for the manipulation of signaling pathways; therefore, the establishment of a model that mimics the conditions of CR in animals is necessary. Utilization of a specialized cell culture model to mimic physiological conditions, while being able to manipulate targeted epigenome modifiers will generate unique information that could not otherwise be obtained from *in vivo* animal models. Future studies are needed where primary isolated myofibers exposed to *in vitro* CR conditions are studied, thus thoroughly exploring the genetic and epigenetic mechanisms that drive TNF expression.

Research conducted in out lab aimed to address this issues by comparing primary isolated myoblasts with commercially available L6 rat myoblasts L6 (ATCC® CRL-1458™). We first aimed to differentiate these cells using diverse protocols: Hydrocortisone/Dexamethasone (H&D) media containing 10% FBS + 5% Horse Serum + 50 uM hydrocortisone + 0.1 uM dexamethasone, or Azacitidine media containing 20 uM azacytidne with 5% horse serum for 3 days, then changed to 10 %FBS + 2% horse serum until myotubes are formed, or lastly Galectin-1 with serum free DMEM with 200 ng/mL Galectin-1. Unfortunately, cells within the last two differentiation conditions (Azacitidine and Galectin-1) did not yield the desired myofiber phenotype. Therefore, we continued hereafter with the H&D media that yielded the expected myofiber fusion following

a 4-week differentiation period (Fig. 7.1A). However, upon closer inspection of the primary cell-derived myofibers, fluorescent staining with Hoechst (red dye, nucleus) and Mitotracker (green dye, mitochondria) showed significant morphological deviations from the L6 control myofibers (Fig. 7.1B). Similar complications related to the differentiation protocol and contamination of the culture prompted us to continue the proposed experiments with L6 myofibers, which require a shorted differentiation period (10 days, Dif10) and easier differentiation media (DMEM +2% Fetal bovine serum +Penicilin/Streptomycin). In the following experiments L6 myofibers (Dif 10) were utilized.

7.1. AIM 1

Determine the change in expression of inflammatory markers following in vitro caloric restriction-mimicking media.

7.1.1. Hypothesis

CR will act through epigenetic modifiers to induce chromatin modifications within the *Tnf* gene, thus repressing inflammation in primary isolated myofiber.

7.1.2. Results

Once the phenotypical shape was observed for L6 rat myofibers, we continued to test our hypothesis of whether a caloric restriction (CR)-mimicking media or a high fat (HF) media will elicit discriminant effects on myofiber gene expression. We used the following conditions:

Table 7.1. Experimental conditions used for incubation media of L6 myoblasts.

CON	HG	DMEM-HF	DMEM-CR
DMEM with low glucose medium (1 g.L-1 glucose, with 1% Pen/Strep)	DMEM with low glucose medium (100 g.L-1 glucose, with 1% Pen/Strep)	DMEM with low glucose medium (1 g.L-1 glucose, with 1% Pen/Strep), 1X glutamic acid (0.0147 g/L), Lipid mixture 1	DMEM with low glucose medium (1 g.L-1 glucose, with 1% Pen/Strep), 2X glutamic acid (0.0294 g/L), without methionine, NEFA (200 uM), 5 µM β-Hydroxybutyrate

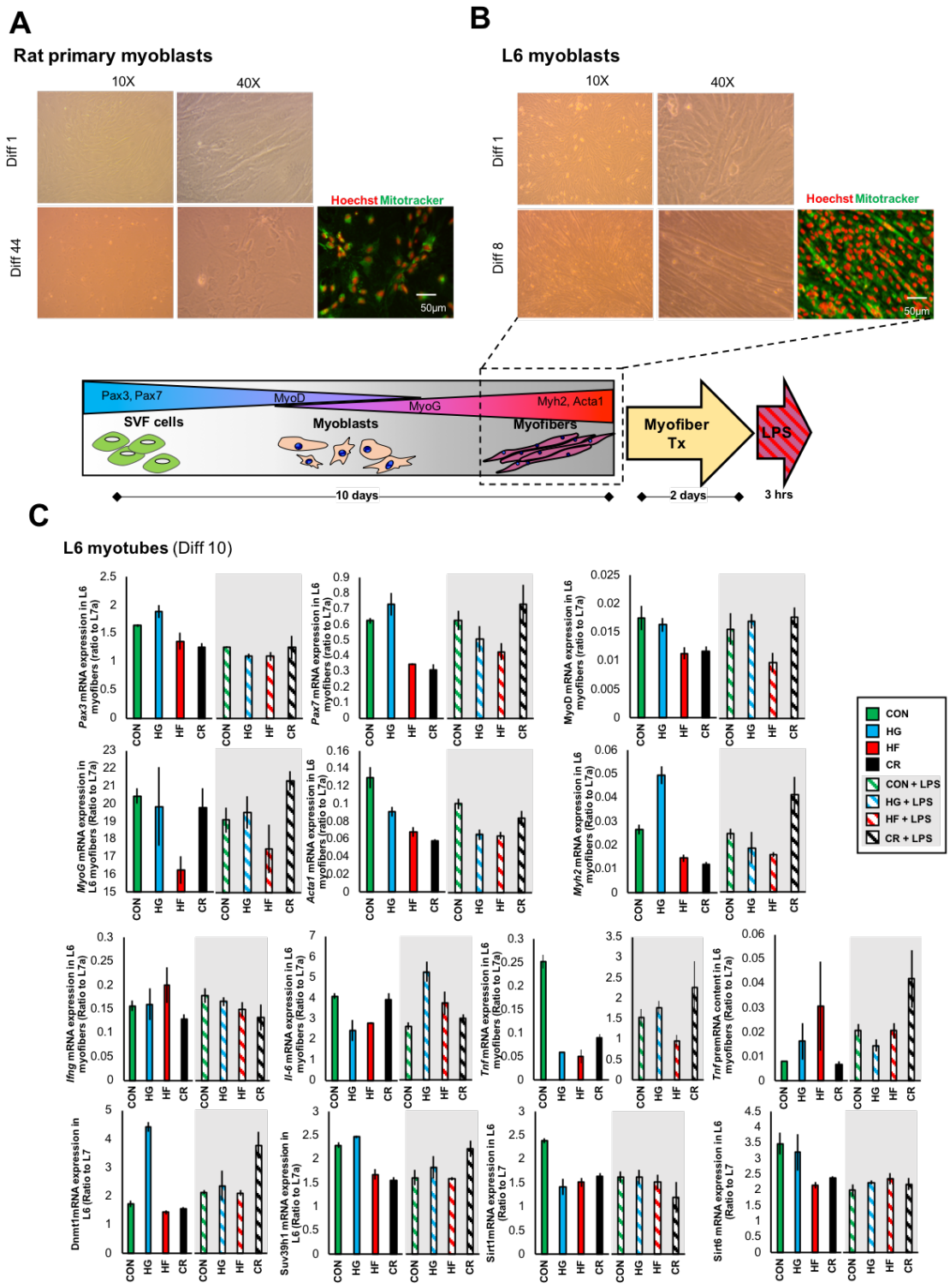

Fig. 7.1. Rat myoblast differentiation and gene expression of inflammatory markers following in vitro caloric restriction-mimicking media. Representative micrographs of **A)** primary isolated rat or **B)** L6 myoblasts and myofibers, and mitochondrial staining. Hoechst is shown in red for nucleus and Mitotracker is shown in green for mitochondria. Diagram of myofiber differentiation depicts the specific stage and morphology of the myofibers. **C)** Gene expression of selected genes is reported as the mean ± SEM.

We used a control (CON) and a high glucose condition (HG) to weed out the specific changes in gene expression. The HF media contained 0.1% of chemically defined lipids with non-animal derived fatty acids (2 µg/ml arachidonic and 10 µg/ml each linoleic, linolenic, myristic, oleic, palmitic and stearic), 0.22 mg/ml cholesterol from New Zealand sheep′s wool, 2.2 mg/ml Tween-80, 70 µg/ml tocopherol acetate and 100 mg/ml Pluronic F-68 solubilized in cell culture water. Myofibers within each group (CON, HG, HF, CR) were incubated for 2 days in the respective media.

We assessed gene expression of L6 myofibers following the treatment period (Fig. 7.1C, white background), and after 3-hr LPS incubation to challenge the immune response (Fig. 7.1C, grey background). Gene expression of differentiated L6 myofibers following treatment failed to produce the same phenotype observed in animals under 6-month 25% CR. Nevertheless, the expression of *Tnf* was similar to that of the animals, but the pre-processed transcript showed a different expression pattern, suggesting that the expression of *Tnf* was not due to our treatment media. Moreover, the CR media showed the lowest protection to an LPS challenge, which tells us that the CR in vitro treatment is not able to produce long-lasting epigenetic changes within the *Tnf* gene to prevent an inflammatory response.

To test whether the cells were responding to the CR-treatment media, we assessed the gene expression in undifferentiated myoblasts. In Fig. 7.2 we can observe the lack

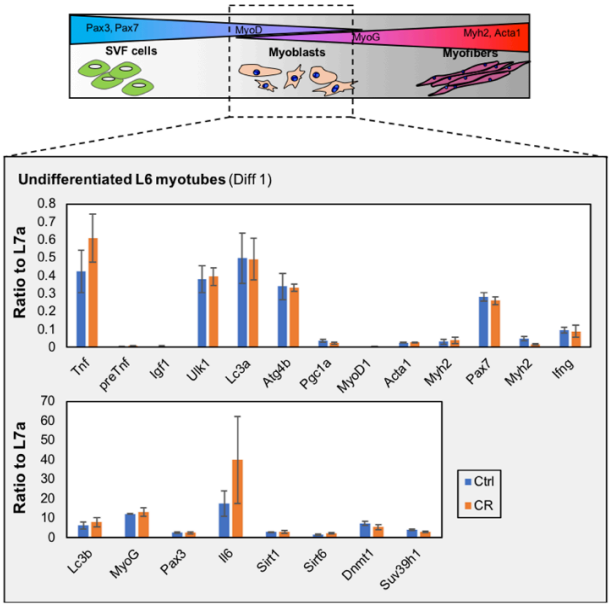

Fig. 7.2. Undifferentiated rat myoblast gene expression of inflammatory markers following *in vitro* caloric restriction-mimicking media. Diagram of myofiber differentiation depicts the specific stage and morphology of the myofibers. Gene expression of selected genes is reported as the mean ± SEM.

of significant effects elicited by our CR media concoction. Therefore, we attributed the changes observed in Fig. 7.1C to variations within the experimental conditions or one of the components of the media. Following this observation, we repeated the experiment >5 times and observed highly variable effects following LPS incubation. For that reason, we then examined the LPS-dose response in two different cell lines L6 myoblasts and H4 hepatoma cells (Fig. 7.3). Following a 3hr incubation with LPS, both L6 and H4 cells were allowed to rest overnight in DMEM media and then gene expression was studied. As seen in Fig. 7.3A, LPS at different concentrations failed to stimulate undifferentiated L6 myoblasts. This prompted us find the best time point at which LPS is able to stimulate Tnf gene expression. This yielded in negative results (Fig. 7.3C), and thus we used the 12-hr period as one with the best induction potential.

Next, we analyzed each individual component of our CR media against the complete concoction (CR), or the DMEM control (CON). The results are shown in Fig. 7.3C. In terms of protection against an LPS challenge, the complete CR

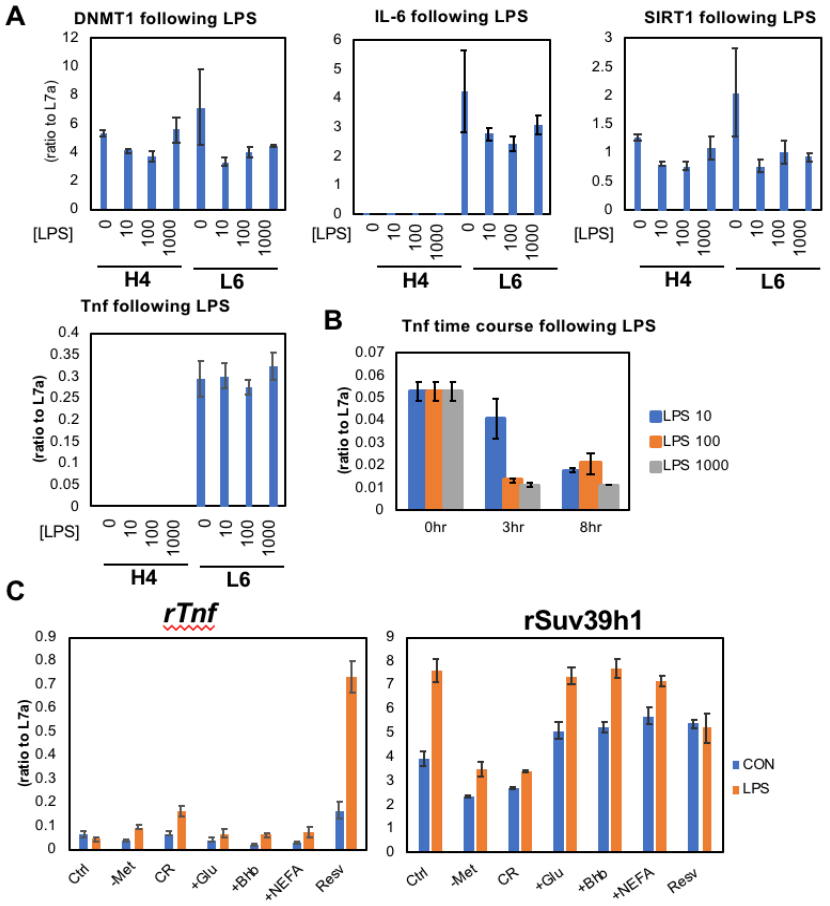

Fig. 7.3. Undifferentiated L6 myoblast and H4 hepatoma cell gene expression of inflammatory markers following LPS incubation. A) H4 and L6 cells were exposed to increasing doses of LPS. **B)** L6 myoblast time course (0, 3, and 8 hr) following exposure to increasing doses of LPS. **C)** Gene expression of *Tnf* and *Suv39h1* following treatment with individual components of CR media. Gene expression is reported as the mean ± SEM.

media showed the worst potential, as the levels of *Tnf* transcription were not decreased. Interestingly, a well-known CR-mimicking component, Resveratrol, was not able to prevent LPS-induced *Tnf* expression. Therefore, we suspect that each individual component of the CR media is not sufficient to produce the anti-inflammatory effect.

7.2. AIM 2

Manipulation of chromatin modifiers and transcription factors will be able to override the effect of CR.

7.2.1. Hypothesis

Overexpression of two forms of transcription factor CEBP-β will be able to differentially induce *Tnf* expression.

7.2.2. Results

Despite the of positive results developing the CR media in Aim 1, we wanted to expand our understanding of the effect of C/EBPβ on *Tnf* expression in undifferentiated L6 myoblasts. Based on our findings that C/EBPβ binding is reduced by CR in animals, we explored the differential effect of two isoforms of the transcription factor. Two isoforms of C/EBPβ exists; the activating form (LAP/LAP*) and the inhibitory form (LIP), which are produced by alternative transcription (Fig. 7.4A). These two isoforms of C/EBPβ differ in length and function, while LAP activates C/EBPβ-target genes, LIP inhibits the targets due to the lack of a transactivating domain (Thiaville, Dudenhausen, Zhong, Pan, & Kilberg, 2008). We validated the size and integrity of the pdDNA empty plasmid, the LAP and LIP plasmids in an agarose gel (Fig. 7.4B), and then proceeded to overexpress the plasmids using lipofectamine (Thermo Fisher) in undifferentiated L6 myoblasts,

and allowed to incubate in DMEM for 24hr. Gene expression results for the C/EBPβ-target genes as well as *Tnf* are shown in (Fig. 7.4C).

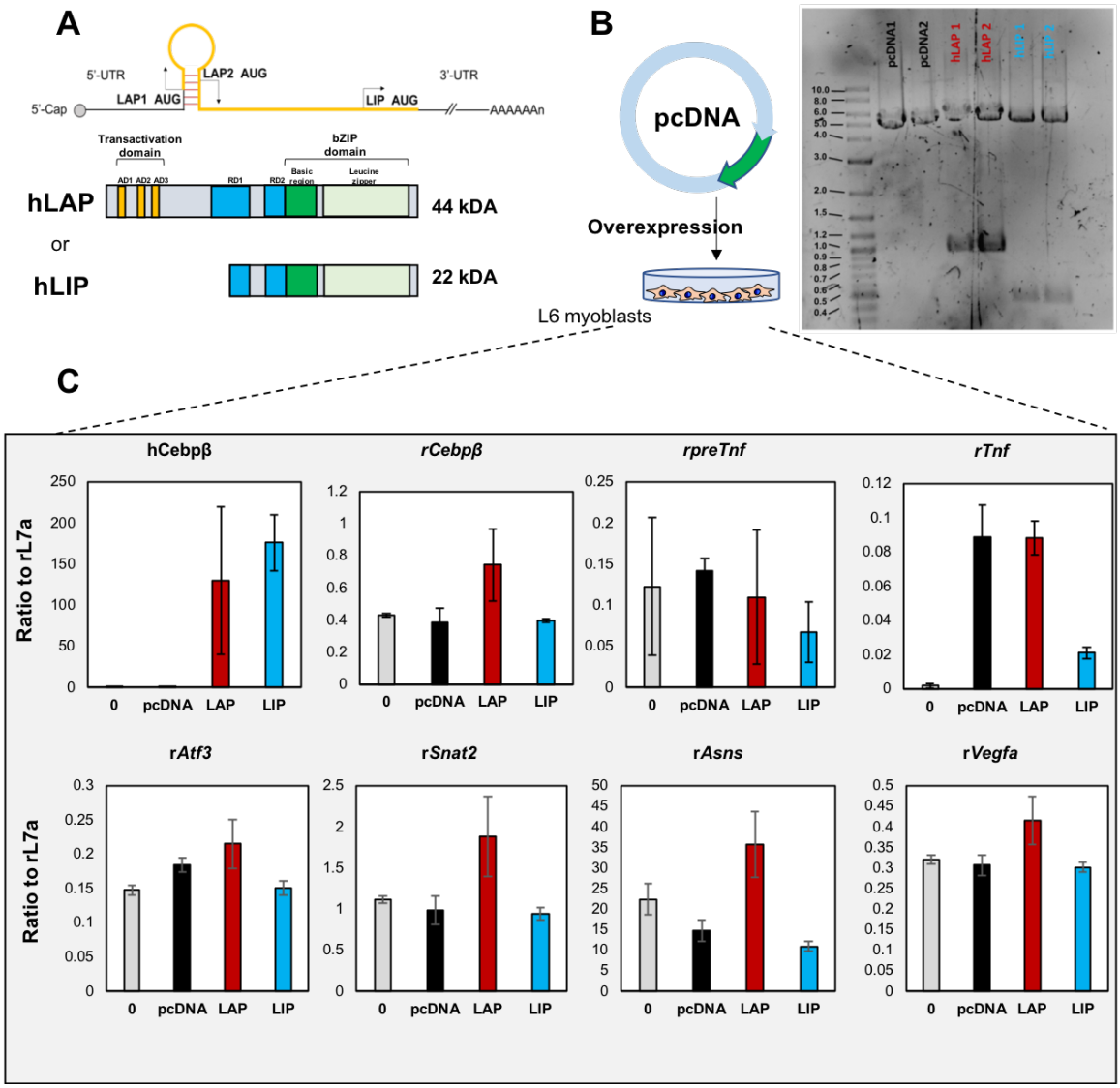

Fig. 7.4. Overexpression of the activating isoform of C/EBPβ in L6 myoblasts stimulates *Tnf* expression. A) Diagram depicting the alternative transcription of C/EBPβ, which produced either the activating (LAP) or the inhibitory isoform (LIP). The activating isoform is longer (44 kDa) and possesses the transactivating domain required for gene activation, whereas the inhibitory form lacks this domain, is shorter (22 kDa), and inhibits the expression of target genes. B) Validation of the pcDNA empty plasmid, and LAP/LIP integrity using EcoRI digestion for 1 hr. C) Gene expression of C/EBPβ target genes and Tnf expression. Data are presented as mean values ± SEM.

Expression of human C/EBPβ demonstrated effective overexpression of the LAP and LIP plasmids, and only LAP is able to activate endogenous rat *Cebpβ*. Further, LAP activates known

target genes *Atf3, Snat, Asns,* and *Vegfa*, whereas LIP is unable to induce transcription. No changes in active transcription were observed for *Tnf* (premRNA), but *Tnf* mature mRNA is induced by LAP and inhibited by LIP. Studies suggest that LAP/LIP ratio is able to regulate myogenesis by inhibiting the myogenic factor MyoD1 in satellite cells (Marchildon et al., 2012). In animals, we observed that MyoD1 was inhibited by chronic HFD and stimulated by chronic CR, thus the ratio of LAP/LIP might be an additional mechanism employed by CR to increase myogenesis. Moreover, CR might increase alternative transcription of LIP and repression of LAP to downregulate inflammation in muscle.

Additional mechanistic studies should be conducted to understand the necessary steps that CR regulates to silence inflammation. Manipulation of the CR-induced silencing might shed light on the core anti-inflammatory mechanism and weed out the redundant inhibitory factors activated by CR.

REFERENCES

Ahrens, M., Ammerpohl, O., von Schonfels, W., Kolarova, J., Bens, S., Itzel, T., . . . Hampe, J. (2013). DNA methylation analysis in nonalcoholic fatty liver disease suggests distinct disease-specific and remodeling signatures after bariatric surgery. *Cell Metab, 18*(2), 296-302. doi:10.1016/j.cmet.2013.07.004

Ahuja, N., Schwer, B., Carobbio, S., Waltregny, D., North, B. J., Castronovo, V., . . . Verdin, E. (2007). Regulation of insulin secretion by SIRT4, a mitochondrial ADP-ribosyltransferase. *J Biol Chem, 282*(46), 33583-33592. doi:10.1074/jbc.M705488200

Akhtar, A., & Becker, P. B. (2000). Activation of transcription through histone H4 acetylation by MOF, an acetyltransferase essential for dosage compensation in Drosophila. *Mol Cell, 5*(2), 367-375.

Albani, D., Ateri, E., Mazzuco, S., Ghilardi, A., Rodilossi, S., Biella, G., . . . Forloni, G. (2014). Modulation of human longevity by SIRT3 single nucleotide polymorphisms in the prospective study "Treviso Longeva (TRELONG)". *Age (Dordr), 36*(1), 469-478. doi:10.1007/s11357-013-9559-2

Alhamdan, B. A., Garcia-Alvarez, A., Alzahrnai, A. H., Karanxha, J., Stretchberry, D. R., Contrera, K. J., . . . Cheskin, L. J. (2016). Alternate-day versus daily energy restriction diets: which is more effective for weight loss? A systematic review and meta-analysis. *Obes Sci Pract, 2*(3), 293-302. doi:10.1002/osp4.52

Andersen, E., Ingerslev, L. R., Fabre, O., Donkin, I., Altintas, A., Versteyhe, S., . . . Barres, R. (2018). Preadipocytes from obese humans with type 2 diabetes are epigenetically reprogrammed at genes controlling adipose tissue function. *Int J Obes (Lond)*. doi:10.1038/s41366-018-0031-3

Anderson, K. A., Huynh, F. K., Fisher-Wellman, K., Stuart, J. D., Peterson, B. S., Douros, J. D., . . . Hirschey, M. D. (2017). SIRT4 Is a Lysine Deacylase that Controls Leucine Metabolism and Insulin Secretion. *Cell Metab, 25*(4), 838-855 e815. doi:10.1016/j.cmet.2017.03.003

Anderson, R., & Prolla, T. (2009). PGC-1alpha in aging and anti-aging interventions. *Biochim Biophys Acta, 1790*(10), 1059-1066. doi:10.1016/j.bbagen.2009.04.005

Anderson, R. M., Shanmuganayagam, D., & Weindruch, R. (2009). Caloric restriction and aging: studies in mice and monkeys. *Toxicol Pathol, 37*(1), 47-51. doi:10.1177/0192623308329476

Anton, S. D., Han, H., York, E., Martin, C. K., Ravussin, E., & Williamson, D. A. (2009). Effect of calorie restriction on subjective ratings of appetite. *J Hum Nutr Diet, 22*(2), 141-147. doi:10.1111/j.1365-277X.2008.00943.x

Bach, E., Nielsen, R. R., Vendelbo, M. H., Moller, A. B., Jessen, N., Buhl, M., . . . Moller, N. (2013). Direct effects of TNF-alpha on local fuel metabolism and cytokine levels in the placebo-controlled, bilaterally infused human leg: increased insulin sensitivity, increased net protein breakdown, and increased IL-6 release. *Diabetes, 62*(12), 4023-4029. doi:10.2337/db13-0138

Bae, J. S., Park, S. H., Jamiyandorj, U., Kim, K. M., Noh, S. J., Kim, J. R., . . . Jang, K. Y. (2016). CK2alpha/CSNK2A1 Phosphorylates SIRT6 and Is Involved in the Progression of Breast Carcinoma and Predicts Shorter Survival of Diagnosed Patients. *Am J Pathol, 186*(12), 3297-3315. doi:10.1016/j.ajpath.2016.08.007

Baehr, L. M., Tunzi, M., & Bodine, S. C. (2014). Muscle hypertrophy is associated with increases in proteasome activity that is independent of MuRF1 and MAFbx expression. *Front Physiol, 5*, 69. doi:10.3389/fphys.2014.00069

Barber, M. F., Michishita-Kioi, E., Xi, Y., Tasselli, L., Kioi, M., Moqtaderi, Z., . . . Chua, K. F. (2012). SIRT7 links H3K18 deacetylation to maintenance of oncogenic transformation. *Nature, 487*(7405), 114-118. doi:10.1038/nature11043

Barres, R., Kirchner, H., Rasmussen, M., Yan, J., Kantor, F. R., Krook, A., . . . Zierath, J. R. (2013). Weight loss after gastric bypass surgery in human obesity remodels promoter methylation. *Cell Rep, 3*(4), 1020-1027. doi:10.1016/j.celrep.2013.03.018

Barrio, L., Dekanty, A., & Milan, M. (2014). MicroRNA-mediated regulation of Dp53 in the Drosophila fat body contributes to metabolic adaptation to nutrient deprivation. *Cell Rep, 8*(2), 528-541. doi:10.1016/j.celrep.2014.06.020

Barthel, R., & Goldfeld, A. E. (2003). T cell-specific expression of the human TNF-alpha gene involves a functional and highly conserved chromatin signature in intron 3. *J Immunol, 171*(7), 3612-3619.

Bastie, C. C., Nahle, Z., McLoughlin, T., Esser, K., Zhang, W., Unterman, T., & Abumrad, N. A. (2005). FoxO1 stimulates fatty acid uptake and oxidation in muscle cells through CD36-dependent and -independent mechanisms. *J Biol Chem, 280*(14), 14222-14229. doi:10.1074/jbc.M413625200

Basu, A., & Haldar, S. (1998). The relationship between BcI2, Bax and p53: consequences for cell cycle progression and cell death. *Mol Hum Reprod, 4*(12), 1099-1109.

Bauer, I., Grozio, A., Lasiglie, D., Basile, G., Sturla, L., Magnone, M., . . . Nencioni, A. (2012). The NAD+-dependent histone deacetylase SIRT6 promotes cytokine production and migration in pancreatic cancer cells by regulating Ca2+ responses. *J Biol Chem, 287*(49), 40924-40937. doi:10.1074/jbc.M112.405837

Belman, J. P., Bian, R. R., Habtemichael, E. N., Li, D. T., Jurczak, M. J., Alcazar-Roman, A., . . . Bogan, J. S. (2015). Acetylation of TUG protein promotes the accumulation of GLUT4 glucose transporters in an insulin-responsive intracellular compartment. *J Biol Chem, 290*(7), 4447-4463. doi:10.1074/jbc.M114.603977

Bento, C. F., Renna, M., Ghislat, G., Puri, C., Ashkenazi, A., Vicinanza, M., . . . Rubinsztein, D. C. (2016). Mammalian Autophagy: How Does It Work? *Annu Rev Biochem, 85*, 685-713. doi:10.1146/annurev-biochem-060815-014556

Benton, M. C., Johnstone, A., Eccles, D., Harmon, B., Hayes, M. T., Lea, R. A., . . . Macartney-Coxson, D. (2015). An analysis of DNA methylation in human adipose tissue reveals differential modification of obesity genes before and after gastric bypass and weight loss. *Genome Biology, 16*. doi:10.1186/S13059-014-0569-X

Bentzinger, C. F., Wang, Y. X., & Rudnicki, M. A. (2012). Building muscle: molecular regulation of myogenesis. *Cold Spring Harb Perspect Biol, 4*(2). doi:10.1101/cshperspect.a008342

Bhardwaj, A., & Das, S. (2016). SIRT6 deacetylates PKM2 to suppress its nuclear localization and oncogenic functions. *Proc Natl Acad Sci U S A, 113*(5), E538-547. doi:10.1073/pnas.1520045113

Bhasin, K. K., van Nas, A., Martin, L. J., Davis, R. C., Devaskar, S. U., & Lusis, A. J. (2009). Maternal low-protein diet or hypercholesterolemia reduces circulating essential amino acids and leads to intrauterine growth restriction. *Diabetes, 58*(3), 559-566. doi:10.2337/db07-1530

Bhatt, A. A., Choudhari, P. K., Mahajan, R. R., Sayyad, M. G., Pratyush, D. D., Hasan, I., . . . Unnikrishnan, A. G. (2017). Effect of a Low-Calorie Diet on Restoration of Normoglycemia in Obese subjects with Type 2 Diabetes. *Indian J Endocrinol Metab, 21*(5), 776-780. doi:10.4103/ijem.IJEM_206_17

Blagosklonny, M. V. (2010). Calorie restriction: decelerating mTOR-driven aging from cells to organisms (including humans). *Cell Cycle, 9*(4), 683-688. doi:10.4161/cc.9.4.10766

Bogan, J. S., Hendon, N., McKee, A. E., Tsao, T. S., & Lodish, H. F. (2003). Functional cloning of TUG as a regulator of GLUT4 glucose transporter trafficking. *Nature, 425*(6959), 727-733. doi:10.1038/nature01989

Bohnert, K. R., McMillan, J. D., & Kumar, A. (2018). Emerging roles of ER stress and unfolded protein response pathways in skeletal muscle health and disease. *J Cell Physiol, 233*(1), 67-78. doi:10.1002/jcp.25852

Bollinger, L. M., Powell, J. J., Houmard, J. A., Witczak, C. A., & Brault, J. J. (2015). Skeletal muscle myotubes in severe obesity exhibit altered ubiquitin-proteasome and autophagic/lysosomal proteolytic flux. *Obesity (Silver Spring), 23*(6), 1185-1193. doi:10.1002/oby.21081

Booij, L., Casey, K. F., Antunes, J. M., Szyf, M., Joober, R., Israel, M., & Steiger, H. (2015). DNA methylation in individuals with anorexia nervosa and in matched normal-eater controls: A genome-wide study. *Int J Eat Disord, 48*(7), 874-882. doi:10.1002/eat.22374

Bordone, L., & Guarente, L. (2005). Calorie restriction, SIRT1 and metabolism: understanding longevity. *Nat Rev Mol Cell Biol, 6*(4), 298-305. doi:10.1038/nrm1616

Bouchard, L., Rabasa-Lhoret, R., Faraj, M., Lavoie, M. E., Mill, J., Perusse, L., & Vohl, M. C. (2010). Differential epigenomic and transcriptomic responses in subcutaneous adipose tissue between low and high responders to caloric restriction. *Am J Clin Nutr, 91*(2), 309-320. doi:10.3945/ajcn.2009.28085

Bowen, T. S., Schuler, G., & Adams, V. (2015). Skeletal muscle wasting in cachexia and sarcopenia: molecular pathophysiology and impact of exercise training. *J Cachexia Sarcopenia Muscle, 6*(3), 197-207. doi:10.1002/jcsm.12043

Brandhorst, S., Choi, I. Y., Wei, M., Cheng, C. W., Sedrakyan, S., Navarrete, G., . . . Longo, V. D. (2015). A Periodic Diet that Mimics Fasting Promotes Multi-System Regeneration, Enhanced Cognitive Performance, and Healthspan. *Cell Metab, 22*(1), 86-99. doi:10.1016/j.cmet.2015.05.012

Brandhorst, S., & Longo, V. D. (2016). Fasting and Caloric Restriction in Cancer Prevention and Treatment. *Recent Results Cancer Res, 207*, 241-266. doi:10.1007/978-3-319-42118-6_12

Branquinho, N. T. D., Cruz, G. H. P., Borrasca, C. L., Alves, L. P. S., de Godoy Gomes, C. R., Ferreira de Godoi, V. A., & Pedrosa, M. M. D. (2017). Early-onset obesity and food restriction alter hepatocyte metabolism in adult Wistar rats. *Arch Physiol Biochem, 123*(5), 297-305. doi:10.1080/13813455.2017.1326942

Braun, J. E., Huntzinger, E., & Izaurralde, E. (2013). The role of GW182 proteins in miRNA-mediated gene silencing. *Adv Exp Med Biol, 768*, 147-163. doi:10.1007/978-1-4614-5107-5_9

Bringman-Rodenbarger, L. R., Guo, A. H., Lyssiotis, C. A., & Lombard, D. B. (2018). Emerging Roles for SIRT5 in Metabolism and Cancer. *Antioxid Redox Signal, 28*(8), 677-690. doi:10.1089/ars.2017.7264

Bruss, M. D., Khambatta, C. F., Ruby, M. A., Aggarwal, I., & Hellerstein, M. K. (2010). Calorie restriction increases fatty acid synthesis and whole body fat oxidation rates. *Am J Physiol Endocrinol Metab, 298*(1), E108-116. doi:10.1152/ajpendo.00524.2009

Buckingham, M., & Rigby, P. W. (2014). Gene regulatory networks and transcriptional mechanisms that control myogenesis. *Dev Cell, 28*(3), 225-238. doi:10.1016/j.devcel.2013.12.020

Buler, M., Aatsinki, S. M., Izzi, V., Uusimaa, J., & Hakkola, J. (2014). SIRT5 is under the control of PGC-1alpha and AMPK and is involved in regulation of mitochondrial energy metabolism. *Faseb j, 28*(7), 3225-3237. doi:10.1096/fj.13-245241

Burton, G. J., Jauniaux, E., & Charnock-Jones, D. S. (2010). The influence of the intrauterine environment on human placental development. *Int J Dev Biol, 54*(2-3), 303-312. doi:10.1387/ijdb.082764gb

Butepage, M., Eckei, L., Verheugd, P., & Luscher, B. (2015). Intracellular Mono-ADP-Ribosylation in Signaling and Disease. *Cells, 4*(4), 569-595. doi:10.3390/cells4040569

Calin, G. A., Sevignani, C., Dumitru, C. D., Hyslop, T., Noch, E., Yendamuri, S., . . . Croce, C. M. (2004). Human microRNA genes are frequently located at fragile sites and genomic regions involved in cancers. *Proc Natl Acad Sci U S A, 101*(9), 2999-3004. doi:10.1073/pnas.0307323101

Calvopina, D. A., Coleman, M. A., Lewindon, P. J., & Ramm, G. A. (2016). Function and Regulation of MicroRNAs and Their Potential as Biomarkers in Paediatric Liver Disease. *Int J Mol Sci, 17*(11). doi:10.3390/ijms17111795

Campion, J., Milagro, F. I., Goyenechea, E., & Martinez, J. A. (2009). TNF-alpha promoter methylation as a predictive biomarker for weight-loss response. *Obesity (Silver Spring), 17*(6), 1293-1297. doi:10.1038/oby.2008.679

Carrico, C., Meyer, J. G., He, W., Gibson, B. W., & Verdin, E. (2018). The Mitochondrial Acylome Emerges: Proteomics, Regulation by Sirtuins, and Metabolic and Disease Implications. *Cell Metab, 27*(3), 497-512. doi:10.1016/j.cmet.2018.01.016

Carthew, R. W., & Sontheimer, E. J. (2009). Origins and Mechanisms of miRNAs and siRNAs. *Cell, 136*(4), 642-655. doi:10.1016/j.cell.2009.01.035

Cava, E., & Fontana, L. (2013). Will calorie restriction work in humans? *Aging (Albany NY), 5*(7), 507-514. doi:10.18632/aging.100581

Cerletti, M., Jang, Y. C., Finley, L. W., Haigis, M. C., & Wagers, A. J. (2012). Short-term calorie restriction enhances skeletal muscle stem cell function. *Cell Stem Cell, 10*(5), 515-519. doi:10.1016/j.stem.2012.04.002

Chalkiadaki, A., & Guarente, L. (2012). Sirtuins mediate mammalian metabolic responses to nutrient availability. *Nat Rev Endocrinol, 8*(5), 287-296. doi:10.1038/nrendo.2011.225

Chang, H. C., & Guarente, L. (2014). SIRT1 and other sirtuins in metabolism. *Trends Endocrinol Metab, 25*(3), 138-145. doi:10.1016/j.tem.2013.12.001

Chang, H. R., Kim, H. J., Xu, X., & Ferrante, A. W., Jr. (2016). Macrophage and adipocyte IGF1 maintain adipose tissue homeostasis during metabolic stresses. *Obesity (Silver Spring), 24*(1), 172-183. doi:10.1002/oby.21354

Chantranupong, L., Wolfson, R. L., & Sabatini, D. M. (2015). Nutrient-sensing mechanisms across evolution. *Cell, 161*(1), 67-83. doi:10.1016/j.cell.2015.02.041

Charles, K. N., Li, M. D., Engin, F., Arruda, A. P., Inouye, K., & Hotamisligil, G. S. (2017). Uncoupling of Metabolic Health from Longevity through Genetic Alteration of Adipose

Tissue Lipid-Binding Proteins. *Cell Rep, 21*(2), 393-402. doi:10.1016/j.celrep.2017.09.051

Chen, P. Y., Ganguly, A., Rubbi, L., Orozco, L. D., Morselli, M., Ashraf, D., . . . Pellegrini, M. (2013). Intrauterine calorie restriction affects placental DNA methylation and gene expression. *Physiol Genomics, 45*(14), 565-576. doi:10.1152/physiolgenomics.00034.2013

Chen, Q., Hao, W., Xiao, C., Wang, R., Xu, X., Lu, H., . . . Deng, C. X. (2017). SIRT6 Is Essential for Adipocyte Differentiation by Regulating Mitotic Clonal Expansion. *Cell Rep, 18*(13), 3155-3166. doi:10.1016/j.celrep.2017.03.006

Chen, T. T., Wu, S. M., Ho, S. C., Chuang, H. C., Liu, C. Y., Chan, Y. F., . . . Lee, K. Y. (2017). SUV39H1 Reduction Is Implicated in Abnormal Inflammation in COPD. *Sci Rep, 7*, 46667. doi:10.1038/srep46667

Chen, X., Li, D., Gao, Y., Cao, Y., & Hao, B. (2018). Histone deacetylase SIRT6 inhibits glioma cell growth through down-regulating NOTCH3 expression. *Acta Biochim Biophys Sin (Shanghai), 50*(4), 417-424. doi:10.1093/abbs/gmy019

Cheng, C., Huang, C., Ma, T. T., Bian, E. B., He, Y., Zhang, L., & Li, J. (2014). SOCS1 hypermethylation mediated by DNMT1 is associated with lipopolysaccharide-induced inflammatory cytokines in macrophages. *Toxicol Lett, 225*(3), 488-497. doi:10.1016/j.toxlet.2013.12.023

Cheong, C. Y., Chng, K., Lim, M. K., Amrithraj, A. I., Joseph, R., Sukarieh, R., . . . Stunkel, W. (2014). Alterations to DNA methylation and expression of CXCL14 are associated with suboptimal birth outcomes. *J Hum Genet, 59*(9), 504-511. doi:10.1038/jhg.2014.63

Choi, K. M., Han, K. A., Ahn, H. J., Lee, S. Y., Hwang, S. Y., Kim, B. H., . . . Min, K. W. (2013). The effects of caloric restriction on fetuin-A and cardiovascular risk factors in rats and humans: a randomized controlled trial. *Clin Endocrinol (Oxf), 79*(3), 356-363. doi:10.1111/cen.12076

Choi, S. E., Fu, T., Seok, S., Kim, D. H., Yu, E., Lee, K. W., . . . Kemper, J. K. (2013). Elevated microRNA-34a in obesity reduces NAD+ levels and SIRT1 activity by directly targeting NAMPT. *Aging Cell, 12*(6), 1062-1072. doi:10.1111/acel.12135

Civitarese, A. E., Carling, S., Heilbronn, L. K., Hulver, M. H., Ukropcova, B., Deutsch, W. A., . . . Team, C. P. (2007). Calorie restriction increases muscle mitochondrial biogenesis in healthy humans. *PLoS Med, 4*(3), e76. doi:10.1371/journal.pmed.0040076

Cole, J. J., Robertson, N. A., Rather, M. I., Thomson, J. P., McBryan, T., Sproul, D., . . . Adams, P. D. (2017). Diverse interventions that extend mouse lifespan suppress shared age-associated epigenetic changes at critical gene regulatory regions. *Genome Biology, 18*. doi:10.1186/s13059-017-1185-3

Collins, K. H., Paul, H. A., Hart, D. A., Reimer, R. A., Smith, I. C., Rios, J. L., . . . Herzog, W. (2016). A High-Fat High-Sucrose Diet Rapidly Alters Muscle Integrity, Inflammation and Gut Microbiota in Male Rats. *Sci Rep, 6*, 37278. doi:10.1038/srep37278

Contreras, A. V., Torres, N., & Tovar, A. R. (2013). PPAR-alpha as a key nutritional and environmental sensor for metabolic adaptation. *Adv Nutr, 4*(4), 439-452. doi:10.3945/an.113.003798

Cordero, P., Campion, J., Milagro, F. I., Goyenechea, E., Steemburgo, T., Javierre, B. M., & Martinez, J. A. (2011). Leptin and TNF-alpha promoter methylation levels measured by MSP could predict the response to a low-calorie diet. *J Physiol Biochem, 67*(3), 463-470. doi:10.1007/s13105-011-0084-4

Csiszar, A., Gautam, T., Sosnowska, D., Tarantini, S., Banki, E., Tucsek, Z., . . . Ungvari, Z. (2014). Caloric restriction confers persistent anti-oxidative, pro-angiogenic, and anti-inflammatory effects and promotes anti-aging miRNA expression profile in cerebromicrovascular endothelial cells of aged rats. *Am J Physiol Heart Circ Physiol, 307*(3), H292-306. doi:10.1152/ajpheart.00307.2014

Cui, X., Yao, L., Yang, X., Gao, Y., Fang, F., Zhang, J., . . . Chang, Y. (2017). SIRT6 regulates metabolic homeostasis in skeletal muscle through activation of AMPK. *Am J Physiol Endocrinol Metab, 313*(4), E493-E505. doi:10.1152/ajpendo.00122.2017

Cummings, N. E., & Lamming, D. W. (2017). Regulation of metabolic health and aging by nutrient-sensitive signaling pathways. *Mol Cell Endocrinol, 455*, 13-22. doi:10.1016/j.mce.2016.11.014

Dai, F., Jiang, T., Bao, Y. Y., Chen, G. J., Chen, L., Zhang, Q., & Lu, Y. X. (2016). Fenofibrate improves high-fat diet-induced and palmitate-induced endoplasmic reticulum stress and inflammation in skeletal muscle. *Life Sci, 157*, 158-167. doi:10.1016/j.lfs.2016.06.008

Dang, W., Steffen, K. K., Perry, R., Dorsey, J. A., Johnson, F. B., Shilatifard, A., . . . Berger, S. L. (2009). Histone H4 lysine 16 acetylation regulates cellular lifespan. *Nature, 459*(7248), 802-807. doi:10.1038/nature08085

Day, S. E., Garcia, L. A., Coletta, R. L., Campbell, L. E., Benjamin, T. R., De Filippis, E. A., . . . Coletta, D. K. (2017). Alterations of sorbin and SH3 domain containing 3 (SORBS3) in human skeletal muscle following Roux-en-Y gastric bypass surgery. *Clin Epigenetics, 9*, 96. doi:10.1186/s13148-017-0396-5

Defossez, P. A., Prusty, R., Kaeberlein, M., Lin, S. J., Ferrigno, P., Silver, P. A., . . . Guarente, L. (1999). Elimination of replication block protein Fob1 extends the life span of yeast mother cells. *Mol Cell, 3*(4), 447-455.

Devlin, K. L., Sanford, T., Harrison, L. M., LeBourgeois, P., Lashinger, L. M., Mambo, E., & Hursting, S. D. (2016). Stage-Specific MicroRNAs and Their Role in the Anticancer Effects of Calorie Restriction in a Rat Model of ER-Positive Luminal Breast Cancer. *PLoS One, 11*(7), e0159686. doi:10.1371/journal.pone.0159686

Dhahbi, J. M., Spindler, S. R., Atamna, H., Yamakawa, A., Guerrero, N., Boffelli, D., . . . Martin, D. I. (2013). Deep sequencing identifies circulating mouse miRNAs that are functionally implicated in manifestations of aging and responsive to calorie restriction. *Aging (Albany NY), 5*(2), 130-141. doi:10.18632/aging.100540

Dhillon, R. S., & Denu, J. M. (2017). Using comparative biology to understand how aging affects mitochondrial metabolism. *Mol Cell Endocrinol, 455*, 54-61. doi:10.1016/j.mce.2016.12.020

do Amaral, C. L., Milagro, F. I., Curi, R., & Martinez, J. A. (2014). DNA methylation pattern in overweight women under an energy-restricted diet supplemented with fish oil. *Biomed Res Int, 2014*, 675021. doi:10.1155/2014/675021

Dutta, D., Xu, J., Dirain, M. L., & Leeuwenburgh, C. (2014). Calorie restriction combined with resveratrol induces autophagy and protects 26-month-old rat hearts from doxorubicin-induced toxicity. *Free Radic Biol Med, 74*, 252-262. doi:10.1016/j.freeradbiomed.2014.06.011

Efeyan, A., Comb, W. C., & Sabatini, D. M. (2015). Nutrient-sensing mechanisms and pathways. *Nature, 517*(7534), 302-310. doi:10.1038/nature14190

Elhanati, S., Ben-Hamo, R., Kanfi, Y., Varvak, A., Glazz, R., Lerrer, B., . . . Cohen, H. Y. (2016). Reciprocal Regulation between SIRT6 and miR-122 Controls Liver Metabolism

and Predicts Hepatocarcinoma Prognosis. *Cell Rep, 14*(2), 234-242. doi:10.1016/j.celrep.2015.12.023
Elhanati, S., Kanfi, Y., Varvak, A., Roichman, A., Carmel-Gross, I., Barth, S., . . . Cohen, H. Y. (2013). Multiple regulatory layers of SREBP1/2 by SIRT6. *Cell Rep, 4*(5), 905-912. doi:10.1016/j.celrep.2013.08.006
Enwere, E. K., Holbrook, J., Lejmi-Mrad, R., Vineham, J., Timusk, K., Sivaraj, B., . . . Korneluk, R. G. (2012). TWEAK and cIAP1 regulate myoblast fusion through the noncanonical NF-kappaB signaling pathway. *Sci Signal, 5*(246), ra75. doi:10.1126/scisignal.2003086
Ertl, R. P., Chen, J., Astle, C. M., Duffy, T. M., & Harrison, D. E. (2008). Effects of dietary restriction on hematopoietic stem-cell aging are genetically regulated. *Blood, 111*(3), 1709-1716. doi:10.1182/blood-2007-01-069807
Ertunc, M. E., & Hotamisligil, G. S. (2016). Lipid signaling and lipotoxicity in metaflammation: indications for metabolic disease pathogenesis and treatment. *J Lipid Res, 57*(12), 2099-2114. doi:10.1194/jlr.R066514
Esposito, K., Petrizzo, M., Maiorino, M. I., Bellastella, G., & Giugliano, D. (2016). Particulate matter pollutants and risk of type 2 diabetes: a time for concern? *Endocrine., 51*(1), 32-37. doi: 10.1007/s12020-12015-10638-12022. Epub 12015 May 12030.
Etchegaray, J. P., Chavez, L., Huang, Y., Ross, K. N., Choi, J., Martinez-Pastor, B., . . . Mostoslavsky, R. (2015). The histone deacetylase SIRT6 controls embryonic stem cell fate via TET-mediated production of 5-hydroxymethylcytosine. *Nat Cell Biol, 17*(5), 545-557. doi:10.1038/ncb3147
Falvo, J. V., Jasenosky, L. D., Kruidenier, L., & Goldfeld, A. E. (2013). Epigenetic control of cytokine gene expression: regulation of the TNF/LT locus and T helper cell differentiation. *Adv Immunol, 118*, 37-128. doi:10.1016/B978-0-12-407708-9.00002-9
Falvo, J. V., Tsytsykova, A. V., & Goldfeld, A. E. (2010). Transcriptional control of the TNF gene. *Curr Dir Autoimmun, 11*, 27-60. doi:10.1159/000289196
Fan, J., Kou, X., Jia, S., Yang, X., Yang, Y., & Chen, N. (2016). Autophagy as a Potential Target for Sarcopenia. *J Cell Physiol, 231*(7), 1450-1459. doi:10.1002/jcp.25260
Farre, D., Roset, R., Huerta, M., Adsuara, J. E., Rosello, L., Alba, M. M., & Messeguer, X. (2003). Identification of patterns in biological sequences at the ALGGEN server: PROMO and MALGEN. *Nucleic Acids Res, 31*(13), 3651-3653.
Fernandez-Marcos, P. J., & Auwerx, J. (2011). Regulation of PGC-1alpha, a nodal regulator of mitochondrial biogenesis. *Am J Clin Nutr, 93*(4), 884S-890. doi:10.3945/ajcn.110.001917
Finley, L. W., Lee, J., Souza, A., Desquiret-Dumas, V., Bullock, K., Rowe, G. C., . . . Haigis, M. C. (2012). Skeletal muscle transcriptional coactivator PGC-1alpha mediates mitochondrial, but not metabolic, changes during calorie restriction. *Proc Natl Acad Sci U S A, 109*(8), 2931-2936. doi:10.1073/pnas.1115813109
Fischle, W., Tseng, B. S., Dormann, H. L., Ueberheide, B. M., Garcia, B. A., Shabanowitz, J., . . . Allis, C. D. (2005). Regulation of HP1-chromatin binding by histone H3 methylation and phosphorylation. *Nature, 438*(7071), 1116-1122. doi:10.1038/nature04219
Fontana, L. (2009). Neuroendocrine factors in the regulation of inflammation: excessive adiposity and calorie restriction. *Exp Gerontol, 44*(1-2), 41-45. doi:10.1016/j.exger.2008.04.005
Fontana, L., & Partridge, L. (2015). Promoting health and longevity through diet: from model organisms to humans. *Cell, 161*(1), 106-118. doi:10.1016/j.cell.2015.02.020

Frieling, H., Bleich, S., Otten, J., Romer, K. D., Kornhuber, J., de Zwaan, M., . . . Hillemacher, T. (2008). Epigenetic downregulation of atrial natriuretic peptide but not vasopressin mRNA expression in females with eating disorders is related to impulsivity. *Neuropsychopharmacology, 33*(11), 2605-2609. doi:10.1038/sj.npp.1301662

Frieling, H., Gozner, A., Romer, K. D., Lenz, B., Bonsch, D., Wilhelm, J., . . . Bleich, S. (2007). Global DNA hypomethylation and DNA hypermethylation of the alpha synuclein promoter in females with anorexia nervosa. *Mol Psychiatry, 12*(3), 229-230. doi:10.1038/sj.mp.4001931

Frieling, H., Romer, K. D., Scholz, S., Mittelbach, F., Wilhelm, J., De Zwaan, M., . . . Bleich, S. (2010). Epigenetic dysregulation of dopaminergic genes in eating disorders. *Int J Eat Disord, 43*(7), 577-583. doi:10.1002/eat.20745

Frye, R. A. (1999). Characterization of five human cDNAs with homology to the yeast SIR2 gene: Sir2-like proteins (sirtuins) metabolize NAD and may have protein ADP-ribosyltransferase activity. *Biochem Biophys Res Commun, 260*(1), 273-279. doi:10.1006/bbrc.1999.0897

Ganguly, A., Chen, Y., Shin, B. C., & Devaskar, S. U. (2014). Prenatal caloric restriction enhances DNA methylation and MeCP2 recruitment with reduced murine placental glucose transporter isoform 3 expression. *J Nutr Biochem, 25*(2), 259-266. doi:10.1016/j.jnutbio.2013.10.015

Gantier, M. P., Stunden, H. J., McCoy, C. E., Behlke, M. A., Wang, D., Kaparakis-Liaskos, M., . . . Williams, B. R. (2012). A miR-19 regulon that controls NF-kappaB signaling. *Nucleic Acids Res, 40*(16), 8048-8058. doi:10.1093/nar/gks521

Gao, M., Li, X., He, Y., Han, L., Qiu, D., Ling, L., . . . Gu, L. (2018). SIRT7 functions in redox homeostasis and cytoskeletal organization during oocyte maturation. *Faseb j*, fj201800078RR. doi:10.1096/fj.201800078RR

Gao, Y., Tan, J., Jin, J., Ma, H., Chen, X., Leger, B., . . . Lan, L. (2018). SIRT6 facilitates directional telomere movement upon oxidative damage. *Sci Rep, 8*(1), 5407. doi:10.1038/s41598-018-23602-0

Garcia-Peterson, L. M., Ndiaye, M. A., Singh, C. K., Chhabra, G., Huang, W., & Ahmad, N. (2017). SIRT6 histone deacetylase functions as a potential oncogene in human melanoma. *Genes Cancer, 8*(9-10), 701-712. doi:10.18632/genesandcancer.153

Garcia-Segura, L., Abreu-Goodger, C., Hernandez-Mendoza, A., Dimitrova Dinkova, T. D., Padilla-Noriega, L., Perez-Andrade, M. E., & Miranda-Rios, J. (2015). High-Throughput Profiling of Caenorhabditis elegans Starvation-Responsive microRNAs. *PLoS One, 10*(11), e0142262. doi:10.1371/journal.pone.0142262

Garg, K., & Boppart, M. D. (2016). Influence of exercise and aging on extracellular matrix composition in the skeletal muscle stem cell niche. *J Appl Physiol (1985), 121*(5), 1053-1058. doi:10.1152/japplphysiol.00594.2016

Garrett, S., Dietzmann-Maurer, K., Song, L., & Sullivan, K. E. (2008). Polarization of primary human monocytes by IFN-gamma induces chromatin changes and recruits RNA Pol II to the TNF-alpha promoter. *J Immunol, 180*(8), 5257-5266.

Gendron, C. M., & Pletcher, S. D. (2017). MicroRNAs mir-184 and let-7 alter Drosophila metabolism and longevity. *Aging Cell, 16*(6), 1434-1438. doi:10.1111/acel.12673

Geng, C. H., Zhang, C. L., Zhang, J. Y., Gao, P., He, M., & Li, Y. L. (2018). Overexpression of Sirt6 is a novel biomarker of malignant human colon carcinoma. *J Cell Biochem, 119*(5), 3957-3967. doi:10.1002/jcb.26539

Ghalandari, H., Kamalpour, M., Alimadadi, A., & Nasrollahzadeh, J. (2018). Comparison of Two Calorie-Reduced Diets of Different Carbohydrate and Fiber Contents and a Simple Dietary Advice Aimed to Modify Carbohydrate Intake on Glycemic Control and Inflammatory Markers in Type 2 Diabetes: A Randomized Trial. *Int J Endocrinol Metab, 16*(1), e12089. doi:10.5812/ijem.12089

Gimeno, R. E. (2007). Fatty acid transport proteins. *Curr Opin Lipidol, 18*(3), 271-276. doi:10.1097/MOL.0b013e3281338558

Giordani, I., Malandrucco, I., Donno, S., Picconi, F., Di Giacinto, P., Di Flaviani, A., . . . Frontoni, S. (2014). Acute caloric restriction improves glomerular filtration rate in patients with morbid obesity and type 2 diabetes. *Diabetes Metab, 40*(2), 158-160. doi:10.1016/j.diabet.2013.12.006

Giralt, A., & Villarroya, F. (2012). SIRT3, a pivotal actor in mitochondrial functions: metabolism, cell death and aging. *Biochem J, 444*(1), 1-10. doi:10.1042/BJ20120030

Goday, A., Bellido, D., Sajoux, I., Crujeiras, A. B., Burguera, B., Garcia-Luna, P. P., . . . Casanueva, F. F. (2016). Short-term safety, tolerability and efficacy of a very low-calorie-ketogenic diet interventional weight loss program versus hypocaloric diet in patients with type 2 diabetes mellitus. *Nutr Diabetes, 6*(9), e230. doi:10.1038/nutd.2016.36

Goyenechea, E., Collins, L. J., Parra, D., Liu, G., Snieder, H., Swaminathan, R., . . . O'Dell, S. D. (2008). CD36 gene promoter polymorphisms are associated with low density lipoprotein-cholesterol in normal twins and after a low-calorie diet in obese subjects. *Twin Res Hum Genet, 11*(6), 621-628. doi:10.1375/twin.11.6.621

Gregor, M. F., & Hotamisligil, G. S. (2011). Inflammatory mechanisms in obesity. *Annu Rev Immunol, 29*, 415-445. doi:10.1146/annurev-immunol-031210-101322

Guarente, L. (2000). Sir2 links chromatin silencing, metabolism, and aging. *Genes Dev, 14*(9), 1021-1026.

Guarente, L. (2005). Calorie restriction and SIR2 genes--towards a mechanism. *Mech Ageing Dev, 126*(9), 923-928. doi:10.1016/j.mad.2005.03.013

Guarente, L. (2006). Sirtuins as potential targets for metabolic syndrome. *Nature, 444*(7121), 868-874. doi:10.1038/nature05486

Guedouari, H., Daigle, T., Scorrano, L., & Hebert-Chatelain, E. (2017). Sirtuin 5 protects mitochondria from fragmentation and degradation during starvation. *Biochim Biophys Acta, 1864*(1), 169-176. doi:10.1016/j.bbamcr.2016.10.015

Hadad, N., Unnikrishnan, A., Jackson, J. A., Masser, D. R., Otalora, L., Stanford, D. R., . . . Freeman, W. M. (2018). Caloric restriction mitigates age-associated hippocampal differential CG and non-CG methylation. *Neurobiol Aging, 67*, 53-66. doi:10.1016/j.neurobiolaging.2018.03.009

Hahn, O., Gronke, S., Stubbs, T. M., Ficz, G., Hendrich, O., Krueger, F., . . . Partridge, L. (2017). Dietary restriction protects from age-associated DNA methylation and induces epigenetic reprogramming of lipid metabolism. *Genome Biology, 18*(1), 56. doi:10.1186/s13059-017-1187-1

Haigis, M. C., Mostoslavsky, R., Haigis, K. M., Fahie, K., Christodoulou, D. C., Murphy, A. J., . . . Guarente, L. (2006). SIRT4 inhibits glutamate dehydrogenase and opposes the effects of calorie restriction in pancreatic beta cells. *Cell, 126*(5), 941-954. doi:10.1016/j.cell.2006.06.057

Hallows, W. C., Yu, W., Smith, B. C., Devries, M. K., Ellinger, J. J., Someya, S., . . . Denu, J. M. (2011). Sirt3 promotes the urea cycle and fatty acid oxidation during dietary restriction. *Mol Cell, 41*(2), 139-149. doi:10.1016/j.molcel.2011.01.002

Hardy, R. W., Meckling-Gill, K. A., Williford, J., Desmond, R. A., & Wei, H. (2002). Energy restriction reduces long-chain saturated fatty acids associated with plasma lipids in aging male rats. *J Nutr, 132*(10), 3172-3177. doi:10.1093/jn/131.10.3172

Hargreaves, D. C., Horng, T., & Medzhitov, R. (2009). Control of inducible gene expression by signal-dependent transcriptional elongation. *Cell, 138*(1), 129-145. doi:10.1016/j.cell.2009.05.047

Hasegawa, A., Iwasaka, H., Hagiwara, S., Asai, N., Nishida, T., & Noguchi, T. (2012). Alternate day calorie restriction improves systemic inflammation in a mouse model of sepsis induced by cecal ligation and puncture. *J Surg Res, 174*(1), 136-141. doi:10.1016/j.jss.2010.11.883

Hashimoto, T., Cook, W. S., Qi, C., Yeldandi, A. V., Reddy, J. K., & Rao, M. S. (2000). Defect in peroxisome proliferator-activated receptor alpha-inducible fatty acid oxidation determines the severity of hepatic steatosis in response to fasting. *J Biol Chem, 275*(37), 28918-28928. doi:10.1074/jbc.M910350199

Hasty, P. (2001). The impact energy metabolism and genome maintenance have on longevity and senescence: lessons from yeast to mammals. *Mech Ageing Dev, 122*(15), 1651-1662.

He, B., Gao, S. Q., Huang, L. D., Huang, Y. H., Zhang, Q. Y., Zhou, M. T., . . . Shan, Y. F. (2015). MicroRNA-155 promotes the proliferation and invasion abilities of colon cancer cells by targeting quaking. *Mol Med Rep, 11*(3), 2355-2359. doi:10.3892/mmr.2014.2994

He, Y., Xiao, Y., Yang, X., Li, Y., Wang, B., Yao, F., . . . Lin, R. (2017). SIRT6 inhibits TNF-alpha-induced inflammation of vascular adventitial fibroblasts through ROS and Akt signaling pathway. *Exp Cell Res, 357*(1), 88-97. doi:10.1016/j.yexcr.2017.05.001

Hebert, A. S., Dittenhafer-Reed, K. E., Yu, W., Bailey, D. J., Selen, E. S., Boersma, M. D., . . . Coon, J. J. (2013). Calorie restriction and SIRT3 trigger global reprogramming of the mitochondrial protein acetylome. *Mol Cell, 49*(1), 186-199. doi:10.1016/j.molcel.2012.10.024

Heilbronn, L. K., & Ravussin, E. (2003). Calorie restriction and aging: review of the literature and implications for studies in humans. *Am J Clin Nutr, 78*(3), 361-369. doi:10.1093/ajcn/78.3.361

Helge, J. W. (2002). Long-term fat diet adaptation effects on performance, training capacity, and fat utilization. *Med Sci Sports Exerc, 34*(9), 1499-1504. doi:10.1249/01.MSS.0000027691.95769.B5

Hernandez-Saavedra, D., Strakovsky, R. S., Ostrosky-Wegman, P., & Pan, Y. X. (2017). Epigenetic Regulation of Centromere Chromatin Stability by Dietary and Environmental Factors. *Adv Nutr, 8*(6), 889-904. doi:10.3945/an.117.016402

Hirschey, M. D., Shimazu, T., Goetzman, E., Jing, E., Schwer, B., Lombard, D. B., . . . Verdin, E. (2010). SIRT3 regulates mitochondrial fatty-acid oxidation by reversible enzyme deacetylation. *Nature, 464*(7285), 121-125. doi:10.1038/nature08778

Hirschey, M. D., Shimazu, T., Huang, J. Y., Schwer, B., & Verdin, E. (2011). SIRT3 regulates mitochondrial protein acetylation and intermediary metabolism. *Cold Spring Harb Symp Quant Biol, 76*, 267-277. doi:10.1101/sqb.2011.76.010850

Hoile, S. P., Lillycrop, K. A., Thomas, N. A., Hanson, M. A., & Burdge, G. C. (2011). Dietary protein restriction during F0 pregnancy in rats induces transgenerational changes in the

hepatic transcriptome in female offspring. *PLoS One, 6*(7), e21668. doi:10.1371/journal.pone.0021668
Holloszy, J. O., & Fontana, L. (2007). Caloric restriction in humans. *Exp Gerontol, 42*(8), 709-712. doi:10.1016/j.exger.2007.03.009
Hotamisligil, G. S. (2006). Inflammation and metabolic disorders. *Nature, 444*(7121), 860-867. doi:10.1038/nature05485
Hotamisligil, G. S. (2017a). Foundations of Immunometabolism and Implications for Metabolic Health and Disease. *Immunity, 47*(3), 406-420. doi:10.1016/j.immuni.2017.08.009
Hotamisligil, G. S. (2017b). Inflammation, metaflammation and immunometabolic disorders. *Nature, 542*(7640), 177-185. doi:10.1038/nature21363
Hotamisligil, G. S., & Bernlohr, D. A. (2015). Metabolic functions of FABPs--mechanisms and therapeutic implications. *Nat Rev Endocrinol, 11*(10), 592-605. doi:10.1038/nrendo.2015.122
Hotamisligil, G. S., & Davis, R. J. (2016). Cell Signaling and Stress Responses. *Cold Spring Harb Perspect Biol, 8*(10). doi:10.1101/cshperspect.a006072
Houtkooper, R. H., Pirinen, E., & Auwerx, J. (2012). Sirtuins as regulators of metabolism and healthspan. *Nat Rev Mol Cell Biol, 13*(4), 225-238. doi:10.1038/nrm3293
Huang, J., & Forsberg, N. E. (1998). Role of calpain in skeletal-muscle protein degradation. *Proc Natl Acad Sci U S A, 95*(21), 12100-12105.
Huang, N., Liu, Z., Zhu, J., Cui, Z., Li, Y., Yu, Y., . . . Yang, Q. (2017). Sirtuin 6 plays an oncogenic role and induces cell autophagy in esophageal cancer cells. *Tumour Biol, 39*(6), 1010428317708532. doi:10.1177/1010428317708532
Huang, Y. T., Maccani, J. Z., Hawley, N. L., Wing, R. R., Kelsey, K. T., & McCaffery, J. M. (2015). Epigenetic patterns in successful weight loss maintainers: a pilot study. *Int J Obes (Lond), 39*(5), 865-868. doi:10.1038/ijo.2014.213
Igarashi, M., & Guarente, L. (2016). mTORC1 and SIRT1 Cooperate to Foster Expansion of Gut Adult Stem Cells during Calorie Restriction. *Cell, 166*(2), 436-450. doi:10.1016/j.cell.2016.05.044
Imai, S., Armstrong, C. M., Kaeberlein, M., & Guarente, L. (2000). Transcriptional silencing and longevity protein Sir2 is an NAD-dependent histone deacetylase. *Nature, 403*(6771), 795-800. doi:10.1038/35001622
Issa, J. P., Ahuja, N., Toyota, M., Bronner, M. P., & Brentnall, T. A. (2001). Accelerated age-related CpG island methylation in ulcerative colitis. *Cancer Res, 61*(9), 3573-3577.
Iwahara, T., Bonasio, R., Narendra, V., & Reinberg, D. (2012). SIRT3 functions in the nucleus in the control of stress-related gene expression. *Mol Cell Biol, 32*(24), 5022-5034. doi:10.1128/MCB.00822-12
Iyer, L. M., Zhang, D., de Souza, R. F., Pukkila, P. J., Rao, A., & Aravind, L. (2014). Lineage-specific expansions of TET/JBP genes and a new class of DNA transposons shape fungal genomic and epigenetic landscapes. *Proc Natl Acad Sci U S A, 111*(5), 1676-1683. doi:10.1073/pnas.1321818111
Jahansouz, C., Xu, H., Hertzel, A. V., Kizy, S., Steen, K. A., Foncea, R., . . . Bernlohr, D. A. (2018). Partitioning of adipose lipid metabolism by altered expression and function of PPAR isoforms after bariatric surgery. *Int J Obes (Lond), 42*(2), 139-146. doi:10.1038/ijo.2017.197

Jiang, H., Khan, S., Wang, Y., Charron, G., He, B., Sebastian, C., . . . Lin, H. (2013). SIRT6 regulates TNF-alpha secretion through hydrolysis of long-chain fatty acyl lysine. *Nature, 496*(7443), 110-113. doi:10.1038/nature12038

Jing, E., Emanuelli, B., Hirschey, M. D., Boucher, J., Lee, K. Y., Lombard, D., . . . Kahn, C. R. (2011). Sirtuin-3 (Sirt3) regulates skeletal muscle metabolism and insulin signaling via altered mitochondrial oxidation and reactive oxygen species production. *Proc Natl Acad Sci U S A, 108*(35), 14608-14613. doi:10.1073/pnas.1111308108

Jing, E., Gesta, S., & Kahn, C. R. (2007). SIRT2 regulates adipocyte differentiation through FoxO1 acetylation/deacetylation. *Cell Metab, 6*(2), 105-114. doi:10.1016/j.cmet.2007.07.003

Johnson, J. B., Summer, W., Cutler, R. G., Martin, B., Hyun, D. H., Dixit, V. D., . . . Mattson, M. P. (2007). Alternate day calorie restriction improves clinical findings and reduces markers of oxidative stress and inflammation in overweight adults with moderate asthma. *Free Radic Biol Med, 42*(5), 665-674. doi:10.1016/j.freeradbiomed.2006.12.005

Johnstone, A. (2015). Fasting for weight loss: an effective strategy or latest dieting trend? *Int J Obes (Lond), 39*(5), 727-733. doi:10.1038/ijo.2014.214

Jones, J. R., Barrick, C., Kim, K. A., Lindner, J., Blondeau, B., Fujimoto, Y., . . . Magnuson, M. A. (2005). Deletion of PPARgamma in adipose tissues of mice protects against high fat diet-induced obesity and insulin resistance. *Proc Natl Acad Sci U S A, 102*(17), 6207-6212. doi:10.1073/pnas.0306743102

Ju, J., Huang, Q., Sun, J., Jin, Y., Ma, W., Song, X., . . . Wang, W. (2018). Correlation between PPAR-alpha methylation level in peripheral blood and inflammatory factors of NAFLD patients with DM. *Exp Ther Med, 15*(2), 1474-1478. doi:10.3892/etm.2017.5530

Jurkowska, R. Z., Jurkowski, T. P., & Jeltsch, A. (2011). Structure and function of mammalian DNA methyltransferases. *Chembiochem, 12*(2), 206-222. doi:10.1002/cbic.201000195

Kanda, Y., Hashiramoto, M., Shimoda, M., Hamamoto, S., Tawaramoto, K., Kimura, T., . . . Kaku, K. (2015). Dietary restriction preserves the mass and function of pancreatic beta cells via cell kinetic regulation and suppression of oxidative/ER stress in diabetic mice. *J Nutr Biochem, 26*(3), 219-226. doi:10.1016/j.jnutbio.2014.10.007

Kanfi, Y., Naiman, S., Amir, G., Peshti, V., Zinman, G., Nahum, L., . . . Cohen, H. Y. (2012). The sirtuin SIRT6 regulates lifespan in male mice. *Nature, 483*(7388), 218-221. doi:10.1038/nature10815

Kawahara, T. L., Michishita, E., Adler, A. S., Damian, M., Berber, E., Lin, M., . . . Chua, K. F. (2009). SIRT6 links histone H3 lysine 9 deacetylation to NF-kappaB-dependent gene expression and organismal life span. *Cell, 136*(1), 62-74. doi:10.1016/j.cell.2008.10.052

Kawasaki, H., Schiltz, L., Chiu, R., Itakura, K., Taira, K., Nakatani, Y., & Yokoyama, K. K. (2000). ATF-2 has intrinsic histone acetyltransferase activity which is modulated by phosphorylation. *Nature, 405*(6783), 195-200. doi:10.1038/35012097

Kazantzis, M., & Stahl, A. (2012). Fatty acid transport proteins, implications in physiology and disease. *Biochim Biophys Acta, 1821*(5), 852-857. doi:10.1016/j.bbalip.2011.09.010

Kennedy, B. K., Austriaco, N. R., Jr., & Guarente, L. (1994). Daughter cells of Saccharomyces cerevisiae from old mothers display a reduced life span. *J Cell Biol, 127*(6 Pt 2), 1985-1993.

Kersten, S., Seydoux, J., Peters, J. M., Gonzalez, F. J., Desvergne, B., & Wahli, W. (1999). Peroxisome proliferator-activated receptor alpha mediates the adaptive response to fasting. *J Clin Invest, 103*(11), 1489-1498. doi:10.1172/JCI6223

Kesselmeier, M., Putter, C., Volckmar, A. L., Baurecht, H., Grallert, H., Illig, T., . . . Wtccc. (2018). High-throughput DNA methylation analysis in anorexia nervosa confirms TNXB hypermethylation. *World J Biol Psychiatry, 19*(3), 187-199. doi:10.1080/15622975.2016.1190033

Khanna, A., Muthusamy, S., Liang, R., Sarojini, H., & Wang, E. (2011). Gain of survival signaling by down-regulation of three key miRNAs in brain of calorie-restricted mice. *Aging (Albany NY), 3*(3), 223-236. doi:10.18632/aging.100276

Kim, C. H., Lee, E. K., Choi, Y. J., An, H. J., Jeong, H. O., Park, D., . . . Chung, H. Y. (2016). Short-term calorie restriction ameliorates genomewide, age-related alterations in DNA methylation. *Aging Cell*. doi:10.1111/acel.12513

Kim, Y. R., Kim, J. H., Kim, M. J., & Treasure, J. (2014). Differential methylation of the oxytocin receptor gene in patients with anorexia nervosa: a pilot study. *PLoS One, 9*(2), e88673. doi:10.1371/journal.pone.0088673

Kinney, S. M., Chin, H. G., Vaisvila, R., Bitinaite, J., Zheng, Y., Esteve, P. O., . . . Pradhan, S. (2011). Tissue-specific distribution and dynamic changes of 5-hydroxymethylcytosine in mammalian genomes. *J Biol Chem, 286*(28), 24685-24693. doi:10.1074/jbc.M110.217083

Kiran, S., Chatterjee, N., Singh, S., Kaul, S. C., Wadhwa, R., & Ramakrishna, G. (2013). Intracellular distribution of human SIRT7 and mapping of the nuclear/nucleolar localization signal. *Febs j, 280*(14), 3451-3466. doi:10.1111/febs.12346

Kirchner, H., Nylen, C., Laber, S., Barres, R., Yan, J., Krook, A., . . . Naslund, E. (2014). Altered promoter methylation of PDK4, IL1 B, IL6, and TNF after Roux-en Y gastric bypass. *Surg Obes Relat Dis, 10*(4), 671-678. doi:10.1016/j.soard.2013.12.019

Kitessa, S. M., & Abeywardena, M. Y. (2016). Lipid-Induced Insulin Resistance in Skeletal Muscle: The Chase for the Culprit Goes from Total Intramuscular Fat to Lipid Intermediates, and Finally to Species of Lipid Intermediates. *Nutrients, 8*(8). doi:10.3390/nu8080466

Klose, R. J., & Bird, A. P. (2006). Genomic DNA methylation: the mark and its mediators. *Trends Biochem Sci, 31*(2), 89-97. doi:10.1016/j.tibs.2005.12.008

Kogure, A., Uno, M., Ikeda, T., & Nishida, E. (2017). The microRNA machinery regulates fasting-induced changes in gene expression and longevity in Caenorhabditis elegans. *J Biol Chem, 292*(27), 11300-11309. doi:10.1074/jbc.M116.765065

Kohli, R. M., & Zhang, Y. (2013). TET enzymes, TDG and the dynamics of DNA demethylation. *Nature, 502*(7472), 472-479. doi:10.1038/nature12750

Kohli, S., Bhardwaj, A., Kumari, R., & Das, S. (2018). SIRT6 Is a Target of Regulation by UBE3A That Contributes to Liver Tumorigenesis in an ANXA2-Dependent Manner. *Cancer Res, 78*(3), 645-658. doi:10.1158/0008-5472.CAN-17-1692

Kraegen, E. W., Cooney, G. J., Ye, J. M., Thompson, A. L., & Furler, S. M. (2001). The role of lipids in the pathogenesis of muscle insulin resistance and beta cell failure in type II diabetes and obesity. *Exp Clin Endocrinol Diabetes, 109 Suppl 2*, S189-201. doi:10.1055/s-2001-18581

Kuang, J., Chen, L., Tang, Q., Zhang, J., Li, Y., & He, J. (2018). The Role of Sirt6 in Obesity and Diabetes. *Front Physiol, 9*, 135. doi:10.3389/fphys.2018.00135

Kugel, S., & Mostoslavsky, R. (2014). Chromatin and beyond: the multitasking roles for SIRT6. *Trends Biochem Sci, 39*(2), 72-81. doi:10.1016/j.tibs.2013.12.002

Kumar, S., & Lombard, D. B. (2018). Functions of the sirtuin deacylase SIRT5 in normal physiology and pathobiology. *Crit Rev Biochem Mol Biol, 53*(3), 311-334. doi:10.1080/10409238.2018.1458071

Kurylowicz, A., Owczarz, M., Polosak, J., Jonas, M. I., Lisik, W., Jonas, M., . . . Puzianowska-Kuznicka, M. (2016). SIRT1 and SIRT7 expression in adipose tissues of obese and normal-weight individuals is regulated by microRNAs but not by methylation status. *Int J Obes (Lond), 40*(11), 1635-1642. doi:10.1038/ijo.2016.131

Kwon, S., Seok, S., Yau, P., Li, X., Kemper, B., & Kemper, J. K. (2017). Obesity and aging diminish sirtuin 1 (SIRT1)-mediated deacetylation of SIRT3, leading to hyperacetylation and decreased activity and stability of SIRT3. *J Biol Chem, 292*(42), 17312-17323. doi:10.1074/jbc.M117.778720

Kwon, S. M., Park, H. G., Jun, J. K., & Lee, W. L. (2014). Exercise, but not quercetin, ameliorates inflammation, mitochondrial biogenesis, and lipid metabolism in skeletal muscle after strenuous exercise by high-fat diet mice. *J Exerc Nutrition Biochem, 18*(1), 51-60. doi:10.5717/jenb.2014.18.1.51

Lagirand-Cantaloube, J., Cornille, K., Csibi, A., Batonnet-Pichon, S., Leibovitch, M. P., & Leibovitch, S. A. (2009). Inhibition of atrogin-1/MAFbx mediated MyoD proteolysis prevents skeletal muscle atrophy in vivo. *PLoS One, 4*(3), e4973. doi:10.1371/journal.pone.0004973

Lagirand-Cantaloube, J., Offner, N., Csibi, A., Leibovitch, M. P., Batonnet-Pichon, S., Tintignac, L. A., . . . Leibovitch, S. A. (2008). The initiation factor eIF3-f is a major target for atrogin1/MAFbx function in skeletal muscle atrophy. *EMBO J, 27*(8), 1266-1276. doi:10.1038/emboj.2008.52

Lamming, D. W., Cummings, N. E., Rastelli, A. L., Gao, F., Cava, E., Bertozzi, B., . . . Fontana, L. (2015). Restriction of dietary protein decreases mTORC1 in tumors and somatic tissues of a tumor-bearing mouse xenograft model. *Oncotarget, 6*(31), 31233-31240. doi:10.18632/oncotarget.5180

Lappas, M. (2012). Anti-inflammatory properties of sirtuin 6 in human umbilical vein endothelial cells. *Mediators Inflamm, 2012*, 597514. doi:10.1155/2012/597514

Lardenoije, R., van den Hove, D. L. A., Vaessen, T. S. J., Iatrou, A., Meuwissen, K. P. V., van Hagen, B. T. J., . . . Rutten, B. P. F. (2015). Epigenetic modifications in mouse cerebellar Purkinje cells: effects of aging, caloric restriction, and overexpression of superoxide dismutase 1 on 5-methylcytosine and 5-hydroxymethylcytosine. *Neurobiol Aging, 36*(11), 3079-3089. doi:10.1016/j.neurobiolaging.2015.08.001

Larsen, T. M., Dalskov, S. M., van Baak, M., Jebb, S. A., Papadaki, A., Pfeiffer, A. F., . . . Genes, P. (2010). Diets with high or low protein content and glycemic index for weight-loss maintenance. *N Engl J Med, 363*(22), 2102-2113. doi:10.1056/NEJMoa1007137

Latouche, C., Heywood, S. E., Henry, S. L., Ziemann, M., Lazarus, R., El-Osta, A., . . . Kingwell, B. A. (2014). Maternal overnutrition programs changes in the expression of skeletal muscle genes that are associated with insulin resistance and defects of oxidative phosphorylation in adult male rat offspring. *J Nutr, 144*(3), 237-244. doi:10.3945/jn.113.186775

Laurent, G., de Boer, V. C., Finley, L. W., Sweeney, M., Lu, H., Schug, T. T., . . . Haigis, M. C. (2013). SIRT4 represses peroxisome proliferator-activated receptor alpha activity to suppress hepatic fat oxidation. *Mol Cell Biol, 33*(22), 4552-4561. doi:10.1128/MCB.00087-13

Lawrence, M., Daujat, S., & Schneider, R. (2016). Lateral Thinking: How Histone Modifications Regulate Gene Expression. *Trends Genet, 32*(1), 42-56. doi:10.1016/j.tig.2015.10.007

Le Couteur, D. G., Solon-Biet, S., Cogger, V. C., Mitchell, S. J., Senior, A., de Cabo, R., . . . Simpson, S. J. (2016). The impact of low-protein high-carbohydrate diets on aging and lifespan. *Cell Mol Life Sci, 73*(6), 1237-1252. doi:10.1007/s00018-015-2120-y

Le May, C., Pineau, T., Bigot, K., Kohl, C., Girard, J., & Pegorier, J. P. (2000). Reduced hepatic fatty acid oxidation in fasting PPARalpha null mice is due to impaired mitochondrial hydroxymethylglutaryl-CoA synthase gene expression. *FEBS Lett, 475*(3), 163-166.

Lee, G. Y., Kim, N. H., Zhao, Z. S., Cha, B. S., & Kim, Y. S. (2004). Peroxisomal-proliferator-activated receptor alpha activates transcription of the rat hepatic malonyl-CoA decarboxylase gene: a key regulation of malonyl-CoA level. *Biochem J, 378*(Pt 3), 983-990. doi:10.1042/BJ20031565

Lee, J., & Zhou, P. (2007). DCAFs, the missing link of the CUL4-DDB1 ubiquitin ligase. *Mol Cell, 26*(6), 775-780. doi:10.1016/j.molcel.2007.06.001

Lee, J. E., Wang, C., Xu, S., Cho, Y. W., Wang, L., Feng, X., . . . Ge, K. (2013). H3K4 mono- and di-methyltransferase MLL4 is required for enhancer activation during cell differentiation. *Elife, 2*, e01503. doi:10.7554/eLife.01503

Lee, N., Kim, D. K., Kim, E. S., Park, S. J., Kwon, J. H., Shin, J., . . . Choi, K. Y. (2014). Comparative interactomes of SIRT6 and SIRT7: Implication of functional links to aging. *Proteomics, 14*(13-14), 1610-1622. doi:10.1002/pmic.201400001

Lee, N., Ryu, H. G., Kwon, J. H., Kim, D. K., Kim, S. R., Wang, H. J., . . . Choi, K. Y. (2016). SIRT6 Depletion Suppresses Tumor Growth by Promoting Cellular Senescence Induced by DNA Damage in HCC. *Plos One, 11*(11), e0165835. doi:10.1371/journal.pone.0165835

Lee, S., & Notterpek, L. (2013). Dietary restriction supports peripheral nerve health by enhancing endogenous protein quality control mechanisms. *Exp Gerontol, 48*(10), 1085-1090. doi:10.1016/j.exger.2012.12.008

Lee, S. S., Chan, W. Y., Lo, C. K., Wan, D. C., Tsang, D. S., & Cheung, W. T. (2004). Requirement of PPARalpha in maintaining phospholipid and triacylglycerol homeostasis during energy deprivation. *J Lipid Res, 45*(11), 2025-2037. doi:10.1194/jlr.M400078-JLR200

Lefevre, M., Redman, L. M., Heilbronn, L. K., Smith, J. V., Martin, C. K., Rood, J. C., . . . Pennington, C. t. (2009). Caloric restriction alone and with exercise improves CVD risk in healthy non-obese individuals. *Atherosclerosis, 203*(1), 206-213. doi:10.1016/j.atherosclerosis.2008.05.036

Leone, T. C., Weinheimer, C. J., & Kelly, D. P. (1999). A critical role for the peroxisome proliferator-activated receptor alpha (PPARalpha) in the cellular fasting response: the PPARalpha-null mouse as a model of fatty acid oxidation disorders. *Proc Natl Acad Sci U S A, 96*(13), 7473-7478.

Li, A. L., Li, H. Y., Jin, B. F., Ye, Q. N., Zhou, T., Yu, X. D., . . . Zhang, X. M. (2004). A novel eIF5A complex functions as a regulator of p53 and p53-dependent apoptosis. *J Biol Chem, 279*(47), 49251-49258. doi:10.1074/jbc.M407165200

Li, C., Sadraie, B., Steckhan, N., Kessler, C., Stange, R., Jeitler, M., & Michalsen, A. (2017). Effects of A One-week Fasting Therapy in Patients with Type-2 Diabetes Mellitus and Metabolic Syndrome - A Randomized Controlled Explorative Study. *Exp Clin Endocrinol Diabetes, 125*(9), 618-624. doi:10.1055/s-0043-101700

Li, F., Li, Y., Duan, Y., Hu, C. A., Tang, Y., & Yin, Y. (2016). Myokines and adipokines: Involvement in the crosstalk between skeletal muscle and adipose tissue. *Cytokine Growth Factor Rev*. doi:10.1016/j.cytogfr.2016.10.003

Li, L. C., & Dahiya, R. (2002). MethPrimer: designing primers for methylation PCRs. *Bioinformatics, 18*(11), 1427-1431.

Li, N., Guenancia, C., Rigal, E., Hachet, O., Chollet, P., Desmoulins, L., . . . Vergely, C. (2016). Short-term moderate diet restriction in adulthood can reverse oxidative, cardiovascular and metabolic alterations induced by postnatal overfeeding in mice. *Sci Rep, 6*, 30817. doi:10.1038/srep30817

Li, N., Mao, D., Cao, Y., Li, H., Ren, F., & Li, K. (2018). Downregulation of SIRT6 by miR-34c-5p is associated with poor prognosis and promotes colon cancer proliferation through inhibiting apoptosis via the JAK2/STAT3 signaling pathway. *Int J Oncol*. doi:10.3892/ijo.2018.4304

Li, W., Sun, Z., Chen, C., Wang, L., Geng, Z., & Tao, J. (2018). Sirtuin7 has an oncogenic potential via promoting the growth of cholangiocarcinoma cells. *Biomed Pharmacother, 100*, 257-266. doi:10.1016/j.biopha.2018.02.007

Li, X., Zhang, Q., Shi, Q., Liu, Y., Zhao, K., Shen, Q., . . . Cao, X. (2017). Demethylase Kdm6a epigenetically promotes IL-6 and IFN-beta production in macrophages. *J Autoimmun, 80*, 85-94. doi:10.1016/j.jaut.2017.02.007

Li, Y. P., Chen, Y., John, J., Moylan, J., Jin, B., Mann, D. L., & Reid, M. B. (2005). TNF-alpha acts via p38 MAPK to stimulate expression of the ubiquitin ligase atrogin1/MAFbx in skeletal muscle. *FASEB J, 19*(3), 362-370. doi:10.1096/fj.04-2364com

Li, Y. Y., Liu, L., & Tollefsbol, T. O. (2010). Glucose restriction can extend normal cell lifespan and impair precancerous cell growth through epigenetic control of hTERT and p16 expression. *Faseb Journal, 24*(5), 1442-1453. doi:10.1096/fj.09-149328

Li, Y. Y., Tang, D., Du, Y. L., Cao, C. Y., Nie, Y. Q., Cao, J., & Zhou, Y. J. (2018). Fatty liver mediated by peroxisome proliferator-activated receptor-alpha DNA methylation can be reversed by a methylation inhibitor and curcumin. *J Dig Dis*. doi:10.1111/1751-2980.12610

Lillycrop, K. A., Phillips, E. S., Torrens, C., Hanson, M. A., Jackson, A. A., & Burdge, G. C. (2008). Feeding pregnant rats a protein-restricted diet persistently alters the methylation of specific cytosines in the hepatic PPAR alpha promoter of the offspring. *Br J Nutr, 100*(2), 278-282. doi:10.1017/S0007114507894438

Lin, H., Hao, Y., Zhao, Z., & Tong, Y. (2017). Sirtuin 6 contributes to migration and invasion of osteosarcoma cells via the ERK1/2/MMP9 pathway. *FEBS Open Bio, 7*(9), 1291-1301. doi:10.1002/2211-5463.12265

Lin, R., Tao, R., Gao, X., Li, T., Zhou, X., Guan, K. L., . . . Lei, Q. Y. (2013). Acetylation stabilizes ATP-citrate lyase to promote lipid biosynthesis and tumor growth. *Mol Cell, 51*(4), 506-518. doi:10.1016/j.molcel.2013.07.002

Lin, S. C., Chung, J. Y., Lamothe, B., Rajashankar, K., Lu, M., Lo, Y. C., . . . Wu, H. (2008). Molecular basis for the unique deubiquitinating activity of the NF-kappaB inhibitor A20. *J Mol Biol, 376*(2), 526-540. doi:10.1016/j.jmb.2007.11.092

Liszt, G., Ford, E., Kurtev, M., & Guarente, L. (2005). Mouse Sir2 homolog SIRT6 is a nuclear ADP-ribosyltransferase. *J Biol Chem, 280*(22), 21313-21320. doi:10.1074/jbc.M413296200

Liu, G. F., Lu, J. Y., Zhang, Y. J., Zhang, L. X., Lu, G. D., Xie, Z. J., . . . Zhang, Y. (2016). C/EBPalpha negatively regulates SIRT7 expression via recruiting HDAC3 to the upstream-promoter of hepatocellular carcinoma cells. *Biochim Biophys Acta, 1859*(2), 348-354. doi:10.1016/j.bbagrm.2015.12.004

Liu, J., Yu, Z., Xiao, Y., Meng, Q., Wang, Y., & Chang, W. (2018). Coordination of FOXA2 and SIRT6 suppresses the hepatocellular carcinoma progression through ZEB2 inhibition. *Cancer Manag Res, 10*, 391-402. doi:10.2147/CMAR.S150552

Liu, W., Wu, M., Du, H., Shi, X., Zhang, T., & Li, J. (2018). SIRT6 inhibits colorectal cancer stem cell proliferation by targeting CDC25A. *Oncol Lett, 15*(4), 5368-5374. doi:10.3892/ol.2018.7989

Loenarz, C., & Schofield, C. J. (2009). Oxygenase catalyzed 5-methylcytosine hydroxylation. *Chem Biol, 16*(6), 580-583. doi:10.1016/j.chembiol.2009.06.002

Longo, V. D., Antebi, A., Bartke, A., Barzilai, N., Brown-Borg, H. M., Caruso, C., . . . Fontana, L. (2015). Interventions to Slow Aging in Humans: Are We Ready? *Aging Cell, 14*(4), 497-510. doi:10.1111/acel.12338

Lu, T., Jackson, M. W., Wang, B., Yang, M., Chance, M. R., Miyagi, M., . . . Stark, G. R. (2010). Regulation of NF-kappaB by NSD1/FBXL11-dependent reversible lysine methylation of p65. *Proc Natl Acad Sci U S A, 107*(1), 46-51. doi:10.1073/pnas.0912493107

Luiken, J. J., Miskovic, D., Arumugam, Y., Glatz, J. F., & Bonen, A. (2001). Skeletal muscle fatty acid transport and transporters. *Int J Sport Nutr Exerc Metab, 11 Suppl*, S92-96.

Lv, M., Zhu, X., Wang, H., Wang, F., & Guan, W. (2014). Roles of caloric restriction, ketogenic diet and intermittent fasting during initiation, progression and metastasis of cancer in animal models: a systematic review and meta-analysis. *Plos One, 9*(12), e115147. doi:10.1371/journal.pone.0115147

Maeda, K., Cao, H., Kono, K., Gorgun, C. Z., Furuhashi, M., Uysal, K. T., . . . Hotamisligil, G. S. (2005). Adipocyte/macrophage fatty acid binding proteins control integrated metabolic responses in obesity and diabetes. *Cell Metab, 1*(2), 107-119. doi:10.1016/j.cmet.2004.12.008

Maegawa, S., Lu, Y., Tahara, T., Lee, J. T., Madzo, J., Liang, S., . . . Issa, J. J. (2017). Caloric restriction delays age-related methylation drift. *Nat Commun, 8*(1), 539. doi:10.1038/s41467-017-00607-3

Makwana, K., Patel, S. A., Velingkaar, N., Ebron, J. S., Shukla, G. C., & Kondratov, R. (2017). Aging and calorie restriction regulate the expression of miR-125a-5p and its target genes Stat3, Casp2 and Stard13. *Aging (Albany NY), 9*(7), 1825-1843. doi:10.18632/aging.101270

Marchildon, F., Lala, N., Li, G., St-Louis, C., Lamothe, D., Keller, C., & Wiper-Bergeron, N. (2012). CCAAT/enhancer binding protein beta is expressed in satellite cells and controls myogenesis. *Stem Cells, 30*(12), 2619-2630. doi:10.1002/stem.1248

Marchlewicz, E. H., Dolinoy, D. C., Tang, L., Milewski, S., Jones, T. R., Goodrich, J. M., . . . Padmanabhan, V. (2016). Lipid metabolism is associated with developmental epigenetic programming. *Sci Rep, 6*, 34857. doi:10.1038/srep34857

Margolis, L. M., Rivas, D. A., Pasiakos, S. M., McClung, J. P., Ceglia, L., & Fielding, R. A. (2017). Upregulation of circulating myomiR following short-term energy restriction is inversely associated with whole body protein synthesis. *Am J Physiol Regul Integr Comp Physiol, 313*(3), R298-R304. doi:10.1152/ajpregu.00054.2017

Marrone, A. K., Edeleva, E. V., Kucherenko, M. M., Hsiao, N. H., & Shcherbata, H. R. (2012). Dg-Dys-Syn1 signaling in Drosophila regulates the microRNA profile. *BMC Cell Biol, 13*, 26. doi:10.1186/1471-2121-13-26

Martinez-Outschoorn, U. E., Sotgia, F., & Lisanti, M. P. (2015). Caveolae and signalling in cancer. *Nat Rev Cancer, 15*(4), 225-237. doi:10.1038/nrc3915

Masoud, G. N., & Li, W. (2015). HIF-1alpha pathway: role, regulation and intervention for cancer therapy. *Acta Pharm Sin B, 5*(5), 378-389. doi:10.1016/j.apsb.2015.05.007

Masternak, M. M., Al-Regaiey, K., Bonkowski, M. S., Panici, J., Sun, L., Wang, J., . . . Bartke, A. (2004). Divergent effects of caloric restriction on gene expression in normal and long-lived mice. *J Gerontol A Biol Sci Med Sci, 59*(8), 784-788.

Masternak, M. M., Al-Regaiey, K. A., Del Rosario Lim, M. M., Jimenez-Ortega, V., Panici, J. A., Bonkowski, M. S., . . . Bartke, A. (2005). Effects of caloric restriction and growth hormone resistance on the expression level of peroxisome proliferator-activated receptors superfamily in liver of normal and long-lived growth hormone receptor/binding protein knockout mice. *J Gerontol A Biol Sci Med Sci, 60*(11), 1394-1398.

Masternak, M. M., & Bartke, A. (2007). PPARs in Calorie Restricted and Genetically Long-Lived Mice. *PPAR Res, 2007*, 28436. doi:10.1155/2007/28436

Mathias, R. A., Greco, T. M., Oberstein, A., Budayeva, H. G., Chakrabarti, R., Rowland, E. A., . . . Cristea, I. M. (2014). Sirtuin 4 is a lipoamidase regulating pyruvate dehydrogenase complex activity. *Cell, 159*(7), 1615-1625. doi:10.1016/j.cell.2014.11.046

Mattison, J. A., Colman, R. J., Beasley, T. M., Allison, D. B., Kemnitz, J. W., Roth, G. S., . . . Anderson, R. M. (2017). Caloric restriction improves health and survival of rhesus monkeys. *Nat Commun, 8*, 14063. doi:10.1038/ncomms14063

Mendelsohn, A. R., & Larrick, J. W. (2017). Epigenetic Drift Is a Determinant of Mammalian Lifespan. *Rejuvenation Res, 20*(5), 430-436. doi:10.1089/rej.2017.2024

Mendes, K. L., Lelis, D. F., & Santos, S. H. S. (2017). Nuclear sirtuins and inflammatory signaling pathways. *Cytokine Growth Factor Rev, 38*, 98-105. doi:10.1016/j.cytogfr.2017.11.001

Meng, Z. X., Gong, J., Chen, Z., Sun, J., Xiao, Y., Wang, L., . . . Lin, J. D. (2017). Glucose Sensing by Skeletal Myocytes Couples Nutrient Signaling to Systemic Homeostasis. *Mol Cell, 66*(3), 332-344 e334. doi:10.1016/j.molcel.2017.04.007

Mercken, E. M., Capri, M., Carboneau, B. A., Conte, M., Heidler, J., Santoro, A., . . . de Cabo, R. (2017). Conserved and species-specific molecular denominators in mammalian skeletal muscle aging. *NPJ Aging Mech Dis, 3*, 8. doi:10.1038/s41514-017-0009-8

Mercken, E. M., Crosby, S. D., Lamming, D. W., JeBailey, L., Krzysik-Walker, S., Villareal, D. T., . . . Fontana, L. (2013). Calorie restriction in humans inhibits the PI3K/AKT pathway and induces a younger transcription profile. *Aging Cell, 12*(4), 645-651. doi:10.1111/acel.12088

Mercken, E. M., Majounie, E., Ding, J., Guo, R., Kim, J., Bernier, M., . . . Abdelmohsen, K. (2013). Age-associated miRNA alterations in skeletal muscle from rhesus monkeys reversed by caloric restriction. *Aging (Albany NY), 5*(9), 692-703. doi:10.18632/aging.100598

Messeguer, X., Escudero, R., Farre, D., Nunez, O., Martinez, J., & Alba, M. M. (2002). PROMO: detection of known transcription regulatory elements using species-tailored searches. *Bioinformatics, 18*(2), 333-334.

Meydani, S. N., Das, S. K., Pieper, C. F., Lewis, M. R., Klein, S., Dixit, V. D., . . . Fontana, L. (2016). Long-term moderate calorie restriction inhibits inflammation without impairing cell-mediated immunity: a randomized controlled trial in non-obese humans. *Aging (Albany NY), 8*(7), 1416-1431. doi:10.18632/aging.100994

Michishita, E., McCord, R. A., Berber, E., Kioi, M., Padilla-Nash, H., Damian, M., . . . Chua, K. F. (2008). SIRT6 is a histone H3 lysine 9 deacetylase that modulates telomeric chromatin. *Nature, 452*(7186), 492-496. doi:10.1038/nature06736

Mico, V., Berninches, L., Tapia, J., & Daimiel, L. (2017). NutrimiRAging: Micromanaging Nutrient Sensing Pathways through Nutrition to Promote Healthy Aging. *Int J Mol Sci, 18*(5). doi:10.3390/ijms18050915

Milagro, F. I., Campion, J., Cordero, P., Goyenechea, E., Gomez-Uriz, A. M., Abete, I., . . . Martinez, J. A. (2011). A dual epigenomic approach for the search of obesity biomarkers: DNA methylation in relation to diet-induced weight loss. *FASEB J, 25*(4), 1378-1389. doi:10.1096/fj.10-170365

Mitchell, S. E., Delville, C., Konstantopedos, P., Hurst, J., Derous, D., Green, C., . . . Speakman, J. R. (2015). The effects of graded levels of calorie restriction: II. Impact of short term calorie and protein restriction on circulating hormone levels, glucose homeostasis and oxidative stress in male C57BL/6 mice. *Oncotarget, 6*(27), 23213-23237. doi:10.18632/oncotarget.4003

Mitchell, S. E., Tang, Z., Kerbois, C., Delville, C., Konstantopedos, P., Bruel, A., . . . Speakman, J. R. (2015). The effects of graded levels of calorie restriction: I. impact of short term calorie and protein restriction on body composition in the C57BL/6 mouse. *Oncotarget, 6*(18), 15902-15930. doi:10.18632/oncotarget.4142

Mitchell, S. J., Bernier, M., Aon, M. A., Cortassa, S., Kim, E. Y., Fang, E. F., . . . de Cabo, R. (2018). Nicotinamide Improves Aspects of Healthspan, but Not Lifespan, in Mice. *Cell Metab, 27*(3), 667-676 e664. doi:10.1016/j.cmet.2018.02.001

Mitterberger, M. C., Mattesich, M., & Zwerschke, W. (2014). Bariatric surgery and diet-induced long-term caloric restriction protect subcutaneous adipose-derived stromal/progenitor cells and prolong their life span in formerly obese humans. *Exp Gerontol, 56*, 106-113. doi:10.1016/j.exger.2014.03.030

Miyamura, Y., Tawa, R., Koizumi, A., Uehara, Y., Kurishita, A., Sakurai, H., . . . Ono, T. (1993). Effects of energy restriction on age-associated changes of DNA methylation in mouse liver. *Mutat Res, 295*(2), 63-69.

Mo, Y. Y., Yu, Y., Theodosiou, E., Ee, P. L., & Beck, W. T. (2005). A role for Ubc9 in tumorigenesis. *Oncogene, 24*(16), 2677-2683. doi:10.1038/sj.onc.1208210

Moody, L., Chen, H., & Pan, Y. X. (2017). Early-Life Nutritional Programming of Cognition-The Fundamental Role of Epigenetic Mechanisms in Mediating the Relation between Early-Life Environment and Learning and Memory Process. *Adv Nutr, 8*(2), 337-350. doi:10.3945/an.116.014209

Mouchiroud, L., Houtkooper, R. H., & Auwerx, J. (2013). NAD(+) metabolism: a therapeutic target for age-related metabolic disease. *Crit Rev Biochem Mol Biol, 48*(4), 397-408. doi:10.3109/10409238.2013.789479

Mulligan, J. D., Stewart, A. M., & Saupe, K. W. (2008). Downregulation of plasma insulin levels and hepatic PPARgamma expression during the first week of caloric restriction in mice. *Exp Gerontol, 43*(3), 146-153. doi:10.1016/j.exger.2007.10.011

Nakamura, M. T., Yudell, B. E., & Loor, J. J. (2014). Regulation of energy metabolism by long-chain fatty acids. *Prog Lipid Res, 53*, 124-144. doi:10.1016/j.plipres.2013.12.001

Nasrin, N., Wu, X., Fortier, E., Feng, Y., Bare, O. C., Chen, S., . . . Bordone, L. (2010). SIRT4 regulates fatty acid oxidation and mitochondrial gene expression in liver and muscle cells. *J Biol Chem, 285*(42), 31995-32002. doi:10.1074/jbc.M110.124164

Negrini, M., Nicoloso, M. S., & Calin, G. A. (2009). MicroRNAs and cancer--new paradigms in molecular oncology. *Curr Opin Cell Biol, 21*(3), 470-479. doi:10.1016/j.ceb.2009.03.002

Nezami, B. G., Mwangi, S. M., Lee, J. E., Jeppsson, S., Anitha, M., Yarandi, S. S., . . . Srinivasan, S. (2014). MicroRNA 375 mediates palmitate-induced enteric neuronal damage and high-fat diet-induced delayed intestinal transit in mice. *Gastroenterology, 146*(2), 473-483 e473. doi:10.1053/j.gastro.2013.10.053

Ng, H. H., & Bird, A. (2000). Histone deacetylases: silencers for hire. *Trends Biochem Sci, 25*(3), 121-126.

Nicoletti, C. F., Nonino, C. B., de Oliveira, B. A., Pinhel, M. A., Mansego, M. L., Milagro, F. I., . . . Martinez, J. A. (2016). DNA Methylation and Hydroxymethylation Levels in Relation to Two Weight Loss Strategies: Energy-Restricted Diet or Bariatric Surgery. *Obes Surg, 26*(3), 603-611. doi:10.1007/s11695-015-1802-8

Nishida, Y., Rardin, M. J., Carrico, C., He, W., Sahu, A. K., Gut, P., . . . Verdin, E. (2015). SIRT5 Regulates both Cytosolic and Mitochondrial Protein Malonylation with Glycolysis as a Major Target. *Mol Cell, 59*(2), 321-332. doi:10.1016/j.molcel.2015.05.022

Noren Hooten, N., Martin-Montalvo, A., Dluzen, D. F., Zhang, Y., Bernier, M., Zonderman, A. B., . . . Evans, M. K. (2016). Metformin-mediated increase in DICER1 regulates microRNA expression and cellular senescence. *Aging Cell, 15*(3), 572-581. doi:10.1111/acel.12469

Oh, K. J., Lee, D. S., Kim, W. K., Han, B. S., Lee, S. C., & Bae, K. H. (2016). Metabolic Adaptation in Obesity and Type II Diabetes: Myokines, Adipokines and Hepatokines. *Int J Mol Sci, 18*(1). doi:10.3390/ijms18010008

Olivo-Marston, S. E., Hursting, S. D., Perkins, S. N., Schetter, A., Khan, M., Croce, C., . . . Lavigne, J. (2014). Effects of calorie restriction and diet-induced obesity on murine colon carcinogenesis, growth and inflammatory factors, and microRNA expression. *PLoS One, 9*(4), e94765. doi:10.1371/journal.pone.0094765

Orom, U. A., Lim, M. K., Savage, J. E., Jin, L., Saleh, A. D., Lisanti, M. P., & Simone, N. L. (2012). MicroRNA-203 regulates caveolin-1 in breast tissue during caloric restriction. *Cell Cycle, 11*(7), 1291-1295. doi:10.4161/cc.19704

Orom, U. A., Nielsen, F. C., & Lund, A. H. (2008). MicroRNA-10a binds the 5'UTR of ribosomal protein mRNAs and enhances their translation. *Mol Cell, 30*(4), 460-471. doi:10.1016/j.molcel.2008.05.001

Oshakbayev, K., Dukenbayeva, B., Togizbayeva, G., Durmanova, A., Gazaliyeva, M., Sabir, A., . . . Idrisov, A. (2017). Weight loss technology for people with treated type 2 diabetes: a randomized controlled trial. *Nutr Metab (Lond), 14*, 11. doi:10.1186/s12986-017-0163-9

Otoda, T., Takamura, T., Misu, H., Ota, T., Murata, S., Hayashi, H., . . . Kaneko, S. (2013). Proteasome dysfunction mediates obesity-induced endoplasmic reticulum stress and insulin resistance in the liver. *Diabetes, 62*(3), 811-824. doi:10.2337/db11-1652

Palacios, D., Mozzetta, C., Consalvi, S., Caretti, G., Saccone, V., Proserpio, V., . . . Puri, P. L. (2010). TNF/p38alpha/polycomb signaling to Pax7 locus in satellite cells links

inflammation to the epigenetic control of muscle regeneration. *Cell Stem Cell, 7*(4), 455-469. doi:10.1016/j.stem.2010.08.013
Pan, P. W., Feldman, J. L., Devries, M. K., Dong, A., Edwards, A. M., & Denu, J. M. (2011). Structure and biochemical functions of SIRT6. *J Biol Chem, 286*(16), 14575-14587. doi:10.1074/jbc.M111.218990
Pannek, M., Simic, Z., Fuszard, M., Meleshin, M., Rotili, D., Mai, A., . . . Steegborn, C. (2017). Crystal structures of the mitochondrial deacylase Sirtuin 4 reveal isoform-specific acyl recognition and regulation features. *Nat Commun, 8*(1), 1513. doi:10.1038/s41467-017-01701-2
Park, J., Chen, Y., Tishkoff, D. X., Peng, C., Tan, M., Dai, L., . . . Zhao, Y. (2013). SIRT5-mediated lysine desuccinylation impacts diverse metabolic pathways. *Mol Cell, 50*(6), 919-930. doi:10.1016/j.molcel.2013.06.001
Parra, D., Gonzalez, A., Martinez, J. A., Labayen, I., & Diez, N. (2003). In vivo assessment of the mitochondrial response to caloric restriction in obese women by the 2-keto[1-C]isocaproate breath test. *Metabolism, 52*(4), 463-467. doi:10.1053/meta.2003.50075
Pedersen, L., & Hojman, P. (2012). Muscle-to-organ cross talk mediated by myokines. *Adipocyte, 1*(3), 164-167. doi:10.4161/adip.20344
Peppa, M., Koliaki, C., Nikolopoulos, P., & Raptis, S. A. (2010). Skeletal muscle insulin resistance in endocrine disease. *J Biomed Biotechnol, 2010*, 527850. doi:10.1155/2010/527850
Peters, A. H., O'Carroll, D., Scherthan, H., Mechtler, K., Sauer, S., Schofer, C., . . . Jenuwein, T. (2001). Loss of the Suv39h histone methyltransferases impairs mammalian heterochromatin and genome stability. *Cell, 107*(3), 323-337.
Phillips, T., & Leeuwenburgh, C. (2005). Muscle fiber specific apoptosis and TNF-alpha signaling in sarcopenia are attenuated by life-long calorie restriction. *FASEB J, 19*(6), 668-670. doi:10.1096/fj.04-2870fje
Picard, F., Kurtev, M., Chung, N., Topark-Ngarm, A., Senawong, T., Machado De Oliveira, R., . . . Guarente, L. (2004). Sirt1 promotes fat mobilization in white adipocytes by repressing PPAR-gamma. *Nature, 429*(6993), 771-776. doi:10.1038/nature02583
Pileggi, C. A., Hedges, C. P., Segovia, S. A., Markworth, J. F., Durainayagam, B. R., Gray, C., . . . Cameron-Smith, D. (2016). Maternal High Fat Diet Alters Skeletal Muscle Mitochondrial Catalytic Activity in Adult Male Rat Offspring. *Front Physiol, 7*, 546. doi:10.3389/fphys.2016.00546
Pileggi, C. A., Segovia, S. A., Markworth, J. F., Gray, C., Zhang, X. D., Milan, A. M., . . . Cameron-Smith, D. (2016). Maternal conjugated linoleic acid supplementation reverses high-fat diet-induced skeletal muscle atrophy and inflammation in adult male rat offspring. *Am J Physiol Regul Integr Comp Physiol, 310*(5), R432-439. doi:10.1152/ajpregu.00351.2015
Piper, M. D., Partridge, L., Raubenheimer, D., & Simpson, S. J. (2011). Dietary restriction and aging: a unifying perspective. *Cell Metab, 14*(2), 154-160. doi:10.1016/j.cmet.2011.06.013
Poulsen, L., Siersbaek, M., & Mandrup, S. (2012). PPARs: fatty acid sensors controlling metabolism. *Semin Cell Dev Biol, 23*(6), 631-639. doi:10.1016/j.semcdb.2012.01.003
Qin, K., Zhang, N., Zhang, Z., Nipper, M., Zhu, Z., Leighton, J., . . . Wang, P. (2018). SIRT6-mediated transcriptional suppression of Txnip is critical for pancreatic beta cell function and survival in mice. *Diabetologia, 61*(4), 906-918. doi:10.1007/s00125-017-4542-6

Qiu, D., Hou, X., Han, L., Li, X., Ge, J., & Wang, Q. (2018). Sirt2-BubR1 acetylation pathway mediates the effects of advanced maternal age on oocyte quality. *Aging Cell, 17*(1). doi:10.1111/acel.12698

Qiu, X., Brown, K., Hirschey, M. D., Verdin, E., & Chen, D. (2010). Calorie restriction reduces oxidative stress by SIRT3-mediated SOD2 activation. *Cell Metab, 12*(6), 662-667. doi:10.1016/j.cmet.2010.11.015

Radford, E. J., Ito, M., Shi, H., Corish, J. A., Yamazawa, K., Isganaitis, E., . . . Ferguson-Smith, A. C. (2014). In utero effects. In utero undernourishment perturbs the adult sperm methylome and intergenerational metabolism. *Science, 345*(6198), 1255903. doi:10.1126/science.1255903

Ranjbar, S., Rajsbaum, R., & Goldfeld, A. E. (2006). Transactivator of transcription from HIV type 1 subtype E selectively inhibits TNF gene expression via interference with chromatin remodeling of the TNF locus. *J Immunol, 176*(7), 4182-4190.

Rardin, M. J., He, W., Nishida, Y., Newman, J. C., Carrico, C., Danielson, S. R., . . . Verdin, E. (2013). SIRT5 regulates the mitochondrial lysine succinylome and metabolic networks. *Cell Metab, 18*(6), 920-933. doi:10.1016/j.cmet.2013.11.013

Robertson, L. T., & Mitchell, J. R. (2013). Benefits of short-term dietary restriction in mammals. *Exp Gerontol, 48*(10), 1043-1048. doi:10.1016/j.exger.2013.01.009

Rogovik, A. L., & Goldman, R. D. (2010). Ketogenic diet for treatment of epilepsy. *Can Fam Physician, 56*(6), 540-542.

Rossi, E. L., Dunlap, S. M., Bowers, L. W., Khatib, S. A., Doerstling, S. S., Smith, L. A., . . . Hursting, S. D. (2017). Energy Balance Modulation Impacts Epigenetic Reprogramming, ERalpha and ERbeta Expression, and Mammary Tumor Development in MMTV-neu Transgenic Mice. *Cancer Res, 77*(9), 2500-2511. doi:10.1158/0008-5472.CAN-16-2795

Ruggenenti, P., Abbate, M., Ruggiero, B., Rota, S., Trillini, M., Aparicio, C., . . . Group, C. R. S. O. S. (2017). Renal and Systemic Effects of Calorie Restriction in Patients With Type 2 Diabetes With Abdominal Obesity: A Randomized Controlled Trial. *Diabetes, 66*(1), 75-86. doi:10.2337/db16-0607

Sadler, A. J., Suliman, B. A., Yu, L., Yuan, X., Wang, D., Irving, A. T., . . . Xu, D. (2015). The acetyltransferase HAT1 moderates the NF-kappaB response by regulating the transcription factor PLZF. *Nat Commun, 6*, 6795. doi:10.1038/ncomms7795

Sahin, K., Yilmaz, S., & Gozukirmizi, N. (2014). Changes in human sirtuin 6 gene promoter methylation during aging. *Biomed Rep, 2*(4), 574-578. doi:10.3892/br.2014.266

Saltiel, A. R., & Kahn, C. R. (2001). Insulin signalling and the regulation of glucose and lipid metabolism. *Nature, 414*(6865), 799-806. doi:10.1038/414799a

Santos-Barriopedro, I., Bosch-Presegue, L., Marazuela-Duque, A., de la Torre, C., Colomer, C., Vazquez, B. N., . . . Vaquero, A. (2018). SIRT6-dependent cysteine monoubiquitination in the PRE-SET domain of Suv39h1 regulates the NF-kappaB pathway. *Nat Commun, 9*(1), 101. doi:10.1038/s41467-017-02586-x

Scher, M. B., Vaquero, A., & Reinberg, D. (2007). SirT3 is a nuclear NAD+-dependent histone deacetylase that translocates to the mitochondria upon cellular stress. *Genes Dev, 21*(8), 920-928. doi:10.1101/gad.1527307

Schneider, A., Dhahbi, J. M., Atamna, H., Clark, J. P., Colman, R. J., & Anderson, R. M. (2017). Caloric restriction impacts plasma microRNAs in rhesus monkeys. *Aging Cell, 16*(5), 1200-1203. doi:10.1111/acel.12636

Schwer, B., North, B. J., Frye, R. A., Ott, M., & Verdin, E. (2002). The human silent information regulator (Sir)2 homologue hSIRT3 is a mitochondrial nicotinamide adenine dinucleotide-dependent deacetylase. *J Cell Biol, 158*(4), 647-657. doi:10.1083/jcb.200205057

Sharples, A. P., Stewart, C. E., & Seaborne, R. A. (2016). Does skeletal muscle have an 'epi'-memory? The role of epigenetics in nutritional programming, metabolic disease, aging and exercise. *Aging Cell, 15*(4), 603-616. doi:10.1111/acel.12486

Shibuya, H., Iinuma, H., Shimada, R., Horiuchi, A., & Watanabe, T. (2010). Clinicopathological and prognostic value of microRNA-21 and microRNA-155 in colorectal cancer. *Oncology, 79*(3-4), 313-320. doi:10.1159/000323283

Shimazu, T., Hirschey, M. D., Hua, L., Dittenhafer-Reed, K. E., Schwer, B., Lombard, D. B., . . . Verdin, E. (2010). SIRT3 deacetylates mitochondrial 3-hydroxy-3-methylglutaryl CoA synthase 2 and regulates ketone body production. *Cell Metab, 12*(6), 654-661. doi:10.1016/j.cmet.2010.11.003

Shogren-Knaak, M., Ishii, H., Sun, J. M., Pazin, M. J., Davie, J. R., & Peterson, C. L. (2006). Histone H4-K16 acetylation controls chromatin structure and protein interactions. *Science, 311*(5762), 844-847. doi:10.1126/science.1124000

Simone, N. L., Soule, B. P., Ly, D., Saleh, A. D., Savage, J. E., Degraff, W., . . . Mitchell, J. B. (2009). Ionizing radiation-induced oxidative stress alters miRNA expression. *Plos One, 4*(7), e6377. doi:10.1371/journal.pone.0006377

Simonet, N. G., & Vaquero, A. (2017). Raising the list of SirT7 targets to a new level. *Proteomics, 17*(13-14). doi:10.1002/pmic.201700137

Simpson, S. J., Le Couteur, D. G., James, D. E., George, J., Gunton, J. E., Solon-Biet, S. M., & Raubenheimer, D. (2017). The Geometric Framework for Nutrition as a tool in precision medicine. *Nutr Healthy Aging, 4*(3), 217-226. doi:10.3233/NHA-170027

Simpson, S. J., Le Couteur, D. G., Raubenheimer, D., Solon-Biet, S. M., Cooney, G. J., Cogger, V. C., & Fontana, L. (2017). Dietary protein, aging and nutritional geometry. *Ageing Res Rev, 39*, 78-86. doi:10.1016/j.arr.2017.03.001

Simpson, S. J., & Raubenheimer, D. (2005). Obesity: the protein leverage hypothesis. *Obes Rev, 6*(2), 133-142. doi:10.1111/j.1467-789X.2005.00178.x

Simpson, S. J., Raubenheimer, D., Cogger, V. C., Macia, L., Solon-Biet, S. M., Le Couteur, D. G., & George, J. (2018). The nutritional geometry of liver disease including non-alcoholic fatty liver disease. *J Hepatol, 68*(2), 316-325. doi:10.1016/j.jhep.2017.10.005

Sinclair, D. A., & Guarente, L. (1997). Extrachromosomal rDNA circles--a cause of aging in yeast. *Cell, 91*(7), 1033-1042.

Skoge, R. H., Dolle, C., & Ziegler, M. (2014). Regulation of SIRT2-dependent alpha-tubulin deacetylation by cellular NAD levels. *DNA Repair (Amst), 23*, 33-38. doi:10.1016/j.dnarep.2014.04.011

Solon-Biet, S. M., McMahon, A. C., Ballard, J. W., Ruohonen, K., Wu, L. E., Cogger, V. C., . . . Simpson, S. J. (2014). The ratio of macronutrients, not caloric intake, dictates cardiometabolic health, aging, and longevity in ad libitum-fed mice. *Cell Metab, 19*(3), 418-430. doi:10.1016/j.cmet.2014.02.009

Solon-Biet, S. M., Mitchell, S. J., Coogan, S. C., Cogger, V. C., Gokarn, R., McMahon, A. C., . . . Le Couteur, D. G. (2015). Dietary Protein to Carbohydrate Ratio and Caloric Restriction: Comparing Metabolic Outcomes in Mice. *Cell Rep, 11*(10), 1529-1534. doi:10.1016/j.celrep.2015.05.007

Solon-Biet, S. M., Walters, K. A., Simanainen, U. K., McMahon, A. C., Ruohonen, K., Ballard, J. W., . . . Simpson, S. J. (2015). Macronutrient balance, reproductive function, and lifespan in aging mice. *Proc Natl Acad Sci U S A, 112*(11), 3481-3486. doi:10.1073/pnas.1422041112

Song, H. Y., Rellinger, E. J., Park, S. H., Paul, P., Qiao, J., Vasilopoulos, A., . . . Chung, D. H. (2018). Inhibition of Sirtuin 6 Induces Neuroblastoma Differentiation. *Anticancer Res, 38*(2), 647-654. doi:10.21873/anticanres.12268

Speakman, J. R., Mitchell, S. E., & Mazidi, M. (2016). Calories or protein? The effect of dietary restriction on lifespan in rodents is explained by calories alone. *Exp Gerontol, 86*, 28-38. doi:10.1016/j.exger.2016.03.011

Stockman, M. C., Thomas, D., Burke, J., & Apovian, C. M. (2018). Intermittent Fasting: Is the Wait Worth the Weight? *Curr Obes Rep, 7*(2), 172-185. doi:10.1007/s13679-018-0308-9

Storlien, L. H., Pan, D. A., Kriketos, A. D., & Baur, L. A. (1993). High fat diet-induced insulin resistance. Lessons and implications from animal studies. *Ann N Y Acad Sci, 683*, 82-90.

Strakovsky, R. S., Lezmi, S., Flaws, J. A., Schantz, S. L., Pan, Y. X., & Helferich, W. G. (2014). Genistein exposure during the early postnatal period favors the development of obesity in female, but not male rats. *Toxicol Sci, 138*(1), 161-174. doi:10.1093/toxsci/kft331

Su, C. H., Lin, I. H., Tzeng, T. Y., Hsieh, W. T., & Hsu, M. T. (2016). Regulation of IL-20 Expression by Estradiol through KMT2B-Mediated Epigenetic Modification. *Plos One, 11*(11), e0166090. doi:10.1371/journal.pone.0166090

Subramaniam, K., Fallon, K., Ruut, T., Lane, D., McKay, R., Shadbolt, B., . . . Taupin, D. (2015). Infliximab reverses inflammatory muscle wasting (sarcopenia) in Crohn's disease. *Aliment Pharmacol Ther, 41*(5), 419-428. doi:10.1111/apt.13058

Subramanian, S., Braun, P. R., Han, S., & Potash, J. B. (2018). Investigation of differential HDAC4 methylation patterns in eating disorders. *Psychiatr Genet, 28*(1), 12-15. doi:10.1097/YPG.0000000000000189

Sullivan, K. E., Reddy, A. B., Dietzmann, K., Suriano, A. R., Kocieda, V. P., Stewart, M., & Bhatia, M. (2007). Epigenetic regulation of tumor necrosis factor alpha. *Mol Cell Biol, 27*(14), 5147-5160. doi:10.1128/MCB.02429-06

Sundaresan, N. R., Samant, S. A., Pillai, V. B., Rajamohan, S. B., & Gupta, M. P. (2008). SIRT3 is a stress-responsive deacetylase in cardiomyocytes that protects cells from stress-mediated cell death by deacetylation of Ku70. *Mol Cell Biol, 28*(20), 6384-6401. doi:10.1128/MCB.00426-08

Syamsunarno, M. R., Iso, T., Hanaoka, H., Yamaguchi, A., Obokata, M., Koitabashi, N., . . . Kurabayashi, M. (2013). A critical role of fatty acid binding protein 4 and 5 (FABP4/5) in the systemic response to fasting. *Plos One, 8*(11), e79386. doi:10.1371/journal.pone.0079386

Tan, M., Peng, C., Anderson, K. A., Chhoy, P., Xie, Z., Dai, L., . . . Zhao, Y. (2014). Lysine glutarylation is a protein posttranslational modification regulated by SIRT5. *Cell Metab, 19*(4), 605-617. doi:10.1016/j.cmet.2014.03.014

Tanny, J. C., Dowd, G. J., Huang, J., Hilz, H., & Moazed, D. (1999). An enzymatic activity in the yeast Sir2 protein that is essential for gene silencing. *Cell, 99*(7), 735-745.

Tasselli, L., Zheng, W., & Chua, K. F. (2017). SIRT6: Novel Mechanisms and Links to Aging and Disease. *Trends Endocrinol Metab, 28*(3), 168-185. doi:10.1016/j.tem.2016.10.002

Taunton, J., Hassig, C. A., & Schreiber, S. L. (1996). A mammalian histone deacetylase related to the yeast transcriptional regulator Rpd3p. *Science, 272*(5260), 408-411.

Teixeira Vde, O., Filippin, L. I., & Xavier, R. M. (2012). Mechanisms of muscle wasting in sarcopenia. *Rev Bras Reumatol, 52*(2), 252-259.
Thiaville, M. M., Dudenhausen, E. E., Zhong, C., Pan, Y. X., & Kilberg, M. S. (2008). Deprivation of protein or amino acid induces C/EBPbeta synthesis and binding to amino acid response elements, but its action is not an absolute requirement for enhanced transcription. *Biochem J, 410*(3), 473-484. doi:10.1042/BJ20071252
Thorne, J. L., Ouboussad, L., & Lefevre, P. F. (2012). Heterochromatin protein 1 gamma and IkappaB kinase alpha interdependence during tumour necrosis factor gene transcription elongation in activated macrophages. *Nucleic Acids Res, 40*(16), 7676-7689. doi:10.1093/nar/gks509
Tian, J., & Yuan, L. (2018). Sirtuin 6 inhibits colon cancer progression by modulating PTEN/AKT signaling. *Biomed Pharmacother, 106*, 109-116. doi:10.1016/j.biopha.2018.06.070
Tilstra, J. S., Clauson, C. L., Niedernhofer, L. J., & Robbins, P. D. (2011). NF-kappaB in Aging and Disease. *Aging Dis, 2*(6), 449-465.
Ting, A. T., & Bertrand, M. J. (2016). More to Life than NF-kappaB in TNFR1 Signaling. *Trends Immunol, 37*(8), 535-545. doi:10.1016/j.it.2016.06.002
Toiber, D., Erdel, F., Bouazoune, K., Silberman, D. M., Zhong, L., Mulligan, P., . . . Mostoslavsky, R. (2013). SIRT6 recruits SNF2H to DNA break sites, preventing genomic instability through chromatin remodeling. *Mol Cell, 51*(4), 454-468. doi:10.1016/j.molcel.2013.06.018
Tong, Z., Wang, M., Wang, Y., Kim, D. D., Grenier, J. K., Cao, J., . . . Lin, H. (2017). SIRT7 Is an RNA-Activated Protein Lysine Deacylase. *ACS Chem Biol, 12*(1), 300-310. doi:10.1021/acschembio.6b00954
Tremolizzo, L., Conti, E., Bomba, M., Uccellini, O., Rossi, M. S., Marfone, M., . . . Nacinovich, R. (2014). Decreased whole-blood global DNA methylation is related to serum hormones in anorexia nervosa adolescents. *World Journal of Biological Psychiatry, 15*(4), 327-333. doi:10.3109/15622975.2013.860467
Trepanowski, J. F., Kroeger, C. M., Barnosky, A., Klempel, M., Bhutani, S., Hoddy, K. K., . . . Varady, K. A. (2017). Effects of alternate-day fasting or daily calorie restriction on body composition, fat distribution, and circulating adipokines: Secondary analysis of a randomized controlled trial. *Clin Nutr*. doi:10.1016/j.clnu.2017.11.018
Trojer, P., & Reinberg, D. (2007). Facultative heterochromatin: is there a distinctive molecular signature? *Mol Cell, 28*(1), 1-13. doi:10.1016/j.molcel.2007.09.011
Tsai, Y. C., Greco, T. M., Boonmee, A., Miteva, Y., & Cristea, I. M. (2012). Functional proteomics establishes the interaction of SIRT7 with chromatin remodeling complexes and expands its role in regulation of RNA polymerase I transcription. *Mol Cell Proteomics, 11*(5), 60-76. doi:10.1074/mcp.A111.015156
Tsytsykova, A. V., Falvo, J. V., Schmidt-Supprian, M., Courtois, G., Thanos, D., & Goldfeld, A. E. (2007). Post-induction, stimulus-specific regulation of tumor necrosis factor mRNA expression. *J Biol Chem, 282*(16), 11629-11638. doi:10.1074/jbc.M611418200
Turcotte, L. P., & Fisher, J. S. (2008). Skeletal muscle insulin resistance: roles of fatty acid metabolism and exercise. *Phys Ther, 88*(11), 1279-1296. doi:10.2522/ptj.20080018
Ueda, Y., Wang, M. C., Ou, B. R., Huang, J., Elce, J., Tanaka, K., . . . Forsberg, N. E. (1998). Evidence for the participation of the proteasome and calpain in early phases of muscle cell differentiation. *Int J Biochem Cell Biol, 30*(6), 679-694.

Unnikrishnan, A., Jackson, J., Matyi, S. A., Hadad, N., Wronowski, B., Georgescu, C., . . . Richardson, A. (2017). Role of DNA methylation in the dietary restriction mediated cellular memory. *Geroscience, 39*(3), 331-345. doi:10.1007/s11357-017-9976-8

Urbanova, M., Mraz, M., Durovcova, V., Trachta, P., Klouckova, J., Kavalkova, P., . . . Haluzik, M. (2017). The effect of very-low-calorie diet on mitochondrial dysfunction in subcutaneous adipose tissue and peripheral monocytes of obese subjects with type 2 diabetes mellitus. *Physiol Res, 66*(5), 811-822.

van de Ven, R. A. H., Santos, D., & Haigis, M. C. (2017). Mitochondrial Sirtuins and Molecular Mechanisms of Aging. *Trends Mol Med, 23*(4), 320-331. doi:10.1016/j.molmed.2017.02.005

Van Gool, F., Galli, M., Gueydan, C., Kruys, V., Prevot, P. P., Bedalov, A., . . . Leo, O. (2009). Intracellular NAD levels regulate tumor necrosis factor protein synthesis in a sirtuin-dependent manner. *Nat Med, 15*(2), 206-210. doi:10.1038/nm.1906

van Niekerk, G., du Toit, A., Loos, B., & Engelbrecht, A. M. (2018). Nutrient excess and autophagic deficiency: explaining metabolic diseases in obesity. *Metabolism, 82*, 14-21. doi:10.1016/j.metabol.2017.12.007

Vaquero, A., & Reinberg, D. (2009). Calorie restriction and the exercise of chromatin. *Genes Dev, 23*(16), 1849-1869. doi:10.1101/gad.1807009

Vaquero, A., Scher, M., Lee, D., Erdjument-Bromage, H., Tempst, P., & Reinberg, D. (2004). Human SirT1 interacts with histone H1 and promotes formation of facultative heterochromatin. *Mol Cell, 16*(1), 93-105. doi:10.1016/j.molcel.2004.08.031

Varady, K. A., & Hellerstein, M. K. (2007). Alternate-day fasting and chronic disease prevention: a review of human and animal trials. *Am J Clin Nutr, 86*(1), 7-13. doi:10.1093/ajcn/86.1.7

Varady, K. A., Tussing, L., Bhutani, S., & Braunschweig, C. L. (2009). Degree of weight loss required to improve adipokine concentrations and decrease fat cell size in severely obese women. *Metabolism, 58*(8), 1096-1101. doi:10.1016/j.metabol.2009.04.010

Vasudevan, S., Tong, Y., & Steitz, J. A. (2007). Switching from repression to activation: microRNAs can up-regulate translation. *Science, 318*(5858), 1931-1934. doi:10.1126/science.1149460

Vella, S., Gnani, D., Crudele, A., Ceccarelli, S., De Stefanis, C., Gaspari, S., . . . Alisi, A. (2013). EZH2 down-regulation exacerbates lipid accumulation and inflammation in in vitro and in vivo NAFLD. *Int J Mol Sci, 14*(12), 24154-24168. doi:10.3390/ijms141224154

Vempati, R. K., Jayani, R. S., Notani, D., Sengupta, A., Galande, S., & Haldar, D. (2010). p300-mediated acetylation of histone H3 lysine 56 functions in DNA damage response in mammals. *J Biol Chem, 285*(37), 28553-28564. doi:10.1074/jbc.M110.149393

Verheggen, R. J., Maessen, M. F., Green, D. J., Hermus, A. R., Hopman, M. T., & Thijssen, D. H. (2016). A systematic review and meta-analysis on the effects of exercise training versus hypocaloric diet: distinct effects on body weight and visceral adipose tissue. *Obes Rev, 17*(8), 664-690. doi:10.1111/obr.12406

Victoria, B., Dhahbi, J. M., Nunez Lopez, Y. O., Spinel, L., Atamna, H., Spindler, S. R., & Masternak, M. M. (2015). Circulating microRNA signature of genotype-by-age interactions in the long-lived Ames dwarf mouse. *Aging Cell, 14*(6), 1055-1066. doi:10.1111/acel.12373

Viljanen, A. P., Karmi, A., Borra, R., Parkka, J. P., Lepomaki, V., Parkkola, R., . . . Raitakari, O. T. (2009). Effect of caloric restriction on myocardial fatty acid uptake, left ventricular

mass, and cardiac work in obese adults. *Am J Cardiol, 103*(12), 1721-1726. doi:10.1016/j.amjcard.2009.02.025

Villeneuve, L. M., Reddy, M. A., Lanting, L. L., Wang, M., Meng, L., & Natarajan, R. (2008). Epigenetic histone H3 lysine 9 methylation in metabolic memory and inflammatory phenotype of vascular smooth muscle cells in diabetes. *Proc Natl Acad Sci U S A, 105*(26), 9047-9052. doi:10.1073/pnas.0803623105

Wahl, D., Cogger, V. C., Solon-Biet, S. M., Waern, R. V., Gokarn, R., Pulpitel, T., . . . Le Couteur, D. G. (2016). Nutritional strategies to optimise cognitive function in the aging brain. *Ageing Res Rev, 31*, 80-92. doi:10.1016/j.arr.2016.06.006

Wang, F., Nguyen, M., Qin, F. X., & Tong, Q. (2007). SIRT2 deacetylates FOXO3a in response to oxidative stress and caloric restriction. *Aging Cell, 6*(4), 505-514. doi:10.1111/j.1474-9726.2007.00304.x

Wang, F., & Tong, Q. (2009). SIRT2 suppresses adipocyte differentiation by deacetylating FOXO1 and enhancing FOXO1's repressive interaction with PPARgamma. *Mol Biol Cell, 20*(3), 801-808. doi:10.1091/mbc.E08-06-0647

Wang, H., & Ye, J. (2015). Regulation of energy balance by inflammation: common theme in physiology and pathology. *Rev Endocr Metab Disord, 16*(1), 47-54. doi:10.1007/s11154-014-9306-8

Wang, L., Guo, W., Ma, J., Dai, W., Liu, L., Guo, S., . . . Li, C. (2018). Aberrant SIRT6 expression contributes to melanoma growth: Role of the autophagy paradox and IGF-AKT signaling. *Autophagy, 14*(3), 518-533. doi:10.1080/15548627.2017.1384886

Wang, Q., Zhang, Y., Yang, C., Xiong, H., Lin, Y., Yao, J., . . . Zhao, G. P. (2010). Acetylation of metabolic enzymes coordinates carbon source utilization and metabolic flux. *Science, 327*(5968), 1004-1007. doi:10.1126/science.1179687

Wang, T., Tsui, B., Kreisberg, J. F., Robertson, N. A., Gross, A. M., Yu, M. K., . . . Ideker, T. (2017). Epigenetic aging signatures in mice livers are slowed by dwarfism, calorie restriction and rapamycin treatment. *Genome Biology, 18*(1), 57. doi:10.1186/s13059-017-1186-2

Wang, W. W., Zeng, Y., Wu, B., Deiters, A., & Liu, W. R. (2016). A Chemical Biology Approach to Reveal Sirt6-targeted Histone H3 Sites in Nucleosomes. *ACS Chem Biol, 11*(7), 1973-1981. doi:10.1021/acschembio.6b00243

Wang, X., & Song, Y. (2018). MicroRNA-340 inhibits the growth and invasion of angiosarcoma cells by targeting SIRT7. *Biomed Pharmacother, 103*, 1061-1068. doi:10.1016/j.biopha.2018.04.148

Wang, Y. P., Zhou, L. S., Zhao, Y. Z., Wang, S. W., Chen, L. L., Liu, L. X., . . . Ye, D. (2014). Regulation of G6PD acetylation by SIRT2 and KAT9 modulates NADPH homeostasis and cell survival during oxidative stress. *Embo j, 33*(12), 1304-1320. doi:10.1002/embj.201387224

Wang, Y. X., Lee, C. H., Tiep, S., Yu, R. T., Ham, J., Kang, H., & Evans, R. M. (2003). Peroxisome-proliferator-activated receptor delta activates fat metabolism to prevent obesity. *Cell, 113*(2), 159-170.

Wang, Z., Al-Regaiey, K. A., Masternak, M. M., & Bartke, A. (2006). Adipocytokines and lipid levels in Ames dwarf and calorie-restricted mice. *J Gerontol A Biol Sci Med Sci, 61*(4), 323-331.

Watanabe, A., Tagawa, H., Yamashita, J., Teshima, K., Nara, M., Iwamoto, K., . . . Sawada, K. (2011). The role of microRNA-150 as a tumor suppressor in malignant lymphoma. *Leukemia, 25*(8), 1324-1334. doi:10.1038/leu.2011.81

Weindruch, R., Walford, R. L., Fligiel, S., & Guthrie, D. (1986). The retardation of aging in mice by dietary restriction: longevity, cancer, immunity and lifetime energy intake. *J Nutr, 116*(4), 641-654.

Weiss, E. P., & Fontana, L. (2011). Caloric restriction: powerful protection for the aging heart and vasculature. *Am J Physiol Heart Circ Physiol, 301*(4), H1205-1219. doi:10.1152/ajpheart.00685.2011

Wirth, M., Karaca, S., Wenzel, D., Ho, L., Tishkoff, D., Lombard, D. B., . . . Fischle, W. (2013). Mitochondrial SIRT4-type proteins in Caenorhabditis elegans and mammals interact with pyruvate carboxylase and other acetylated biotin-dependent carboxylases. *Mitochondrion, 13*(6), 705-720. doi:10.1016/j.mito.2013.02.002

Witt, S. H., Granzier, H., Witt, C. C., & Labeit, S. (2005). MURF-1 and MURF-2 target a specific subset of myofibrillar proteins redundantly: towards understanding MURF-dependent muscle ubiquitination. *J Mol Biol, 350*(4), 713-722. doi:10.1016/j.jmb.2005.05.021

Wolfson, R. L., & Sabatini, D. M. (2017). The Dawn of the Age of Amino Acid Sensors for the mTORC1 Pathway. *Cell Metab, 26*(2), 301-309. doi:10.1016/j.cmet.2017.07.001

Wood, S. H., van Dam, S., Craig, T., Tacutu, R., O'Toole, A., Merry, B. J., & de Magalhaes, J. P. (2015). Transcriptome analysis in calorie-restricted rats implicates epigenetic and post-translational mechanisms in neuroprotection and aging. *Genome Biology, 16*, 285. doi:10.1186/s13059-015-0847-2

Wronska, A., Lawniczak, A., Wierzbicki, P. M., & Kmiec, Z. (2016). Age-Related Changes in Sirtuin 7 Expression in Calorie-Restricted and Refed Rats. *Gerontology, 62*(3), 304-310. doi:10.1159/000441603

Wu, H., & Zhang, Y. (2011). Mechanisms and functions of Tet protein-mediated 5-methylcytosine oxidation. *Genes Dev, 25*(23), 2436-2452. doi:10.1101/gad.179184.111

Xu, Y., Rubin, B. R., Orme, C. M., Karpikov, A., Yu, C., Bogan, J. S., & Toomre, D. K. (2011). Dual-mode of insulin action controls GLUT4 vesicle exocytosis. *J Cell Biol, 193*(4), 643-653. doi:10.1083/jcb.201008135

Yadava, R. S., Foff, E. P., Yu, Q., Gladman, J. T., Kim, Y. K., Bhatt, K. S., . . . Mahadevan, M. S. (2015). TWEAK/Fn14, a pathway and novel therapeutic target in myotonic dystrophy. *Hum Mol Genet, 24*(7), 2035-2048. doi:10.1093/hmg/ddu617

Yan, C., & Boyd, D. D. (2006). Histone H3 acetylation and H3 K4 methylation define distinct chromatin regions permissive for transgene expression. *Mol Cell Biol, 26*(17), 6357-6371. doi:10.1128/MCB.00311-06

Yang, L., Licastro, D., Cava, E., Veronese, N., Spelta, F., Rizza, W., . . . Fontana, L. (2016a). Long-Term Calorie Restriction Enhances Cellular Quality-Control Processes in Human Skeletal Muscle. *Cell Rep, 14*(3), 422-428. doi:10.1016/j.celrep.2015.12.042

Yang, L., Licastro, D., Cava, E., Veronese, N., Spelta, F., Rizza, W., . . . Fontana, L. (2016b). Long-Term Calorie Restriction Enhances Cellular Quality-Control Processes in Human Skeletal Muscle. *Cell Rep, 14*(3), 422-428. doi:10.1016/j.celrep.2015.12.042

Yang, W., Cao, M., Mao, X., Wei, X., Li, X., Chen, G., . . . Liu, C. (2016). Alternate-day fasting protects the livers of mice against high-fat diet-induced inflammation associated with the

suppression of Toll-like receptor 4/nuclear factor kappaB signaling. *Nutr Res, 36*(6), 586-593. doi:10.1016/j.nutres.2016.02.001

Yang, W., Nagasawa, K., Munch, C., Xu, Y., Satterstrom, K., Jeong, S., . . . Haigis, M. C. (2016). Mitochondrial Sirtuin Network Reveals Dynamic SIRT3-Dependent Deacetylation in Response to Membrane Depolarization. *Cell, 167*(4), 985-1000 e1021. doi:10.1016/j.cell.2016.10.016

Yang, Y. B., Wu, X. L., Ke, B., Huang, Y. J., Chen, S. Q., Su, Y. Q., & Qin, J. (2017). Effects of caloric restriction on peroxisome proliferator-activated receptors and positive transcription elongation factor b expression in obese rats. *Eur Rev Med Pharmacol Sci, 21*(19), 4369-4378.

Yoshizawa, T., Karim, M. F., Sato, Y., Senokuchi, T., Miyata, K., Fukuda, T., . . . Yamagata, K. (2014). SIRT7 controls hepatic lipid metabolism by regulating the ubiquitin-proteasome pathway. *Cell Metab, 19*(4), 712-721. doi:10.1016/j.cmet.2014.03.006

Yu, J., Qiu, Y., Yang, J., Bian, S., Chen, G., Deng, M., . . . Huang, L. (2016). DNMT1-PPARgamma pathway in macrophages regulates chronic inflammation and atherosclerosis development in mice. *Sci Rep, 6*, 30053. doi:10.1038/srep30053

Yu, W., Dittenhafer-Reed, K. E., & Denu, J. M. (2012). SIRT3 protein deacetylates isocitrate dehydrogenase 2 (IDH2) and regulates mitochondrial redox status. *J Biol Chem, 287*(17), 14078-14086. doi:10.1074/jbc.M112.355206

Zemach, A., McDaniel, I. E., Silva, P., & Zilberman, D. (2010). Genome-wide evolutionary analysis of eukaryotic DNA methylation. *Science, 328*(5980), 916-919. doi:10.1126/science.1186366

Zhang, C., Zhai, Z., Tang, M., Cheng, Z., Li, T., Wang, H., & Zhu, W. G. (2017). Quantitative proteome-based systematic identification of SIRT7 substrates. *Proteomics, 17*(13-14). doi:10.1002/pmic.201600395

Zhang, L., Hou, X., Ma, R., Moley, K., Schedl, T., & Wang, Q. (2014). Sirt2 functions in spindle organization and chromosome alignment in mouse oocyte meiosis. *FASEB J, 28*(3), 1435-1445. doi:10.1096/fj.13-244111

Zhang, M., Pan, Y., Dorfman, R. G., Yin, Y., Zhou, Q., Huang, S., . . . Zhao, S. (2017). Sirtinol promotes PEPCK1 degradation and inhibits gluconeogenesis by inhibiting deacetylase SIRT2. *Sci Rep, 7*(1), 7. doi:10.1038/s41598-017-00035-9

Zhang, N., Li, Z., Mu, W., Li, L., Liang, Y., Lu, M., . . . Wang, Z. (2016). Calorie restriction-induced SIRT6 activation delays aging by suppressing NF-kappaB signaling. *Cell Cycle, 15*(7), 1009-1018. doi:10.1080/15384101.2016.1152427

Zhang, X., Khan, S., Jiang, H., Antonyak, M. A., Chen, X., Spiegelman, N. A., . . . Lin, H. (2016). Identifying the functional contribution of the defatty-acylase activity of SIRT6. *Nat Chem Biol, 12*(8), 614-620. doi:10.1038/nchembio.2106

Zhang, Y., & Reinberg, D. (2001). Transcription regulation by histone methylation: interplay between different covalent modifications of the core histone tails. *Genes Dev, 15*(18), 2343-2360. doi:10.1101/gad.927301

Zhang, Y., Wang, H., Zhou, D., Moody, L., Lezmi, S., Chen, H., & Pan, Y. X. (2015). High-fat diet caused widespread epigenomic differences on hepatic methylome in rat. *Physiol Genomics, 47*(10), 514-523. doi:10.1152/physiolgenomics.00110.2014

Zhao, Q., Fan, Y. C., Zhao, J., Gao, S., Zhao, Z. H., & Wang, K. (2013). DNA methylation patterns of peroxisome proliferator-activated receptor gamma gene associated with liver

fibrosis and inflammation in chronic hepatitis B. *J Viral Hepat, 20*(6), 430-437. doi:10.1111/jvh.12048

Zhong, L., D'Urso, A., Toiber, D., Sebastian, C., Henry, R. E., Vadysirisack, D. D., . . . Mostoslavsky, R. (2010). The histone deacetylase Sirt6 regulates glucose homeostasis via Hif1alpha. *Cell, 140*(2), 280-293. doi:10.1016/j.cell.2009.12.041

Zhou, D., Wang, H., Cui, H., Chen, H., & Pan, Y. X. (2015). Early-life exposure to high-fat diet may predispose rats to gender-specific hepatic fat accumulation by programming Pepck expression. *J Nutr Biochem, 26*(5), 433-440. doi:10.1016/j.jnutbio.2014.10.009

Zhou, J., Liu, B., Liang, C., Li, Y., & Song, Y. H. (2016). Cytokine Signaling in Skeletal Muscle Wasting. *Trends Endocrinol Metab, 27*(5), 335-347. doi:10.1016/j.tem.2016.03.002

Zhou, J., Wu, A., Yu, X., Zhu, J., & Dai, H. (2017). SIRT6 inhibits growth of gastric cancer by inhibiting JAK2/STAT3 pathway. *Oncol Rep, 38*(2), 1059-1066. doi:10.3892/or.2017.5753

Zhu, B., Yan, Y., Shao, B., Tian, L., & Zhou, W. (2018). Downregulation of SIRT6 is associated with poor prognosis in patients with non-small cell lung cancer. *J Int Med Res, 46*(4), 1517-1527. doi:10.1177/0300060517750298

Zou, R., Shi, W., Tao, J., Li, H., Lin, X., Yang, S., & Hua, P. (2018). SIRT5 and post-translational protein modifications: A potential therapeutic target for myocardial ischemia-reperfusion injury with regard to mitochondrial dynamics and oxidative metabolism. *Eur J Pharmacol, 818*, 410-418. doi:10.1016/j.ejphar.2017.11.005

APPENDIX A: CHAPTER 3 APPENDIX

Supplemental Table 3.1. Algorithm search for miRNA and CR

miRNA	%CR	Tissue	Change by CR*	Ref.
cel-miR-1824-5p	2-day fasting	Whole animals	Downregulated	(Kogure et al., 2017)
cel-miR-1829b	2-day fasting	Whole animals	Downregulated	(Kogure et al., 2017)
cel-miR-2210-5p	2-day fasting	Whole animals	Downregulated	(Kogure et al., 2017)
cel-miR-2221	2-day fasting	Whole animals	Downregulated	(Kogure et al., 2017)
cel-miR-239a-5p	2-day fasting	Whole animals	Downregulated	(Kogure et al., 2017)
cel-miR-243-3p	2-day fasting	Whole animals	Downregulated	(Kogure et al., 2017)
cel-miR-259-3p	2-day fasting	Whole animals	Downregulated	(Kogure et al., 2017)
cel-miR-259-5p	2-day fasting	Whole animals	Downregulated	(Kogure et al., 2017)
cel-miR-35-5p	2-day fasting	Whole animals	Downregulated	(Kogure et al., 2017)
cel-miR-38-5p	2-day fasting	Whole animals	Downregulated	(Kogure et al., 2017)
cel-miR-40-5p	2-day fasting	Whole animals	Downregulated	(Kogure et al., 2017)
cel-miR-43-3p	2-day fasting	Whole animals	Downregulated	(Kogure et al., 2017)
cel-miR-4809-3p	2-day fasting	Whole animals	Downregulated	(Kogure et al., 2017)
cel-miR-4936	2-day fasting	Whole animals	Downregulated	(Kogure et al., 2017)
cel-miR-49-5p	2-day fasting	Whole animals	Downregulated	(Kogure et al., 2017)
cel-miR-50-3p	2-day fasting	Whole animals	Downregulated	(Kogure et al., 2017)
cel-miR-52-3p	2-day fasting	Whole animals	Downregulated	(Kogure et al., 2017)
cel-miR-55-5p	2-day fasting	Whole animals	Downregulated	(Kogure et al., 2017)
cel-miR-5592-3p	2-day fasting	Whole animals	Downregulated	(Kogure et al., 2017)
cel-miR-5592-5p	2-day fasting	Whole animals	Downregulated	(Kogure et al., 2017)
cel-miR-58b-5p	2-day fasting	Whole animals	Downregulated	(Kogure et al., 2017)
cel-miR-63-3p	2-day fasting	Whole animals	Downregulated	(Kogure et al., 2017)
cel-miR-75-3p	2-day fasting	Whole animals	Downregulated	(Kogure et al., 2017)
cel-miR-75-5p	2-day fasting	Whole animals	Downregulated	(Kogure et al., 2017)
cel-miR-784-3p	2-day fasting	Whole animals	Downregulated	(Kogure et al., 2017)
cel-miR-789	2-day fasting	Whole animals	Downregulated	(Kogure et al., 2017)
cel-miR-791-5p	2-day fasting	Whole animals	Downregulated	(Kogure et al., 2017)
cel-miR-79-3p	2-day fasting	Whole animals	Downregulated	(Kogure et al., 2017)
cel-miR-80-5p	2-day fasting	Whole animals	Downregulated	(Kogure et al., 2017)
cel-miR-83-5p	2-day fasting	Whole animals	Downregulated	(Kogure et al., 2017)
cel-miR-1832b-3p	2-day fasting	Whole animals	Downregulated	(Kogure et al., 2017)
cel-miR-4808-5p	2-day fasting	Whole animals	Downregulated	(Kogure et al., 2017)
cel-let-7-3p	12-hr starvation	Whole animals	Downregulated	(Garcia-Segura et al., 2015)
cel-mir-79	12-hr starvation	Whole animals	Downregulated	(Garcia-Segura et al., 2015)
cel-mir-85	12-hr starvation	Whole animals	Downregulated	(Garcia-Segura et al., 2015)
cel-miR-85-5p	12-hr starvation	Whole animals	Downregulated	(Garcia-Segura et al., 2015)
dme-miR-305	24-hr, 72hr starved media	Whole animals	Downregulated	(Barrio et al., 2014)
mmu-miR-126-5p	40% CR	Serum	Downregulated	(Dhahbi et al., 2013)
mmu-miR-127-3p	40% CR	Serum	Downregulated	(Dhahbi et al., 2013)
mmu-miR-136-3p	40% CR	Serum	Downregulated	(Dhahbi et al., 2013)
mmu-miR-139-5p	40% CR	Serum	Downregulated	(Dhahbi et al., 2013)
mmu-miR-194-5p	40% CR	Serum	Downregulated	(Dhahbi et al., 2013)
mmu-miR-27b-3p	40% CR	Serum	Downregulated	(Dhahbi et al., 2013)
mmu-miR-29c-3p	40% CR	Serum	Downregulated	(Dhahbi et al., 2013)
mmu-miR-322-3p	40% CR	Serum	Downregulated	(Dhahbi et al., 2013)
mmu-miR-335-5p	40% CR	Serum	Downregulated	(Dhahbi et al., 2013)
mmu-miR-34a-5p	40% CR	Serum	Downregulated	(Dhahbi et al., 2013)
mmu-miR-381-3p	40% CR	Serum	Downregulated	(Dhahbi et al., 2013)
mmu-miR-411-5p	40% CR	Serum	Downregulated	(Dhahbi et al., 2013)
mmu-miR-434-5p	40% CR	Serum	Downregulated	(Dhahbi et al., 2013)
mmu-miR-540-3p	40% CR	Serum	Downregulated	(Dhahbi et al., 2013)
mmu-miR-541-5p	40% CR	Serum	Downregulated	(Dhahbi et al., 2013)
mmu-miR-101a-3p	40% CR	Liver	Downregulated	(Noren Hooten et al., 2016)
mmu-miR-101b-3p	40% CR	Liver	Downregulated	(Noren Hooten et al., 2016)
mmu-miR-106b-5p	40% CR	Liver	Downregulated	(Noren Hooten et al., 2016)
mmu-miR-107-3p	40% CR	Liver	Downregulated	(Noren Hooten et al., 2016)
mmu-miR-122-5p	40% CR	Liver	Downregulated	(Noren Hooten et al., 2016)
mmu-miR-125a-3p	40% CR	Liver	Downregulated	(Noren Hooten et al., 2016)
mmu-miR-142-3p	40% CR	Liver	Downregulated	(Noren Hooten et al., 2016)
mmu-miR-148a-3p	40% CR	Liver	Downregulated	(Noren Hooten et al., 2016)
mmu-miR-152-3p	40% CR	Liver	Downregulated	(Noren Hooten et al., 2016)
mmu-miR-15a-5p	40% CR	Liver	Downregulated	(Noren Hooten et al., 2016)

Supplemental Table 3.1. (cont.)

mmu-miR-192-5p	40% CR	Liver	Downregulated	(Noren Hooten et al., 2016)
mmu-miR-1937b_v16.0	40% CR	Liver	Downregulated	(Noren Hooten et al., 2016)
mmu-miR-1937c_v16.0	40% CR	Liver	Downregulated	(Noren Hooten et al., 2016)
mmu-miR-1939_v16.0	40% CR	Liver	Downregulated	(Noren Hooten et al., 2016)
mmu-miR-193a-3p	40% CR	Liver	Downregulated	(Noren Hooten et al., 2016)
mmu-miR-19b-3p	40% CR	Liver	Downregulated	(Noren Hooten et al., 2016)
mmu-miR-203-3p	40% CR	Liver	Downregulated	(Noren Hooten et al., 2016)
mmu-miR-212-3p	40% CR	Liver	Downregulated	(Noren Hooten et al., 2016)
mmu-miR-21a-5p	40% CR	Liver	Downregulated	(Noren Hooten et al., 2016)
mmu-miR-26b-5p	40% CR	Liver	Downregulated	(Noren Hooten et al., 2016)
mmu-miR-27b-3p	40% CR	Liver	Downregulated	(Noren Hooten et al., 2016)
mmu-miR-29b-3p	40% CR	Liver	Downregulated	(Noren Hooten et al., 2016)
mmu-miR-29c-3p	40% CR	Liver	Downregulated	(Noren Hooten et al., 2016)
mmu-miR-30a-5p	40% CR	Liver	Downregulated	(Noren Hooten et al., 2016)
mmu-miR-30e-5p	40% CR	Liver	Downregulated	(Noren Hooten et al., 2016)
mmu-miR-34a-5p	40% CR	Liver	Downregulated	(Noren Hooten et al., 2016)
mmu-miR-466f-3p	40% CR	Liver	Downregulated	(Noren Hooten et al., 2016)
mmu-miR-5097	40% CR	Liver	Downregulated	(Noren Hooten et al., 2016)
mmu-miR-720_v18.0	40% CR	Liver	Downregulated	(Noren Hooten et al., 2016)
mmu-miR-155	30% CR	Colon mucosa	Downregulated	(Olivo-Marston et al., 2014)
mmu-miR-30e	40% CR	brain	Downregulated	(Khanna et al., 2011)
mmu-miR-34a	40% CR	brain	Downregulated	(Khanna et al., 2011)
mmu-miR-181a-1*	40% CR	brain	Downregulated	(Khanna et al., 2011)
mmu-miR-200a	30% CR	breast tissue	Downregulated	(Devlin et al., 2016)
mml-miR-106b-5p	30% restriction, starting at 10%	Plasma	Downregulated	(Schneider et al., 2017)
mml-miR-125a-5p	30% restriction, starting at 10%	Plasma	Downregulated	(Schneider et al., 2017)
mml-miR-125b-5p	30% restriction, starting at 10%	Plasma	Downregulated	(Schneider et al., 2017)
mml-miR-133b-5p	30% restriction, starting at 10%	Plasma	Downregulated	(Schneider et al., 2017)
mml-miR-133c-5p	30% restriction, starting at 10%	Plasma	Downregulated	(Schneider et al., 2017)
mml-miR-143-5p	30% restriction, starting at 10%	Plasma	Downregulated	(Schneider et al., 2017)
mml-miR-16-5p	30% restriction, starting at 10%	Plasma	Downregulated	(Schneider et al., 2017)
mml-miR-182	30% restriction, starting at 10%	Plasma	Downregulated	(Schneider et al., 2017)
mml-miR-20a-5p	30% restriction, starting at 10%	Plasma	Downregulated	(Schneider et al., 2017)
mml-miR-224-5p	30% restriction, starting at 10%	Plasma	Downregulated	(Schneider et al., 2017)
mml-miR-92a-3p	30% restriction, starting at 10%	Plasma	Downregulated	(Schneider et al., 2017)
mml-miR-486-5p	30% restriction, starting at 10%	Plasma	Downregulated	(Schneider et al., 2017)
mmu-miR-100-5p	40% CR	Serum	Downregulated	(Dhahbi et al., 2013)
cel-miR-1822-5p	2-day fasting	Whole animals	Upregulated	(Kogure et al., 2017)
cel- miR-34-3p	2-day fasting	Whole animals	Upregulated	(Kogure et al., 2017)
cel- miR-1817	2-day fasting	Whole animals	Upregulated	(Kogure et al., 2017)
cel- miR-4810	2-day fasting	Whole animals	Upregulated	(Kogure et al., 2017)
cel- miR-64-3p	2-day fasting	Whole animals	Upregulated	(Kogure et al., 2017)
cel- miR-5552-3p	2-day fasting	Whole animals	Upregulated	(Kogure et al., 2017)
cel- miR-796	2-day fasting	Whole animals	Upregulated	(Kogure et al., 2017)
cel-miR-253-5p	2-day fasting	Whole animals	Upregulated	(Kogure et al., 2017)
cel-miR-359	2-day fasting	Whole animals	Upregulated	(Kogure et al., 2017)
cel-miR-266	2-day fasting	Whole animals	Upregulated	(Kogure et al., 2017)
cel-miR-2210-3p	2-day fasting	Whole animals	Upregulated	(Kogure et al., 2017)
cel-miR-1823	2-day fasting	Whole animals	Upregulated	(Kogure et al., 2017)
cel-miR-1829a-5p	2-day fasting	Whole animals	Upregulated	(Kogure et al., 2017)
cel-miR-1832a	2-day fasting	Whole animals	Upregulated	(Kogure et al., 2017)
cel-miR-255-3p	2-day fasting	Whole animals	Upregulated	(Kogure et al., 2017)
cel-miR-4812-5p	2-day fasting	Whole animals	Upregulated	(Kogure et al., 2017)
cel-miR-235-5p	2-day fasting	Whole animals	Upregulated	(Kogure et al., 2017)
cel-miR-2214-5p	2-day fasting	Whole animals	Upregulated	(Kogure et al., 2017)
cel-miR-797-5p	2-day fasting	Whole animals	Upregulated	(Kogure et al., 2017)
cel-miR-798	2-day fasting	Whole animals	Upregulated	(Kogure et al., 2017)
cel-miR-39-3p	12-hr starvation	Whole animals	Upregulated	(Garcia-Segura et al., 2015)
cel-miR-37-3p	12-hr starvation	Whole animals	Upregulated	(Garcia-Segura et al., 2015)
cel-miR-35-3p	12-hr starvation	Whole animals	Upregulated	(Garcia-Segura et al., 2015)
cel-miR-38-3p	12-hr starvation	Whole animals	Upregulated	(Garcia-Segura et al., 2015)
cel-miR-41-3p	12-hr starvation	Whole animals	Upregulated	(Garcia-Segura et al., 2015)
cel-miR-36-3p	12-hr starvation	Whole animals	Upregulated	(Garcia-Segura et al., 2015)
cel-miR-4813-5p	12-hr starvation	Whole animals	Upregulated	(Garcia-Segura et al., 2015)
cel-miR-40-3p	12-hr starvation	Whole animals	Upregulated	(Garcia-Segura et al., 2015)
cel-miR-34-3p	12-hr starvation	Whole animals	Upregulated	(Garcia-Segura et al., 2015)
cel-miR-41-5p	12-hr starvation	Whole animals	Upregulated	(Garcia-Segura et al., 2015)

Supplemental Table 3.1. (cont.)

cel-mir-35	12-hr starvation	Whole animals	Upregulated	(Garcia-Segura et al., 2015)
cel-miR-359	12-hr starvation	Whole animals	Upregulated	(Garcia-Segura et al., 2015)
cel-miR-39-5p	12-hr starvation	Whole animals	Upregulated	(Garcia-Segura et al., 2015)
cel-miR-240-5p	12-hr starvation	Whole animals	Upregulated	(Garcia-Segura et al., 2015)
cel-miR-246-3p	12-hr starvation	Whole animals	Upregulated	(Garcia-Segura et al., 2015)
dme-mir-184	High to low energy switch	Whole animals	Upregulated	(Gendron & Pletcher, 2017)
dme-let-7	High to low energy switch	Whole animals	Upregulated	(Gendron & Pletcher, 2017)
dme-mir-125	High to low energy switch	Whole animals	Upregulated	(Gendron & Pletcher, 2017)
dme-mir-100	High to low energy switch	Whole animals	Upregulated	(Gendron & Pletcher, 2017)
mmu-miR-150	30% CR	Colon mucosa	Upregulated	(Olivo-Marston et al., 2014)
mmu-miR-351	30% CR	Colon mucosa	Upregulated	(Olivo-Marston et al., 2014)
mmu-miR-16	30% CR	Colon mucosa	Upregulated	(Olivo-Marston et al., 2014)
mmu-let-7f	30% CR	Colon mucosa	Upregulated	(Olivo-Marston et al., 2014)
mmu-miR-34c	30% CR	Colon mucosa	Upregulated	(Olivo-Marston et al., 2014)
mmu-miR-29c	30% CR	breast tissue	Upregulated	(Orom et al., 2012)
mmu-miR-203	30% CR	breast tissue	Upregulated	(Orom et al., 2012)
mmu-miR-150	30% CR	breast tissue	Upregulated	(Orom et al., 2012)
mmu-miR-30	30% CR	breast tissue	Upregulated	(Orom et al., 2012)
mmu-miR-139-5p	40% CR	Liver	Upregulated	(Noren Hooten et al., 2016)
mmu-miR-92a-3p	40% CR	Liver	Upregulated	(Noren Hooten et al., 2016)
mmu-miR-338-5p	40% CR	Liver	Upregulated	(Noren Hooten et al., 2016)
mmu-miR-1187	40% CR	Liver	Upregulated	(Noren Hooten et al., 2016)
mmu-let-7c-5p	40% CR	Liver	Upregulated	(Noren Hooten et al., 2016)
mmu-miR-125b-5p	40% CR	Liver	Upregulated	(Noren Hooten et al., 2016)
mmu-let-7b-5p	40% CR	Liver	Upregulated	(Noren Hooten et al., 2016)
mmu-miR-1944_v16.0	40% CR	Liver	Upregulated	(Noren Hooten et al., 2016)
mmu-miR-1906	40% CR	Liver	Upregulated	(Noren Hooten et al., 2016)
mmu-miR-574-5p	40% CR	Liver	Upregulated	(Noren Hooten et al., 2016)
mmu-miR-2134_v15.0	40% CR	Liver	Upregulated	(Noren Hooten et al., 2016)
mmu-miR-2133_v15.0	40% CR	Liver	Upregulated	(Noren Hooten et al., 2016)
mmu-miR-2141_v15.0	40% CR	Liver	Upregulated	(Noren Hooten et al., 2016)
mmu-miR-2135_v15.0	40% CR	Liver	Upregulated	(Noren Hooten et al., 2016)
mmu-miR-2146_v15.0	40% CR	Liver	Upregulated	(Noren Hooten et al., 2016)
mmu-miR-486-3p	40% CR	Serum	Upregulated	(Dhahbi et al., 2013)
mmu-miR-3107-3p	40% CR	Serum	Upregulated	(Dhahbi et al., 2013)
mmu-miR-34b-5p	Young vs. old vs. CR (no CR)	Serum	Upregulated	(Victoria et al., 2015)
mmu-miR-344d-2-5p	Young vs. old vs. CR (no CR)	Serum	Upregulated	(Victoria et al., 2015)
mmu-miR-592-5p	Young vs. old vs. CR (no CR)	Serum	Upregulated	(Victoria et al., 2015)
mmu-mir-136	Young vs. old vs. CR (no CR)	Serum	Upregulated	(Victoria et al., 2015)
mmu-mir-127	Young vs. old vs. CR (no CR)	Serum	Upregulated	(Victoria et al., 2015)
mmu-miR-540	Young vs. old vs. CR (no CR)	Serum	Upregulated	(Victoria et al., 2015)
mmu-miR-449	Young vs. old vs. CR (no CR)	Serum	Upregulated	(Victoria et al., 2015)
mmu-miR-379	Young vs. old vs. CR (no CR)	Serum	Upregulated	(Victoria et al., 2015)
mmu-miR-5107	Young vs. old vs. CR (no CR)	Serum	Upregulated	(Victoria et al., 2015)
mmu-miR-146	Young vs. old vs. CR (no CR)	Serum	Upregulated	(Victoria et al., 2015)
mmu-miR-342	Young vs. old vs. CR (no CR)	Serum	Upregulated	(Victoria et al., 2015)
mmu-miR-368	Young vs. old vs. CR (no CR)	Serum	Upregulated	(Victoria et al., 2015)
mmu-miR-154	Young vs. old vs. CR (no CR)	Serum	Upregulated	(Victoria et al., 2015)
mmu-mir-15	Young vs. old vs. CR (no CR)	Serum	Upregulated	(Victoria et al., 2015)
mmu-miR-34c-5p	Young vs. old vs. CR (no CR)	Serum	Upregulated	(Victoria et al., 2015)
rno-miR-667	lifelong 40% CR	CEVC	Upregulated	(Csiszar et al., 2014)
rno-miR-383	lifelong 40% CR	CEVC	Upregulated	(Csiszar et al., 2014)
rno-miR-328a	lifelong 40% CR	CEVC	Upregulated	(Csiszar et al., 2014)
rno-let-7b	lifelong 40% CR	CEVC	Upregulated	(Csiszar et al., 2014)
rno-miR-92a	lifelong 40% CR	CEVC	Upregulated	(Csiszar et al., 2014)
rno-miR-532-3p	lifelong 40% CR	CEVC	Upregulated	(Csiszar et al., 2014)
rno-miR-181c	lifelong 40% CR	CEVC	Upregulated	(Csiszar et al., 2014)
rno-miR-145	lifelong 40% CR	CEVC	Upregulated	(Csiszar et al., 2014)
rno-let-7c	lifelong 40% CR	CEVC	Upregulated	(Csiszar et al., 2014)
rno-miR-329	lifelong 40% CR	CEVC	Upregulated	(Csiszar et al., 2014)
rno-miR-23a	lifelong 40% CR	CEVC	Upregulated	(Csiszar et al., 2014)
rno-miR-214	lifelong 40% CR	CEVC	Upregulated	(Csiszar et al., 2014)
rno-miR-125b-5p	lifelong 40% CR	CEVC	Upregulated	(Csiszar et al., 2014)
rno-miR-15b	lifelong 40% CR	CEVC	Upregulated	(Csiszar et al., 2014)
rno-let-7e	lifelong 40% CR	CEVC	Upregulated	(Csiszar et al., 2014)
rno-miR-181a	lifelong 40% CR	CEVC	Upregulated	(Csiszar et al., 2014)
rno-miR-221	lifelong 40% CR	CEVC	Upregulated	(Csiszar et al., 2014)
rno-let-7d	lifelong 40% CR	CEVC	Upregulated	(Csiszar et al., 2014)
rno-miR-34a	lifelong 40% CR	CEVC	Upregulated	(Csiszar et al., 2014)

Supplemental Table 3.1. (cont.)

rno-miR-24	lifelong 40% CR	CEVC	Upregulated	(Csiszar et al., 2014)
rno-miR-872	lifelong 40% CR	CEVC	Upregulated	(Csiszar et al., 2014)
rno-miR-29a	lifelong 40% CR	CEVC	Upregulated	(Csiszar et al., 2014)
rno-miR-140	lifelong 40% CR	CEVC	Upregulated	(Csiszar et al., 2014)
rno-miR-301a	lifelong 40% CR	CEVC	Upregulated	(Csiszar et al., 2014)
rno-miR-30c	lifelong 40% CR	CEVC	Upregulated	(Csiszar et al., 2014)
rno-miR-30b	lifelong 40% CR	CEVC	Upregulated	(Csiszar et al., 2014)
rno-miR-27a	lifelong 40% CR	CEVC	Upregulated	(Csiszar et al., 2014)
rno-miR-26a	lifelong 40% CR	CEVC	Upregulated	(Csiszar et al., 2014)
rno-miR-542-5p	lifelong 40% CR	CEVC	Upregulated	(Csiszar et al., 2014)
rno-miR-152	lifelong 40% CR	CEVC	Upregulated	(Csiszar et al., 2014)
rno-miR-26b	lifelong 40% CR	CEVC	Upregulated	(Csiszar et al., 2014)
rno-miR-186	lifelong 40% CR	CEVC	Upregulated	(Csiszar et al., 2014)
rno-miR-20a	lifelong 40% CR	CEVC	Upregulated	(Csiszar et al., 2014)
rno-miR-126	lifelong 40% CR	CEVC	Upregulated	(Csiszar et al., 2014)
rno-miR-29c	lifelong 40% CR	CEVC	Upregulated	(Csiszar et al., 2014)
rno-miR-192	lifelong 40% CR	CEVC	Upregulated	(Csiszar et al., 2014)
rno-miR-30e	lifelong 40% CR	CEVC	Upregulated	(Csiszar et al., 2014)
rno-miR-301b	lifelong 40% CR	CEVC	Upregulated	(Csiszar et al., 2014)
rno-miR-101a	lifelong 40% CR	CEVC	Upregulated	(Csiszar et al., 2014)
rno-miR-210	lifelong 40% CR	CEVC	Upregulated	(Csiszar et al., 2014)
rno-miR-106b	lifelong 40% CR	CEVC	Upregulated	(Csiszar et al., 2014)
rno-miR-449a	lifelong 40% CR	CEVC	Upregulated	(Csiszar et al., 2014)
rno-miR-17	lifelong 40% CR	CEVC	Upregulated	(Csiszar et al., 2014)
rno-miR-130b	lifelong 40% CR	CEVC	Upregulated	(Csiszar et al., 2014)
rno-miR-16	lifelong 40% CR	CEVC	Upregulated	(Csiszar et al., 2014)
rno-miR-19b	lifelong 40% CR	CEVC	Upregulated	(Csiszar et al., 2014)
rno-miR-503	lifelong 40% CR	CEVC	Upregulated	(Csiszar et al., 2014)
mml-miR-6529-5p	30% restriction, starting at 10%	Plasma	Upregulated	(Schneider et al., 2017)
mml-miR-21-5p	30% restriction, starting at 10%	Plasma	Upregulated	(Schneider et al., 2017)
mml-miR-340-5p	30% restriction, starting at 10%	Plasma	Upregulated	(Schneider et al., 2017)
mml-miR-130a-5p	30% restriction, starting at 10%	Plasma	Upregulated	(Schneider et al., 2017)
mml-miR-1260b	30% restriction, starting at 10%	Plasma	Upregulated	(Schneider et al., 2017)
mml-miR-130b-5p	30% restriction, starting at 10%	Plasma	Upregulated	(Schneider et al., 2017)
mml-miR-411-5p	30% restriction, starting at 10%	Plasma	Upregulated	(Schneider et al., 2017)
mml-miR-598-5p	30% restriction, starting at 10%	Plasma	Upregulated	(Schneider et al., 2017)
mml-miR-500a-5p	30% restriction, starting at 10%	Plasma	Upregulated	(Schneider et al., 2017)
mml-miR-501-5p	30% restriction, starting at 10%	Plasma	Upregulated	(Schneider et al., 2017)
mml-miR-122a-5p	30% restriction, starting at 10%	Plasma	Upregulated	(Schneider et al., 2017)
mml-miR-337-5p	30% restriction, starting at 10%	Plasma	Upregulated	(Schneider et al., 2017)
hsa-miR-1-3p	7-day weight maintenance (WM) period was followed by 28 days of 30% ER	Serum	Upregulated	(Margolis et al., 2017)
hsa- miR-133a-3p	7-day weight maintenance (WM) period was followed by 28 days of 30% ER	Serum	Upregulated	(Margolis et al., 2017)
hsa-miR-133b	7-day weight maintenance (WM) period was followed by 28 days of 30% ER	Serum	Upregulated	(Margolis et al., 2017)
hsa-miR-206	7-day weight maintenance (WM) period was followed by 28 days of 30% ER	Serum	Upregulated	(Margolis et al., 2017)

APPENDIX B: CHAPTER 4 APPENDIX

Supplemental Table 4.1. Primer sequences used for qPCR of skeletal muscle.

Gene (Ensembl ID)	Forward sequence (5'→3')	Reverse sequence (5'→3')
Igf-1 (+454 to +545) (ENSRNOT00000081822.1)	GGTGGACGCTCTTCAGTTCGTG	TCTGTGGTGCCCTCCGAATG
Igf-1r (+2239 to +2304) (ENSRNOT00000019267.6)	CTGAGAGGAGGCGGAGAGATG	TGTTCCTGCTTCGGCTGG
mTor (+196 to +263) (ENSRNOT00000014167.7)	TCCAGCACTATGTCACCA	CTGGTCATAGAAGCGAGTAG
Rptor (+1128 to +1200) (ENSRNOT00000005337.6)	CTCCAGATGTGGTGAAGACC	TGAGGACCCATAGACAGAGG
Akt2 (+252 to +319) (ENSRNOT00000025303.3)	GCTAGGTGACAGCGTGTTAATG	TGGAGCCAGCCTTCTTTG
Lkb1 (+1497 to +1573) (ENSRNOT00000060683.3)	CAATGGACTGGACACCTT	CCGTGGTGATGTTGTAGA
Pik3ca (+289 to +365) (ENSRNOT00000025687.7)	ACTGTCAGTCAGAGGTTCAG	CTGTTCAGGTGCTTCAGA
Ampkg (+12 to +77) (ENSRNOT00000083354)	TAGCAATGGAGTCGGTTG	GGGTCTCTTGAGAGTGTTCA
Phkg1 (+157 to+233) (ENSRNOT00000001222.4)	ACCTAACTAGGTGCTTGGG	AGAATGAGAGTCAGGGAGG
Pgc1a (+15 to +98) (ENSRNOT00000006071.5)	TGGCGTCATTCAGGAGCTGG	CAACCAGGGCAGCACACTCTATG
Cebpb (+1607 to +1670) (ENSRNOT00000083876.1)	CGCAACCCACGTGTAACTGTCAG	CAGCAACAAGCCCGTAGGAACA
Cpt1a (+1027 to +1102) (ENSRNOT00000019652.3)	GAGCGACTCTTCAATACTTCCC	TGTGCCTGCTGTCCTTGATA
Cpt1c (+291 to +366) (ENSRNOT00000035908.4)	TTACCTCTCTGCCCTACGCTCCTG	CGGGACCACACCAGCAAGAAA
Mlycd (+673 to +749) (ENSRNOT00000019923.5)	GCCCTGTGAGGTGCTTCAGAAGA	GCCGCTTCATGTCCATCCAGT
Lpl (+506 to +581) (ENSRNOT00000016543.3)	AGTAGACTGGTTGTATCGGG	CACATCATTTCCCACCAG
Acc2 (+1146 to +1229) (ENSRNOE00000005258)	CTCCTCCACCATTGTAGCCCAGAC	TCCTCCGTCCACTCCACTGTGA
Chrebp (+2281 to +2344) (ENSRNOT00000071067.2)	CGGGACATGTTTGATGACTATGTC	AATAAAGGTCGGATGAGGATGCT
Pfk1(+1653 to +1743) (ENSRNOT00000001625.5)	CCACCATCAGCAACAATGTC	TTGATGCGGTCACAACTCTC
Atf4 (+253 to +315) (ENSRNOT00000065304.4)	GGCTCCTCAGAATGGCTGGCTAT	ATCCTCCTTGCCGGTGTCTGAG
Atf3 (+949 to +1028) (ENSRNOT00000089841.1)	CGGCCATTCTCAGATGACCTAGC	TCTGCCTGCATCCCATTAGTGC
Bnip3 (+652 to +739) (ENSRNOT00000023477.6)	AAGGCGTCTGACAACTTCCA	TCACAGCTCAGCGTGAAT
Atg2a (+190 to +306) (ENSRNOT00000090100.1)	GCTACAGCACTACTTGGGTC	ACAGACCAGGTTTCCAGG
Chop (+636 to +731) (ENSRNOT00000083472.1)	CTCTGATCGACCGCATGGTCAG	TGGCGTGATGGTGCTGGG
Bcl2 (+730 to +817) (ENSRNOT00000003768.2)	CCCTGGTGGACAACATCGCTC	GCATCCCAGCCTCCGTTATCC
Lc3b (+626 to +726) (ENSRNOT00000051352.6)	GTGTTGTGGAAGAATGCC	TCACCCTTGTATCGCTCT
Lc3a (+443 to +536R) (ENSRNOT00000035060.4)	AGTGTATCCACACCCATCGC	AGCCGAAGGTTTCTTGGG
Ulk1 (+2780 to +2849) (ENSRNOT00000056790.3)	GCTTACAGACTGCCATTGACCAGA	ACCACCTGCTTCACAGTAGACGAA
Gcn2 (+356 to +426) (ENSRNOT00000009222.7)	GCAGTGTGGAGAGGTGATGATA	GCTTGTTATGCTCGCTGAGA
Pon1 (+1149 to +1221) (ENSRNOT00000011823.6)	AGTGAGGCCATCATTTCAGCC	ATTCGTTGGTGAGCGGAGATC
Pon2 (+584 to +658) (ENSRNOT00000036460.3)	TACGCCACCAATGACCACT	TGCCCAACGTAGGTTCAAG

Supplemental Table 4.1. (cont.)

Sod1 (+239 to +310) (ENSRNOT00000002885.6)	CAGCGGATGAAGAGAGGCA	ACACATTGGCCACACCGTC
Capn1 (+534 to +596) (ENSRNOT00000028431.6)	CTGGCATCTTTCATTTCCA	AATCATCCACGACCACATCTA
Capn2 (+949 to +1020) (ENSRNOT00000045326.3)	GAGTTCTGGAGTGCCCTTCTGGA	ACCCCCTGAGAGTGCTTCATAGC
Murf1 (+210 to +283) (ENSRNOT00000067524.3)	TCCTGCCCTGCCAGCACAA	GGTCCAGTAGGGATTGGCAGCC
Atrogin1 (+276 to +347) (ENSRNOT00000010361.3)	GATGAGAAAAGCGGCACCTT	CAGGCTGTTGAACAGATTCTCC
Mstn (+403 to +493) (ENSRNOT00000038093.3)	CAGAGGGATGACAGCAGT	AGTCAGACTCGGTAGGCA
Inha (+293 to +364) (ENSRNOT00000027227.4)	GCTTCATGCACAGGACCTCTGAAC	CACCTGTGGCTGGGAAAAGGAT
Ihnba (+608 to +682) (ENSRNOT00000019272.5)	AGATCATCACCTTTGCCGAGTCAG	GGTCACTGCCTTCCTTGGAAATCT
Fst (+42 to +103) (ENSRNOT00000015680.4)	CTCCTGCTGCTGCTACTCTGC	CAGCAATTCCCAGCCTGG
Foxo1a (+994 to +1056) (ENSRNOT00000018244.5)	AGGATAAGGGCGACAGCAACAG	GGGACAGATTGTGGCGAATTG
Foxo3 (+2424 to +2516) (ENSRNOT00000000327.5)	TTGCCAAATCTGCTCTCAGC	TCTCTGCTGGGTTAGGAAGATG
Mapk14 (+727 to +817) (ENSRNOT00000000617.8)	CACTCGGCTGACATAATCCA	CCAGCCCAAAATCCAGAA
Pax3 (+824 to +900) (ENSRNOT00000018652.5)	CTGTGCCCTCAGTGAGTTCCATCA	TAAATCCGCCTCCTCCTCTTCTCC
Pax7 (+1333 to +1402) (ENSRNOT00000025488.6)	TACAGCACCACGGGCTACAGT	CAGCAGTTTGACCGTACTGGC
Myod1 (+160 to +227) (ENSRNOT00000015109.2)	GACGACTCTTCAGGCTTG	GGCGATAGTAGCTCCATG
Mrf4 (+682 to +779) (ENSRNOT00000006523.5)	CCTGGTGATAACTGCTAAGG	CTGAGGAAATACTGTCCACG
Myog (+547 to +623) (ENSRNOT00000042046.1)	GAGTGGGGCAATGCACTGGA	TTGTGGGCACCTGTAGGGTCAG
Myf5 (+697 to +763) (ENSRNOT00000006453.5)	CACCAGCCCCACCTCCAACT	CTTTCGGGACCAGACAGGGC
Nfkb (p50)(+1907 to +1985) (ENSRNOT00000045233.3)	AGGCAGCACTCCTTATCAACCACC	GACAGGCTGTTGCTCATCACAGCT
Ikbke (+1189 to +1257) (ENSRNOT00000038151.3)	CCCTGCTCTGGATGTCCCAAAG	CCCTTAGCGGTGCTGTAATCGG
Il-1b (+793 to +871) (ENSRNOT00000006308.4)	CACCTCTCAAGCAGAGCACAG	GGGTTCCATGGTGAAGTCAAC
Il-6 (+559 to +637) (ENSRNOT00000013732.6)	TCCTACCCCAACTTCCAATGCTC	TTGGATGGTCTTGGTCCTTAGCC
Ifng (+116 to +182) (ENSRNOT00000009919.2)	CTCAAGTAGCATGGATGCTATGGA	CTTTTGCCAGTTCCTCCAGATATC
Tnfa (+339 to +449) (ENSRNOT00000079677.1)	AAATGGGCTCCCTCTCATCAGTTC	TCCGCTTGGTGGTTTGCTACGAC
Nfatc1 (+1447 to +1537) (ENSRNOT00000058382.4)	GCCTTTTGTGAGCAGTATCTGTCG	ATGGGCTCATGTATGACGTTGG
Nfatc2 (+1599 to +1674) (ENSRNOT00000065615.1)	GGAGCCAAAGAACAACATGCGGG	CAGCTCGATGTCAGCGTTTCGGA
Nfatc3 (+1837 to +1898) (ENSRNOT00000089783.1)	GCATCTATTCCTGTTGAGTG	TACTTCTCAATGTGAGGGAG
Nfatc4 (+1293 to +1372) (ENSRNOT00000089584.1)	CTTAGCAGTTCCTTCTCCCCTC	GTAGGGCAGAGGTCCTGAAGAT
Nfat5 (+994 to +1068) (ENSRNOT00000017005.5)	CAGCATCAATGAGTCAGACAAGCG	AAGAAGCATCGGCAGCAACTACAG
Sirt1 (+734 to +810) (ENSRNOT00000078739.1)	TTAATCAGGTAGTTCCTCGG	GAAGACAATCTCTGGCTTCA
Sirt6 (+582 to +660) (ENSRNOT00000008758.5)	GCCTGTAGAGGGGAGCTGAGAGAC	CATCAGCGAGCGTTAGGTCCC
Hdac3 (+1011 to +1128) (ENSRNOT00000084735.1)	GCTCCATCCAGATGTCAGCACCCGCAT	CTGGACACTGGGTGCATGGTTCAGC
Suv39h1 (+1127 to +1200) (ENSRNOT00000008399.5)	GCTGTTGCTGTGGCTATGACTGC	GCGGAAGATGCAGAGGTTGTAGC

Supplemental Table 4.1. (cont.)

Ezh2 (+1110 to +1180) (ENSRNOT00000008149.5)	CCACAGTGTTATCAGCATCTGGAGG	GTCTTTATCCGCTCAGCAGTAAGGG
Kmt2b (+961 to +1049) (ENSRNOT00000080842.1)	CTAGAATCAGGTCAGGGTCGTGGTC	GGTCCCCTTTCCTGTTCATCTCC
Dnmt1 (+1713 to +1792) (ENSRNOT00000064932.4)	TCCTACGCCATGCCCAGTTTG	GAAGATGGGCGTCTCATCATCG
Dnmt3b (+1197 to +1274) (ENSRNOT00000015482.6)	AATGCGCTGGGTACAGTGGTTTG	AACAGACCCAGAGCCACCAGCT

APPENDIX C: CHAPTER 5 APPENDIX

Supplemental Table 5.1. Primer sequences used for qPCR of skeletal muscle.

Gene (Ensembl ID)	Forward sequence (5'→3')	Reverse sequence (5'→3')
mTor (+196 to +263) (ENSRNOT00000014167.7)	TCCAGCACTATGTCACCA	CTGGTCATAGAAGCGAGTAG
Akt2 (+252 to +319) (ENSRNOT00000025303.3)	GCTAGGTGACAGCGTGTTAATG	TGGAGCCAGCCTTCTTTG
Lkb1 (+1497 to +1573) (ENSRNOT00000060683.3)	CAATGGACTGGACACCTT	CCGTGGTGATGTTGTAGA
Pik3ca (+289 to +365) (ENSRNOT00000025687.7)	ACTGTCAGTCAGAGGTTCAG	CTGTTCAGGTGCTTCAGA
Ampkg (+12 to +77) (ENSRNOT00000083354)	TAGCAATGGAGTCGGTTG	GGGTCTCTTGAGAGTGTTCA
Pgc1a (+15 to +98) (ENSRNOT00000006071.5)	TGGCGTCATTCAGGAGCTGG	CAACCAGGGCAGCACACTCTATG
Atf4 (+253 to +315) (ENSRNOT00000065304.4)	GGCTCCTCAGAATGGCTGGCTAT	ATCCTCCTTGCCGGTGTCTGAG
Bnip3 (+652 to +739) (ENSRNOT00000023477.6)	AAGGCGTCTGACAACTTCCA	TCACAGCTCAGCGTGAAT
Lc3b (+626 to +726) (ENSRNOT00000051352.6)	GTGTTGTGGAAGAATGCC	TCACCCTTGTATCGCTCT
Mstn (+403 to +493) (ENSRNOT00000038093.3)	CAGAGGGATGACAGCAGT	AGTCAGACTCGGTAGGCA
Fst (+42 to +103) (ENSRNOT00000015680.4)	CTCCTGCTGCTGCTACTCTGC	CAGCAATTCCCAGCCTGG
Tnfa (+339 to +449) (ENSRNOT00000079677.1)	AAATGGGCTCCCTCTCATCAGTTC	TCCGCTTGGTGGTTTGCTACGAC
Sirt1 (+734 to +810) (ENSRNOT00000078739.1)	TTAATCAGGTAGTTCCTCGG	GAAGACAATCTCTGGCTTCA
Fbp2 (+4 to +77) (ENSRNOT00000023865.3)	TGAGAGAGCAAGGATTCCTACGAGG	GCTTCTGTCCGTCATTGTGGCA
Cdkn2d (p19) (+753 to +821) (BC088350.1)	TTTTCCCCCCATTACTCCGA	GGAAAGCCCAAAATGCCA
G6pc (+825 to +883) (ENSRNOT00000028033.6)	CTCCAGCATGTACCGCAAGA	AACGGAATGGGAGCGACTT
Camkk2 (+966 to +1034) (ENSRNOT00000001774.6)	CGGGCACATCAAGATAGC	TTAGACAGCAAGGCGTCG
Pepck (+1177 to +1253) (ENSRNOT00000025260.7)	CGAACGCCATTAAGACCATCCAG	CCAGTAAACACCCCCATCACTTGTC

Supplemental Table 5.2. Serum Biochemical Parameters from animals following 6-month ADCR.

	CHOL[1]	HDL[1]	TAG[1]	nHDL[1]	TC/H[2]	LDL[1]	VLDL[1]	IGF1[1]	Glucose[1]	Insulin[3]	HOMA[2]
OL	103.8 ± 14.28 ^{a}	59.0 ± 9.72 ^{a}	160.8 ± 19.77 ^{ab}	44.4 ± 6.88 ^{a}	1.8 ± 0.13 ^{a}	13.6 ± 6.19 ^{a}	32.2 ± 3.99 ^{ab}	1.10 ± 0.04 ^{a}	128.25 ± 7.57 ^{a}	0.79 ± 0.20 ^{ab}	5.96 ± 1.41
ML	100.1 ± 9.54 ^{a}	50.6 ± 6.82 ^{a}	186.8 ± 27.38 ^{a}	49.8 ± 3.21 ^{a}	2.0 ± 0.07 ^{a}	14.8 ± 4.29 ^{a}	37.3 ± 5.51 ^{a}	1.01 ± 0.03 ^{ab}	107.08 ± 8.21 ^{a}	0.96 ± 0.10 ^{ab}	5.39 ± 0.42
CR	98.71 ± 12.89 ^{a}	45.83 ± 2.5 ^{a}	109.4 ± 10.94 ^{ab}	41.0 ± 2.59 ^{a}	1.9 ± 0.04 ^{a}	19.0 ± 3.11 ^{a}	21.85 ± 2.20 ^{ab}	0.73 ± 0.04 ^{de}	115.18 ± 9.78 ^{a}	0.65 ± 0.12 ^{b}	3.85 ± 0.56
IF1	102.1 ± 19.09 ^{a}	40.2 ± 6.27 ^{a}	224.3 ± 30.64 ^{a}	45.0 ± 7.20 ^{a}	2.2 ± 0.20 ^{a}	7.0 ± 1.77 ^{a}	46.0 ± 6.44 ^{a}	1.01 ± 0.05 ^{ab}	115.50 ± 7.81 ^{a}	1.27 ± 0.25 ^{a}	9.94 ± 2.63
IF2	112.1 ± 15.04 ^{a}	63.5 ± 11.77 ^{a}	169.0 ± 41.80 ^{ab}	45.7 ± 8.19 ^{a}	2.0 ± 0.18 ^{a}	10.0 ± 4.96 ^{a}	33.8 ± 8.32 ^{ab}	1.00 ± 0.04 ^{ab}	122.45 ± 10.62 ^{a}	0.97 ± 0.11 ^{ab}	8.10 ± 1.40
IF3	101.3 ± 8.50 ^{a}	54.8 ± 5.13 ^{a}	122.8 ± 19.40 ^{ab}	46.5 ± 5.21 ^{a}	1.9 ± 0.09 ^{a}	21.8 ± 2.99 ^{a}	24.5 ± 3.80 ^{ab}	0.97 ± 0.03 ^{abc}	134.50 ± 6.11 ^{a}	0.91 ± 0.11 ^{ab}	7.64 ± 1.04
IF4	104.4 ± 6.01 ^{a}	59.5 ± 4.63 ^{a}	147.7 ± 24.47 ^{ab}	44.8 ± 4.82 ^{a}	1.7 ± 0.12 ^{a}	15.7 ± 6.26 ^{a}	29.71 ± 4.85 ^{ab}	1.08 ± 0.04 ^{a}	141.92 ± 8.79 ^{a}	0.95 ± 0.08 ^{ab}	8.01 ± 0.59
IF5	94.8 ± 12.98 ^{a}	51.5 ± 11.11 ^{a}	118.8 ± 13.89 ^{ab}	43.6 ± 4.69 ^{a}	2.1 ± 0.15 ^{a}	18.8 ± 6.09 ^{a}	23.8 ± 2.82 ^{ab}	0.93 ± 0.03 ^{abcd}	119.58 ± 8.29 ^{a}	0.80 ± 0.07 ^{ab}	5.92 ± 0.84
IF6	129.0 ± 37.29 ^{a}	52.0 ± 4.09 ^{a}	119.0 ± 29.57 ^{ab}	39.6 ± 0.93 ^{a}	1.8 ± 0.08 ^{a}	21.4 ± 2.18 ^{a}	23.8 ± 5.93 ^{ab}	0.78 ± 0.04 ^{cde}	120.00 ± 13.93 ^{a}	0.57 ± 0.05 ^{b}	3.96 ± 0.51
IF7	102.2 ± 12.50 ^{a}	53.2 ± 10.71 ^{a}	160.6 ± 28.80 ^{ab}	48.8 ± 3.35 ^{a}	2.0 ± 0.14 ^{a}	16.8 ± 4.50 ^{a}	32.0 ± 5.79 ^{ab}	1.10 ± 0.08 ^{a}	123.75 ± 9.25 ^{a}	1.12 ± 0.20 ^{ab}	7.75 ± 1.00
IF8	80.2 ± 8.48 ^{a}	42.5 ± 3.97 ^{a}	105.7 ± 12.65 ^{ab}	39.5 ± 4.26 ^{a}	1.9 ± 0.05 ^{a}	16.7 ± 2.91 ^{a}	21.3 ± 2.47 ^{ab}	0.82 ± 0.08 ^{bcde}	130.33 ± 11.29 ^{a}	0.81 ± 0.17 ^{ab}	6.84 ± 0.97
IF9	76. 7 ± 5.31 ^{a}	41. 3 ± 4.10 ^{a}	86.8 ± 23.14 ^{b}	35.1 ± 3.93 ^{a}	1.9 ± 0.13 ^{a}	17.7 ± 4.20 ^{a}	17.3 ± 4.70 ^{b}	0.64 ± 0.04 ^{e}	129.25 ± 8.21 ^{a}	0.52 ± 0.04 ^{b}	4.20 ± 0.40

Data are expressed as means ± SEM. [1]Espressed as mg/dL. [2]Expressed as arbitrary units. [3]Expressed as ng/mL.

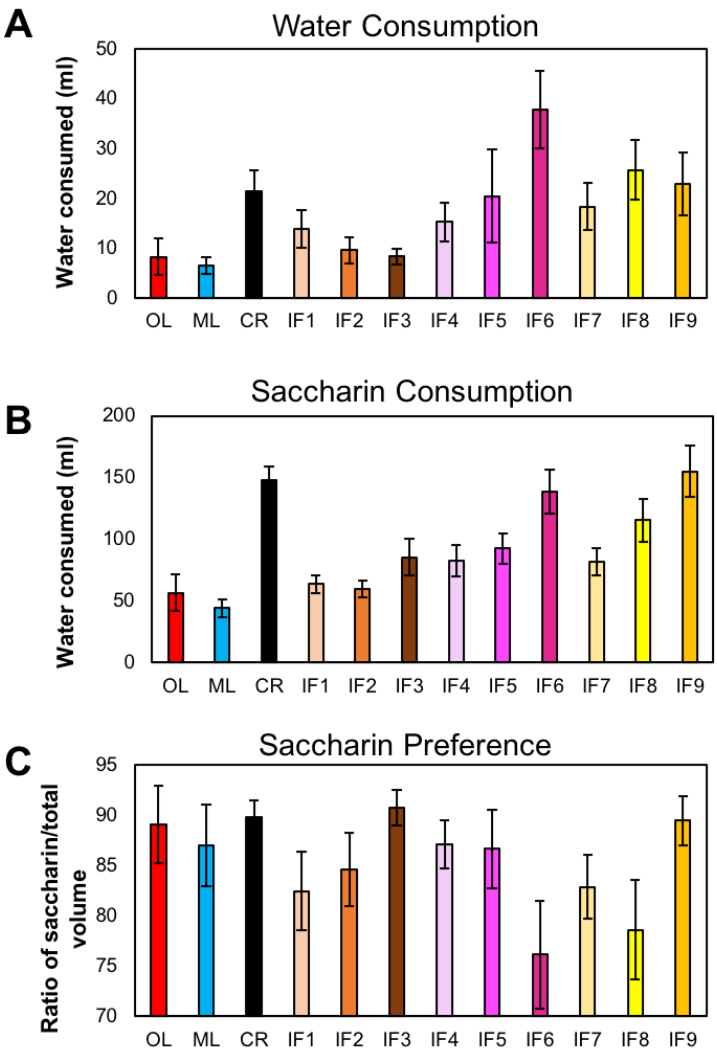

Supplemental Figure 5.1. Conditioned water and saccharin consumption and saccharin preference following ADCR. Volume of A) water of B) saccharine consumed in a two-bottle test paradigm. Values are expressed as means ± SEM. [abc]Different letters between treatments indicate significant statistical difference with Tukey post hoc test at $p<0.05$. Saccharin preference assessed as the ratio of saccharin consumed (in ml) to total volume consumed. Data reported was collected from the second day of exposure to allow for habituation to the two-bottle paradigm using two water bottles in each cage.

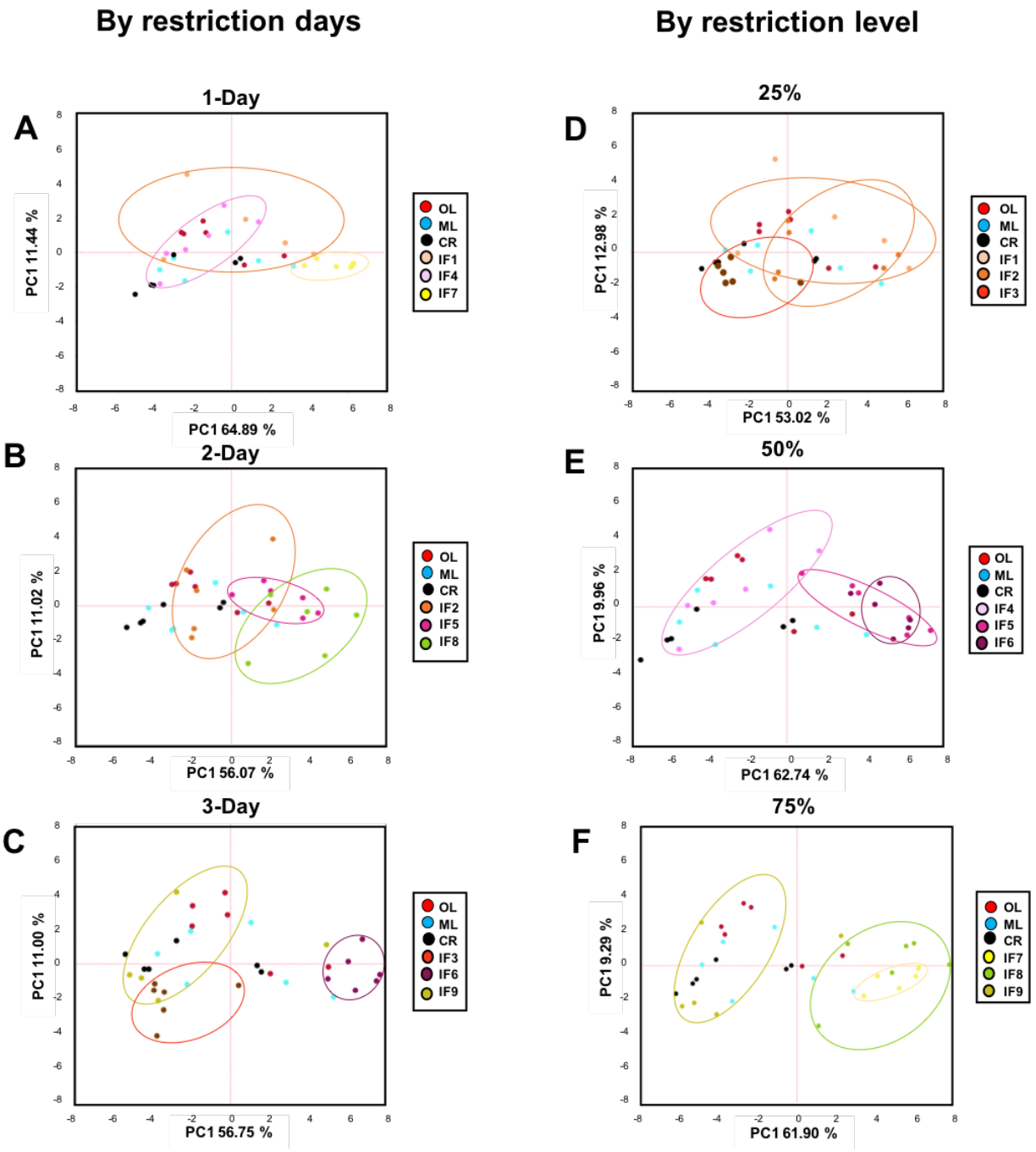

Supplemental Figure 5.2. Subgroup analysis of gene expression of nutrient sensing and proteostasis related pathways by restriction level or day from skeletal muscle using qPCR. Principal component analysis of the expression of groups in two components categorized by A) 1-, B) 2-, and C) 3-day restriction. Principal component analysis of the expression of groups in two components categorized by A) 25%, B) 50%, and C) 75% restriction. Ellipses show 95% confidence interval for each control group. Each dot represents one biological sample.

APPENDIX D: CHAPTER 6 APPENDIX

Supplemental Table 6.1. List of Primers.

Gene (Ensembl ID)	Forward sequence (5'➔3')	Reverse sequence (5'➔3')
Tnfrsf1a (+1285 to +1363) (ENSRNOT00000048529.4)	CTGTTCGGAAATGGGAAG	ACAGCATACAGCATCGCA
Tnfrsf12a (+313 to +379) (ENSRNOT00000004842.5)	TTTCTGGTTTCCTGGTCTGG	GTCTCCTCTATGGGGGTAGTAAAC
Ripk1 (+1978 to +2057) (ENSRNOT00000004842.5)	TGGACCGAGTTCACAACCACCA	TGGTGTTAGCGAAGACGGCTTG
Nfkb1 **mRNA(p50)** (+1907 to +1985) (ENSRNOT00000045233.3)	AGGCAGCACTCCTTATCAACCACC	GACAGGCTGTTGCTCATCACAGCT
Cebp-β **mRNA** (+1220 to +1287) (ENSRNOT00000083876.1)	AGAACGAGCGGCTGCAGAAGA	GAACAAGTTCCGCAGCGTGC
Nfkbia **mRNA (Ikba)** (+701 to +763) (ENSRNOT00000009894.6)	CTACCTGGGCATCGTGGAGCA	CAGGGCTCCTGAGCGTTGACA
Ikbke **mRNA** (+1189 to +1257) (ENSRNOT00000038151.3)	CCCTGCTCTGGATGTCCCAAAG	CCCTTAGCGGTGCTGTAATCGG
Ikbkg **mRNA** (+494 to +563) (ENSRNOT00000038151.3)	GAGGCTGCTACCAAGGAACGACA	GCTGTCTGACCTGCTCACTAACTGC
Tnf **mRNA** (+339 to +449) (ENSRNOT00000079677.1)	AAATGGGCTCCCTCTCATCAGTTC	TCCGCTTGGTGGTTTGCTACGAC
Tnf **premRNA** (+1279 to +1370) (ENSRNOT00000079677.1)	CGGAAGTGAAGTGTGGGTAGAAGT	GTTTGCTGAGGGAGGGAGAATT
Dnmt1 **mRNA** (+1713 to +1792) (ENSRNOT00000064932.4)	TCCTACGCCATGCCCAGTTTG	GAAGATGGGCGTCTCATCATCG
Dnmt3b mRNA (+1197 to +1274) (ENSRNOT00000015482.6)	AATGCGCTGGGTACAGTGGTTTG	AACAGACCCAGAGCCACCAGCT
Tnf **MSP Meth** (-4850 to -4789) (ENSRNOT00000079677.1)	AACTTACCGCTACCTAAAATTACTTTAAACG	GGTTTGTGGGTGAGGTTTTTTGT
Tnf **MSP Meth** (-4850 to -4789) (ENSRNOT00000079677.1)	ACCAACTTACCACTACCTAAAATTACTTTAAAC	AAAGGTTTATATCGTGTCGTTCGAGT
Tnf **MSP Meth** (-2922 to -2834) (ENSRNOT00000079677.1)	TTTTGGTTTTTTATATTAGTGTGCG	AATAACAACAAAAACGTCCCGTA
Tnf **MSP Unmeth** (-2921 to -2831) (ENSRNOT00000079677.1)	TTTGGTTTTTTATATTAGTGTGTGG	AAAAATAACAACAAAAACATCCCATA
Tnf **MSP Meth** (-1902 to -1832) (ENSRNOT00000079677.1)	GCGTATAGAAATTTGTGTATTCGGG	AACACAACCCCCTAATACATTAAACGTA
Tnf **MSP Unmeth** (-1902 to -1832) (ENSRNOT00000079677.1)	TTAGTGTATAGAAATTTGTGTATTTGGGG	AACACAACCCCCTAATACATTAAACATA
Tnf **MSP Meth** (-1018 to -950) (ENSRNOT00000079677.1)	GTTTTTAGTAATATGATGGATTCGT	CTTATCCTTTAAATCTCCTCCGAC
Tnf **MSP Unmeth** (-1018 to -947) (ENSRNOT00000079677.1)	GTTTTTAGTAATATGATGGATTTGT	AACCTTATCCTTTAAATCTCCTCCA
Tnf **MSP Meth** (-253 to -155) (ENSRNOT00000079677.1)	TGTTATAGAATTTTGGTGAGGACG	TCTCAATTTCTTCTCCAATACGAA

Supplemental Table 6.1. (cont.)

***Tnf* MSP Unmeth** (-252 to -153) (ENSRNOT00000079677.1)	GTTATAGAATTTTGGTGAGGATGG	TCTCTCAATTTCTTCTCCAATACAAA
***Tnf* MSP Meth** (+540 to +604) (ENSRNOT00000079677.1)	CGTGTAGAGATGTGTAGAGACGTGG	CTCGAATTTTTATCTCTTACTTCTTCCCTA
***Tnf* MSP Unmeth** (+540 to +604) (ENSRNOT00000079677.1)	TGTGTAGAGATGTGTAGAGATGTGGTTAG	TCTCAAATTTTTATCTCTTACTTCTTCCC
***Tnf* ChIP** (-1389 to -1322) (ENSRNOT00000079677.1)	AAGAGGGGAGAGATGGAA	TGTGGTAACTGACGCCTT
***Tnf* ChIP** (-970 to -897) (ENSRNOT00000079677.1)	GGAGGAGACCCAAAGGATAAGGCT	TCACTTCTCCCAGAACCTCCGTCT
***Tnf* ChIP** (-453 to -378) (ENSRNOT00000079677.1)	CTCCCAATGCTAAGTTCTC	AGAGACACCATGCCTATGT
***Tnf* ChIP** (+110 to +182) (ENSRNOT00000079677.1)	CCCGAGGCAACACATCTC	GCCAGTTCCACATCTCGG
***Tnf* ChIP** (+614 to +688) (ENSRNOT00000079677.1)	GGAGACGAGGGAGATAAGGAGATA	CCCTCTGTGCTTGATCTGTTGT
***Tnf* ChIP** (+1117 to +1254) (ENSRNOT00000079677.1)	CAGGTGAGAGAGTCAGAGCGGTGA	ACGTCCCATTGGCTACGAGGTC
***Tnf* ChIP** (+1710 to +1788) (ENSRNOT00000079677.1)	GCTGAGGTCAACCTGCCCAAGT	CGCCTCACAGAGCAATGACTCC
***Sirt1* mRNA** (+734 to +810) (ENSRNOT00000078739.1)	TTAATCAGGTAGTTCCTCGG	GAAGACAATCTCTGGCTTCA
***Sirt6* mRNA** (+582 to +660) (ENSRNOT00000008758.5)	GCCTGTAGAGGGGAGCTGAGAGAC	CATCAGCGAGCGTTAGGTCCC
***Hdac3* mRNA** (+1011 to +1128) (ENSRNOT00000084735.1)	GCTCCATCCAGATGTCAGCACCCGCAT	CTGGACACTGGGTGCATGGTTCAGC
***Suv39h1* mRNA** (+1127 to +1200) (ENSRNOT00000008399.5)	GCTGTTGCTGTGGCTATGACTGC	GCGGAAGATGCAGAGGTTGTAGC
***Ezh2* mRNA** (+1110 to +1180) (ENSRNOT00000008149.5)	CCACAGTGTTATCAGCATCTGGAGG	GTCTTTATCCGCTCAGCAGTAAGGG
***Kmt2b* mRNA** (+961 to +1049) (ENSRNOT00000080842.1)	CTAGAATCAGGTCAGGGTCGTGGTC	GGTCCCCTTTCCTGTTCATCTCC
***Kdm6b* mRNA** (+367 to +441) (ENSRNOT00000067677.3)	AGCAGTAACAACACTGGTCTTC	AGGGTTTTGGTAATGGTCAG
***Lrrfip1* mRNA** (+467 to +545) (ENSRNOT00000050191.2)	CAGGGAGATCAAGGACTCTC	GTTGTCTAGCTGGGCGTT
***Kdm2a* mRNA** (+1063 to +1149) (ENSRNOE00000186026)	CAAGGTGGAAAGGTCTTCTGGC	TCCCTGTTTCCCTGATAGCAGC
***Tnfaip3* mRNA** (+394 to +473) (ENSRNOT00000074583.1)	CTGAAAACCAACGGTGATG	ACCAAGTCAGTATCCTGGACA
***Zbtb16* mRNA** (+1759 to +1838) (ENSRNOT00000045356.3)	TCAAAGGAAGATGCCCTGGA	TTCCCACACAGCAGACAGAAGA

Supplemental Table 6.2. List of Antibodies.

Name	Cat. No.	Origin	Company
TNF	ab6671	Rabbit	Abcam
β-Actin	sc-1616 (I-19)	Goat	Santa Cruz
IgG	sc-2027	Rabbit	Santa Cruz
NF-kB	ab16502	Rabbit	Abcam
C/EBPβ	sc-150	Rabbit	Santa Cruz
H3K4me3	07-442	Rabbit	Millipore Sigma
H3Ac	06-599	Rabbit	Millipore Sigma

Supplemental Table 6.3. miRNA Database search for rat *Tnf* 3'-UTR, and miRNA in PubMed for Myomir and CR.

3'-UTR Tnf		Myomir and *Tnf*				CR and miRNA			
miR ID	**Database**	**miRNA**	**Reference**	**miRNA**	**Reference**	**miRNA**	**Reference**	**miRNA**	**Reference**
mir-411	miRanda-miRSVF	miRNA-29b	Kulkarni, AS et al 2018	mml-miR-1271	Mercken, EM et al 2013	mml-miR-486-5p	Schneider, A et al 2017	rno-let-7c	Csiszar, A et al 2014
mir-240	miRanda-miRSVF	miRNA-29b	Li, J et al. 2017	mml-miR-17	Mercken, EM et al 2013	mml-miR-92a-3p	Schneider, A et al 2017	rno-miR-329	Csiszar, A et al 2014
mir-211	miRanda-miRSVF	miR-1	Fan, J et al 2016	mml-miR-221	Mercken, EM et al 2013	mml-miR-16-5p	Schneider, A et al 2017	rno-miR-23a	Csiszar, A et al 2014
mir-212	miRanda-miRSVF	miR-133	Fan, J et al 2016	mml-miR-339	Mercken, EM et al 2013	mml-miR-125a-5p	Schneider, A et al 2017	rno-miR-214	Csiszar, A et al 2014
mir-132	miRanda-miRSVF	miR-206	Fan, J et al 2016	mml-miR-16	Mercken, EM et al 2013	mml-miR-125b-5p	Schneider, A et al 2017	rno-miR-125b-5p	Csiszar, A et al 2014
mir-27b	miRanda-miRSVF	miR-208	Fan, J et al 2016	mml-miR-34a	Mercken, EM et al 2013	mml-miR-143-5p	Schneider, A et al 2017	rno-miR-15b	Csiszar, A et al 2014
mir-27a	miRanda-miRSVF	miR-486	Fan, J et al 2016	mml-miR-15a	Mercken, EM et al 2013	mml-miR-106b-5p	Schneider, A et al 2017	rno-let-7e	Csiszar, A et al 2014
mir-125a-3p	miRanda-miRSVF	miR-431	Fan, J et al 2016	mml-miR-192	Mercken, EM et al 2013	mml-miR-20a-5p	Schneider, A et al 2017	rno-miR-181a	Csiszar, A et al 2014
mir-19b	miRanda-miRSVF	miR-499	Fan, J et al 2016	mml-miR-19b	Mercken, EM et al 2013	mml-miR-133c-5p	Schneider, A et al 2017	rno-miR-221	Csiszar, A et al 2014
mir-19a	miRanda-miRSVF	miR-155	Fan, J et al 2016	mml-miR-29b	Mercken, EM et al 2013	mml-miR-133b-5p	Schneider, A et al 2017	rno-let-7d	Csiszar, A et al 2014
mir-181d	miRanda-miRSVF	miR-146a	Fan, J et al 2016	mml-miR-181b	Mercken, EM et al 2013	mml-miR-182	Schneider, A et al 2017	rno-miR-34a	Csiszar, A et al 2014
mir-181c	miRanda-miRSVF	miR-181a	Fan, J et al 2016; Li, QJ et al 2007; Mercken, EM et al 2013	mml-miR-181a	Mercken, EM et al 2013	mml-miR-224-5p	Schneider, A et al 2017	rno-miR-24	Csiszar, A et al 2014
mir-181b	miRanda-miRSVF	let-7c	Yu, JH et al. 2016	mml-miR-653	Mercken, EM et al 2013	mml-miR-6529-5p	Schneider, A et al 2017	rno-miR-872	Csiszar, A et al 2014
mir-181a	miRanda-miRSVF	miR-155	Seok, HY et al. 2011	mml-miR-489	Mercken, EM et al 2013	mml-miR-21-5p	Schneider, A et al 2017	rno-miR-29a	Csiszar, A et al 2014
mir-499	miRanda-miRSVF	miR-10a	Xu, D et al 2016	mml-miR-1323	Mercken, EM et al 2013	mml-miR-340-5p	Schneider, A et al 2017	rno-miR-140	Csiszar, A et al 2014
mir-208	miRanda-miRSVF	miR-16	Talari, M et al 2015.			mml-miR-130a-5p	Schneider, A et al 2017	rno-miR-301a	Csiszar, A et al 2014
mir-99a	miRanda-miRSVF	miR-146b	Fiorillo, A et al 2015			mml-miR-1260b	Schneider, A et al 2017	rno-miR-30c	Csiszar, A et al 2014

Supplemental Table 6.3. (cont.)

mir-99b	miRanda-miRSVF
mir-100	miRanda-miRSVF
rno-miR-540-3p	miRDB
rno-miR-181b-5p	miRDB
rno-miR-181c-5p	miRDB
rno-miR-181d-5p	miRDB
rno-miR-181a-5p	miRDB
rno-miR-298-5p	miRDB
rno-miR-204-5p	miRDB
rno-miR-211-5p	miRDB
rno-mir-181-5p	TargetScan
rno-mir-27-3p	TargetScan

miR-374a	Fiorillo, A et al 2015
miR-31	Fiorillo, A et al 2015
miR-146a	Fiorillo, A et al 2015
miR-223	Fiorillo, A et al 2015
miR-320a	Fiorillo, A et al 2015
miR-382	Fiorillo, A et al 2015
miR-206	Režen, T et al 2014
miR-23a	Režen, T et al 2014
let-7	Režen, T et al 2014
mml-miR-451	Mercken, EM et al 2013
mml-miR-144	Mercken, EM et al 2013
mml-miR-129	Mercken, EM et al 2013
mml-miR-200c	Mercken, EM et al 2013
mml-miR-942	Mercken, EM et al 2013
mml-miR-141	Mercken, EM et al 2013
mml-miR-142-3p	Mercken, EM et al 2013
mml-miR-18a	Mercken, EM et al 2013
mml-miR-106b	Mercken, EM et al 2013
mml-miR-15b	Mercken, EM et al 2013
mml-miR-215	Mercken, EM et al 2013
mml-miR-223	Mercken, EM et al 2013

mml-miR-130b-5p	Schneider, A et al 2017	rno-miR-30b	Csiszar, A et al 2014
mml-miR-411-5p	Schneider, A et al 2017	rno-miR-27a	Csiszar, A et al 2014
mml-miR-598-5p	Schneider, A et al 2017	rno-miR-26a	Csiszar, A et al 2014
mml-miR-500a-5p	Schneider, A et al 2017	rno-miR-542-5p	Csiszar, A et al 2014
mml-miR-501-5p	Schneider, A et al 2017	rno-miR-152	Csiszar, A et al 2014
mml-miR-122a-5p	Schneider, A et al 2017	rno-miR-26b	Csiszar, A et al 2014
mml-miR-337-5p	Schneider, A et al 2017	rno-miR-186	Csiszar, A et al 2014
miR-1-3p	Margolis, LM et al 2017	rno-miR-20a	Csiszar, A et al 2014
miR-133a-3p	Margolis, LM et al 2017	rno-miR-126	Csiszar, A et al 2014
miR-133b	Margolis, LM et al 2017	rno-miR-29c	Csiszar, A et al 2014
miR-206	Margolis, LM et al 2017	rno-miR-192	Csiszar, A et al 2014
miR-221	Ortega, FJ et al 2015;	rno-miR-30e	Csiszar, A et al 2014
scarna-17	Serna, E et al 2013	rno-miR-301b	Csiszar, A et al 2014
miR-21	Serna, E et al 2013	rno-miR-101a	Csiszar, A et al 2014
miR-130a	Serna, E et al 2013	rno-miR-210	Csiszar, A et al 2014
miR-494	Serna, E et al 2013	rno-miR-106b	Csiszar, A et al 2014
miR-19b	Serna, E et al 2013	rno-miR-449a	Csiszar, A et al 2014
mmu-miR-34c-5p	Victoria, B et al	rno-miR-17	Csiszar, A et al 2014
mmu-miR-34b-5p	Victoria, B et al	rno-miR-130b	Csiszar, A et al 2014
mmu-miR-344d-2-5p	Victoria, B et al	rno-miR-16	Csiszar, A et al 2014
mmu-miR-592-5p	Victoria, B et al	rno-miR-19b	Csiszar, A et al 2014

Supplemental Table 6.3. (cont.)

	mml-miR-194	Mercken, EM et al 2013	rno-miR-667	Csiszar, A et al 2014	rno-miR-503	Csiszar, A et al 2014
	mml-miR-409-5p	Mercken, EM et al 2013	rno-miR-383	Csiszar, A et al 2014	mmu-miR-150	Olivo-Marston, SE et al 2014
	mml-miR-93	Mercken, EM et al 2013	rno-miR-328a	Csiszar, A et al 2014	mmu-miR-351	Olivo-Marston, SE et al 2014
	mml-miR-17-5p	Mercken, EM et al 2013	rno-let-7b	Csiszar, A et al 2014	mmu-miR-16	Olivo-Marston, SE et al 2014
	mml-miR-495	Mercken, EM et al 2013	rno-miR-92a	Csiszar, A et al 2014	mmu-let-7f	Olivo-Marston, SE et al 2014
	mml-miR-32	Mercken, EM et al 2013	rno-miR-532-3p	Csiszar, A et al 2014	mmu-miR-34c	Olivo-Marston, SE et al 2014
	mml-miR-19a	Mercken, EM et al 2013	rno-miR-181c	Csiszar, A et al 2014	mmu-miR-155	Olivo-Marston, SE et al 2014
	mml-miR-20a	Mercken, EM et al 2013	rno-miR-145	Csiszar, A et al 2014		

mml: *Macaca mulatta*; rno: *Rattus norvegicus*; mmu: *Mus musculus*.